ENERGY AND RESOURCE VALORISATION OF BIOMASS AND WASTE TOWARDS SUSTAINABLE ENVIRONMENT VIA THERMOCHEMICAL AND BIOLOGICAL APPLICATION

EDITED BY: Su Shiung Lam, Yiu Fai Tsang, Armando Tibigin Quitain, Seyed Ehsan Hosseini and Dai-Viet N. Vo

PUBLISHED IN: Frontiers in Energy Research

frontiers Research Topics

frontiers

ISSN 1664-8714
ISBN 978-2-88966-517-4
DOI 10.3389/978-2-88966-517-4

About Frontiers

Frontiers is more than just an open-access publisher of scholarly articles: it is a pioneering approach to the world of academia, radically improving the way scholarly research is managed. The grand vision of Frontiers is a world where all people have an equal opportunity to seek, share and generate knowledge. Frontiers provides immediate and permanent online open access to all its publications, but this alone is not enough to realize our grand goals.

Frontiers Journal Series

The Frontiers Journal Series is a multi-tier and interdisciplinary set of open-access, online journals, promising a paradigm shift from the current review, selection and dissemination processes in academic publishing. All Frontiers journals are driven by researchers for researchers; therefore, they constitute a service to the scholarly community. At the same time, the Frontiers Journal Series operates on a revolutionary invention, the tiered publishing system, initially addressing specific communities of scholars, and gradually climbing up to broader public understanding, thus serving the interests of the lay society, too.

Dedication to Quality

Each Frontiers article is a landmark of the highest quality, thanks to genuinely collaborative interactions between authors and review editors, who include some of the world's best academicians. Research must be certified by peers before entering a stream of knowledge that may eventually reach the public - and shape society; therefore, Frontiers only applies the most rigorous and unbiased reviews.
Frontiers revolutionizes research publishing by freely delivering the most outstanding research, evaluated with no bias from both the academic and social point of view. By applying the most advanced information technologies, Frontiers is catapulting scholarly publishing into a new generation.

What are Frontiers Research Topics?

Frontiers Research Topics are very popular trademarks of the Frontiers Journals Series: they are collections of at least ten articles, all centered on a particular subject. With their unique mix of varied contributions from Original Research to Review Articles, Frontiers Research Topics unify the most influential researchers, the latest key findings and historical advances in a hot research area! Find out more on how to host your own Frontiers Research Topic or contribute to one as an author by contacting the Frontiers Editorial Office: frontiersin.org/about/contact

ENERGY AND RESOURCE VALORISATION OF BIOMASS AND WASTE TOWARDS SUSTAINABLE ENVIRONMENT VIA THERMOCHEMICAL AND BIOLOGICAL APPLICATION

Topic Editors:
Su Shiung Lam, University of Malaysia Terengganu, Malaysia
Yiu Fai Tsang, The Education University of Hong Kong, Hong Kong
Armando Tibigin Quitain, Kumamoto University, Japan
Seyed Ehsan Hosseini, Arkansas Tech University, United States
Dai-Viet N. Vo, Nguyen Tat Thanh University, Vietnam

Citation: Lam, S. S., Tsang, Y. F., Quitain, A. T., Hosseini, S. E., Vo, D.-V. N., eds. (2021). Energy and Resource Valorisation of Biomass and Waste Towards Sustainable Environment via Thermochemical and Biological Application. Lausanne: Frontiers Media SA. doi: 10.3389/978-2-88966-517-4

Table of Contents

frontiers in Energy Research

EDITORIAL
published: 25 January 2021
doi: 10.3389/fenrg.2020.632403

Editorial: Energy and Resource Valorization of Biomass and Waste Toward Sustainable Environment *via* Thermochemical and Biological Application

Su Shiung Lam[1]*, *Yiu Fai Tsang*[2], *Armando Tibigin Quitain*[3,4], *Seyed Ehsan Hosseini*[5] and *Dai-Viet N. Vo*[6]

[1]Higher Institution Centre of Excellence (HICoE), Institute of Tropical Aquaculture and Fisheries (AKUATROP), Universiti Malaysia Terengganu, Terengganu, Malaysia, [2]Department of Science and Environmental Studies, The Education University of Hong Kong, Tai Po, Hong Kong, [3]Faculty of Advanced Science and Technology, Kumamoto University, Kumamoto, Japan, [4]Center for International Education, Kumamoto University, Kumamoto, Japan, [5]Combustion and Sustainable Energy Laboratory (ComSEL), Department of Mechanical Engineering, Arkansas Tech University, Russellville, AR, United States, [6]Center of Excellence for Green Energy and Environmental Nanomaterials (CE@GrEEN), Nguyen Tat Thanh University, Ho Chi Minh City, Vietnam

OPEN ACCESS

Edited by:
Hu Li,
Guizhou University, China

Reviewed by:
Denny K. S. NG,
Heriot-Watt University Malaysia, Malaysia
Saravanamurugan Shunmugavel, Center of Innovative and Applied Bioprocessing (CIAB), India

***Correspondence:**
Su Shiung Lam
lam@umt.edu.my

Specialty section:
This article was submitted to Bioenergy and Biofuels, a section of the journal Frontiers in Energy Research

Received: *23 November 2020*
Accepted: *17 December 2020*
Published: *25 January 2021*

Citation:
Lam SS, Tsang YF, Quitain AT, Hosseini SE and Vo D-VN (2021) Editorial: Energy and Resource Valorization of Biomass and Waste Toward Sustainable Environment via Thermochemical and Biological Application. Front. Energy Res. 8:632403. doi: 10.3389/fenrg.2020.632403

Keywords: valorization, waste biorefinery, biofuel, pyrolysis, fermentation, gasification

Editorial on the Research Topic

Energy and Resource Valorization of Biomass and Waste toward Sustainable Environment *via* Thermochemical and Biological Application

Innovation toward a sustainable environment is important in maintaining a circular economy and making it a key priority in most countries. This demands practical efforts in resource recovery from biomass, energy production, waste valorization, and reducing environmental pollution through joint ventures among education, research institutions, public services, and private industry.

This Frontiers Research Topic was designed to inaugurate the ongoing developments of thermochemical and biological approaches, including the novel and latest measures that have been initiated in resource and energy valorization of biomass and its wastes, revolutionizing our society toward a sustainable environment.

Ten research articles have been received, reviewed, and published in this research topic. The articles were contributed by academics and researchers from various institutions at different countries including Finland, Ireland, Thailand, China, Belgium, Malaysia, Sweden, Greece, and Colombia. The editorial team of this research topic expresses gratitude to all the authors for their contributions toward the successful publication of this research topic.

THERMOCHEMICAL APPLICATION TO BIOMASS AND WASTE

Bonilla et al. studied fixed-bed gasification of coffee husk using pure oxygen-steam blends to convert agro-industrial waste into fuel. This study also highlighted the estimation of uncertainty in the flows of oxygen, steam, biomass fuel, and syngas composition, energy recovery from gasification process, and the performance of oxygen-steam blends vs. airsteam.

In this research topic, Vamvuka et al. investigated and developed a multi-fuel residential boiler for combustion of agricultural residues. This study also discussed raw fuel analysis,

combustion performance of agricultural residues, and co-combustion performance of agricultural residues blends. Prurapark et al. studied the effect of temperature during pyrolysis of high-density polyethylene and polyethylene terephthalate on the production and properties of pyrolysis oil.

BIOLOGICAL TREATMENT OF BIOMASS AND WASTE

Zhang et al. in this research topic highlighted on how to convert agricultural biomass wastes (e.g., pig manure, corn straw, and fertilizers) into energy using mixed fermentation technology. The authors have also discussed the pretreatment methods including physical, chemical, and biological means to improve the biomass anaerobic and mixed fermentation.

Nickel et al. proposed an evaluation framework for a wheat straw–based ethanol biorefinery derived from multi-scale variability analysis using a flow sheet process model, life cycle assessment, and techno-economic analysis to describe the simultaneous saccharification and ethanol fermentation.

The biological treatment of dairy wastewater in this research topic was also studied by Singh et al., who performed methanization of long-chain fatty acid in a dynamic sludge chamber–fixed film bioreactor. Vergote et al. compared the effect of composition fraction separation between unseparated liquid pig manure and its separated fecal fraction on the stability of thermophilic mono-digestion process.

An proposed a new model for the circular economy development in the garden industry by introducing a static composting treatment for landscape waste recycle. Another study by Zhang et al. demonstrated a potent extraction method for *Cinnamomum camphora* leaves that are rich in bioactive compounds. The study shows the potential conversion of *Cinnamomum camphora* into chemical materials, bioenergy, and biomedicine.

APPLICATION OF NOVEL MATERIALS (E.G., CATALYSTS) IN WASTE AND BIOMASS TO ENERGY

Mohammed et al. improved gasification reaction and tar cracking efficiency of empty fruit bunch using primary Malaysian dolomite catalysts. The effects of calcined dolomite catalysts on product yield (especially syngas), gasification performance, and tar cracking were discussed.

CONCLUSION

This research topic highlights the potential, recent development and needs to retrieve the chemical and energy value of biomass materials and its wastes for various applications, while hindering the waste dumping to landfill sites. This effort is realized by the innovations of emerging thermochemical and biological processes for useful products manufacture especially as chemical feedstock and energy carriers rather than opting the common volume-reducing "incineration." The aim is placed on the description of the design, operation, and products of advanced thermochemical and biological technologies, along with understanding of their fundamentals and applications.

AUTHOR CONTRIBUTIONS

All authors listed have made a substantial, direct, and intellectual contribution to the work and approved it for publication.

Conflict of Interest: The authors declare that the research was conducted in the absence of any commercial or financial relationships that could be construed as a potential conflict of interest.

frontiers in Energy Research

ORIGINAL RESEARCH
published: 26 November 2019
doi: 10.3389/fenrg.2019.00127

Experimental Gasification of Coffee Husk Using Pure Oxygen-Steam Blends

Javier Bonilla[1]*, *Gerardo Gordillo*[2] and *Carlos Cantor*[3]

[1] Grupo de Investigación de Aprovechamiento Tecnológico de Materiales y Energía, Universidad ECCI, Bogota, Colombia, [2] Research Group of Energy Conversion, Department of Mechanical Engineering, Universidad de los Andes, Bogota, Colombia, [3] Department of Mechanical Engineering, School of Basic Sciences, Technology and Engineering, Universidad Nacional Abierta y a Distancia, Bogota, Colombia

This work discusses results on temperature profile, syngas composition, High Heating Value, and efficiency of a Coffee Husk counter-current fixed-bed gasification process, in which oxygen-steam blends were used as an oxidizing agent. The experimentation was carried out for various Equivalence Ratios (ER) and Steam-Fuel Ratios (SF), whose ranges were [1.6–5.6] and [0.4–0.8], respectively. The results show that increased steam (higher steam fuel ratios) improves the H_2/CO molar ratio i.e., for a constant ER = 3.7 and SF at 0.4, 0.6, and 0.8, the H_2/CO ratio was 1.2, 1.4, and 1.8, respectively. Also, the addition of steam tends to increase the syngas Higher Heating Value, which ranged between 7,714 kJ/m^3 at ER = 1.6 and SF = 0.4 and 8,841 kJ/m^3 at ER = 3.2 and SF = 0.8. On the other hand, increased ER (lower oxygen) decreases the Net Cold Gasification Efficiency (CGE_{NET}) which was between 53% at ER = 5.6 and SF = 0.6 and 82% at ER = 1.6 and SF = 0.4. Results were also compared to results published before for gasification of the same biomass but using air-steam mixtures for partial oxidation. This comparison shows that the use of oxygen increases both the temperature profile in the bed and the yield of CO and H_2 contained in the syngas.

Keywords: biomass gasification, coffee husk, updraft gasifier, oxygen gasifying agent, syngas

OPEN ACCESS

Edited by:
Su Shiung Lam,
Universiti Malaysia Terengganu, Malaysia

Reviewed by:
Fehmi Akgun,
Tubitak Marmara Research Centre Energy Institute, Turkey
Azlina Karim,
Putra Malaysia University, Malaysia

***Correspondence:**
Javier Bonilla
jbonillap@ecci.edu.co

Specialty section:
This article was submitted to Bioenergy and Biofuels, a section of the journal Frontiers in Energy Research

Received: *17 July 2019*
Accepted: *29 October 2019*
Published: *26 November 2019*

Citation:
Bonilla J, Gordillo G and Cantor C (2019) Experimental Gasification of Coffee Husk Using Pure Oxygen-Steam Blends. Front. Energy Res. 7:127. doi: 10.3389/fenrg.2019.00127

HIGHLIGHTS

- Use of coffee husk as agro-industrial waste for generation of fuel.
- Quality enhancement of syngas by yielding oxygen-steam agents into the gasifier.
- Small-scale gasification technology very appropriate to generate syngas to low cost for many farms.

INTRODUCTION

The continuous increase in both energy consumption and emissions, generated in the combustion of fossil fuels, around the world (International Energy Agency, 2016) has stimulated the study of new sustainable energy technologies to reduce the dependence of the population on fossil fuels. The economies of many countries are based on agro-industry, a sector that produces a lot of biomass residues that can be used as feedstock for the production of solid, liquid, and gas biofuels via

thermochemical or biological gasification processes (Abbasi and Abbasi, 2010; Gírio et al., 2010; Yang et al., 2014; Aslan, 2016; Chen, 2016; Cutz et al., 2016; Joselin Herbert and Unni Krishnan, 2016; Bilgili et al., 2017; Toklu, 2017). Thermochemical processes to produce biofuels under biomass conversion include partial oxidation with pure air or pure oxygen to produce a syngas rich in CO and CH_4, reforming with steam to produce mixtures of CO_2 and H_2, partial oxidation and partial reforming with air-steam or oxygen-steam to produce a syngas rich in H_2, and pure pyrolysis without any oxidizer to produce liquid and gas fuels (Hernandez et al., 2016; Pacioni et al., 2016; Kirsanovs et al., 2017; Li et al., 2017; Sansaniwal et al., 2017b; Tanczuk et al., 2017; Xiao et al., 2017; Zhang and Pang, 2017). Thus, one of the most performed thermochemical processes is coal and biomass air-gasification have been used for a long time to produce syngas with a high heating value (HHV) ranging from 4 to 6 MJ/SATP m^3 (Gordillo and Annamalai, 2010; Sandeep and Dasappa, 2014). However, in order to improve syngas quality (HHV and composition), the other gasification processes mentioned above have been studied. For instance, the use of pure oxygen as oxidizing agent instead of air enhances the energy density of the syngas produced (Kurkela et al., 2016; Hussein et al., 2017). On the other hand, biomass oxygen-steam gasification is a process used when it is required improving both gas composition and HHV of the mixtures produced.

Colombia is a country known for its coffee agroindustry and whose production of green coffee in 2016 was of 870,000 metric tons, which produced about 141,627 metric tons of coffee husk (CH) waste. This waste can be used as feedstock for the *in situ* production of gaseous fuels via small-scale gasification, which can take advantage for energy generation in order to reduce the dependency of farms on fossil fuels. Updraft fixed-bed gasification technology is the most suitable for the control of the composition of the mixtures produced since the gasification stages are known as drying, pyrolysis, reduction, and combustion occur in different zones in the bed of the gasifier. Also, updraft gasifiers are very good for small-scale energy generation requirements because of its simple operation (Gordillo and Annamalai, 2010; Plis and Wilk, 2011; Sansaniwal et al., 2017a). The mixture contained in biomass releases at temperatures ranging from 373 to 450 K in the drying zone, placed on the top of the bed, whereas the volatile matter, contained in the dry biomass coming from the drying zone, is released at 450 K < T < 990 K in the pyrolysis zone. The char (fixed carbon and ash) produced in the pyrolysis zone downwards through the reduction zone where it reacts, at 990 K < T < 1,100 K, with the species (CO_2, CO, H_2, H_2O) yielded in the combustion zone to produce secondary species such as CH_4, CO, CO_2, H_2, etc. In the combustion zone, the remaining char from the reduction zone reacts with the oxidizing agent supplied through the plenum of the gasifier to produce the heat required in the process. The peak of temperature occurs in the combustion zone where the global heterogeneous-exothermic reactions of char with oxygen take place and release the heat required in the global gasification process. Above of the combustion zone, the temperature starts to decrease because the global reactions occurring in these zones (pyrolysis, reduction, and drying) are endothermic. **Table 1** shows the global reactions occurring during a gasification process. Reactions with enthalpy lower than zero are exothermic and those with enthalpy higher than zero are endothermic.

Gordillo and Rodriguez (2011) researched adiabatic gasification and pyrolysis of coffee husk. Via simulation, the NASA CEA software was used in order to obtain the compounds and HHV of Syngas as well as the Energy Conversion Efficiency of the gasification. Among the results, it is highlighted that the syngas is rich in CO_2 and H_2 and the Activation Energy of coffee husk is close to 221 kJ/mol. Wilson et al. (2010) published results on a (coffee husk) CH gasification study, carried out at constant temperatures of 700, 800, and 900°C and using oxygen-nitrogen blends as an oxidizing source. The results showed that increasing both the temperature and the oxygen concentration enhances the CO content in mixtures, e.g., raising the temperature from 700 to 900°C in an environment of pure nitrogen (100% nitrogen and 0% oxygen) and for an environment with 3% of oxygen (97% nitrogen and 3% oxygen) on a molar basis increased the CO concentration in the syngas from 2.17 to 5.49% and from 3.28 to 5.93%, respectively. In Van Huynh and Kong (2013) carried out an experimental study on a pilot-scale biomass gasifier using oxygen—steam as the gasifying agents. The biomasses used as feedstock to feed the gasification facility were pinewood, maple-oak mixture, and discarded seed corn. They concluded that the H_2/CO ratio increases when the oxygen supplied also increased—e.g., increasing the oxygen from 21 to 40% enhanced the H_2/CO ratio from 0.59 to 0.75, 0.36 to 0.43, and 0.67 to 0.84 for pine, discarded seed corn, and maple-oak, respectively. Lenis et al. (2016) performed research on fixed-bed gasification of Jacaranda Copaia wood where air enriched with oxygen (21, 24, and 29% vol) was used as a gasifying agent. The conclusion of these experimental results showed that an increase in the oxygen concentration raises the biomass consumption in the

TABLE 1 | Chemical reactions in the gasification process.

	Chemical reaction	ΔH_r^θ [kJ/mol]
R_1	Solid Biomass → VM + Char + Tar	
	Char combustion	
R_2	$C_2 + \frac{1}{2}O_2 \rightarrow C + CO$	−111
R_3	$C + O_2 \rightarrow CO_2$	−394
	Char gasification	
R_4	$C + CO_2 \rightarrow 2CO$	173
R_5	$C + H_2O \rightarrow CO + H_2$	131
R_6	$C + 2H_2 \rightarrow CH_4$	−75
	Homogeneous reactions	
R_7	$CO + \frac{1}{2}O_2 \rightarrow CO_2$	−283
R_8	$H_2 + \frac{1}{2}O_2 \rightarrow H_2O$	−242
R_9	$CH_4 + 2O_2 \rightarrow CO_2 + 2H_2O$	−803
R_{10}	$CO + H_2O \rightarrow CO_2 + H_2$	−41
R_{11}	$CH_4 + H_2O \rightarrow CO + 3H_2$	206

Adapted from Gírio et al. (2010), Bilgili et al. (2017), and Toklu (2017).

gasifier due to lower nitrogen amount, which reduces syngas thermal energy losses by heating of nitrogen. In Liu et al. (2018) carried out experimental research on a two-stage fluidized bed gasifier using oxygen-enriched air as gasifying agent and rice straw as fuel. The oxygen concentrations of the gasifying agent were from 21 up to 45%. Thus, the findings present that increasing the oxygen concentration is conducive to raising the gasification temperature, leading to enhancement of the HHV of syngas (4–5.24 MJ/kg) and improving the gasification efficiency. A secondary oxygen injection of 33% of primary oxygen reduced the tar concentration from 15.78 to 10.24 g/Nm^3. Bonilla and Gordillo (2017) performed experimental research on autothermal gasification of CH using air-steam blends as gasifying agents. In their research, Equivalence Ratio (ER) and Steam-Fuel Ratio (SF) were the parameters set which ranged 1.53–6.11 and 0.23–0.89, respectively. The HHV of the syngas obtained was between 3,112 and 5,085 kJ/SATP m^3. The main chemical composite concentrations (%) of syngas on a dry basis at its maximum HHV were $H_2 = 18.81$, $CO = 10.13$, $CO_2 = 19.33$, and $CH_4 = 3.52$. The results evidence that even though supplying steam into the gasifier decreases the main temperature of the fixed-bed, the HHV of syngas increases.

A literature review shows that there are no previous studies on fixed bed counter-flow gasification of CH using oxygen-steam mixtures as an oxidizing source. Also, the previous study on biomass gasification (Gordillo and Rodriguez, 2011) with nitrogen-oxygen showed only the effect of increasing the oxygen (21–40%) on the H_2/CO ratio. Thus, this paper presents results from a study carried out in fixed-bed counter-flow gasification of CH using oxygen-steam as an oxidizing agent. As a principal contribution, this study discusses the effect of operating parameters such as Equivalence Ratio (ER) and Steam-Oxygen ratio (SF) on temperature profiles along the gasifier axis, syngas composition, syngas HHV, and Cold Gas Efficiency (CGE), and Total Energy Improvement Ratio (TEIR). Also, the results are compared to results previously published (Bonilla and Gordillo, 2017) on gasification of CH but using air-steam mixtures as an oxidizing agent. The thermochemical characterization (empirical formula, DAF-HHV, formation enthalpy, etc.) of the CH also is presented. ER and SF are defined in Equations (1) and (2), respectively.

$$ER = \frac{\text{stoichiometric oxygen moles}}{\text{actual oxygen moles}} \quad (1)$$

$$SF = \frac{\text{actual steam moles}}{\text{actual fuel moles}} \quad (2)$$

The Equivalence Ratio is defined according to the USA definition.

MATERIALS AND EXPERIMENTAL METHOD

Fuel Biomass

CH samples were obtained from Colombian agroindustry and characterized under proximate and ultimate analysis. The samples were prepared under the ASTM D2013 standard as required for the proximate analysis, which were carried out under the following standards: moisture (ASTM D3302), volatile matter (ASTM D3175/D7582), ash content (ASTM D4239), fixed carbon (ASTM D3172), sulfur (ASTM 2492), high heating value (ASTM D5865). The elemental analysis was done as follows: carbon, hydrogen, and nitrogen (ASTM D5373), sulfur (ASTM 2492), ashes (ASTM D3174-12/D7582-15). Also, the particle size of the biomass was determined by using the ASTM D422.

Experimental Setup and Procedure

Figure 1 shows the experimental facility where the experimentation was developed. It is a low-scale (about 10 kW) counter-flow fixed-bed gasifier that can use air-steam or oxygen-steam blends as an oxidizing source. The main facility components are (i) fixed-bed gasifier, (ii) biomass hoper, (iii) temperature data logger, (iv) pneumatic vibrator coupled to the grate, (v) steam generator, (vi) gas cleaning system, (vii) a gas analyzer (GS), and (viii) syngas burner.

(i) The fixed-bed gasifier is 1 m height and built of a castable alumina refractory tube whose inner and outer diameters are 127 and 254 mm, respectively. The tube is surrounded by a 5 cm insulating fiberglass blanket layer to reduce the heat loss. The biomass hopper has a worm screw in the bottom to feed the biomass continuously. The temperature data logger (Omega RD8800) records every minute the temperature obtained from 8 k-type thermocouples placed along the axis of the bed in a way that it gives the profile of the temperature along the gasifier bed. The steam generator is built of a 10 cm stainless steel tube surrounded by an electric tape resistance with variable power from 350 to 1,000 W. The tube and resistance are externally isolated with a 10-cm layer of fiberglass blanket to avoid heat loss. The mass rate of vapor generated in this device depends on the power supplied by the electrical resistance and varies from 1.3 to 17.3 g/min. The oxygen volumetric flows supplied to the gasifier were measured by an oxygen flowmeter (Dwyer), whereas the steam flows were measured using a certificated calibrated rotameter (Aalborg P11A1-VA0). The pneumatic vibrator is joined to the conical cast grate to maintain continuous ash removal from the bed to gasifier plenum, placed under the grate at gasifier bottom. The cleaning gas system has a moisture and tar collector that are preceded by a set of filters to retain the particle material flowing with the syngas. Samples of the clean syngas leaving the filters are taken to the gas analyzer (Gasboard-3100 Infrared Syngas), which analyzes the mole fraction of H_2, CO, CO_2, CH_4, and C_nH_m between the following ranges: $0 < CO2 < 50\%$, $0 < CO < 100\%$, $0 < CH_4 < 10\%$, $0 < H_2 < 50\%$, and $0 < C_nH_m < 10\%$. Gas samples analyzed are mixed downstream, with the remaining syngas to be burned in the syngas burner.

Operating Conditions

The experiments were carried out according to the parameters specified in **Table 2** and under the following sequence: (i) the gasifier grate was heated at 550°C using a torch, (ii) the gasifier plenum was closed and the temperature recorder was turned on in order to store temperature every minute, (iii) the bed was fed with biomass until the bed height was 16 cm, (iv) the flows of steam and oxygen were adjusted as required for each experiment (ER, and SF), (v) the fed biomass continued as it

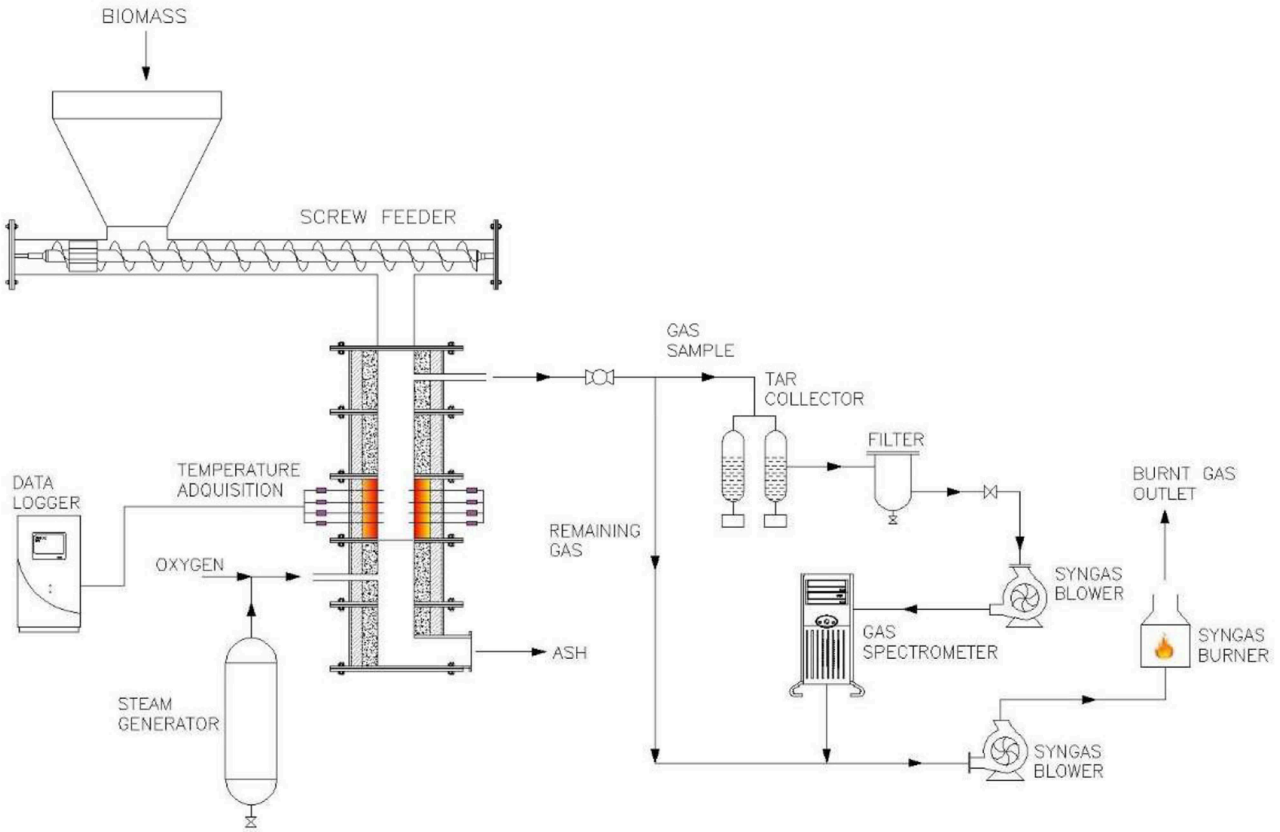

FIGURE 1 | Gasification facility.

TABLE 2 | Experimental parameters.

Oxygen pressure and temperature	0.76 bar, 18°C
Steam pressure and temperature	0.76 bar, 92°C
Bed height	160 mm
Fuel biomass	Coffee husk
Particle size	Flake where 80% of the mass is $d_p < 4$ mm
Biomass flow rate	0.166 g/s (600 g/h)
Oxygen flow	15 SFCH–4 SFCH (0.42 SATP m^3/h–0.11 SATP m^3/h)
Steam flow	2.18–4.99 g/min (130.8–299.4 g/h)
ER	1.49–5.59
SF	0.38–0.87

was burned until the gasifier was at almost steady-state, i.e., peak temperature at the bed did not change, (vi) the syngas samples were carried out toward a gas analyzer at a flow rate of 1 l/min to be analyzed, (vii) the samples analyzed and the syngas remaining were fixed downstream and burned in the gas burner, (viii) the sample analysis continued at real time during 10 min, (ix) the biomass screw feeder was stopped and the gasifier cooled down until room conditions, (x) char samples were taken from the gasifier plenum to be analyzed, and (xi) all systems compounding the experimental facility were cleaned to prepare the facility for the next experiment. All experimentation was carried out at $P = 76$ kPa and temperatures of oxygen and steam of 18 and 92°C, respectively.

RESULTS AND DISCUSSION

Biomass Characteristics

Table 3 shows the results on ultimate, proximate, lignocellulose analyses, the biomass empirical formula and formation enthalpy as well as the particle size distribution of CH. The empirical formula was determined based on the atom balance on components given by proximate and ultimate analyses, whereas the formation enthalpy was derived using the dry ash-free high heating value (DAF HHV) in order to perform an energy balance between reactants and products of the theoretical combustion of a kmol of biomass defined as the empirical formula ($CH_{1.63}N_{0.015}O_{0.82}S_{0.0024}$).

Proximate analysis results show that the CH has a high volatile matter content, which makes this biomass a good feedstock for gasification processes in order to produce clean fuels. Due to its dry ash-free high heating value (21,217 kJ/kg), CH is

TABLE 3 | Characterization of CH.

Proximate analysis	
Moisture %	10.10
Volatiles %	79.86
Ash %	1.20
FC %	8.84
Ultimate analysis	
C %	44.52
H %	6.03
N %	0.78
O %	48.38
S %	0.29
HHV (kJ/kg)	18,740
DRY HHV (kJ/kg)	20,845
DAF HHV (kJ/kg)	21,127
Empirical formula	$CH_{1.63}N_{0.015}O_{0.82}S_{0.0024}$
Enthalpy formation (kJ/mol)	−103,957
Analysis of lignocellulose	
Cellulose %	30.12
Hemicellulose %	15.90
Lignin %	27.87
Particle size	
[0,0; 0,5] mm	13.15%
[0,5; 1,0] mm	14.01%
[1,0; 1,7] mm	20.54%
[1,7; 2,0] mm	9.94%
[2,0; 2,8] mm	20.6%
[2,8; 4,0] mm	19.33%
[4,0; 5,6] mm	2.33%

appropriate for combustion processes to produce heat or for gasification process with steam-oxygen mixtures rich in steam without heat supply. More steam supplied to the gasifier implies low gasification temperatures. In gasification processes when the temperature is very low, the gasification process is not sustainable by itself and requires heat addition.

Uncertainty Analysis

The uncertainty in the flows of oxygen, steam, biomass fuel, and syngas composition was estimated according to Equations (3) and (4), which give the total uncertainty and the uncertainty propagation, respectively.

$$\sigma_{x_i}^2 = B_{x_i}^2 + P_{x_i}^2 \tag{3}$$

$$\sigma_r^2 = \sum_{i=1}^{j} \left(\frac{\partial r}{\partial x_i} \right)^2 \sigma_{x_i}^2 \tag{4}$$

Where, B_{x_i} and P_{x_i} are systematic uncertainties and random uncertainties of x_i; $r = r(x_1, x_2, ..., x_2)$ is function of x_i measured variables of j; σ_r, σ_{x_i} are uncertainties of r and x_i, respectively. The temperature was tested with thermocouples of the accuracy of ±0.75%. The uncertainty derived from thermocouple operation was ±0.15% which gives an uncertainty total, given by Equation 4, in temperature, of ±0.76%. The oxygen flow rate was measured by a rotameter with 20 SFCH-full scale (0.57 m^3/h), 1 SFCH (0.0285 m^3/h) of resolution, and accuracy of ±4%; the total uncertainty of airflow, given by Equation (3), was ±4%. Steam flows entering the gasifier were measured with a rotameter of 9.96 cm^3/min full scale, 0.066 cm^3/min resolution, and an accuracy ±1%. Thus, total uncertainty to water flow rate measurement was ±1%. The feeding system (screw feeder) was calibrated previously and its systematic uncertainty was ±3.42%. The total uncertainty of scale used to measure the sample weight was ±1%, and the total uncertainty of the timer used to measure the feed rate was ±3.87%. The uncertainties of ER and SF are functions of two variables, which were calculated by using Equation (4), resulting in ±5.57% for ER and ±4.12% for the SF ratio. The total uncertainty about syngas compounds measured by a mass spectrometer was ±1% accuracy only.

Temperature Profiles Along the Gasifier Axis

Figures 2–4 show the temperature profiles along the gasifier axis for different SF and ER ratios. The temperature curves show that the temperature peak occurred at about 4 cm above of the grate, indicating the midpoint of the combustion zone where the char reacts with the oxygen-steam mixture supplied, releasing CO and CO_2 via the oxidation of C ($C + \frac{1}{2}O_2 \rightarrow CO$, $C + O_2 \rightarrow CO_2$) and H_2 and CO via the Carbon steam reforming reaction ($C + H_2O \rightarrow H_2 + CO$). Also, the heat required to drive the gasification process is released in the combustion zone by the oxidation of C. Downstream of the combustion zone (height > 4 cm), the trend of the temperature curves is decreasing since almost all the oxygen supplied to the gasifier is consumed in the combustion zone, and hence the reactions occurring over there are endothermic. Immediately above the combustion zone is the pyrolysis zone, where the volatile matter contained in biomass is released as a mixture of gases composed basically of CO, CO_2, H_2O, H_2, CH_4, C_2H_6, and other heavier gases. Above the pyrolysis zone, one of the more important reactions is the shift reaction ($CO + H_2O \rightarrow H_2 + CO_2$), in which the CO coming from the combustion and pyrolysis zone reacts with the steam released in the dry zone to produce more H_2 and CO_2. In general, pyrolysis and drying processes are endothermic, consuming an amount of the heat produced in the combustion zone.

Figures 2, **3** show the effect of the ER on the temperature profiles. All curves show that increased ER tends to decrease the temperature along the gasifier axis. i.e., the pick temperature (T_p) that occurs in the combustion zone decreases with increased ER (lower oxygen supplied). Lower oxygen in the combustion zone implies poor oxidation of C (rich oxidation) and hence a lower heat released—i.e., at SF = 0.4, increasing the ER from 1.6 to 5.6 decreases the peak temperature from 979 to 864°C. Also, results show that the increase in SF decreases temperature along the gasifier. Increased SF implies more steam supplied to the gasifier and hence the steam reforming reactions, which in general are endothermic, are favored—i.e., at ER = 1.6, the peak temperature is 979°C for a SF = 0.4 whereas it is 825°C for a SF = 0.8.

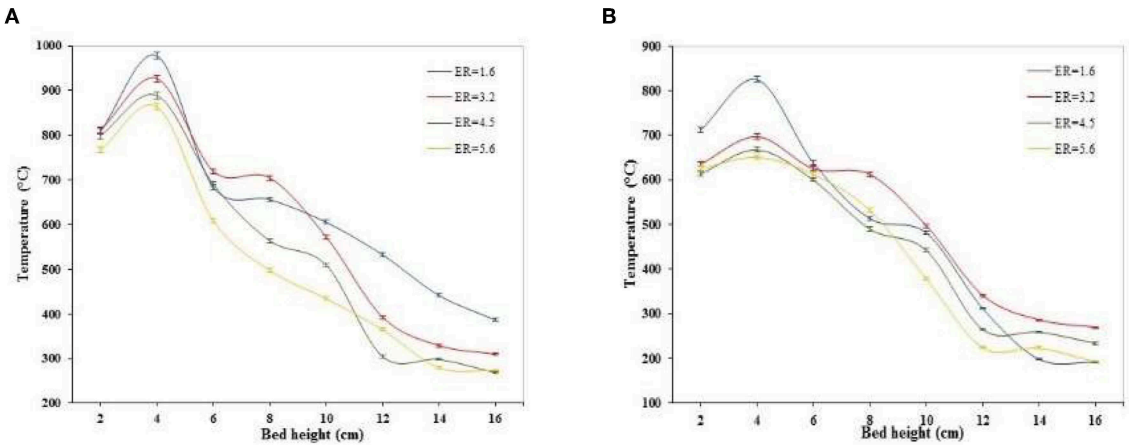

FIGURE 2 | Temperature profile along of gasifier bed axis at **(A)** SF = 0.4; **(B)** SF = 0.8.

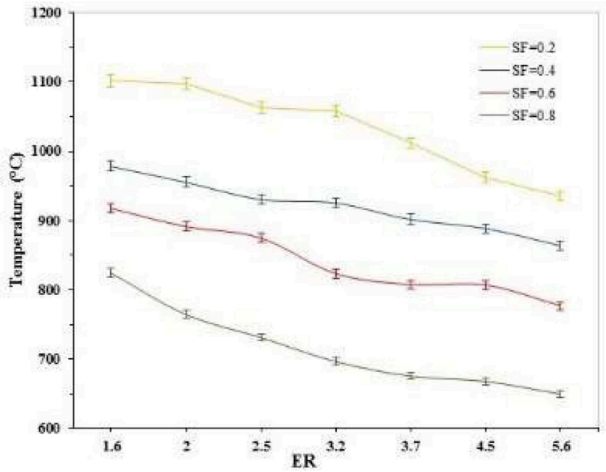

FIGURE 3 | Temperature peaks vs. ER for several SF ratio values for air and oxygen gasification of CH.

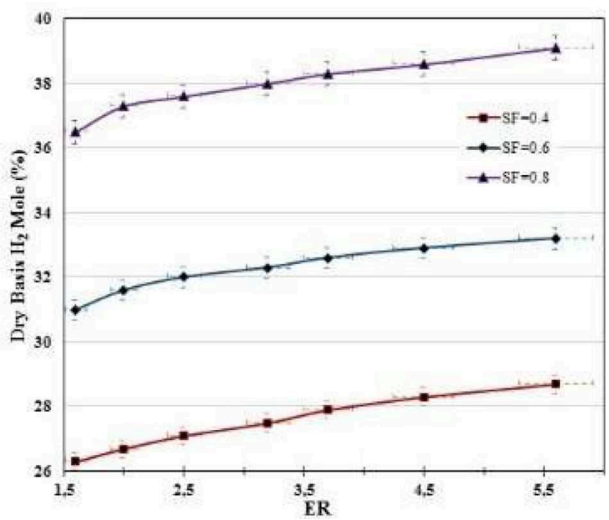

FIGURE 4 | H_2 production vs. ER for several SFs for air and oxygen gasification of CH.

Figure 3 shows the effect of the ER and SF ratios on the combustion temperature (peak temperature). All curves show that the temperature in the combustion zone decreases with increased ER and SF ratios. Increased ER implies a lower oxygen supply to the gasifier, hence the combustion of char ($C_2 + \frac{1}{2}O_2 \rightarrow C + CO$, $C + O_2 \rightarrow CO_2$) in the combustion zone occurs in an environment poor in oxygen leading to more production of CO than CO_2. Partial oxidation of C to produce CO released lower heat than those to produce CO_2. On the other hand, when the SF is increased, at constant ER, the steam-reforming reaction of char ($C + H_2O \rightarrow H_2 + CO$) to produce CO and H_2 is favored due to more steam entering the gasifier. This leads to lower temperatures in the combustion zone because of more head consumed by the steam reforming reaction, which is endothermic. Also, when the combustion zone is poor in oxygen, due to increased ER, the carbon burnt decreases, leading a lower heat release.

Syngas Composition

Figures 4–**7** show the percentages of H_2, CO, CO_2, and CH_4 contents in syngas as a function of ER and SF ratios. As shown in **Figure 4**, H_2 content increases as ER and SF increase. At constant SF, the H_2 curves tend to be linear with ER for ER $>$ 1.75. i. e., at SF = 0.4, increasing the ER from 1.6 to 5.6 raises the H_2 content from 26.3 to 28.7%, which corresponds to an increase of the H_2 production of 9.12%. However, at SF = 0.8, for the same increase in ER (1.6–5.6) the increase in H_2 content (36.5–39.1%) is only 7.1%. This implies that at higher SF the effect of the ER on the H_2 production tends to

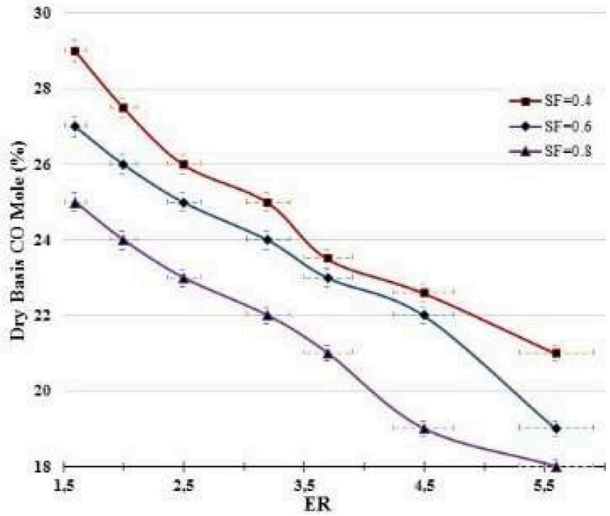

FIGURE 5 | CO concentration vs. ER at several SF values.

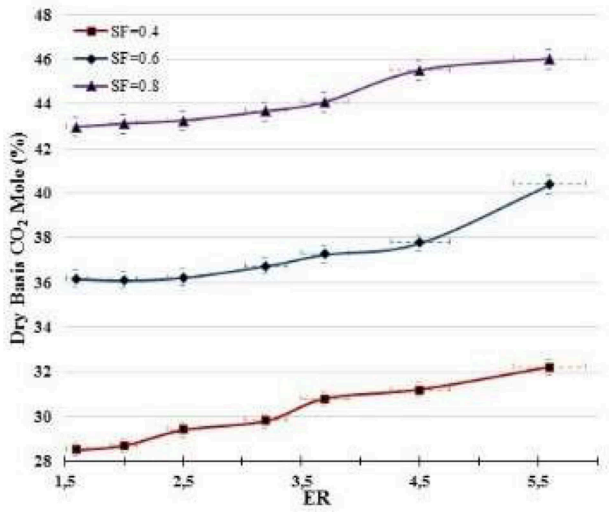

FIGURE 6 | CO_2 concentration at several SF vs. ER.

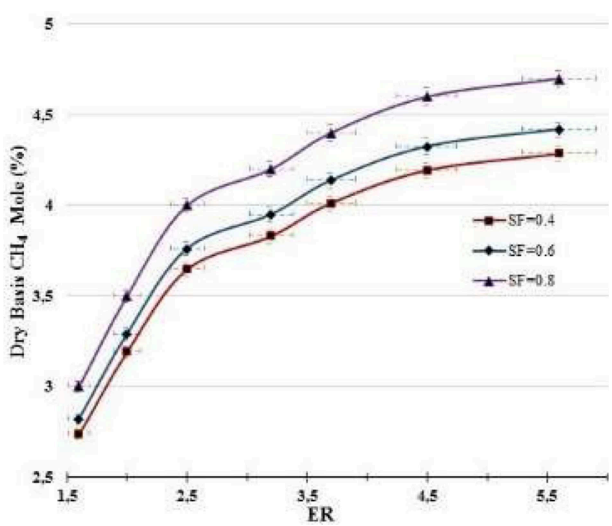

FIGURE 7 | CH_4 concentration at several SF vs. ER.

be less important. At constant SF, increased ER leads to lower oxygen entering the gasifier and hence the combustion of char in the combustion zone ($C + O_2 \rightarrow \frac{1}{2}CO$, $C + O_2 \rightarrow CO_2$) occurs in a poor oxygen ambient, which favors the production of CO instead of CO_2. More CO produced in the combustion zone by partial oxidation of C implies more production of H_2 through the reaction of CO with both the steam supplied to the gasifier and the moisture released in the drying zone ($CO + H_2O \rightarrow H_2 + CO_2$). Thus, H_2 production starts in the combustion zone and continues through the other zones (reduction, pyrolysis, and drying). **Figure 4** also shows the effect of SF on H_2 production. At constant ER, the effect of increasing SF is to produce more H_2 due to more steam supply with the oxidizing source, which favors the shift reaction ($CO + H_2O \rightarrow H_2 + CO_2$) and carbon reforming reaction ($C + H_2O \rightarrow H_2 + CO$)–i.e., at ER = 1.6, rising SF from 0.4 to 0.8 increases the H_2 production from 26.3 to 36.5%, which corresponds to an increase of 38.8%, whereas at ER = 5.5 the same increase in SF (0.4–0.8) increases the production of H_2 by 36.2% (from 28.7 and 39.1%). This suggests that the effect of SF on the H_2 is almost linear for the ranges of the ER ($1.6 \leq ER \leq 5.6$) and SF ($0.4 \leq SF \leq 0.6$) studied.

Figure 5 shows the effect of the ER and SF ratios on the CO production. The trend of the curves is to decrease with increased both ER and SF. Increased SF implies more steam free downstream the combustion zone, which favors the shift reaction ($CO + H_2O \rightarrow H_2 + CO_2$) that consumes more of the CO produced by the carbon steam reforming reaction ($CO + H_2O \rightarrow H_2 + CO_2$) in the combustion zone. At constant SF, increasing ER leads to a combustion zone poor in oxygen concentration, with partial oxidation of carbon (C) producing CO since the combustion of char is almost diffusion-controlled (Hernández et al., 2012). At much higher ER, the gasification process tends to be near to pyrolysis, in which more of the species produced are due to the volatilization of volatile matter contained in biomass. Also, increased ER decreases the temperature peak in the combustion zone where the oxidation of carbon occurs, which disfavors the reaction $C_2 + O_2 \rightarrow 2CO$, since it is more important at T > 800°C than that of the carbon ($C + O_2 \rightarrow CO_2$) to produce CO_2.

Figure 6 illustrates that an oxidizer source richer in H_2O (increased SF) and poorer in O_2 (decreased ER) produces syngas with higher CO_2 content. More H_2O supplied to the gasifier implies a combustion zone with a high H_2O concentration, which favors the carbon reforming reaction ($C + H_2O \rightarrow H_2 + CO$) that produces CO and H_2. Also, environments richer in both H_2O and CO favor the shift reaction ($CO + H_2O \rightarrow H_2 + CO_2$), which consumes CO to produce CO_2 downstream the combustion zone.

In general, from results presented in **Figures 5**, **6**, it is apparent that under the parametric experimental conditions in which the research was developed the shift reaction ($CO + H_2O \rightarrow H_2 + CO_2$) was more important than the Boudouard reaction ($C + CO_2 \rightarrow 2CO$). Shift and Boudouard reactions are competitive for CO and CO_2 productions. Also, Boudouard reaction is dominant at extremely high temperatures or when the O_2 concentration is very low (Hernández et al., 2012).

Methane production is shown in **Figure 7** for different ER and SF ratios. In general, the production of CH_4 was below 5%. Increasing both ER and SF enhances the production of H_2 (**Figure 4**) and hence the production of CH_4 through the reaction ($C + 2H_2 \rightarrow CH_4$), occurring in the reduction zone, which is important at extremely high temperature or at high H_2 concentration.

HHV of Syngas

The Syngas High Heating Values (HHV_{syngas}) or energy density of syngas was calculated using Equation (5).

$$HHV_{syngas} = \sum_{i=1}^{j} X_i \cdot HHV_i \quad (5)$$

where, X_i and HHV_i are the molar fraction and high heating value of each gas fuel, contained in syngas, respectively. HHV_{syngas} is the high heating value (kJ/ SATP m^3 of dry syngas). **Table 4** presents the syngas energy density in a dry base for the operating parameters (ER and SF) used during the experimentation. At constant SF, the energy density of the syngas increases with increased ER until ER = 2.5, where it starts to decrease as the ER increases. On the other hand, at constant ER the increase in SF always increases the syngas energy density. As SF increases, the production of CH_4 and H_2 increases although the production of CO decreases. The syngas energy density is strongly affected by the production of CH_4 which is a gas that has the highest HHV as compared to other species in the syngas produced—i.e., the CH_4 energy density is 36,264 kJ/SATP m^3 while those of the CO and H_2 are 12,048 and 12,123 kJ/SATP m^3, respectively. The syngas HHV (HHV_{syngas}) was 7,625–8,841 kJ/SATP m^3, which corresponds to 21.0 and 24.4% of the methane-HHV.

Energy Recovery

Although HHV_{syngas} gives information on the energy density of the syngas produced, it does not provide information about the energy recovered per biomass unit gasified. Cold gas efficiency (CGE) or energy recovery typically is a parameter used to estimate the energy recovered in syngas (room conditions) per unit of biomass gasified. The recovery energy fraction in the syngas is calculated using Equation (6), the remaining energy is in char, tar, and syngas sensible heat.

$$CGE_{net} = \frac{\dot{\forall}_{syngas} \cdot HHV_{syngas}}{\dot{m}_{biomass} \cdot HHV_{biomass} + \dot{m}_{steam} \cdot \triangle h_{water-steam} + \dot{\forall}_{oxygen} \cdot EV_{oxygen}} \quad (6)$$

Where, CGE_{net} is the net Cold Gas Efficiency or energy recovery, $\dot{\forall}_{syngas}$ (m^3/h) is the syngas flow, HHV_{syngas} (kJ/m^3) is syngas density on a dry basis, $\dot{m}_{biomass}$ (kg/h) is the mass of CH gasified per hour, $HHV_{biomass}$ (kJ/kg) is the Higher Heating Value of DAF-CH, $\dot{m}_{steam}$ (kg/h) is the mass rate of steam supplied to the gasifier, $\triangle h_{water-steam}$ is the difference of specific enthalpy (kJ/kg) between steam (0.76 bar, 92°C) and water (0.76 bar, 20°C), $\dot{\forall}_{oxygen}$ is the supplied flow of oxygen (m^3/h) entering into the gasifier, and EV_{oxygen} is the energetic value of oxygen (1,129 kJ/m^3) (Cerone et al., 2016).

Figure 8 presents the CGE_{net} at constant SF, the CGE_{net} always decreases as ER values increase. Increased ER increases the production of char due to lower oxygen available in the

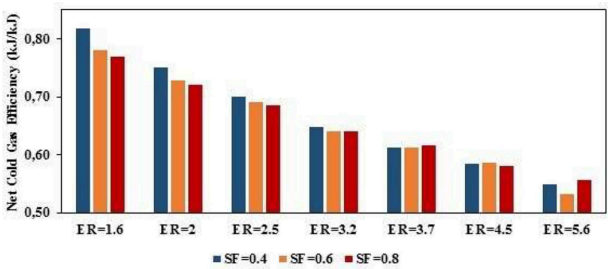

FIGURE 8 | Net cold gas efficiency for several ER and SF values.

TABLE 5 | Model summarize.

Fuel gas	R	R^2	Adjusted R^2	Standard error of the estimate	Durbin-Watson
CO	0.990	0.981	0.979	0.41937	1.363
H_2	0.998	0.996	0.995	0.30434	0.700

TABLE 4 | HHV of syngas [kJ/SATP m^3].

SF	ER						
	1.6	2.0	2.5	3.2	3.7	4.5	5.6
0.4	7,714	7,753	7,793	7,790	7,726	7,735	7,625
0.6	8,074	8,204	8,309	8,296	8,283	8,269	7,980
0.8	8,568	8,733	8,837	8,841	8,832	8,703	8,681

combustion zone for the combustion of char—i.e., when the ER tends to zero the gasification process tends to be pure pyrolysis, in which the syngas produced corresponds to the volatile matter content in biomass. At ER $\geq$ 3.2, the effect of the SF ratio on energy recovery is to increase. In general, increased SF tends to produce syngas with higher HHV due to more production of both CH_4 and H_2. Increased SF implies more H_2O in the combustion zone, which favors the char steam reforming reaction and hence more char consumed to produce H_2 and CO and lower char in gasifier plenum. The energy recovery ranged between 53 and 82%.

Multiple Linear Model for CO and H_2 Concentration

Since the behavior of CO and H_2 concentration as a function of ER is near to that of a straight line for several SF values, the hypothesis of a linear function of CO concentration which depends on ER and SF was evaluated in the current study. Thus, a statistic model under multiple linear regression conditions was performed in the software IBM® SPSS® STATISTICS 24 where the results that confirm the viability of the model are shown in **Table 5**.

According to the correlation coefficient (R) and the coefficient of determination (R^2), the data points have an adequate dispersion, but an adjusted coefficient of determination allows knowing the dispersion based on all of the independent variables (ER and SF) and not only based on one of them. On the other hand, the standard error of the estimate calculated means that the data has excellent accuracy, and Durbin-Watson number indicates that there is a positive autocorrelation for the analysis of regression [0; 2]. Further, the CO and H_2 concentration in dry basis equations were calculated as functions of ER and SF as shown in Equations (7) and (8). **Figure 9** shows the trend for H_2:

$$\boldsymbol{CO} = -8.071\,\boldsymbol{SF} - 1.847\boldsymbol{ER} + 34.369 \quad (7)$$

$$\boldsymbol{H_2} = 26.036\,\boldsymbol{SF} + 0.564\,\boldsymbol{ER} + 15.074 \quad (8)$$

Oxygen-Steam Blends vs. Air-Steam

This section compares the results of this study to others carried out by the authors, using steam-air mixtures as an oxidizer and the same biomass (Bonilla and Gordillo, 2017). The use of oxygen–mixtures as gasifying agent enhances the temperature along the gasifier, and hence the mole fractions of CO and H_2 in the syngas yield as compared to the use of steam-air—i.e., at SF = 0.4 and ER = 3.2, the CO and H_2 dry basis concentrations were 25 and 27.5%, respectively, for oxygen-steam, whereas these for gasification with air-steam were 12.4 and 12.4%, respectively. More oxygen supplied implies more heat released by higher

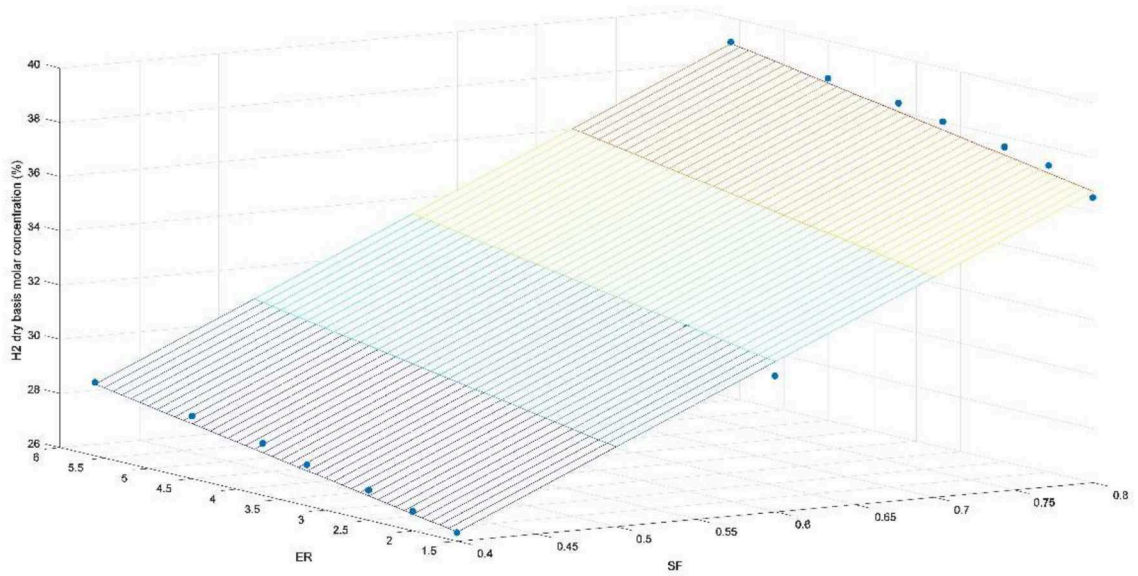

FIGURE 9 | Fitted plane as a function of ER and SF for dry H_2 concentration.

TABLE 6 | TEIR is the energy recovery ratio between oxygen-steam and air-steam gasification.

SF	ER						
	1.6	**2.0**	**2.5**	**3.2**	**3.7**	**4.5**	**5.6**
0.4	4.61	4.44	4.42	4.65	4.41	5.40	6.53
0.6	3.88	3.88	3.47	3.59	3.67	4.17	4.69
0.8	2.57	2.62	2.77	2.72	2.72	3.03	3.58

char oxidation (more production of CO_2). Also, when the air is supplied as oxidizer, a fraction of the heat released by the oxidation of char is consumed as sensible heat of the N_2. Also, using oxygen instead of air increases both the HHV and CGE_{NET}, respectively i.e., at SF = 0.6 and ER = 3.7, the HHV and CGE_{NET} were 8,283 kJ/SATP m^3 and 0.61 by using oxygen, whereas the HHV and CGE_{NET} were 4,391 kJ/SATP m^3 and 0.32, respectively, for air-steam gasification. In general, the comparison of results shows that the use of oxygen instead of air improves syngas quality. **Table 6** shows a ratio, defined by Equation (9), that gives information about the total energy recovered in the syngas produced for each mass unit of CH gasified, using oxygen-steam and air-steam gasification.

$$TEIR = \frac{\left[HHV_{syngas} \cdot CGE_{net}\right]_{Oxy}}{\left[HHV_{syngas} \cdot CGE_{net}\right]_{Air}} \quad (9)$$

Where, TEIR is the Total Energy Improvement Ratio, HHV_{syngas} is the syngas Higher Heating Value and CGE_{net} is the net Cold Gas Efficiency.

CONCLUSIONS

Results show that increased ER and SF ratios tend to decrease both the temperature in the combustion zone and the CO contained in syngas, whereas the H_2 content in syngas increases as ER and SF increase. On the other hand, increased SF and decreased ER increase the production of CO_2. The methane production was lower than 5% and increased as both ER and SF ratios increased. At constant ER, the HHV of syngas increases as when SF ratio is increased. The effect of the ER on HHV is to increase until ER = 3.2, while at ER > 3.2 increasing ER tends to decrease HHV. At constant SF, the CGE_{net} always decreases as ER increases. The comparison between oxygen-steam and air-steam gasification of CH shows that under the same operating conditions, the gasification with oxygen-steam increases the temperature along the gasifier, the HHV of the syngas, and the energy recovery. Additionally, the maximum cold energy recovery was 82% for oxygen-steam and 62% for air-steam gasification.

DATA AVAILABILITY STATEMENT

All datasets generated for this study are included in the article/**Supplementary Material**.

AUTHOR CONTRIBUTIONS

JB conceived and designed the analysis, collected the data, contributed data, performed the analysis, and wrote the paper. GG conceived and designed the analysis, collected the data, performed the analysis, and wrote the paper. CC collected the data, contributed data, and performed the analysis.

ACKNOWLEDGMENTS

The financial support from the internal financing grants of the Universidad de Los Andes is gratefully acknowledged.

SUPPLEMENTARY MATERIAL

The Supplementary Material for this article can be found online at: https://www.frontiersin.org/articles/10.3389/fenrg.2019.00127/full#supplementary-material

REFERENCES

Abbasi, T., and Abbasi, S. A. (2010). Biomass energy and the environmental impacts associated with its production and utilization. *Renew. Sustain. Energy Rev.* 14, 919–937. doi: 10.1016/j.rser.2009.11.006

Aslan, A. (2016). The causal relationship between biomass energy use and economic growth in the United States. *Renew. Sustain. Energy Rev.* 57, 362–366. doi: 10.1016/j.rser.2015.12.109

Bilgili, F., Koçak, E., Bulut, Ü., and Kuşkaya, S. (2017). Can biomass energy be an efficient policy tool for sustainable development? *Renew. Sustain. Energy Rev.* 71, 830–845. doi: 10.1016/j.rser.2016.12.109

Bonilla, J., and Gordillo, G. (2017). Adiabatic fixed-bed gasification of colombian coffee husk using air-steam blends for partial oxidation. *J. Combust.* 2017, 1–26. doi: 10.1155/2017/3576509

Cerone, N., Zimbardi, F., Villone, A., Strjiugas, N., and Kiyikci, E. G. (2016). Gasification of wood and torrefied wood with air, oxygen, and steam in a fixed-bed pilot plant. *Energy Fuels* 30, 4034–4043. doi: 10.1021/acs.energyfuels.6b00126

Chen, X. (2016). Economic potential of biomass supply from crop residues in China. *Appl. Energy.* 166, 141–149. doi: 10.1016/j.apenergy.2016.01.034

Cutz, L., Haro, P., Santana, D., and Johnsson, F. (2016). Assessment of biomass energy sources and technologies: the case of Central America. *Renew. Sustain. Energy Rev.* 58, 1411–1431. doi: 10.1016/j.rser.2015.12.322

Gírio, F. M., Fonseca, C., Carvalheiro, F., Duarte, L. C., Marques, S., and Bogel-Łukasik, R. (2010). Hemicelluloses for fuel ethanol: a review. *Bioresour. Technol.* 101, 4775–4800. doi: 10.1016/j.biortech.2010.01.088

Gordillo, G., and Annamalai, K. (2010). Adiabatic fixed bed gasification of dairy biomass with air and steam. *Fuel* 89, 384–391. doi: 10.1016/j.fuel.2009.07.018

Gordillo, G., and Rodriguez, C. (2011). Adiabatic gasification and pyrolysis of coffee husk using air-steam for partial oxidation. *J. Combust.* 2011:303168. doi: 10.1155/2011/303168

Hernández, J. J., Aranda, G., Barba, J., and Mendoza, J. M. (2012). Effect of steam content in the air-steam flow on biomass entrained flow gasification. *Fuel Process. Technol.* 99, 43–55. doi: 10.1016/j.fuproc.2012.01.030

Hernandez, J. J., Lapuerta, M., and Monedero, E. (2016). Characterisation of residual char from biomass gasification: effect of the gasifier operating conditions. *J. Clean. Prod.* 138, 83–93. doi: 10.1016/j.jclepro.2016.05.120

Hussein, M. S., Burra, K. G., Amano, R. S., and Gupta, A. K. (2017). Effect of oxygen addition in steam gasification of chicken manure. *Fuel* 189, 428–435. doi: 10.1016/j.fuel.2016.11.005

International Energy Agency (2016). *Colombia: Balances for 2010.*

Joselin Herbert, G. M., and Unni Krishnan, A. (2016). Quantifying environmental performance of biomass energy. *Renew. Sustain. Energy Rev.* 59, 292–308. doi: 10.1016/j.rser.2015.12.254

Kirsanovs, V., Blumberga, D., Karklina, K., Veidenbergs, I., Rochas, C., Vigants, E., et al. (2017). Biomass gasification for district heating. *Energy Procedia.* 113, 217–223. doi: 10.1016/j.egypro.2017.04.057

Kurkela, E., Kurkela, M., and Hiltunen, I. (2016). Steam-oxygen gasification of forest residues and bark followed by hot gas filtration and catalytic reforming of tars: results of an extended time test. *Fuel Process. Technol.* 141, 148–158. doi: 10.1016/j.fuproc.2015.06.005

Lenis, Y. A., Pérez, J. F., and Melgar, A. (2016). Fixed bed gasification of Jacaranda Copaia wood: effect of packing factor and oxygen enriched air. *Ind. Crops Prod.* 84, 166–175. doi: 10.1016/j.indcrop.2016.01.053

Li, H., Zhang, X., Liu, L., Wang, S., and Zhang, G. (2017). Proposal and research on a combined heating and power system integrating biomass partial gasification with ground source heat pump. *Energy Convers. Manag.* 145, 158–168. doi: 10.1016/j.enconman.2017.04.090

Liu, L., Huang, Y., Cao, J., Liu, C., Dong, L., Xu, L., et al. (2018). Experimental study of biomass gasification with oxygen-enriched air in fluidized bed gasifier. *Sci. Tot. Environ.* 626, 423–433. doi: 10.1016/j.scitotenv.2018.01.016

Pacioni, T. R., Soares, D., Di Domenico, M., Rosa, M. F. R., de Muniz Moreira, F. P., and José, H. J. (2016). Bio-syngas production from agro-industrial biomass residues by steam gasification. *Waste Manag.* 58, 221–229. doi: 10.1016/j.wasman.2016.08.021

Plis, P., and Wilk, R. K. (2011). Theoretical and experimental investigation of biomass gasification process in a fixed bed gasifier. *Energy* 36, 3838–3845. doi: 10.1016/j.energy.2010.08.039

Sandeep, K., and Dasappa, S. (2014). First and second law thermodynamic analysis of air and oxy-steam biomass gasification. *Int. Hydrogen Energy J.* 39, 19474–19484. doi: 10.1016/j.ijhydene.2014.09.134

Sansaniwal, S. K., Pal, K., Rosen, M. A., and Tyagi, S. K. (2017a). Recent advances in the development of biomass gasification technology: a comprehensive review. *Renew. Sustain. Energy Rev.* 72, 363–384. doi: 10.1016/j.rser.2017.01.038

Sansaniwal, S. K., Rosen, M. A., and Tyagi, S. K. (2017b). Global challenges in the sustainable development of biomass gasification: an overview. *Renew. Sustain. Energy Rev*. 80, 23–43. doi: 10.1016/j.rser.2017.05.215

Tanczuk, M., Junga, R., Werle, S., Chabinski, M., and Ziólkowski. (2017). Experimental analysis of the fixed bed gasification process of the mixtures of the chicken manure with biomass. *Renew. Energy* 136, 1055–1063. doi: 10.1016/j.renene.2017.05.074

Toklu, E. (2017). Biomass energy potential and utilization in Turkey. *Renew. Energy*. 107, 235–244. doi: 10.1016/j.renene.2017.02.008

Van Huynh, C., and Kong, S. C. (2013). Performance characteristics of a pilot-scale biomass gasifier using oxygen-enriched air and steam. *Fuel* 103, 987–996. doi: 10.1016/j.fuel.2012.09.033

Wilson, L., John, G. R., Mhilu, C. F., Yang, W., and Blasiak, W. (2010). Coffee husks gasification using high temperature air/steam agent. *Fuel Process. Technol.* 91, 1330–1337. doi: 10.1016/j.fuproc.2010.05.003

Xiao, Y., Xu, S., Tursun, Y., Wang, C., and Wang, G. (2017). Catalytic steam gasification of lignite for hydrogen-rich gas production in a decoupled triple bed reaction system. *Fuel* 189, 57–65. doi: 10.1016/j.fuel.2016.10.078

Yang, Y., Brammer, J. G., Mahmood, A. S. N., and Hornung, A. (2014). Intermediate pyrolysis of biomass energy pellets for producing sustainable liquid, gaseous and solid fuels. *Bioresour. Technol.* 169, 794–799. doi: 10.1016/j.biortech.2014.07.044

Zhang, Z., and Pang, S. (2017). Experimental investigation of biomass devolatilization in steam gasification in a dual fluidised bed gasifier. *Fuel* 188, 628–635. doi: 10.1016/j.fuel.2016.10.074

Conflict of Interest: The authors declare that the research was conducted in the absence of any commercial or financial relationships that could be construed as a potential conflict of interest.

frontiers in Energy Research

ORIGINAL RESEARCH
published: 25 February 2020
doi: 10.3389/fenrg.2020.00024

The Method for Static Composting Treatment of the Landscaping Waste

Liwei An [1,2]*

[1] College of Agriculture, Inner Mongolia University for Nationalities, Tongliao, China, [2] Institute of Ecological Civilization and Green Development, Inner Mongolia University for Nationalities, Tongliao, China

In order to speed up the process of landscape garbage composting and reduce environmental pollution, the static composting method of landscape garbage was studied in depth. The spring landscape garbage in Beijing Xiangshan Park was used as the main raw material, and an appropriate amount of dried chicken manure was added for high-temperature composting experiments. Furfural residue was added to landscape waste compost, and the dynamic changes of compost quality, total nitrogen, carbon-nitrogen ratio, and plant inhibitors were studied. Through orthogonal experiments, chicken manure was used as a C/N regulator, and bacteria and wood vinegar were used as additives. The total volume of each treatment, changes in pH and EC values, and seed germination index were analyzed and compared. The results show that this method reduces the bulk density of 39 mg/kg, increases the total porosity by 11.6%, and increases the water holding porosity by 7.74%, which can significantly increase the N, P, and K content of landscape waste compost products and reduce the product. The bulk density of the fertilizer has increased the total porosity and water holding porosity of the fertilizer, and the quality of the fertilizer has been significantly improved.

Keywords: landscaping, waste, static, composting, treatment effect

OPEN ACCESS

Edited by:
Su Shiung Lam,
University of Malaysia Terengganu, Malaysia

Reviewed by:
Mukesh Kumar Awasthi,
Northwest A&F University, China
Muhammad Aqeel Ashraf,
China University of Geosciences Wuhan, China
Dangquan Zhang,
Henan Agricultural University, China

***Correspondence:**
Liwei An
imaualw@126.com

Specialty section:
This article was submitted to Bioenergy and Biofuels, a section of the journal Frontiers in Energy Research

Received: *11 December 2019*
Accepted: *07 February 2020*
Published: *25 February 2020*

Citation:
An L (2020) The Method for Static Composting Treatment of the Landscaping Waste. Front. Energy Res. 8:24. doi: 10.3389/fenrg.2020.00024

INTRODUCTION

In recent years, with the rapid development of landscape industry in China, the city's green level and overall green volume are also constantly improving, followed by the rapid increase in the number of the landscape waste, which has become one of the main sources of urban solid waste (Antonio, 2016). How to deal with and utilize the huge amount of the landscape waste has become one of the problems to be solved in the research of urban ecological environment in China (Zhang et al., 2016). The landscape waste refers to the green trimmings, fallen leaves, dead branches, and grass scraps produced in urban greening maintenance, as well as the by-products produced in the operation of other industries (i.e., wood waste). If the treatment measures are improper, it will not only affect the beauty of urban human settlements, but also pollute the air, soil and groundwater, and cause permanent harm to the environment (Wu et al., 2016).

The traditional way of treating the landscape waste in China is landfill or incineration. Although the number of the landscape waste can be reduced, the two non environmental treatment methods cause serious air pollution and resource waste. On the one hand, the landfilling of the landscape waste will lead to a large number of land resources being occupied (Yang et al., 2016). At present, the amount of the landscape waste in China is increasing gradually. If it cannot be dealt with and utilized timely and effectively, the problem of its occupation of agricultural land will become more

and more serious (Shahid et al., 2016). At the same time, the burning of the landscape waste will produce a large number of greenhouse gases and toxic gases such as dioxin and hydrogen sulfide, which will cause serious air pollution (Yang, 2016). On the other hand, excessive removal of the landscape waste will also cause the interruption of soil nutrient cycle, the decrease of organic matter content in the soil and the damage of soil acid-base environment. Finally, it leads to many problems such as soil surface hardening, salinization or sand dust (Svetlana et al., 2016). In fact, from the perspective of resource science, the landscape waste is not only a waste but also a resource, and it is a growing organic resource in the world. The landscape waste contains a certain amount of beneficial nutrients, a large number of lignin, cellulose, hemicellulose, and some organic substances. In the future, it will become an inevitable trend for social development to reuse it as a raw material that can participate in production (Qiao, 2016). Chen et al. (2018) found that the composting of landscape waste can not only reduce the landfill area and the propagation of pathogens, but also return it to the soil, which can increase the soil nutrient content. Improve the physical properties of soil and reduce the occurrence of urban dust, soil invasion, and surface runoff. At the same time, it also greatly reduces the maintenance cost of urban green space and drives the rapid development of circular economy. More importantly, compost product is a kind of substance similar to humus, which can be used as soil improver, organic fertilizer, and peat alternative matrix with remarkable effect. Therefore, the composting treatment of the landscape waste is the best environmental protection technology, which is also conducive to the development of environment and economy (Gao and Li, 2016).

Therefore, the recycling of the landscape waste is of strategic significance for the coordinated development of society, economy, and environment (Swarnam et al., 2016). The growth trend of the amount of the landscape waste in foreign countries is basically consistent with that in China, which is increasing with the rapid development of urban greening. For example, according to the data, EC countries produce about 2.5 billion tons of waste every year. Among them, the number of the landscape water accounts for more than half (Jin and Gao, 2016). Therefore, many foreign scholars have done a lot of research on the processing and reuse of the landscape waste. Vergara and Tchobanoglous (2012) has established a model of the cost of urban solid waste collection in the United States, and reduced the cost of collection to promote the recycling of the landscape waste; According to the situation of urban organic waste collection, according to the collection time, line and artificial needs, Everett and Shahi designed the method of street collection of the landscape waste (Wei et al., 2017). For the research on the resource-based processing of the landscape water, compared with foreign countries, it is still in the exploratory stage, and has not formed a series of related theoretical and technical support (Lin et al., 2016).

Landscape waste recycling has become an important way to achieve sustainable development of organic waste. It can make full and reasonable use of the garden ecosystem, reduce the negative impact of landscaping activities on the nature and the urban environment, and provide a new model for the development of circular economy in the garden industry. Therefore, a static combined treatment method for landscape waste is proposed, which provides theoretical and technical support for the static combined treatment of landscape pollutants.

TABLE 1 | Basic physical and chemical properties of composting materials.

Material	Green waste	Chicken manure	Furfural residue
Water content/%	20.11 ± 0.83	15.32 ± 0.36	36.06 ± 0.56
pH	5.790 ± 0.15	7.020 ± 0.31	2.840 ± 0.18
Total nitrogen/%	0.730 ± 0.09	4.390 ± 0.17	0.89 ± 0.02
C/N ratio	43.10 ± 0.66	7.570 ± 0.24	32.30 ± 0.65
Bulk density/kg/m^3	171.0 ± 0.99	861.0 ± 10.07	351.0 ± 3.60

TABLE 2 | Experiment design of garden waste composting.

Handle	1	2	3
Material	Landscaping waste	Landscaping waste + chicken manure	Landscaping waste + chicken manure + furfural residue
C/N ratio	43.1 ± 0.59	25.1 ± 0.35	28.1 ± 0.29

MATERIALS AND METHODS

Test Time and Place

The field experiment was conducted in Beijing Xiangshan Park in May 2019, and the indoor experiment was conducted in the laboratory of soil science of Beijing Forestry University in August 2019 (Hanc et al., 2016).

Test Materials

Effect of Furfural Residue on the Composting of the Landscaping Waste

The landscape waste used in this experiment is the spring garden waste of Beijing Xiangshan Park, mainly the pruned branches and leaves of poplar and willow (Touceda-González et al., 2016). Furfural residue is provided by a furfural factory in Siping City, Jilin Province. Rinse with water before use to remove particles and water soluble substances attached to the surface of furfural residue, and dilute its own acidity. Then, air dry and standby under natural conditions (Bolocan et al., 2016). Chicken manure is obtained from dry chicken manure produced by a company in Shijiazhuang. The basic physical and chemical properties of each compost raw material are shown in **Table 1**.

There are three composting treatments, namely pure garden waste compost, garden waste compost with chicken manure, garden waste compost with furfural residue and chicken manure. The C/N ratio of each treatment in the early stage is shown in **Table 2**.

Before composting, adjust the moisture content to 55–60%, and pile into a pile with the height of about 1.5 m. The ventilation is carried out by means of manual turning over, from the beginning of composting to the end of high

TABLE 3 | Basic physicochemical properties of main composting materials.

Raw material	Landscaping waste	Chicken manure
Total nitrogen (%)	0.81	1.11
Total organic carbon (%)	46.10	9.51
C/N	57.51	8.61
Water content (%)	10.10	2.21

TABLE 4 | Orthogonal experimental design L_9 (3^4).

Treatment	Factor			
	Microbe fungus	Wood vinegar	Microbe fungus × Wood vinegar	C/N
C/N21 + W/951	1 (0)	1 (951 times dilution)	1.1	1 (21)
C/N31 + W/501	1 (0)	2 (501 times dilution)	2.1	2 (31)
C/N41 + W/51	1 (0)	3 (51 times dilution)	3.1	3 (41)
C/N41 + 0.3%M + W/951	2 (0.3%)	1 (951 times dilution)	2.1	3 (41)
C/N21 + 0.3%M + W/501	2 (0.3%)	2 (501 times dilution)	3.1	1 (21)
C/N31 + 0.3%M + W/51	2 (0.3%)	3 (51 times dilution)	1.1	2 (31)
C/N31 + 0.5%M + W/951	3 (0.5%)	1 (951 times dilution)	3.1	2 (31)
C/N41 + 0.5%M + W/501	3 (0.5%)	2 (501 times dilution)	1.1	3 (41)
C/N21 + 0.5%M + W/51	3 (0.5%)	3 (51 times dilution)	2.1	1 (21)

temperature, turning over once every 2 days; after the high temperature period, turning over once every 5 days until the compost is mature. During composting, samples were taken at 0, 3.1, 5.1, 10.1, 15.1, 20.1, 25.1, 30.1, 35.1, and 40.1 d respectively, and relevant indexes were determined. It includes pH value, total nitrogen, alkali hydrolyzed nitrogen, available phosphorus, available potassium, bulk density, total porosity and water holding porosity (Zhu et al., 2016).

The Effect of C/N, Adding Bacteria and Wood Sorrel on the Landscape Waste Composting

The dead branches and dead leaves of plants pruned in autumn in Beijing Xiangshan Park were used as the main raw materials and chicken manure as the conditioner. The basic physical and chemical properties of the main composting materials are shown in **Table 3**.

The used fungicide is Sufubao organic material maturity fungicide, which is a kind of high-efficiency compound microbial fungicide, mainly composed of protein, fat, cellulose, chitin, etc. It has strong decomposition ability and fast decomposition speed, and is suitable for fast composting of a variety of different substrates (Ling et al., 2018). The wood vinegar used is the light yellow to reddish brown condensate produced by wood pyrolysis in the process of burning charcoal. It has the special smoky smell and is acidic.

The orthogonal design $L_9\left(3^4\right)$ of the interaction of C/N, fungus and wood vinegar (dilution ratio 3) is adopted, and the details are shown in **Table 4**.

According to the test design requirements, adjust the C/N according to the weight ratio of the landscape waste and chicken manure, add the bacterial agent and mix well. Then add 951, 501, and 51 times of wood sorrel with equal volume dilution, spray and stir at the same time, so that the moisture content of the pile is about 65%. This can not only meet the water content requirements, but also help to mix the wood vinegar evenly and save labor. Finally, the piles with length of 2 m, width of 1.5 m and height of 1 m were made, respectively.

Data Processing Method

SPSS software was used for variance analysis and multiple comparisons of test data (LSD method); Microsoft Office Excel 2003 was used for data processing and chart drawing (Li et al., 2018).

RESULTS

Effect of Furfural Residue on the Composting of the Landscape Waste

Effect of Furfural Residue on the Quality of the Landscape Waste Compost

The quality character of compost product is an important index to restrict whether compost can be used in agriculture or not, and it is also an important decisive factor to influence whether the municipal solid waste can realize its "resource." It can be seen from **Table 5** that adding chicken manure and furfural residue can significantly improve the quality of compost products. The content of basic n, available P and available K in the compost of treatment 3 with furfural residue was significantly higher than that of treatment 2 with pure chicken manure. Compared with treatment 1, treatment 2 increased 14.9% of basic n, 45.4% of available P and 18.0% of available K. Compared with treatment 2, treatment 3 increased basic n by 20.5%, available P by 25.2%, and available K by 33.3%. The effect of furfural residue on the quality of the landscape waste compost is shown in **Table 5**.

TABLE 5 | Quality characteristics of compost products from landscaping wastes.

Handle	1	2	3
Hydrolyzable nitrogen/(mg/kg)	58.18	66.84	80.52
Available phosphorus/(mg/kg)	6.04	8.78	10.99
Available potassium/(mg/kg)	128.22	151.30	201.64
Bulk density/(mg/kg)	139	122	83
Total porosity/%	48.2	55.68	67.28
Water holding porosity/%	24.19	27.74	35.48

Different capitals and lowercase letters in the same column indicate significant and extremely significant differences in LSR test at the level of 0.05 and 0.01 respectively.

Compared with Treatment 1, Treatment 2 reduced the bulk density by 17 mg/kg, increased the total porosity by 7.48%,

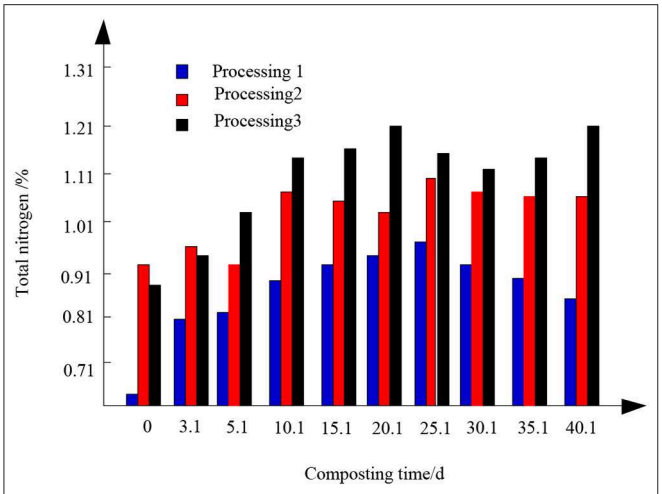

FIGURE 1 | Changes of total nitrogen content in different composting treatments.

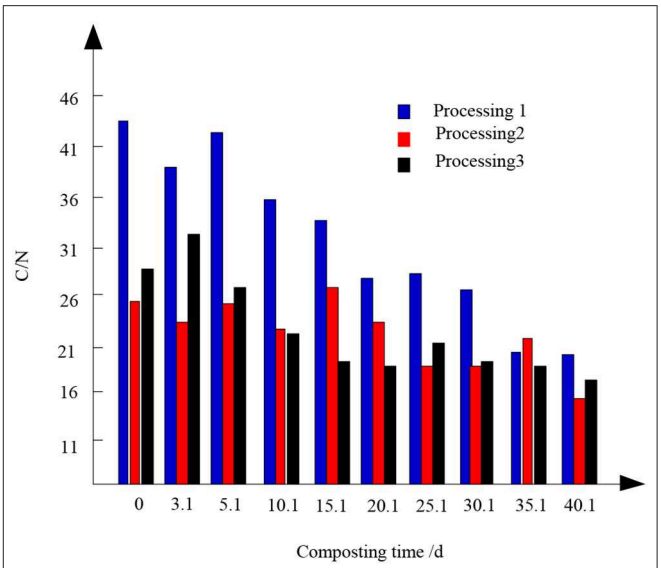

FIGURE 2 | The change of C/N ratio in different composting treatments.

and increased the water holding porosity by 3.55%. Compared with Treatment 2, Treatment 3 reduced the bulk density by 39 mg/kg, total porosity increased by 11.6%, and water holding porosity increased by 7.74%. The addition of chicken manure and furfural residues can effectively reduce the compost density and significantly increase the total porosity and water holding porosity of the compost product.

Effect of Furfural Residue on Total Nitrogen Content in Landscape Waste Compost

If the compost is not treated properly, a lot of nitrogen will be lost. When this kind of compost product is applied to the soil, not only the fertilizer effect is not high, but also it may capture the nitrogen in the soil and destroy the nutrient balance of the soil. The dynamic change of total nitrogen content in this composting process is shown in **Figure 1**.

From the test results, 3.1 days after composting, the total nitrogen content increased rapidly, then decreased and gradually flattened. At 20.1 d, the total nitrogen content of treatment 3 increased to the highest. After composting, the total nitrogen content of each treatment was 0.87, 1.05, and 1.18, respectively. Compared with treatment 1, the total nitrogen content of pure chicken manure treatment 2 increased, while that of furfural residue treatment 3 was higher than that of treatment 2. Furfural residues can significantly increase the total nitrogen content during composting. The total nitrogen content of each treatment in the test showed an overall growth trend.

Effect of Furfural Residue on C/N Ratio in Landscape Waste Composting

Generally speaking, when the C/N ratio of compost is below 21, it is considered that the compost is mature. The effect of furfural residue on the C/N ratio of the landscape waste compost is shown in **Figure 2**.

It can be seen from **Figure 2** that in the whole composting process, the C/N ratio obtained by different treatment methods shows the downward trend, and finally achieves relative stability. In the composting process, although the decline trend of treatment 1 is obvious, at the end of the composting cycle, its C/N ratio is only 21, which does not meet the requirements of composting maturity. The C/N of treatment 2 and treatment 3 decreased from 25 and 28 at the beginning to 17 and 16 at the end of composting, which indicated that the addition of furfural residue had a positive effect on C/N in composting. This is mainly because in the early stage of composting, with the increase of temperature, the microbial activity in the reactor is strong, the decomposition of organic matter in the reactor is intense, and the carbon content decreases faster than the nitrogen loss. Therefore, the overall C/N ratio decreased, while the content of carbon in furfural residue was rich, and the content of organic matter easy to be decomposed by microorganisms was more, so the C/N ratio of treatment 3 with furfural residue decreased significantly compared with other treatments.

Effect of Furfural Residue on Degradation of Plant Inhibitor in the Landscape Waste Compost

The degradation of organic matter in composting will produce many intermediate products. Immature compost is rich in organic acids, polyphenols, and other plant growth inhibitors, which are gradually transformed or disappeared with the composting process. Through the germination index (GI) of plant seeds, the degradation of plant inhibitors can be determined rapidly. Generally speaking, when GI $>$ 0.50, compost is considered to be basically non-toxic, and GI $>$ 0.80, compost is considered to be completely mature. In this experiment, water celery seed is selected as the indicator plant of germination test, and the test results are shown in **Figure 3**.

In the composting, GI increased with time. However, the GI value of compost decreased from 3.1 to 10.1 d, which may be due to the inhibition of NH_4^+ – N and organic acid produced by

microbial degradation of organic matter on water celery seeds. At 20.1 d, the germination indexes of celery seeds treated with different methods were 0.59, 0.73, and 0.81, respectively. The GI value of treatment 2 was higher than that of treatment 1, and that of treatment 3 with furfural residue was higher than that of treatment 2. After composting, the germination indexes of the three treatments were 73, 87, and 90%, respectively. Except treatment 1, the other two treatments have reached the compost maturity standard.

Effect of C/N Regulation and Addition of Bacteria and Wood Sorrel on the Composting of the Landscape Waste

Changes of Bulk Volume, pH, and EC Value Before and After Composting With Different Treatments

With the passage of time, the gap between the piles becomes smaller and smaller, and the volume of the piles gradually decreases. By the end of composting, the volume of compost obtained by C/N41 + 0.5%m + W/501 treatment was the smaller than that of the initial treatment, and the volume change caused by C/N21 + W/951 treatment was the least. The pH value not only affects the decomposition of organic matter, the oxidation-reduction of minerals and the activity intensity of microorganisms, but also directly affects the biochemical reaction speed participated by enzymes. It is one of the important indexes to evaluate the maturity of compost.

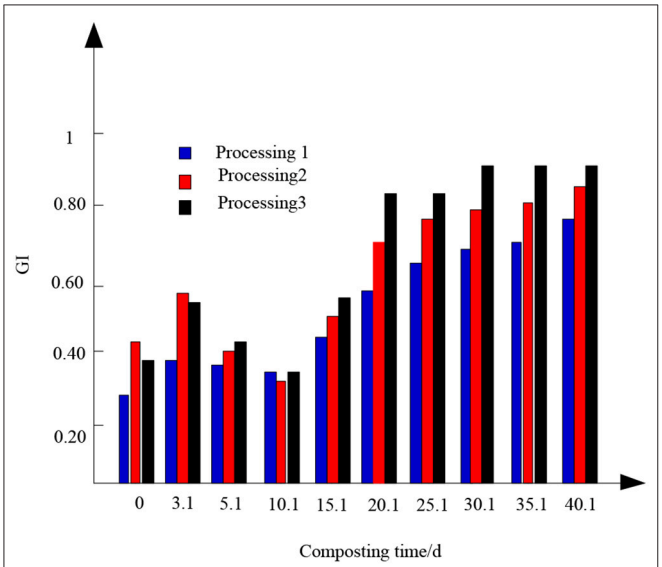

FIGURE 3 | Changes of seed germination index in different composting treatments.

The pH value of each treatment increased from the beginning to the end of composting. The increase of pH value is caused by the decomposition of organic matter and the production of NH_3.

As shown in **Table 6**, the rising range of pH value of compost obtained by each treatment method is different. Before and after composting, the pH value of compost obtained by C/N41 + 0.3% m + W/951 and C/N31 + 0.5% m + W/951 treatments changed the most. This is because the C/N of compost treated by these two methods is higher, enough carbon sources provide necessary nutrients for the growth and reproduction of microorganisms, and the degradation degree of organic matter is higher. However, the addition of exogenous bacteria makes the decomposition of organic matter more intense, and the volatile part of NH_3 fills the compost, which makes the pH of the compost increase continuously.

It can be seen from **Table 6** that the pH of compost can be reduced by adding wood vinegar under certain C/N conditions. This phenomenon may be due to the acidity of wood sorrel. Adding wood sorrel provides a lot of H+ for composting, which reacts with NH_3 to form NH_4^+ dissolved in water, and reduces the pH. It can be seen that the proper C/N regulation and the addition of fungicides are conducive to the increase of compost pH, while wood sorrel can reduce the pH of compost products. The pH value specified in the organic fertilizer standard is 5.5–8.0, and the pH value of each treatment in this compost does not meet the organic fertilizer standard. It can be seen that the use of compost products also needs to add other additives according to the actual situation to reduce pH.

The size of EC is related to the salt content of compost. The EC of compost used as soil conditioner should not be too large, otherwise it will affect the normal growth of crops. From the data analysis in **Table 6**, it is found that the EC Value of the

TABLE 6 | Variations of volume, pH value, and EC value of the composting at the start and the end of different treatments.

Treatment	Volume			PH			EC		
	Start	End	Decrease	Start	End	Increase	Start	End	Increase
C/N21 + W/951	0.57	0.52	8.98	7.3	8.1	11.2	1,153	2,331	103
C/N31 + W/501	0.57	0.35	39.25	6.9	8.6	25.1	1,091	1,537	42
C/N41 + W/51	0.56	0.42	25.98	6.5	7.4	14.2	1,032	1,307	28
C/N41 + 0.3%M + W/951	0.57	0.32	44.88	6.6	8.7	32.4	1,041	1,215	18
C/N21 + 0.3%M + W/501	0.57	0.42	27.86	7.2	8.6	19.8	1,130	1,961	75
C/N31 + 0.3%M + W/51	0.55	0.39	30.27	6.8	8.4	23.8	1,073	1,452	36
C/N31 + 0.5%M + W/951	0.58	0.34	42.51	6.8	8.8	32.9	1,104	1,272	16
C/N41 + 0.5%M + W/501	0.58	0.3	50.01	6.5	8.3	28.2	1,037	1,117	9
C/N21 + 0.5%M + W/51	0.59	0.48	18.53	7.3	7.8	6.8	1,148	2,217	94

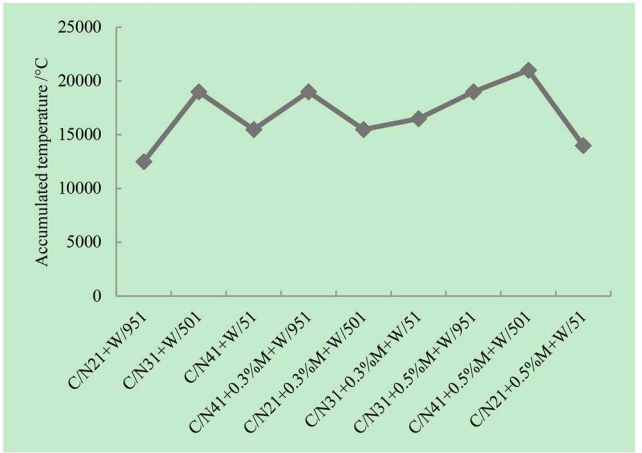

FIGURE 4 | Compost accumulated temperature of different treatments.

finished compost is higher than that of the raw material. The lower the C/N was, the higher the EC value was, and the lower the EC value was. The increase of EC Value of compost products is caused by a large number of ammonium ions and mineral salts produced in the compost and the gradual decrease of the volume of the compost. However, the low EC Value of compost with proper amount of bacteria and wood vinegar is due to the accelerated decomposition of compost materials, the formation of more humus and the reduction of EC value. It can be seen that the regulation of C/N and the addition of bacteria and wood sorrel can prevent the EC Value of compost products from being too high and improve the quality of compost products.

Compost Accumulated Temperature Changes of Different Treatment Methods

It has been shown that the accumulated temperature can be used as an important parameter to consider both temperature intensity and holding time in the composting process, which is related to the composting process and maturity of compost. The compost accumulated temperature of different treatment methods is shown in **Figure 4**.

It can be seen from **Figure 4** that the compost treated by C/N41 + 0.5m + W/501 has the largest accumulated temperature, while the compost treated by C/N21 + W/951 has the smallest accumulated temperature. It can be seen that the higher the C/N ratio is, the higher the composting temperature is, and the addition of proper amount of bacteria and wood sorrel can improve the composting temperature.

From the point of view of temperature change and accumulated temperature, C/N31 + W/501, C/N41 + 0.3% m + W/951, C/N31 + 0.5% m + W/951, C/N41 + 0.5% m + W/501 had the best fermentation effect, and the high temperature retention time and accumulated temperature were longer in the whole fermentation stage. However, the compost treated with C/N41 + W/51 and C/N21 + 0.5% m + W/51 had the lowest accumulated temperature and the shortest duration of high temperature, which may be related to the lack of effective carbon source at low C/N and the lack of effective nitrogen source at high C/N and the inhibition of microbial quantity by adding high concentration of wood vinegar. The addition of proper amount of bacteria and wood sorrel can advance and prolong the high temperature period of compost and shorten the fermentation period of compost. The reason may be that the addition of fungicides increased the total number of microorganisms in the pile layer, while the addition of appropriate amount of wood vinegar provided food for microorganisms. This makes the microorganisms in the compost layer propagate rapidly and maintain at a relatively stable high level, which makes the high temperature period of compost come ahead of time. At the same time, a certain amount of microorganisms can rapidly decompose the organic matter in the compost, so as to accelerate the compost maturity and greatly shorten the composting time.

Germination Index (GI)

Table 7 shows the analysis results of the variance of the orthogonal test.

Table 8 shows the significance test results of differences between different treatments and factor effects.

It can be seen from **Table 7** that there is no significant difference in GI among the treatment repeats, and the interaction among C/N, fungicide, wood sorrel, fungicide and wood sorrel is extremely significant, which shows that the interaction among C/N, fungicide, wood sorrel, fungicide, and wood sorrel is an important factor affecting GI.

It can be seen from **Table 8** that the range of C/N is the largest, which shows that C/N has the greatest influence on GI of compost, and wood vinegar has the smallest influence among the three factors. This is related to the degradation rate of organic matter in compost mainly depends on C/N, rather than the number or species of microorganisms. The comparison between composting treatments and multiple comparison of the effects of various factors (**Table 8**) shows that the treatment effect is the best when the C/N is 31, the effect is the best when the amount of bacteria is 0.4%, and the effect of wood vinegar is the best when the dilution is 501 times. When the C/N is 41 and the wood sorrel is diluted 51 times, the effect is poor, which may be related to the lack of effective nitrogen source to inhibit microbial activity under the condition of high C/N, and the high concentration wood sorrel also has a certain inhibition effect on microbial activity. F test showed that the interaction between 0.5% bacteria and 501 times diluted wood sorrel was the most significant, and the interaction between 0.5% bacteria and 501 times diluted wood sorrel was significantly different from other levels. The interaction value between the added amount of each fungus and the 51 times diluted wood sorrel solution was negative, which indicated that the 51 times diluted wood sorrel solution had a certain inhibition on the effect of fungus.

In this experiment, the GI value of the compost treated by C/N31 + 0.5% m + W/951 method is larger than that of C/N41 + 0.5% m + W/501 treatment, and the difference is significant, which shows that the interaction between 0.4% bacteria and the diluted 501 times wood vinegar is large. However, the effect of C/N on GI was much greater than that of 0.5% fungicide and 501 times diluted wood sorrel. The GI of C/N21 + W/951,

TABLE 7 | Analysis of variance of orthogonal test.

Source of variation	Processing room	Repeating room	Microbial inoculum	Wood vinegar	C/N	C/inoculant × Wood vinegar	Error	Total
df	8.1	2.1	2.1	2.1	2.1	4.1	16.1	26.1
SS	8858.2	78.58	2551.21	2224.86	3629.72	452.46	297.13	9233.93
MS	1107.3	39.28	1275.61	1112.43	1814.87	113.12	18.58	
F	59.64**	2.13	69.68**	59.91**	97.74**	6.08**		
$F_{0.05}$	2.58	3.24				3.02		
$F_{0.01}$	3.88	6.24				4.78		
Range			23.64	21.63	28.25			

***Conspicuousness.*

TABLE 8 | Significance test of difference between different treatments and factor effect.

Treatment	Multiple comparisons between processes		Multiple comparison of various factors					
	GI (%)	Saliency	Level	GI (%)	Saliency	Level	GI (%)	Saliency
C/N21 + W/951	68.78	e D	Microbial inoculum			Wood vinegar		
C/N31 + W/501	98.58	c BC	1.1	79.18	c C	1.1	94.86	b A
C/N41 + W/51	70.23	e D	2.1	93.54	b B	2.1	101.17	a A
C/N41 + 0.3%M + W/951	89.86	d C	3.1	102.83	a A	3.1	79.55	c B
C/N21 + 0.3%M + W/501	94.68	ed C	C/N			Interaction value of fungicide and wood sorrel		
C/N31 + 0.3%M + W/51	96.07	ed BC						
C/N31 + 0.5%M + W/951	125.92	a A	1.1	78.62	c C	M_2W_2	6.29	b B
C/N41 + 0.5%M + W/501	110.23	b AB	2.1	106.86	a A	M_2W_2	−22.14	d D
C/N21 + 0.5%M + W/51	72.35	e D	3.1	90.11	b B	M_3W_2	44.05	a A
						M_3W_3	−8.11	a A

C/N41 + W/51, C/N20 + 0.5% m + W/51 was the smallest and the difference between them was not significant, which did not meet the standard of no toxicity to plants. This shows that too high or too low C/N is not conducive to the improvement of compost maturity, which may be related to the fact that low C/N will make EC too high, too high salt will inhibit the normal germination of seeds, and high C/N will make the compost nutrient content low. The difference of GI value between C/N21 + 0.3% m + W/501 and C/N21 + W/951 and C/N21 + 0.5% m + W/51 treatment was extremely significant, which indicated that the addition of proper amount of bacteria and wood vinegar could effectively improve the maturity of compost. Therefore, the optimal combination of C/N, fungicide and wood sorrel was determined as C/N31 + 0.5% m + W/501, that is, C/N31 + 0.5% fungicide + dilution 501 times wood sorrel.

DISCUSSION

(1) The importance of preprocessing: The degradation resistance of lignocellulose is an important factor limiting the effective transformation of landscape litter. Exploring an effective method for removing lignin from lignocellulose will help shorten the maturation time of landscape waste compost and improve the compost efficiency. Guangzhou Institute of Landscape Architecture has developed three chemical maturation agents: 1,1-cyclohexanediacetic acid (CDA), 4,4′-bis (9-carbazolyl)−2, 2′-dimethylbiphenyl (CDB), and Cinnamyl 3,4-dihydroxy-alpha- cyanocinnamate (CDC) chemistry, combined with the results of SEM, IR, and XRD, we can see that after pretreatment with chemical curing agent, the wall swelled and the wall thickness of lignocellulose increased by more than 25%. Because the chemical bond between lignin and cellulose was partially destroyed, the crystal structure of the lignocellulose crystal region was destroyed, and the relative crystallinity was reduced by more than 2.6%. It can be seen that chemical maturation agents have good application potential in landscape waste composting.

(2) By the end of composting, the volume of compost obtained by C/N41 + 0.5%m + W/501 treatment was the smaller than that of the initial treatment, and the volume change caused by C/N21 + W/951 treatment was the least. When the C/N content of compost is fixed, adding wood sorrel can reduce the pH of compost, which may be due to the acidity of wood sorrel. The addition of wood sorrel provides a large amount of H+ for composting, which reacts with NH3 to form NH+4 dissolved in water, reducing pH. The EC values of the compost products were higher than those of the raw materials, and the lower the C/N was, the higher the EC values were, and the lower the EC values of the compost products were.

(3) The accumulated temperature of compost treated with C/N41 + 0.5m + W/501 method was the largest, and that of compost treated with C/N21 + W/951 method was the smallest. The higher the value of C/N was, the

higher the accumulated temperature of compost was. Adding proper amount of bacteria and wood sorrel can improve the compost temperature.

(4) There was no significant difference in GI among the treatments, and C/N, fungicide, wood sorrel, the interaction of fungicide and wood sorrel was very significant. This shows that they are all important factors affecting GI, and the optimal combination of C/N, fungicide and wood sorrel is C/N31 + 0.5% m + W/501, That is, C/N31 + 0.5% bacterial agent + wood sorrel diluted by 501 times.

CONCLUSIONS

In order to promote the recycling of resources, according to the characteristics of landscape waste, a rapid composting treatment method was studied. The landscape waste in Beijing Xiangshan Park was used as an experimental object to conduct a composting test. The experimental results show that chicken manure and furfural residue can effectively reduce the bulk density of compost, and significantly increase the total porosity and water holding porosity of compost products. Furfural residue can significantly increase the content of total nitrogen in compost. Compared with other treatments, the C/N ratio of furfural residue decreased significantly. After composting, the germination indexes of the three treatments were 73, 87, and 90%, respectively. Except treatment 1, the other two treatments have reached the compost maturity standard. There was no significant difference in GI among the treatments, and C/N, fungicide, wood sorrel, the interaction of fungicide and wood sorrel was very significant. This shows that they are all important factors affecting GI, and the optimal combination of C/N, fungicide and wood sorrel is C/N31 + 0.5% m + W/501, That is, C/N31 + 0.5% bacterial agent + wood sorrel diluted by 501 times.

DATA AVAILABILITY STATEMENT

All datasets generated for this study are included in the article/supplementary files.

AUTHOR CONTRIBUTIONS

LA did the whole work of the research, used the landscape waste in spring as the main raw material to add proper proportion of dry chicken manure for high temperature composting experiment, analyzed and compared the bulk volume, the changes of pH and EC Value, and seed germination index in every treatment, and wrote the manuscript.

REFERENCES

Antonio, P. (2016). Wood products and green chemistry. *Ann. For. Sci.* 73, 185–203. doi: 10.1007/s13595-014-0448-3

Bolocan, A. S., Bolocan, V., O'Connor, P. M., Coffey, A., Nicolau, A. I., and McAuliffe, O. (2016). Inhibition of listeria monocytogenes biofilms by bacteriocin-producing bacteria isolated from mushroom substrate. *J. Appl. Microbiol.* 122, 279–293. doi: 10.1111/jam.13337

Chen, Z., Kim, J., and Jiang, X. (2018). Survival of *Escherichia coli* O157:H7 and *Salmonella enterica* in animal waste-based composts as influenced by compost type, storage condition and inoculum level. *J. Appl. Microbiol.* 124, 1311–1323. doi: 10.1111/jam.13719

Gao, L., and Li, C. (2016). Palmprint recognition based on features weighted and kernel principal component analysis. *J. Jilin Univ.* 54, 1361–1366. doi: 10.13413/j.cnki.jdxblxb.2016.06.31

Hanc, A., Boucek, J., Svehla, P., Dreslova, M., Tlustos, P. (2016). Properties of vermicompost aqueous extracts prepared under different conditions. *Environ. Technol.* 38, 1428–1434. doi: 10.1080/09593330.2016.1231225

Jin, Y., and Gao, Y. (2016). Optimal piecewise real-time pricing strategy for smart grid. *Comp. Simul.* 33, 171–175.

Li, Z., Ji, Q., and Zhao, S. (2018). Changes in C and N fractions with composted manure plus chemical fertilizers applied in apple orchard soil: an *in-situ* field incubation study on the loess plateau, *China. Soil Use Manag.* 34, 276–285. doi: 10.1111/sum.12417

Lin, Z., Bai, J., and Zhen, Z. (2016). Enhancing pentachlorophenol degradation by vermicomposting associated bioremediation. *Ecol. Eng.* 87, 288–294. doi: 10.1016/j.ecoleng.2015.12.004

Ling, L., Xiao, P., and Guo, C. (2018). Adsorption behaviors and mechanisms of heavy metal ions on municipal waste composts with different degree of maturity. *Environ. Technol.* 40, 1–43. doi: 10.1080/09593330.2018.1458908

Qiao, G. (2016). Design and research of landscape platform for mobile devices. *Automat. Instrument.* 10, 168–169. doi: 10.14016/j.cnki.1001-9227.2016.10.168

Shahid, I., Andrey, K., Guber, H., and Zaman, K. (2016). Estimating nitrogen leaching losses after compost application in furrow irrigated soils of Pakistan using HYDRUS-2D software. *Agric. Water Manag.* 168, 85–95. doi: 10.1016/j.agwat.2016.01.019

Svetlana, M., Miloš, S., and Biljana, T. (2016). Biological control of green mould on *Agaricus bisporus* by a native *Bacillus subtilis* strain from mushroom compost. *Eur. J. Plant Pathol.* 148, 1–11. doi: 10.1007/s10658-016-1107-3

Swarnam, T. P., Velmurugan, A., Pandey, S. K., and Dam Roy. S. (2016). Enhancing nutrient recovery and compost maturity of coconut husk by vermicomposting technology. *Bioresour. Technol.* 207, 76–84. doi: 10.1016/j.biortech.2016.01.046

Touceda-González, M., Álvarez-López, V., Prieto-Fernández, Á., Rodríguez-Garrido, B., Trasar-Cepeda, C. and Mench, M. (2016). Aided phytostabilisation reduces metal toxicity, improves soil fertility and enhances microbial activity in Cu-rich mine tailings. *J. Environ. Manage.* 186, 301–313. doi: 10.1016/j.jenvman.2016.09.019

Vergara, S. E., and Tchobanoglous, G. (2012). Municipal solid waste and the environment: a global perspective. *Annu. Rev. Environ. Resour.* 37, 277–309. doi: 10.1146/annurev-environ-050511-122532

Wei, F., Jie, Y., and Panyue, Z. (2017). Solid-state anaerobic fermentation of spent mushroom compost for volatile fatty acids production by ph regulation. *Int. J. Hydrogen Energy* 42, 18295–18300. doi: 10.1016/j.ijhydene.2017.04.148

Wu, Q., Li, G., and Chen, W. (2016). An overview of sustainable green 5G networks. *IEEE Wirel. Commun.* 24, 72–80. doi: 10.1109/MWC.2017.1600343

Yang, B., Zhao, H., Zeng, G., and Zhong, Y. (2016). DC capacitors voltage balancing strategy for cascaded statcom. *J. Power Supply* 14, 128–136. doi: 10.13234/j.issn.2095-2805.2016.5.128

Yang, H. (2016). Communication power supply monitoring system based on TCP/IP protocol. *Chin. J. Power Sources* 40, 1298–1299.

Zhang, P., Qin, Z., and Lu, Z. (2016). An analytical model of space backbone network capacity for space information transmission. *J. China Acad. Electron. Inf. Technol.* 11, 66–72.

Zhu, Y. L., Zheng, G. D., Gao, D., Chen, T. B., Wu, F. K., and Niu, M. J. (2016). Odor composition analysis and odor indicator selection during sewage sludge composting. *J. Air Waste Manage. Assoc.* 66, 930–940. doi: 10.1080/10962247.2016.1188865

Conflict of Interest: The author declares that the research was conducted in the absence of any commercial or financial relationships that could be construed as a potential conflict of interest.

frontiers in Energy Research

ORIGINAL RESEARCH
published: 24 March 2020
doi: 10.3389/fenrg.2020.00038

The Evaluation on Three Types of Malaysian Dolomites as a Primary Catalyst in Gasification Reaction of EFB and Tar Cracking Efficiency

M. A. A. Mohammed[1], *I. Nor Shafizah*[1], *A. Salmiaton*[1,2]*, *W. A. K. G. Wan Azlina*[1,2] *and Y. H. Taufiq-Yap*[3]

[1] Department of Chemical & Environmental Engineering, Faculty of Engineering, Universiti Putra Malaysia, Serdang, Malaysia,
[2] Sustainable Process Engineering Research Centre, Faculty of Engineering, Universiti Putra Malaysia, Serdang, Malaysia,
[3] Department of Chemistry, Faculty of Science, Universiti Putra Malaysia, Serdang, Malaysia

The conversion of biomass into hydrogen-rich syngas has been getting attention recently, as it has potential sustainability benefits of agricultural residues. In this study, gasification of empty fruit bunch (EFB) was performed using various calcined Malaysian dolomite catalysts, which were denoted as P1, P2, and P3. The physicochemical properties of the catalysts were examined using X-ray fluorescence (XRF), X-ray diffraction (XRD), Brunauer–Emmett–Teller (BET), and scanning electron microscopy (SEM). The effect of various catalyst to biomass (C/B) ratios (varied in the range of 0.05–0.3 in an increment of 0.05) of P1, P2, and P3 catalyst in EFB gasification was evaluated at a gasifier temperature of 850°C. The gas produced was analyzed by gas chromatography (GC). The effect of various C/B ratios on tar conversion was also examined. The result showed that, with lower impurities in calcined dolomites and high content of active sites (CaO–MgO), improved characteristics of P1 and P2 in crystalline structure contributes to a significant reduction in tar cracking (~78 and 75%, respectively) and higher H_2 yield (32.25 mg H_2/g EFB).

Keywords: empty fruit bunch, gasification, Malaysian dolomite, hydrogen yield, tar cracking

OPEN ACCESS

Edited by:
Su Shiung Lam,
University of Malaysia Terengganu, Malaysia

Reviewed by:
C. K. Cheng,
Universiti Malaysia Pahang, Malaysia
Muhammad Aziz,
The University of Tokyo, Japan
Jude Onwudili,
Aston University, United Kingdom

***Correspondence:**
A. Salmiaton
mie@upm.edu.my

Specialty section:
This article was submitted to Bioenergy and Biofuels, a section of the journal Frontiers in Energy Research

Received: *19 November 2019*
Accepted: *25 February 2020*
Published: *24 March 2020*

Citation:
Mohammed MAA, Shafizah IN, Salmiaton A, Wan Azlina WAKG and Taufiq-Yap YH (2020) The Evaluation on Three Types of Malaysian Dolomites as a Primary Catalyst in Gasification Reaction of EFB and Tar Cracking Efficiency. Front. Energy Res. 8:38. doi: 10.3389/fenrg.2020.00038

INTRODUCTION

Syngas can be obtained from various sources, such as coal, natural gas, and petroleum distillate through thermochemical processes (Shen et al., 2018). Syngas technology is a well-known alternative process to produce valuable chemical products. The main components of syngas are hydrogen and carbon monoxide. Hydrogen is a clean and efficient energy source, also known as a safe source because it can be stored as a gas or a liquid, and it has good properties in fueling automobile engines (Mohammed et al., 2011). Dependence on fossil fuels as the main source has led to price instability, excessive carbon dioxide emissions, and unprecedented global warming (Li and Chen, 2018). Owing to the ever-increasing demand of energy for modern civilization and rapid depletion of fossil fuel, there is a need to find for alternative energy sources (González-Vázquez et al., 2018). The production of hydrogen not only accomplish the growing demand energy but also is economically feasible and a sustainable development of the world by utilizing the same infrastructure without any major modification to replace fossil fuel (Shahbaz et al., 2019).

Biomass gasification is regarded to be one of the viable routes for a sustainable future in hydrogen gas production. Biomass is a cheap, abundant, carbon-neutral energy source and has good synergy with current fossil fuel power plants (Li and Chen, 2018). Malaysia has produced a huge amount of palm oil wastes ∼54.1 Mt/year. The palm oil wastes, also known as biomass, consists of empty fruit bunch (EFB), palm kernel shell (PKS), palm oil fronds (POFs), trunks, and fiber (Abdulrazik et al., 2017). Malaysia has implemented a biofuel program and embarked on renewable energy growth to ensure sustainable development in the energy sector. In line with government policy, it has led to strong interest among researchers to utilize biomass for green biofuels (Mohammed et al., 2011). Till now, many works have been reported on the transformation of solid biomass into combustible gases, such as the mixture of hydrogen, methane, carbon monoxide, carbon dioxide, light hydrocarbon, and char, through gasification (Mutlu and Yucel, 2018). Nevertheless, many reported works have shown low conversion efficiency of syngas, which is low H_2/CO ratio, hence resulting in higher tar formation and reduction in gas yield. To achieve high-quality syngas, high gas yield, suitable gas components, low tar yield, and low content of impurities must be obtained (Shen et al., 2018). Many studies have been conducted to produce high-quality syngas by various techniques, such as high-temperature gasification, gasification agent, bio-oil reforming, inline reforming, and type of catalysts.

Nonetheless, high tar yield can cause several operational issues, such as corrosion in equipment and pipeline blockage and high maintenance cost on the filtration system (Tian et al., 2018). Tars can be removed by several ways, such as collection and disposal of tars (non-catalytic), catalytic tar conversion, and cogasification of biomass and coal (Tian et al., 2018). Tar can be eliminated by a catalytic pathway to convert it into the lower molecular weight of hydrocarbon. Tar conversion reaction during gasification in the presence of the catalyst can be shown in Equation (1) (Aydin et al., 2018):

$$\text{Tar} + \left\{\frac{H_2O}{CO_2}\right\} \rightarrow H_2 + CO + CH_4 + C_2H_n \quad (1)$$

The use of catalyst has proven to benefit the gasification process in terms of the economic point of view. According to Shahbaz et al. (2019), the use of a catalyst can augment the quantity of the desired product, lower the gasification temperature condition, and capable of converting tar into gases, although it has a minor problem in sintering as well as regeneration. However, some catalyst can be easily deactivated during the process due to high tar contamination and particle agglomeration after several sorption–desorption cycles (Xu et al., 2017).

There is strong interest to use low-cost and abundantly available sources, such as dolomite as catalyst for EFB gasification as well as tar cracking (Waheed et al., 2016). Quitete and Souza (2017) stated that they evaluated the three dolomites from different origins and Ni-based mixed metal oxides containing Ce and La for tar removal. Mixed metal oxide showed a higher toluene conversion than dolomites due to hydration and carbonation. They also mentioned that dolomites can retain a portion of H_2S and HCl and promote tar cracking and are significantly active above 800°C. Herein, this study aimed to evaluate the tar cracking efficiency in EFB gasification reaction using various calcined Malaysian dolomite catalysts as the primary catalyst. Moreover, the effect of different catalyst to biomass (C/B) ratios on product yield and selectivity, the performance of gasification reaction, and tar conversion efficiency were determined in the study.

TABLE 1 | Properties of empty fruit bunch.

Component	Measured
Cellulose (%)	22.24
Hemicellulose (%)	20.58
Lignin (%)	30.45
PROXIMATE ANALYSIS	
Moisture (wb) (%)	55.6
Moisture (db) (%)	5.18
Volatiles matter (%)	82.58
Fixed carbon (%)	8.97
Ash (%)	3.27
ULTIMATE ANALYSIS (db)	
C (%)	46.62
H (%)	6.45
N (%)	1.21
S (%)	0.035
O (by diff.) (%)	45.69
Calorific value (MJ/kg)	17.02

wb, wet basis; db, dry basis.

MATERIALS AND METHODS

Materials

The feedstock used was dried EFB, ∼0.3–0.5 mm in diameter. The properties of the dried EFB are shown in **Table 1**. Silica sand was used as the bed material in the gasifier with a mean size of 0.10–0.15 mm. Three types of natural Malaysian dolomite stones (P1, P2, and P3) were used as catalysts. All dolomites were ground and sieved with an average diameter of 0.5–1.0 mm. Then, the dolomites were calcined at 900–1,000°C with nitrogen purging for 4 h before being used in the gasification process. Analytical-grade solvents and reagents were used for sample preparation and chemicals for the preparation of calibration and internal standards. All chemicals as follows were received in minimum purity of 98–99% (Sigma–Aldrich, United States): dichloromethane (DCM), isopropanol (IPA), *N*, *O*-bis(trimethylsilyl) trifluoroacetamide (BSTFA), *p*-ethoxyphenol (PEP), and 2-promonaphthalene. Solid-phase extraction (SPE) tubes (VARIAN, United States) used for tar sampling and sample preparation were loaded with 500 mg of aminoporpylsilane (NH_2) phase (surface area, ∼460–520 m^2/g) bonded to a silica gel (average particle size of 47–60 μm and average pore diameter of 60–87 Å).

Catalyst Characterization

The chemical composition of catalysts was estimated using wavelength-dispersive X-ray fluorescence (WDXRF) (model BRUKER, S8 TIGER, United States). The fused-bead technique was used to prepare the samples for XRF analysis. Approximately 0.5 g of the sample was mixed with 5.0 g of spectra-flux LT-110 ($Li_2B_4O_7$ = 66.5%, $LiBO_2$ = 33.5%) and placed in a platinum crucible. The mixture was then fused at temperatures between 900 and 1,250°C and cast in a platinum casting dish. The samples were subjected to precise control of the cooling process to ensure the reproducibility of the flat glass disks and to avoid cracking or crystallization.

To examine the structural changes induced by the calcination process, the samples were characterized using a diffractrometer X-ray diffraction (XRD) system (model Shimadzu XRD6000, Japan), using Cu Kα (at wavelength of 1.5406 Å) radiation, fitted with a Cu filter on the secondary optics and operated under 40 kV power and 30 mA current. The scanning 2θ range was from 20 to 90°, at a scan rate of 3°/min.

The physical properties of the dolomites, such as specific surface area, total pore volume, and pore size distribution, were obtained by measuring their nitrogen adsorption–desorption isotherm at 77 K using a Quantachrome instrument (model Atosorb-1, United States). The Brunauer–Emmet–Teller (BET) surface area was estimated from the adsorption–isotherm data using the relative pressure (p/po) range of 10^{-6}-1. The total pore volume was assessed by converting the amount of nitrogen gas adsorbed at relative pressure to the volume of the liquid adsorbate. The analytical method consisted of three steps, including dehydration, degassing under low vacuum pressure, and nitrogen gas adsorption at 77 K. The resulting isotherm was analyzed using the BET adsorption method, and the pore-size distributions were derived by the Barret–Joyner–Halena (BJH) desorption method.

The surface and microstructure analysis of the catalysts was carried out using a scanning electron microscopy (SEM) instrument (model HITACHI, S-3400N, Japan). The catalyst powder was mounted onto the SEM stubs (layered with sticky carbon tape). The stub was then placed in a sputter coater (EMITECH, K550X, United States) for 5 min for coating with gold to provide high reflectivity during the scanning process. The samples were then placed at 40°C in an oven before SEM analysis.

Catalytic Gasification

The catalysis experiments were performed to inspect the effect of the catalyst on the EFB gasification process when it was directly dry mixed with EFB samples as primary catalyst. The weight ratio of C/B varied in the range of 0.05–0.3 in increments of 0.05 at a gasifier temperature of 850°C. The experimental setup for a primary catalyst is illustrated in **Figure 1**. The results were compared with the results published previously (Mohammed et al., 2011), in which non-catalytic gasification was performed to assess the influence of gasification temperature, the equivalence ratio (ER), and feedstock particle size.

Tar Analysis Using Solid-Phase Adsorption Method

The sampling and analysis of tar compounds were achieved using the solid-phase adsorption (SPA) method. In this paper, tar was referred to as major gas chromatography (GC)-detectable aromatic and phenolic compounds. In this method, 100 ml of gas product was withdrawn from the sampling gas line through the SPE tube using a syringe within ∼1 min. The sampling point was kept at 250°C using a heating tape to prevent or minimize any tar condensation. Subsequently, the SPE tubes were eluted using 1.5 ml DCM to get an aromatic fraction, and then with 1 ml of IPA-DCM (1:1 *v*/*v*) and 0.5 ml of IPA to get a phenolic fraction. The fractions were collected in vials (1.5 ml) and closed with a

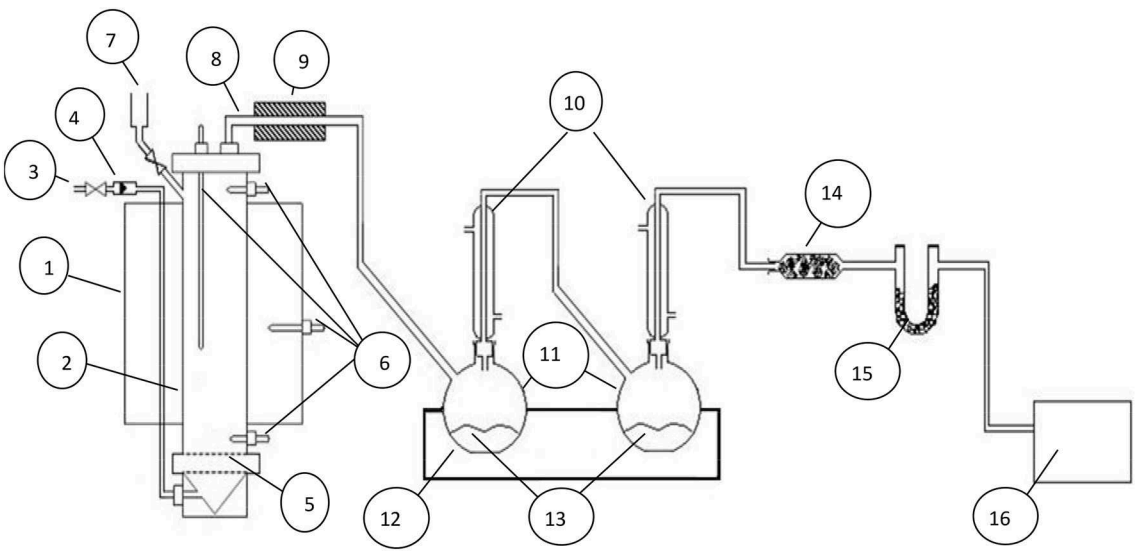

FIGURE 1 | A schematic diagram of the gasification setup: (1) gasifier, (2) electric furnace, (3) air inlet, (4) air flow meter, (5) air distributor, (6) thermocouples, (7) feeder, (8) gas outlet, (9) heating tape, (10) condenser, (11) neck flask, (12) ice path, (13) dichloromethane, (14) fiber-glass wool filter, (15) silica gel, and (16) gas bag.

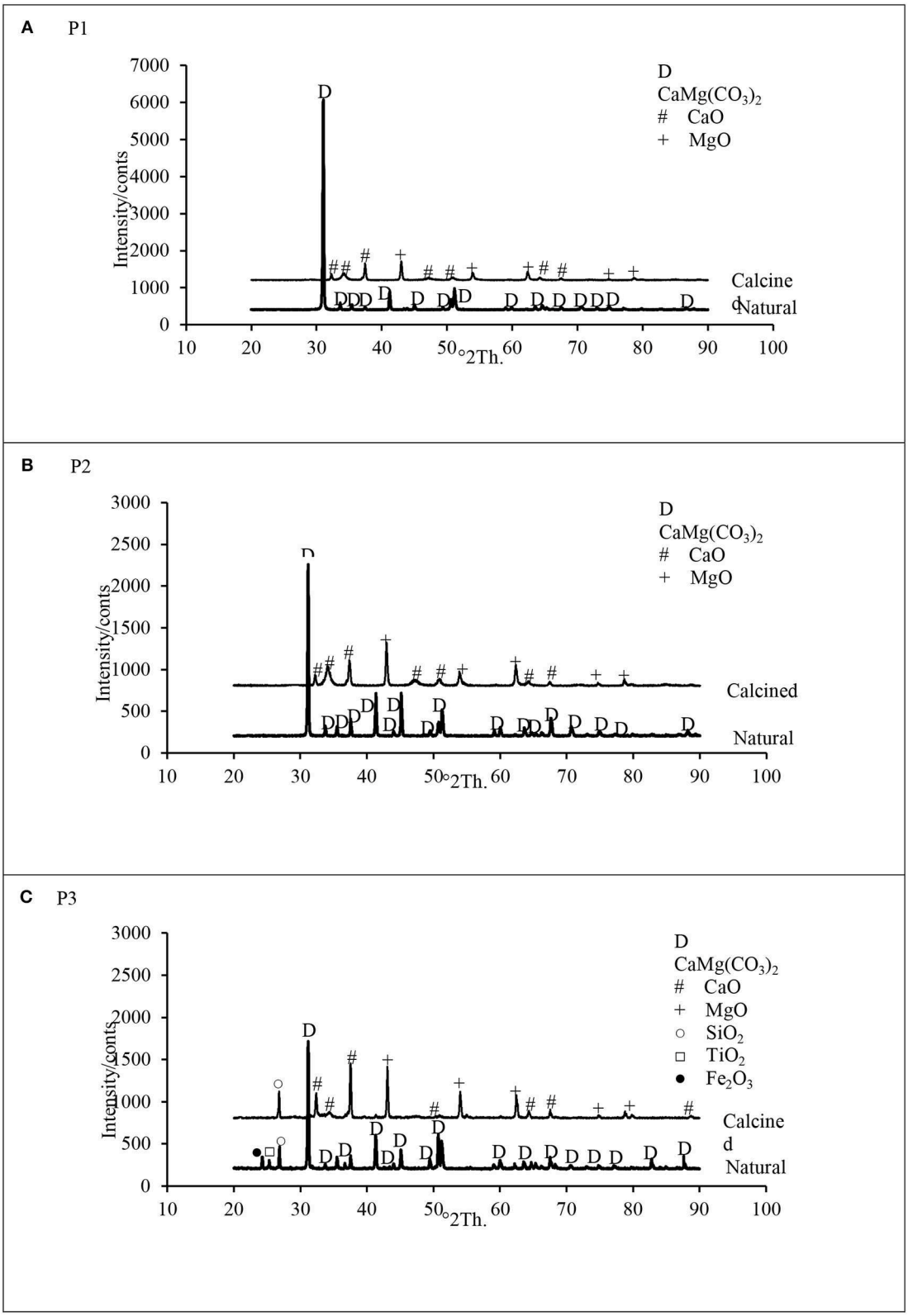

FIGURE 2 | X-ray diffraction (XRD) diffractogram of natural and calcined dolomite catalyst for **(A)** P1, **(B)** P2, and **(C)** P3.

septum cap. The known amounts of 2-bromonaphthalene and p-ethoxyphenol were added as internal standards for aromatic and phenolic fractions, respectively. Phenols were derivatized to form trimethylsilyl ethers by the addition of 50 μl BSTFA to the phenolic fractions and allowed for the reaction to occur for 1 h before GC analysis. The aromatic and phenolic fractions were analyzed using a GC (model Agilent Technologies, 7890A, United States) equipped with a flame-ionization detector (FID) operated at 300°C and an Agilent HP-5 column with 30 m length, 0.325 mm internal diameter, and 0.25 μm film thickness. The splitter/splitless injector port was operated in a split mode at 280°C. A constant flow of helium at 0.8 ml/min through the column was automatically maintained using electronic pressure control programming (60–100 kPa) to follow the temperature program. The sample size was 1 μl. The oven temperature was programmed from 50°C isothermally for 5 min and then at 8°C/min to 280°C with 5-min final delay time.

Gas Product Analysis Using Gas Chromatography

The gas product was qualitatively and quantitatively analyzed using GC (model Agilent technology, HP6890N, United States) equipped with a thermal conductive detector (TCD) and a capillary column HP Molesieve (J&W Scientific, United States) to measure the volume fraction of permanent gas. The length, internal diameter, and film thickness of the column were 30 m, 0.53 mm, and 50 μm, respectively. The oven temperature was set at 70°C, and the carrier gas flowrate (argon) was 3.4 ml/min. The splitless inlet temperature was 60°C, while the detector temperature was 200°C. The TCD was calibrated using a standard gas (Air Products, Singapore) mixture containing CO, CO_2, H_2, and CH_4 in N_2 at periodic intervals.

RESULTS AND DISCUSSION

Physicochemical Properties of Activated Dolomite Catalysts

The catalysts were characterized before and after calcination using XRD to analyze the effect of the calcination process on the catalyst structure. From **Figure 2**, XRD patterns for natural dolomites show that all peaks correspond to those of dolomite $CaMg(CO_3)_2$ [Joint Committee on Powder Diffraction Standards (JCPDS) 36-0426]. The XRD pattern for calcined dolomites, however, changes drastically compared to that of natural dolomites. New dominant peaks that belong to CaO (JCPDS 04-0777) and MgO (JCPDS 87-0652) are observed. Natural P3 sample (**Figure 3C**) shows three additional peaks between $2\theta = 20^\circ$ and $2\theta = 30^\circ$, which belongs to Fe_2O_3 (JCPDS 26-1319), TiO_2 (JCPDS 71-1169), and SiO_2 (JCPDS 83-0539), occurring at $2\theta = 25.2$, 26.7, and 28°, respectively. The changing in the peaks illuminates the calcination of Malaysian dolomites, resulting in the formation of MgO–CaO, which is the active component.

The chemical composition of the dolomite in addition to its physical properties (i.e., surface area, pore volume, and average pore diameter) is an important factor in evaluating the tar cracking capacity of the dolomite. Calcined dolomite is a porous catalyst; its large surface area and the presence of CaO and MgO in its matrix make it an active catalyst concerning tar reduction. The BET surface area, pore volume, and average pore size for dolomites are summarized in **Table 2**. A comparison of the surface area and pore volume (17–3,000 Å) shows that the P1 and P2 catalysts has the highest surface area and pore volume compared to P3. The pore size distribution of P1 and P2 dolomites differs from that of P3. The pore size of P1 and P2 catalysts is mainly in the 400-Å region, whereas the major pore size of P3 is in the 150-Å region.

Catalyst micrographs before and after calcination process are shown in **Figure 3**. The SEM images of the calcined dolomites are significantly different from those of the dolomites before calcination. As illustrated in **Figure 3**, the SEM images of natural dolomite show a rough and disorderly surface with low-porosity grains, whereas the calcined dolomite samples show high-porosity surface, especially in the case of P1 and P2 catalysts. The pores are homogeneous and well-pronounced, which confirms the structural transformation of dolomites.

The Influence of Calcined Dolomite Catalysts on Tar Cracking

Figure 4A shows the effect of different amounts of calcined dolomite catalysts on tar conversion in the EFB gasification process. The tar content decreased with the use of dolomites in the gasifier due to the cracking of tar by wet- and dry-reforming reaction. Further reductions were achieved by increasing the amount of catalyst in the reaction. P1 and P2 catalysts showed higher catalytic activity for tar reduction compared to P3 dolomite. It might be due to the higher surface area and pore volume that contributes to higher tar cracking efficiency, as shown in **Table 2**. On the contrary, P3 contains low quantities of CaO and MgO with high amounts of impurities, such as SiO_2, Al_2O_3, and TiO_2, which strongly reduced its catalytic activity. In the presence of P1 dolomite, the total tar content in the produced gas decreased from 41.2 mg/g obtained with zero catalyst addition in the gasification to 8.8 mg/g obtained at 850°C with 30% catalyst, while under the same conditions, the total tar reduced to 10.2 and 12.2 mg/g in the case of P2 and P3, respectively. The tar conversion efficiencies of all calcined dolomite catalysts are shown in **Figure 4B**. The calculated tar reduction (%) relative to that obtained with zero catalyst for P1, P2, and P3 were ∼78, 75, and 70%, respectively (Mohammed et al., 2011).

Analysis of the characteristics of tar content in the produced gas from EFB gasification were performed before and after decomposition with PI, P2, and P3 catalysts for their aromatic and phenolic compounds using the SPA method. As can be seen in **Figure 4B**, P1 dolomite showed the highest activity for the decomposition of the total light aromatics and naphthalene compared to P2 and P3 catalysts, while for the decomposition of phenolic compounds, P1 and P2 dolomites showed similar activity. Besides, the naphthalene conversion for P1, P2, and P3 were ∼52, 39, and 21%, respectively.

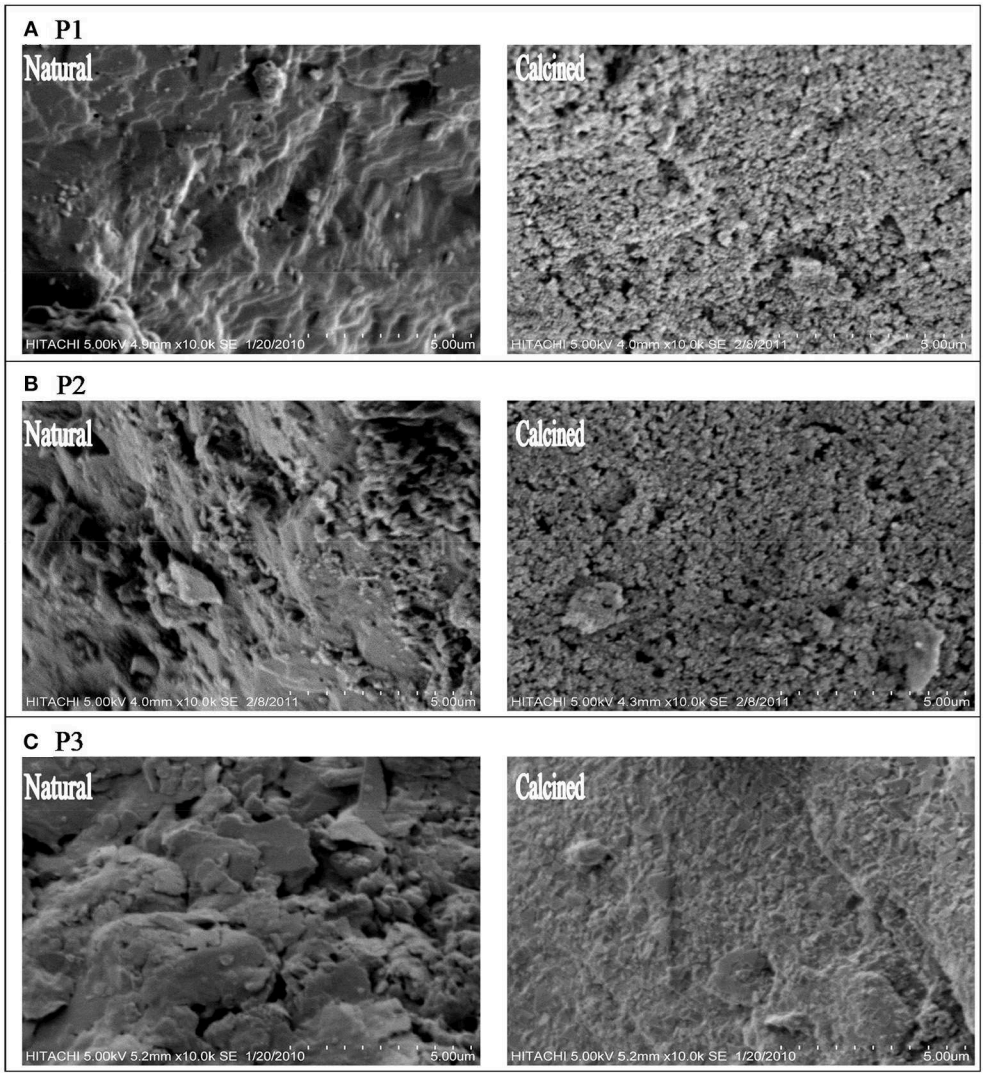

FIGURE 3 | Morphology of calcined dolomite catalysts **(A)** P1, **(B)** P2, and **(C)** P3.

The Influence of Calcined Dolomite Catalysts on Overall Product Yields and Syngas Composition

The results for the EFB gasification yields and performance using calcined dolomite, which are P1, P2, and P3 catalysts, are shown in **Figure 5**. All dolomites conferred more positive influence on the gas yield. The gas product increased with increasing the C/B ratio, whereas the char and tar yields decreased. The results indicate that the dolomite catalyst tends to produce a larger quantity of gas with a smaller amount of tar. This contributes to a significant effect on gasification yields and performance. As shown in **Figure 5**, the P1 catalyst appeared to have a stronger catalytic effect than other types of dolomites used in the EFB gasification reaction. As the C/B ratio of P1 increased from 0.05 to 0.30, the total gas yield increased ∼8% (1.57 N m^3/kg) compared to non-catalytic gasification (1.46 N m^3/kg), whereas the total tar yield dramatically decreased approximately by 78% (8.8 mg/g) compared to the former process (non-catalytic, 41.2 mg/g). Char yield also decreased from 51.5 mg/g with zero catalyst addition to 15.4 mg/g with the addition of P1 at a C/B ratio of 0.30 (Mohammed et al., 2011).

TABLE 2 | Brunauer–Emmett–Teller (BET) surface area and porosity of the calcined dolomites.

	BET surface area (m^2/g)	Pore volume (cm^3/g)	Average pore diameter (Å)
P1	15.3	0.32	815
P2	16.9	0.12	692
P3	6.2	0.09	258

Figure 6 shows the specific gas composition for the EFB gasification under the influence of the different C/B ratios of

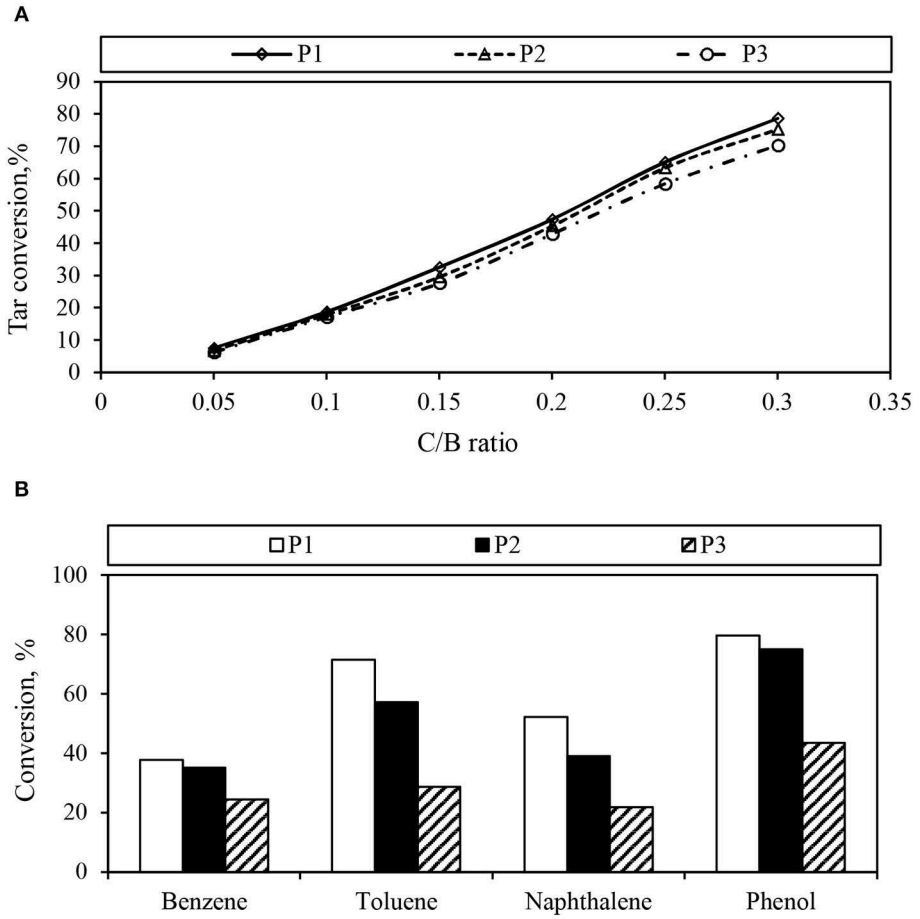

FIGURE 4 | Effect of different catalyst to biomass (C/B) ratio on **(A)** tar conversion and **(B)** gas conversion.

TABLE 3 | Chemical composition of calcined dolomites.

Compounds (%)	Calcined dolomites		
	P1	P2	P3
SiO_2	0.07	0.09	15.37
Al_2O_3	0.04	0.08	1.69
Fe_2O_3	0.07	0.12	0.51
CaO	30.00	32.00	23.00
MgO	21.00	21.00	17.20
K_2O	0.014	0.026	0.195
Na_2O	0.013	0.013	0.013
P_2O_5	0.013	0.017	0.019
MnO	0.010	0.011	0.013
SrO	0.008	0.009	0.009
TiO_2	0.006	0.007	0.015

P1, P2, and P3 catalysts. The percentage in volume of produced gas components had a marked change with the increasing C/B ratio. As for the individual gases, dolomites had a noticeable effect of favoring the production of H_2 and CO at higher C/B ratios, whereas the CO_2 formation was reduced. These results could be explained by the effect of shifting reactions (Mohammed et al., 2011) and tar destruction (by reforming, cracking) reaction.

The presence of dolomites as primary catalyst favored the production of H_2, although different effects could be observed. The product yield and gas species distributions were quite similar for both additions of P1 and P2 catalysts, and they were slightly different in the case of adding the P3 catalyst. This can be explained by the fact that the chemical compositions of the dolomites (**Table 3**) are different from each other. The chemical composition of P3 dolomite differed significantly from that of P1 and P2. The CaO and MgO contents of P1 and P2 dolomites were very close, whereas in the case of P3, these contents were relatively low. Furthermore, P1 and P2 had a much lower content of impurities than P3, whereas P3 had a higher level of impurities, especially silica (SiO_2, 15.37%) and alumina (Al_2O_3, 1.69%).

As shown in **Figure 6**, the P1 catalyst shows a higher catalytic activity for gas yield and a better selectivity for H_2 production than P2 and P3 dolomites. The highest H_2 content of 36.87%

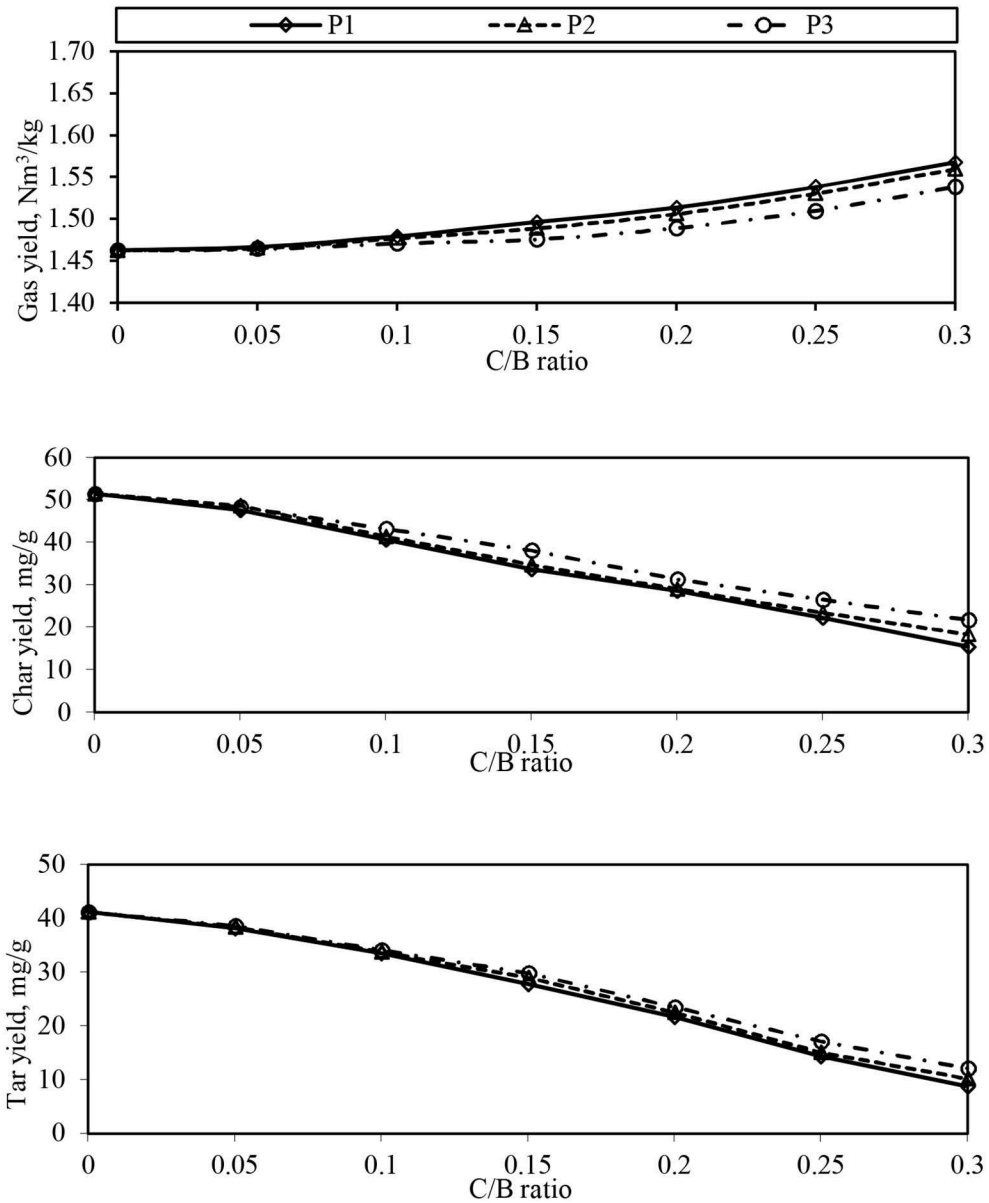

FIGURE 5 | Effect of different catalyst to biomass (C/B) ratio on overall product yield.

(32.25 mg H_2/g EFB) was obtained with P1 as the primary catalyst at an C/B ratio of 0.30 compared to 27.31% (21.55 mg H_2/g EFB) obtained from gasification process with zero catalyst addition. Besides, the CO and CH_4 contents were increased from 33.08 to 36.56% and from 13.76 to 16.26%, respectively. The CO_2 content significantly decreased from 25.63%, obtained from non-catalytic gasification process, to 9.93% with the presence of P1 dolomite.

The Influence of Dolomite on Gasification Performance

As the gas yield increased with increasing the loading of catalyst to EFB, the cold gas efficiency and carbon conversion were also increased accordingly. The increasing trend in the higher heating value (HHV) of produced gas was also observed due to increment in H_2, CO, and CH_4 contents. As can be seen in **Figure 7**, the cold gas efficiency, carbon conversion, and HHV of produced gas were higher in the presence of dolomites. In case of P1 catalyst, an increase in C/B ratio from 0.05 to 0.30 improved the gas HHV from 8.38 to 9.96 MJ/N m^3 compared to 8.20 MJ/N m^3 for the non-catalytic gasification process. In addition, the carbon conversion was improved due to the improvement of water–gas and Boudouard reactions (Mohammed et al., 2011) through which more carbon was converted to gaseous products. The presence of P1 dolomite in the gasification system increased the cold gas efficiency from 55.80 to 70.90% at a C/B ratio of 0.30 due to the high gas yield and heating value.

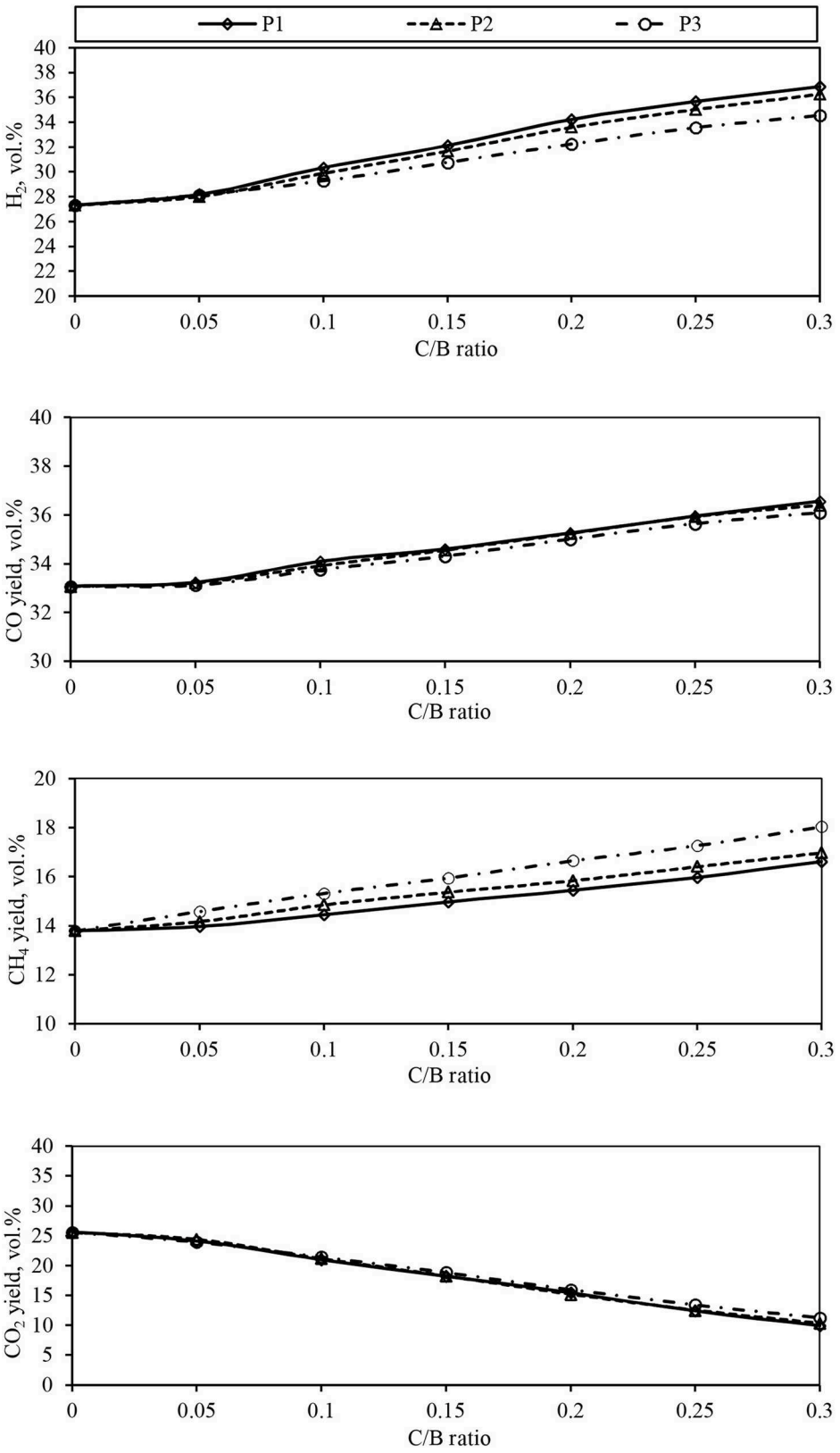

FIGURE 6 | Effect of different catalyst to biomass (C/B) ratio on syngas product composition.

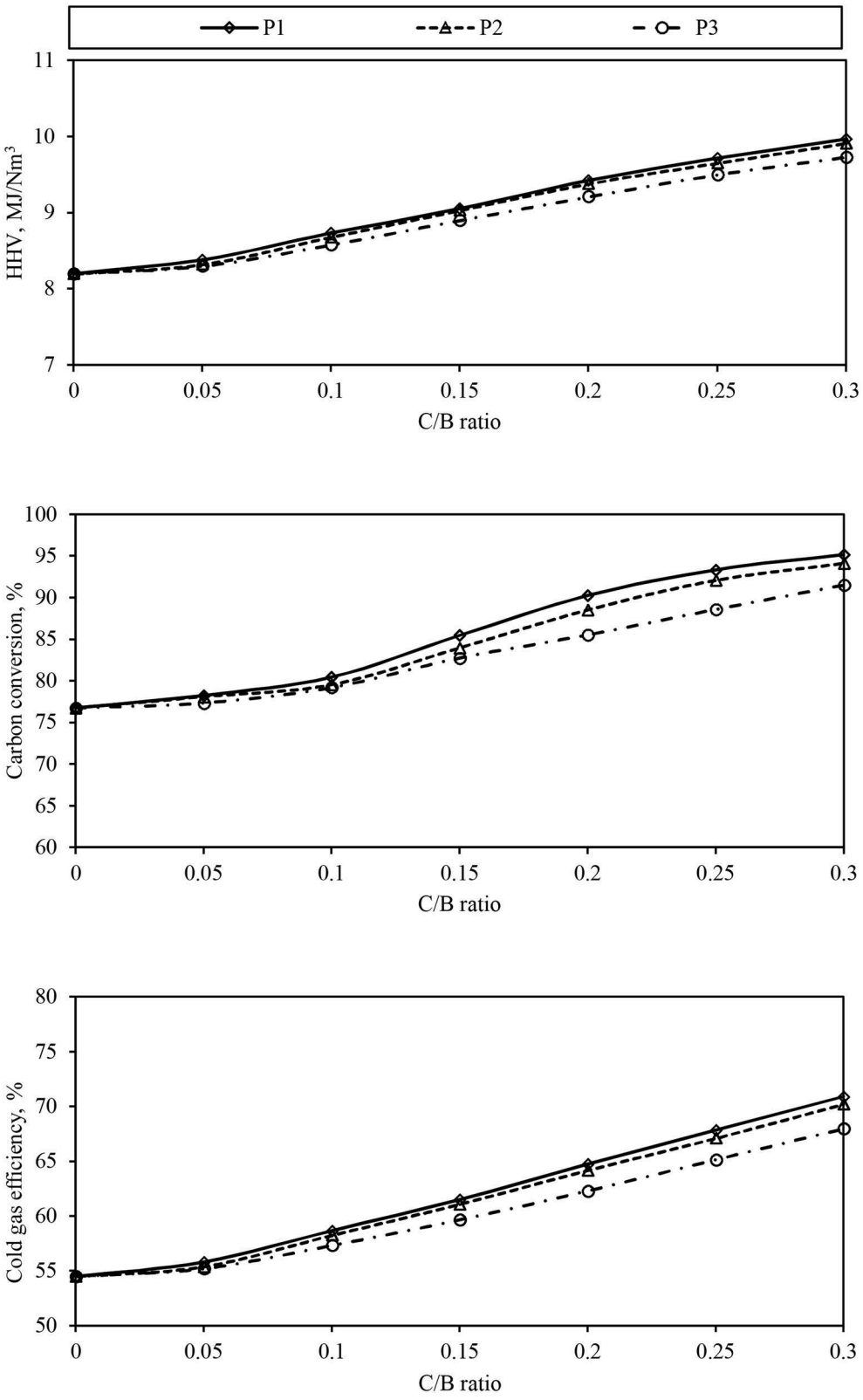

FIGURE 7 | Effect of different catalyst to biomass (C/B) ratio on gasification performance.

CONCLUSION

Calcined dolomites denoted as PI, P2, and P3 catalysts are an effective catalyst for reducing tar in EFB gasification for syngas production. The results indicate that besides chemical composition, the dolomites' surface properties are also important factors for efficient tar cracking capacity. Higher surface area and pore volume contribute to higher tar reduction and catalytic activity when using P1 and P2 catalysts as compared to P3 catalysts. P3 contains low quantities of actives sites (CaO–MgO) with high amounts of impurities, which strongly reduced its catalytic activity. The calculated tar reduction (%) relative to that obtained with zero catalyst for P1, P2, and P3 were ∼78, 75, and 70%, respectively. The PI catalyst increased the total yield by 8% (1.57 N m^3/kg), reduced the char to 15.4 mg/g, and significantly reduced tar by 78% (8.8 mg/g) as compared to EFB gasification without a catalyst. The P1 catalyst showed higher selectivity of H_2 production (32.25 mg H_2/g EFB), cold gas efficiency, and carbon conversion than P2 and P3.

DATA AVAILABILITY STATEMENT

The datasets generated for this study are available on request to the corresponding author.

AUTHOR CONTRIBUTIONS

MM: carried out the main experimental activities and wrote the first draft of the manuscript. IS: carried out validation of the work and revised the manuscript. AS: designed the methodology of the work, supervision of the work, validation, and revised the manuscript. WW and YT-Y: supervision, conceptualization, and validation of the work.

FUNDING

The authors would like to acknowledge the financial support for this work by Universiti Putra Malaysia under the project 05/01/07/0210RU.

REFERENCES

Abdulrazik, A., Elsholkami, M., Elkamel, A., and Simon, L. (2017). Multi-products productions from Malaysian oil palm empty fruit bunch (EFB): analyzing economic potentials from the optimal biomass supply chain. *J. Clean. Prod.* 168, 131–148. doi: 10.1016/j.jclepro.2017.08.088

Aydin, E. S., Yucel, O., and Sadikoglu, H. (2018). Numerical and experimental investigation of hydrogen-rich syngas production via biomass gasification. *Int. J. Hydrogen Energy* 43, 1105–1115. doi: 10.1016/j.ijhydene.2017.11.013

González-Vázquez, M. P., García, R., Gil, M. V., Pevida, C., and Rubiera, F. (2018). Comparison of the gasification performance of multiple biomass types in a bubbling fluidized bed. *Energy Convers. Manag.* 176, 309–323. doi: 10.1016/j.enconman.2018.09.020

Li, Y. H., and Chen, H. H. (2018). Analysis of syngas production rate in empty fruit bunch steam gasification with varying control factors. *Int. J. Hydrogen Energy* 43, 667–675. doi: 10.1016/j.ijhydene.2017.11.117

Mohammed, M. A. A., Salmiaton, A., Wan Azlina, W. A. K. G., Mohammad Amran, M. S., and Fakhru'L-Razi, A. (2011). Air gasification of empty fruit bunch for hydrogen-rich gas production in a fluidized-bed reactor. *Energy Convers. Manag.* 52, 1555–1561. doi: 10.1016/j.enconman.2010.10.023

Mutlu, A. Y., and Yucel, O. (2018). An artificial intelligence based approach to predicting syngas composition for downdraft biomass gasification. *Energy* 165, 895–901. doi: 10.1016/j.energy.2018.09.131

Quitete, C. P. B., and Souza, M. M. V. M. (2017). Application of Brazilian dolomites and mixed oxides as catalysts in tar removal system. *Appl. Catal. A Gen.* 536, 1–8. doi: 10.1016/j.apcata.2017.02.014

Shahbaz, M., Taqvi, S. A., Minh Loy, A. C., Inayat, A., Uddin, F., Bokhari, A., et al. (2019). Artificial neural network approach for the steam gasification of palm oil waste using bottom ash and CaO. *Renew. Energy* 132, 243–254. doi: 10.1016/j.renene.2018.07.142

Shen, Y., Liu, Y., and Yu, H. (2018). Enhancement of the quality of syngas from catalytic steam gasification of biomass by the addition of methane/model biogas. *Int. J. Hydrogen Energy* 43, 20428–20437. doi: 10.1016/j.ijhydene.2018.09.068

Tian, Y., Zhou, X., Lin, S., Ji, X., Bai, J., and Xu, M. (2018). Syngas production from air-steam gasification of biomass with natural catalysts. *Sci. Total Environ.* 645, 518–523. doi: 10.1016/j.scitotenv.2018.07.071

Waheed, Q. M. K., Wu, C., and Williams, P. T. (2016). Pyrolysis/reforming of rice husks with a Ni–dolomite catalyst : in fl uence of process conditions on syngas and hydrogen yield. *J. Energy Inst.* 89, 657–667. doi: 10.1016/j.joei.2015.05.006

Xu, C., Chen, S., Soomro, A., Sun, Z., and Xiang, W. (2017). Hydrogen rich syngas production from biomass gasification using synthesized Fe/CaO active catalysts. *J. Energy Inst.* 91, 805–816. doi: 10.1016/j.joei.2017.10.014

Conflict of Interest: The authors declare that the research was conducted in the absence of any commercial or financial relationships that could be construed as a potential conflict of interest.

frontiers in Energy Research

ORIGINAL RESEARCH
published: 15 April 2020
doi: 10.3389/fenrg.2020.00040

Stability of Thermophilic Pig Manure Mono-digestion: Effect of Thermal Pre-treatment and Separation

Tine L. I. Vergote[1,2], Anke E. J. De Dobbelaere[3], Bernard Willems[4], Jan Leenknegt[3], Jeroen Buysse[2], Eveline I. P. Volcke[1] and Erik Meers[1]*

[1] Department of Green Chemistry and Technology, Faculty of Bioscience Engineering, Ghent University, Ghent, Belgium, [2] Department of Agricultural Economics, Faculty of Bioscience Engineering, Ghent University, Ghent, Belgium, [3] Inagro vzw, Research and Advice in Agriculture and Horticulture, Rumbeke-Beitem, Belgium, [4] Innolab, Oostkamp, Belgium

Anaerobic pig manure digestion holds potential to contribute to a bio-based economy. This work assesses the stability of the thermophilic mono-digestion process. Thermophilic mono-digestion experiments with (i) fresh liquid pig manure and (ii) the fresh fecal fraction from source separation by a pig housing construction were conducted in semi pilot-scale continuous stirred tank reactors. The effect of separation on the digestion stability was studied by comparing thermophilic mono-digestion of fresh liquid (unseparated) and fresh source separated pig manure. Influencing factors and inhibitors were identified during the experiments. An unstable thermophilic mono-digestion process was observed for fresh liquid pig manure at a digester retention time of 60 days, due to high levels of ammonia and sulfur-containing components. Thermophilic mono-digestion of the fresh fecal fraction was more promising in terms of stability, provided enough time for digestion. In addition, the effect of low temperature (70°C) thermal pre-treatment of manure on the digestion stability was investigated. In the case of liquid pig manure, no improvement in the digestion stability was noted upon thermal pre-treatment. For the fecal fraction, the stability of the thermophilic mono-digestion process did improve. Moreover, thermal treatment and subsequent thermophilic mono-digestion of the fresh fecal fractions from two different farms with a similar pig housing construction suggested an effect of the (organic) dry matter content on the process stability.

Keywords: anaerobic digestion, thermophilic mono-digestion, fresh pig manure, process stability, semi pilot-scale digesters, thermal pre-treatment, source separation

OPEN ACCESS

Edited by:
Su Shiung Lam,
University of Malaysia Terengganu, Malaysia

Reviewed by:
Ao Xia,
Chongqing University, China
Obulisamy Parthiba Karthikeyan,
University of Houston, United States

****Correspondence:***
Tine L. I. Vergote
Tine.Vergote@UGent.be

Specialty section:
This article was submitted to Bioenergy and Biofuels, a section of the journal Frontiers in Energy Research

Received: *09 December 2019*
Accepted: *26 February 2020*
Published: *15 April 2020*

Citation:
Vergote TLI, De Dobbelaere AEJ, Willems B, Leenknegt J, Buysse J, Volcke EIP and Meers E (2020) Stability of Thermophilic Pig Manure Mono-digestion: Effect of Thermal Pre-treatment and Separation. Front. Energy Res. 8:40. doi: 10.3389/fenrg.2020.00040

INTRODUCTION

Pig production in Flanders, the Northern part of Belgium, has a very high density of animals per surface area. The more than 5.8 million animals in 2018 accounted for 90% of the total pig population in Belgium and were divided over approximately 3,750 farms[1] Given the actual annual manure production per pig category in terms of nitrogen (VLM, 2019b) and considering the fixed composition of liquid manure from these pig categories (VLM, 2019c), the estimated annual mass of pig manure produced is close to 10 million tons.

Manure can be valorized to energy through the process of anaerobic digestion. Under anaerobic conditions, organic substrate such as manure is converted to biogas, i.e., a mixture of mainly

[1] https://statbel.fgov.be/nl/themas/landbouw-visserij/land-en-tuinbouwbedrijven#figures

carbon dioxide and methane, and digestate by a wide diversity of micro-organisms (Pavlostathis and Giraldo-Gomez, 1991). The produced biogas can be burned in a combined heat and power unit to supply electricity and heat, while digestate can serve as an organic fertilizer. The World Biogas Association recently stated that the total agricultural energy demand could be met by renewable energy generated from only livestock manure (Jain et al., 2019). Scarlat et al. (2018) estimated the electricity production potential by digestion of manure from livestock and poultry in Europe to be close to 58 TWh per year, only taking into account collectable manure. For the specific case of Belgium, it was nearly 1.5 TWh.

Despite the high potential for anaerobic manure digestion, this technology is not yet fully exploited in Flanders, especially not in the pig sector. If pig manure is digested, it is almost exclusively in large, centralized installations within the concept of co-digestion. In addition, the manure is usually not collected fresh, leading to a reduced biogas potential (de Buisonjé and Verheijen, 2014). About a decade ago, small-scale, decentralized digestion on farms was introduced in Flanders (Decorte et al., 2019). Farm-scale digestion comprises the conversion of on-farm organic substrate to on-farm energy in a dedicated digestion reactor, allowing digester-owning farmers to become (partly) energy self-sufficient (De Dobbelaere et al., 2015). Furthermore, digestion of fresh manure has potential to reduce the overall carbon footprint of farms, as was demonstrated for the dairy sector by Vergote et al. (2019). Note that the term farm-scale anaerobic digestion applies in this case to digesters treating <5,000 tons of proprietary organic substrates per year and having a maximum electrical capacity of 200 kW (De Dobbelaere et al., 2015).

In 2018, the majority of the 53 active farm-scale digesters in Flanders were mono-digesters treating dairy manure (Decorte et al., 2019). Most of these digesters were operated under mesophilic conditions, i.e., at temperatures ranging from 30 to 40°C (Parkin and Owen, 1986; van Lier, 1995). However, thermophilic digestion (>50°C) poses some advantages, among which an increased microbial growth rate, and thus an accelerated energy generation, as well as an enhanced digestibility (Al Seadi et al., 2008), which is important for substrates such as manure, mainly consisting of non-readily biodegradable compounds (Vavilin et al., 1996). Furthermore, despite the large pig population in Flanders, farm-scale anaerobic digesters only treating pig manure are rare, due to the challenges that arise not only during the collection of fresh pig manure but also during the digestion process itself. Pig manure is rich in nitrogen, thereby inducing a high risk for ammonia inhibition (Hashimoto, 1983; Chen et al., 2008). Furthermore, it can contain a lot of sulfuric components depending on the pig's feed ration (Chen et al., 2008; Trabue et al., 2019) and it is sensitive to foam formation (Lindorfer and Demmig, 2016). All these aspects can cause the digestion process to become unstable, resulting in a low, non-constant production of methane or even complete termination of the process. As long as process stability cannot be guaranteed, investments in this technology will be limited, leaving the renewable energy potential by pig manure digestion unused.

In Flanders, pig manure is mostly present in liquid form, with a low dry matter content and a low methane potential in terms of fresh mass (Møller et al., 2007). Thermal pre-treatment could enhance methane production by increasing the soluble organic matter content of the substrate to be digested. Both high (>100°C) and low temperature (<100°C) thermal treatment prior to anaerobic digestion have already been frequently studied for wastewater treatment excess sludge, in batch and small-scale continuous mode, ranging treatment times from several minutes to multiple days (Wang et al., 1997; Gavala et al., 2003; Valo et al., 2004; Skiadas et al., 2005; Climent et al., 2007; Appels et al., 2010). For liquid pig manure, some studies are available focusing on possible improvement of the methane production (potential) by thermal pre-treatment (Bonmatí et al., 2001; González-Fernández et al., 2008; Carrère et al., 2009; Sutaryo et al., 2014). However, thermal pre-treatment could also have a (positive) effect on digestion stability, i.e., the continuation of the anaerobic digestion process under normal conditions, without sudden changes in gas production or methane content in the gas due to limiting or inhibitory components (Drosg, 2013). Indeed, there could be hypothesized that thermal treatment partially converts foam forming agents and other (inhibitory) components before digestion, thereby limiting the risk for instability during digestion. None of the mentioned studies specifically investigated this hypothesis, while process stability is an essential prerequisite for the implementation in practice.

Manure can be separated mechanically into a liquid and solid fraction or by specific animal housing constructions into a fecal and urine fraction (Hjorth et al., 2010). In Flanders, interest in separation techniques has recently been growing because of their possible role in optimizing manure disposal (by mechanical separation; Vannecke et al., 2018) and in the reduction of ammonia emissions and odor nuisance (by source separation in the animal housing; Vermeulen, 2019). Soluble minerals, such as ammonium nitrogen, mainly accumulate in the liquid or urine fraction. Most of the organic matter is present in the solid or fecal fraction, which thus can be useful for digestion (Vannecke et al., 2018). Due to partial removal of the liquid fraction or urine, the remaining fraction has a much higher methane potential and thus energy content in terms of mass than unseparated pig manure, if fresh (Asam et al., 2011; Deng et al., 2014). However, the higher methane potential is only beneficial toward digestion if the process can be kept stable. Available results from experimental research on inhibition and stability are contradictory. Sutaryo et al. (2013) found that raw acidified liquid sow and pig slurry were inhibited by sulfide during mesophilic digestion, while this was not the case for the solid fraction obtained through mechanical separation. In contrast, Møller et al. (2007) obtained a stable thermophilic digestion process for fresh liquid pig manure as such and for fresh liquid pig manure partly substituted by its solid fraction (up to 60% on mass base), though latter process

Abbreviations: BMP_0, Biochemical methane potential; CSTR, Continuous stirred tank reactor; DM, Dry matter; FOS, Volatile organic acids; HRT, Hydraulic retention time; LPM, Liquid pig manure; oDM, Organic dry matter; OLR, Organic loading rate; SPM, Separated pig manure; SRB, Sulfate reducing bacteria; TAC, Total inorganic carbonates; TAN, Total ammonia nitrogen; TN, Total nitrogen; VFA, Volatile fatty acids.

was inhibited by ammonia. Other studies on mono-digestion of (fresh) separated pig manure have mostly been conducted in view of identifying the influence of thermal pre-treatment on methane production (Rafique et al., 2010; Raju et al., 2013; Sutaryo et al., 2014). Available research is mainly focused on the solid fraction of separated pig manure instead of the fecal fraction resulting from source separation by a pig housing construction. However, such construction meets an important condition for valuable anaerobic digestion: fresh substrate (collection). Furthermore, due to inconsistency in results from previous research, it is clear that more studies on mono-digestion of fresh separated pig manure are required to assess its process stability. Moreover, the effect of thermal pre-treatment on this stability has not yet been clarified.

The objective of the current work is to study the stability of thermophilic mono-digestion of fresh pig manure, using semi pilot-scale digesters. Both fresh liquid pig manure and the fresh fecal fraction from source separation by a specific pig housing construction are digested, thereby assessing the effect of separation on the process stability. In addition, the effect of thermal pre-treatment on the digestion stability is investigated. Low temperature thermal pre-treatment (70°C) with a short treatment time (1 h) is studied to ensure high probability for an economically feasible farm-scale implementation. Influencing factors and inhibitors are identified during the experiments. In general, this study aims to gain insight into the conditions necessary for stable mono-digestion of pig manure in order to support potential future implementations on pig farms.

MATERIALS AND METHODS

Substrate and Inoculum

Fresh liquid (LPM) and separated pig manure (SPM) were obtained periodically from different Flemish pig farms. Liquid pig manure is present on standard pig farms, in the manure pit below the slatted floor of the animal housing. As this specific pig housing construction does not allow for collection of fresh manure, collection took place at a more advanced facility in a manure pit with separate manure and water channels. The water channel mainly contains feed residuals, besides some manure. Such manure pit construction reduces the ammonia emitting surface and thus limits ammonia emissions. Furthermore, it enables fresh manure collection, as the channels are connected to a central pipe and can be flushed (Van Overbeke et al., 2010). Fresh excreta from the manure and water channels were collected and mixed proportionally, more specifically 4 to 1 L, to obtain representative fresh LPM for the experiments. SPM was in this case the fresh fecal fraction collected from a VeDoWS (Vermeulen Dobbelaere Welfare System) pig housing construction. Its design, a shallow manure pit with gutters and a manure scraper below the slatted floor, allows for source separation, i.e., primary separation of freshly excreted manure into a fecal and urine fraction[2] This specific pig housing construction is recognized as an ammonia-reducing technique in Flanders (VLM, 2019a). Note that the substrate choice was driven by the current animal housing situation, and thus manure collection systems, in the Flemish pig sector and was aimed at enlarging pig manure digestion possibilities.

Manure was collected as fresh as possible (<2 days old) to avoid any effect of pre-digestion. The collected substrates were stored at 4°C prior to the digestion experiments. The anaerobic digestate used as inoculum was obtained from a properly running thermophilic reactor in Flanders, co-digesting mainly organic biological waste and a small fraction of manure (up to 10% of the total mass fed per year). Inoculum is necessary to expedite process start-up in the reactors (Liebetrau et al., 2019). Furthermore, a volume of inoculum (**Table 2**), which amounted to 10%of the total reactor volume, was added to the reactor when a temporary stop of the feeding was not sufficient for recovery and continuation of the process after instability.

Experimental Set-Up

Experiments were conducted in semi pilot-scale continuous stirred tank reactors (CSTRs) at the Flemish biogas laboratory Innolab. Four reactors were used, two in vertical configuration (CSTR 1 and 2) and two in horizontal configuration (CSTR 3 and 4) (**Supplementary Figure A.1**). The working volume of the CSTRs was respectively, 72 and 33 L. Every 10 min, the CSTRs were mixed for 1 min by a central shaft, rotating at 20 or 15 rpm depending on the reactor. All CSTRs were operated under thermophilic conditions (50–52°C). The reactors were fed manually once per day and up to seven days per week. Before feeding, the biogas production was read from a Drum-type gas meter (Ritter, TG 0.5 model) connected to the reactor. The gas composition, including the percentage of methane, carbon dioxide and oxygen in the gas as well as the hydrogen sulfide content, was measured by a portable gas analyzer (Geotech, Biogas 5000 model). The specific time and mass of ingoing manure were recorded at each feeding. Excess digestate was periodically removed via the overflow. The reactor set-up is further elaborated in **Supplementary Material A.2**.

The stability of thermophilic pig manure mono-digestion was investigated based on three experiments (**Table 1**). The effect of low temperature thermal pre-treatment on the digestion stability was studied in experiment 1 and 2, for LPM from farm A and SPM from farm B, respectively, by simultaneously digesting raw and pre-treated substrate. The hydraulic retention time (HRT) was varied during the experiments with SPM B_1. Experiment 3 studied the digestion stability of SPM, from two different farms (farm B and C) with the same pig housing construction, after thermal treatment. By comparing the results for LPM (experiment 1) and SPM (experiment 2 and 3), the possible influence of separation on the process stability was assessed. The digestion process was defined as unstable when the relative biogas or methane production on organic dry matter base (Equation 2) or the methane content in the biogas suddenly dropped without fast recovery (Drosg, 2013), or when the biogas production process (almost) completely stopped despite daily feeding.

A thermal pre-treatment was performed under the hypothesis that it will partially convert foam forming agents and other (inhibitory) components before digestion, thereby limiting the risk for instability during digestion. Low temperature thermal

[2]https://www.vermeulenconstruct.be/nl/stalinrichting/

TABLE 1 | Overview of the experiments performed to investigate the stability of thermophilic pig manure mono-digestion.

No.	Substrate	Specification	Period*	Duration (days)	HRT** (days)	Reactor	Pre-treatment
1	Fresh liquid pig manure from farm A	LPM A	1a	23	60	CSTR 1	–
		LPM A	1b	25	60	CSTR 1	–
		LPM A_p	1a	23	60	CSTR 2	Thermal
		LPM A_p	1b	25	60	CSTR 2	Thermal
2	Fresh fecal fraction from farm B	SPM B_1	2a	55	60	CSTR 3	–
		SPM B_1	2b	33	45	CSTR 3	–
		SPM B_{p1}	2a	55	60	CSTR 4	Thermal
		SPM B_{p1}	2b	33	45	CSTR 4	Thermal
3	Fresh fecal fraction from farm B and C	SPM B_{p2}	–	72	60	CSTR 3	Thermal
		SPM C_p	–	72	60	CSTR 4	Thermal

During each experiment, mono-digestion of two different substrates was tested simultaneously. Thermal pre-treatment was performed for 1 h at 70°C.
**The occurrence of instability or an adaptation of the HRT required division of the experiments with LPM A (experiment 1) and SPM B_1 (experiment 2) into subperiods.*
***Fixed HRTs were maintained during the subperiods of the experiments. As the manure composition differed (**Table 2**), the OLR varied between the experiments.*

pre-treatment with a short treatment time was studied to increase the probability for an economically feasible implementation on farm-scale. Manure was heated in an oven to a temperature of 70°C after which it was kept at that temperature for 1 h. At a temperature of 70°C, denaturation can be induced (Ichimura, 1991; Ahmed et al., 2007). Moreover, the activity of part of the thermophilic bacteria population may be improved by thermal pre-treatment at 70°C (Climent et al., 2007). During heating, manure was mixed manually every 20–30 min. Each time, about 15 kg of manure was pre-treated at once.

An HRT of 100 days was set at the beginning of the experiments to ensure good start-up and proper adaptation of the microbiology. The HRT was decreased to 60 days by increasing the daily ingoing mass of manure. A change in HRT happened gradually, meaning that the ingoing mass of manure was daily increased by 10% until the desired HRT was reached. This approach allowed for steady adaptation of the microbial community to higher loading rates.

Chemical Analysis

Raw and pre-treated manure samples were analyzed prior to reactor feeding each time after a pre-treatment was performed, i.e., up to five times depending on the length of the experiment and the necessary mass for feeding. A representative digestate sample was taken every week from each CSTR for analysis.

The substrate and digestate samples were analyzed for dry matter (DM), i.e., total solids, organic dry matter (oDM), i.e., volatile solids, total nitrogen (TN), total ammonia nitrogen (TAN) and pH. The DM content was determined gravimetrically after drying at 105°C for 24 h. The oDM content was measured based on the dried sample after incineration at 550°C for 4 h in a muffle furnace. TN was determined by Kjeldahl destruction, TAN by steam distillation, after addition of MgO to the sample, and subsequent titration (Van Ranst et al., 1999). The pH was measured with a pH-meter (PCD 6500, Eutech Instruments). Ammonia nitrogen was calculated based on the TAN, pH and temperature (Equation 4).

Besides, manure samples were analyzed for degradable carbohydrates, proteins and lipids based on the Weende analysis (Henneberg and Stohman, 1860). The biogas and methane potential were determined by the EPi test (Flash biochemical methane potential test)[3] Digestate samples were additionally analyzed for volatile fatty acids (VFA), including acetic, propionic, (iso)butyric, (iso)valeric, and caproic acid, by extraction with diethyl ether and subsequent separation and detection by the GC-FID. Volatile organic acids (FOS) and total inorganic carbonates (TAC) were determined by the Nordmann method (Nordmann, 1977). Viscosity was measured by using the Brookfield method (ASTM/DIN ISO 2555).

The density of the different substrates was calculated as the ratio between the mass and the volume of a sample. For LPM substrates, the density was directly measured with a graduated cylinder of 0.250 L. For SPM substrates, having a high DM content, a graduated cylinder (0.100 L) containing demineralized water was used. The density was determined based on the added mass of manure and the volume increase due to this addition.

Calculations

The relative methane production $CH_{4,rel}$ (L CH_4 kg^{-1} manure) was calculated based on the measured volume of biogas produced per day $V_{biogas,daily}$ (L biogas d^{-1}), the measured methane content in the gas $CH_{4,daily}$ (L CH_4 L^{-1} biogas) and the mass of manure daily fed to the digester $m_{fed,daily}$ (kg manure d^{-1}) (Equation 1). The relative methane production on oDM base $CH_{4,rel,oDM}$ (L CH_4 kg^{-1} oDM) was determined based on $CH_{4,rel}$, the DM (kg DM kg^{-1} manure) and oDM (kg oDM kg^{-1} DM) content of the manure (Equation 2).

$$CH_{4,rel} = \frac{V_{biogas,daily} \cdot CH_{4,daily}}{m_{fed,daily}} \quad (1)$$

$$CH_{4,rel,oDM} = \frac{CH_{4,rel}}{DM \cdot oDM} \quad (2)$$

[3]http://www.innolab.be/nl/productendetail/methaanpotentieel-biogaspotentieel-sneltest

TABLE 2 | Average chemical composition of the substrates, being fresh liquid pig manure (LPM) and the fresh fecal fraction from source separation by a specific pig housing construction (SPM), and the inoculum used for the thermophilic mono-digestion experiments.

		Experiment 1		Experiment 2		Experiment 3		
Parameter	**Unit**	**LPM A**	**LPM A_p**	**SPM B_1**	**SPM B_{p1}**	**SPM B_{p2}**	**SPM C_p**	**Inoculum**
DM	%; 10^{-2} kg DM kg^{-1}	9.3	9.1	26	26	25	21	7.4
oDM	%DM; 10^{-2} kg oDM kg^{-1} DM	77	76	87	87	87	83	58
Composition								
- *Carbohydrates*	kg ton^{-1}	28	26	64	90	68	40	–
- *Proteins*	kg ton^{-1}	15	14	51	51	48	36	–
- *Lipids*	kg ton^{-1}	7.6	7.8	22	21	22	25	–
BMP	m^3 CH_4 ton^{-1}	24	23	67	75	66	53	–
BMP_{oDM}	10^3 m^3 CH_4 ton^{-1} oDM	0.34	0.33	0.30	0.33	0.31	0.29	–
pH	–	7.5	8.4	6.2	6.1	6.3	7.1	8.6
TAN	g N kg^{-1}	5.1	5.3	3.8	3.9	4.0	3.5	3.6
TN	g N kg^{-1}	7.6	7.7	12	12	12	9.3	6.0

The relative efficiency α_{rel} (%) indicates how much the methane production obtained during the experiments deviates from the biochemical methane potential of the substrate. It was calculated based on $CH_{4,rel,oDM}$ and the analyzed biochemical methane potential on oDM base BMP_{oDM} (L CH_4 kg^{-1} oDM) (Equation 3).

$$\alpha_{rel} = \frac{CH_{4,rel,oDM}}{BMP_{oDM}} \cdot 100 \quad (3)$$

The ammonia nitrogen concentration NH_3-N (g N kg^{-1} manure) was calculated based on the measured TAN concentration (g N kg^{-1} manure), which is the sum of ionized ammonium nitrogen (NH_4^+) and unionized ammonia nitrogen (NH_3), the prevailing digester temperature T (K) and the measured pH (–) (Equation 4; Hansen et al., 1998).

$$NH_3 - N = \frac{TAN}{1 + 10^{(0.09018 + \frac{2729.92}{T}) - pH}} \quad (4)$$

The organic loading rate (OLR) (kg oDM m^{-3} d^{-1}) indicates how much organic matter enters the reactor per unit of time. This parameter thus gives an idea about possible overloading of the system. The OLR was calculated based on Equation 5 with V the working volume of the CSTR (m^3).

$$OLR = \frac{m_{fed,daily} \cdot DM \cdot oDM}{V} \quad (5)$$

RESULTS AND DISCUSSION

Both fresh liquid pig manure and the fresh fecal fraction from source separation by a specific pig housing construction were mono-digested under thermophilic conditions. The average chemical composition of the used substrates and inoculum was analyzed and discussed. The stability of raw substrate mono-digestion was determined and described as such, as well as the effect of a thermal pre-treatment and of separation on the digestion stability. Based on the acquired insights, suggestions were given toward further research, focusing on the possible implementation in practice.

Characterization of Substrates

Table 2 shows the average chemical composition of the used substrates and inoculum. The average density of all substrates was close to 1 kg L^{-1}. In general, the measured parameter values of the substrates were in line with typical values from literature.

LPM is generally characterized by a DM content below 10% and an oDM content ranging from 65 to 85% (Møller et al., 2004; Al Seadi et al., 2008; Coppens, 2009; Deublein and Steinhauser, 2009; Verdoes, 2013; Sommer et al., 2015). The DM content of separated manure depends on the technique used for separation (Hjorth et al., 2010). For the fecal fraction from the pig housing construction considered in this study, the DM content typically varies between 22 and 32%, depending on the feed ration and the season (Vermeulen, 2019). Variability in the DM content is thus common, as was the case for the used source SPM with values ranging from 21 (for SPM C) to 26% (for SPM B) (**Table 2** and **Supplementary Table A.1**). Similar DM contents can be reached with mechanical separators, such as a screw press or decanter, depending on the machine settings and the addition of coagulants and flocculants (Verdoes, 2013; Vannecke et al., 2018). The oDM content of SPM commonly ranges between 75 and 90% (Deublein and Steinhauser, 2009; Sommer et al., 2015). The DM content of SPM was higher than that of LPM due to removal of part of the urine. Because of the difference in DM and oDM content between LPM and SPM (**Table 2**) and since fixed HRTs were maintained

TABLE 3 | (Average of) the measured values of the gas production and composition parameters obtained during the thermophilic mono-digestion experiments with fresh liquid pig manure (LPM) and the fresh fecal fraction from source separation by a specific pig housing construction (SPM), excluding the values before complete process failure.

Exp.	Substrate	Period	HRT (days)	Duration (days)	$CH_{4,rel,oDM}$ (L CH_4 kg^{-1} oDM)	CH_4 % (%)	α_{rel} (%)	H_2S^m (ppm)
1	LPM A	1a	60	23	359	61–67	113	3,500
		1b[s]	60	25	225	50–70	63	4,400
	LPM A_p	1a	60	23	363	63–69	112	2,900
		1b	60	25	258	53–70	77	4,000
2	SPM B_1	2a	60	55	259	56–67	89	1,700
		2b	45	33	58	35–60	19	2,100
	SPM B_{p1}	2a	60	55	234	56–66	74	1,700
		2b	45	33	124	50–62	38	2,200
3	SPM B_{p2}	–	60	72	226	59–66	74	1,100
	SPM C_p	–	60	72	280	58–66	95	900

Data obtained during the acclimation period at an HRT of 100 days were not included in the table. The duration of the experiments and HRT were specified.
[s]Addition of a new volume of inoculum (10% of the reactor volume) before the start of this period to allow for process recovery and continuation of the experiment after process instability.
[m]Maximum value measured during the experimental period.

TABLE 4 | Measured values of the digestate parameters obtained during the thermophilic mono-digestion experiments with fresh liquid pig manure (LPM) and the fresh fecal fraction from source separation by a specific pig housing construction (SPM), excluding the values before complete process failure.

Exp.	Substrate	Period	pH* (-)	TAN* (g N kg^{-1})	NH_3-N* (g NH_3-N kg^{-1})	FOS/TAC (mg mg^{-1})	VFA^m (mg kg^{-1})
1	LPM A	1a	8.4	3.4	1.5	0.11–0.33	500
		1b[s]	8.5	4.1	2.1	0.22–0.36	5,000
	LPM A_p	1a	8.3	3.8	1.3	0.11–0.30	1,900
		1b	8.5	4.3	2.2	0.22–0.37	3,800
2	SPM B_1	2a	8.3	5.4	2.2	0.15–0.40	5,800
		2b	8.1	6.3	1.8	0.39–0.84	17,400
	SPM B_{p1}	2a	8.4	5.3	2.3	0.22–0.41	6,600
		2b	8.3	6.2	2.2	0.38–0.77	12,500
3	SPM B_{p2}	-	8.3	6.0	2.2	0.22–0.63	9,000
	SPM C_p	-	8.4	5.2	2.2	0.17–0.46	4,400

Data obtained during the acclimation period at an HRT of 100 days were not included in the table.
[s]Addition of a new volume of inoculum (10% of the reactor volume) before the start of this period to allow for process recovery and continuation of the experiment after process instability.
**Value reached at the end of the period.*
[m]Maximum value measured during the experimental period.

in the reactors during the subperiods (**Table 1**), the OLR varied during the experiments.

The protein and lipid content were in line with values proposed by Møller et al. (2004) for LPM. The proposed carbohydrate content was almost double the value in this study as besides degradable also non-degradable carbohydrates were included. The lipid content was significantly higher than the values found by Matulaitis et al. (2015) for fresh LPM and the solid fraction of SPM, which amounted to respectively 3.5 and 0.5 kg lipids per ton, probably due to dissimilarities in the pig's feed ration and the separation technique. Manure composition in terms of carbohydrates, proteins and lipids is directly related to the methane potential (Weinrich, 2019). For LPM, the methane potential typically ranges from 150 to 480 m^3 per ton of oDM (Al Seadi et al., 2008; Deublein and Steinhauser, 2009; Matulaitis et al., 2015), given a methane content of 60% (Al Seadi et al., 2008). Values for SPM on oDM base are comparable to those for LPM (Deublein and Steinhauser, 2009; Matulaitis et al., 2015; Vermeulen, 2019). However, the methane potential and thus energy content in terms of mass is much higher for SPM due to (partial) removal of the urine, containing a limited amount of organic matter (Vannecke et al., 2018) and therefore having a low methane potential (Asam et al., 2011; Deng et al., 2014).

Pig manure in general has a high nitrogen content, as it is a protein-rich substrate (Chen et al., 2008; Sommer et al., 2013). In this case, 30 to 40% of the degradable fraction was related to proteins. The TAN and TN content of LPM commonly vary from 3.2 to 6.3 g N kg^{-1} and 6.3 to 9.9 g N kg^{-1}, respectively (Coppens, 2009; de Haan et al., 2013; Verdoes, 2013; Sommer et al., 2015). For SPM, these values range from 2.7 to 6.0 g N kg^{-1} and 7.4 to 12.0 g N kg^{-1}, respectively (de Haan et al., 2013; Sommer et al., 2015; Vermeulen, 2019). The TN content is in general higher for mechanically SPM since the mass separation efficiency is higher than the nitrogen separation efficiency from raw manure to the solid fraction (Smets et al., 2018). The TAN content is slightly lower for SPM as soluble minerals rather accumulate in the liquid

than in the solid fraction (Vannecke et al., 2018). The same trends were found when comparing the values of the LPM and the source SPM used in this study. The pH of the SPM was slightly more acidic than expected, the pH of the LPM was mostly close to neutral (Sommer et al., 2015).

Thermal pre-treatment of LPM (A vs. A_p) did not change the manure composition, taking into account a mass loss of 1–2%. No significant increase in methane potential was thus induced, which contrasts with most results for substrates treated at higher temperatures or longer contact times (Wang et al., 1997; Bonmatí et al., 2001; González-Fernández et al., 2008). The obtained results were however in line with research on low temperature thermal pre-treatment such as the work of Appels et al. (2010), in which no significant solubilization of carbohydrates and proteins was detected after thermal treatment of sludge from a waste water treatment plant during 1 h at 70°C. Thermal pre-treatment of SPM did have an effect on the manure composition, though the effect was variable depending on the used manure. The protein and lipid content remained rather constant after thermal treatment. The change in carbohydrate content differed among the investigated samples (**Table 2** and **Supplementary Table A.1**). The difference in composition between SPM B_{p1} and SPM B_{p2} could be attributed to the difficulty for homogeneous and representative sampling, due to the high DM content, as the composition of the not pre-treated substrates was comparable.

Stability of Raw Substrate Digestion

Fresh Liquid Pig Manure

Digestion of LPM from farm A (experiment 1) yielded an average methane production of 359 L CH_4 kg^{-1} oDM during period 1a (**Table 3**). Methane production was higher than the analyzed methane potential of the substrate (**Table 2**), shown by an average relative efficiency exceeding 100% (**Figure 1A** and **Table 3**). This high percentage is due to the residual methane potential of the inoculum, with which the reactors were completely filled at the beginning of the experiments. The methane content remained relatively constant during the digestion period (**Supplementary Figure B.1**). However, after an operational period of about 1/2 of the HRT, it suddenly dropped from 66 to 55%. Likewise, the biogas production decreased by 33% (**Supplementary Figure B.1**), resulting in a drop in relative efficiency (**Figure 1A**). The sudden change in methane content and biogas production is a consequence of digester instability (Drosg, 2013). During period 1b, on average 225 L CH_4 kg^{-1} oDM was produced, which equals to an average relative efficiency of 63% (**Figure 1A** and **Table 3**). After an operational period of about 1/3 of the HRT, instability occurred again, characterized by a drop in methane content from 61 to 46% over a few days and a 37% decreased biogas production (**Supplementary Figure B.1**).

The concentration of TAN and ammonia were high with values of respectively, 3.4 g N kg^{-1} and 1.5 g NH_3-N kg^{-1} at the end of period 1a (**Table 4** and **Supplementary Figure B.1**). During the experimental period, the levels increased by 30–55% due to mineralization of organic nitrogen and preservation of a rather constant pH (Equation 4). Angelidaki and Ahring (1994) stated that for thermophilic digestion of manure inhibition may happen at an ammonia concentration exceeding 0.7 g NH_3-N kg^{-1}. Hansen et al. (1998) found values of 1.1 g NH_3-N kg^{-1} for thermophilic pig manure digestion. Rajagopal et al. (2013) summarized that digestion instability can be the result of TAN concentrations ranging from 1.5 to 7.0 g N kg^{-1}. The experimental values mostly exceeded the maximum values stated in literature, suggesting the occurrence of inhibition or even intoxication. However, ammonia inhibition and intoxication remain case-specific as they depend on pH, temperature, ionic strength, type of micro-organisms and their adaptation (Chen et al., 2008). At the end of period 1b, the concentration of TAN and ammonia were even higher with values of respectively 4.1 g N kg^{-1} and 2.1 g NH_3-N kg^{-1} (**Table 4**), resulting in more process inhibition and thus lower methane production values and relative efficiencies than during period 1a (**Figure 1A**).

H_2S concentrations up to 3,500 ppm were measured in the gas during period 1a (**Table 3** and **Supplementary Figure B.1**). An increasing H_2S concentration in the gas indicates the presence of sulfur-containing components in the liquid (manure). Sulfate reducing bacteria (SRB) compete with other micro-organisms for substrate to form sulfides (Deublein and Steinhauser, 2009; Chen et al., 2014). With methanogens, they compete for H_2 and acetic acid, thereby hindering methane production (Shah et al., 2014). Moreover, sulfides in the liquid, resulting from SRB activity, will at some point become inhibitory or even toxic for both methanogens and SRB (Chen et al., 2014). The inhibitory or toxic effect depends on the prevailing pH and temperature (Koster et al., 1986) as well as on the microbial adaptation (Chen et al., 2008). Not long after values of 1,500–2,000 ppm were reached, methane production started to decrease gradually until the point of failure (**Supplementary Figure B.1**). Both competition and high sulfide concentrations in the liquid presumably contributed to sudden process instability. In period 1b, H_2S concentrations of more than 4,000 ppm were detected in the gas (**Table 3**). The concentration varied strongly over time (**Supplementary Figure B.1**). Variation of H_2S concentration in the biogas can take place due to unexplainable reasons (Deublein and Steinhauser, 2009). Nonetheless, a sudden decrease in concentration could have been caused by the occurrence of some microaeration during the measurements, inducing biochemical oxidation of sulfide to elemental sulfur (Krayzelova et al., 2015). H_2S values were higher during period 1b and thus contributed to the reduced methane production and relative efficiency (**Table 3**), as was the case for ammonia. Nevertheless, the microbial community seemed to be slightly adapted to these inhibitors, by being subjected to gradually increasing concentrations during period 1a, as the digestion process was not disrupted immediately after exceeding high inhibitor values.

The total VFA concentration during period 1a (**Table 4**) was low to normal compared to the suggested values for proper digestion by Wiese and König (2007), ranging from 500 to 3,000 mg kg^{-1}. The acid production and consumption were thus in balance, indicating that the instability was not caused by overloading the system. This observation was confirmed by a FOS/TAC ratio lower than 0.4 (**Table 4**) which shows that the buffer capacity (TAC) was high compared

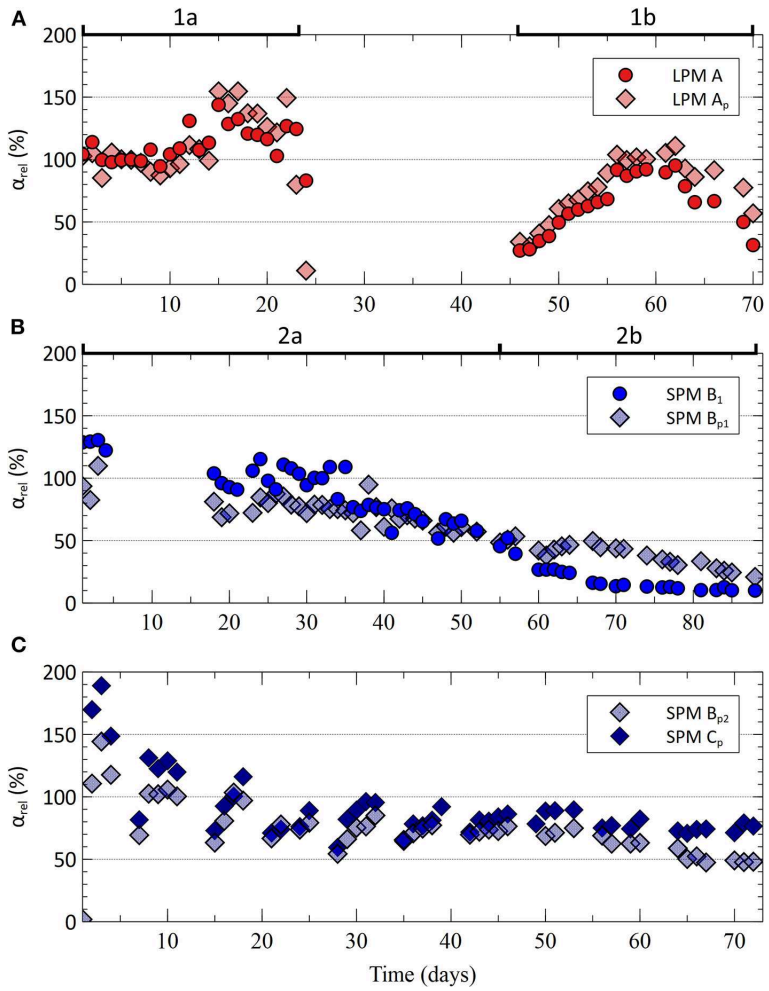

FIGURE 1 | Relative efficiency α_{rel}, defined as the ratio between the methane production obtained during the thermophilic mono-digestion experiments and the biochemical methane potential, on oDM base. **(A)** represents experiment 1 with the (not) pre-treated fresh liquid pig manure from farm A (LPM A and LPM A_p), digested at an HRT of 60 days (in period 1a and 1b), **(B)** experiment 2 with the (not) pre-treated fresh fecal fraction from source separation by a specific pig housing construction on farm B (SPM B_1 and SPM B_{p1}), digested at an HRT of 60 (period 2a) and 45 days (period 2b) and **(C)** experiment 3 with the pre-treated fresh fecal fractions from source separation by a similar pig housing construction on farm B and C (SPM B_{p2} and SPM C_p), digested at an HRT of 60 days. Data obtained during the acclimation period at an HRT of 100 days were not included in the figures.

to the FOS content (Wiese and König, 2007; Drosg, 2013). Immediately after instability, the VFA concentration, and more specifically the acetic acid concentration, increased rapidly indicating a disturbed digestion process. Due to (extreme) inhibition and intoxication, methanogenic activity can decrease, leading to an accumulation in VFAs (Parkin and Owen, 1986; Angelidaki and Ahring, 1994). At the beginning of period 1b, the microbiology had to cope with the restart of the feeding after instability, leading to somewhat higher VFA concentrations. However, after a while normal values were again reached (**Supplementary Figure B.1**). In contrast to period 1a, a constantly higher propionic acid concentration, sometimes exceeding the acetic acid concentration, was observed. Propionic acid accumulation can occur due to inhibition of propionate degrading acetogens by high ammonia concentrations (Calli et al., 2005). Furthermore, conversion of propionic acid is not thermodynamically favorable anymore at a hydrogen partial pressure exceeding values of 10^{-4} bar (McCarty and Smith, 1986). Such values can be induced by imbalance in the syntrophic relation between hydrogen-producing acetogens and hydrogen-consuming methanogens, due to inhibition of the latter (Parkin and Owen, 1986; Deublein and Steinhauser, 2009).

Fresh Separated Pig Manure

An average methane production of 259 L CH_4 kg^{-1} oDM and a relative efficiency of 89% were obtained during digestion of SPM from farm B (experiment 2) in period 2a (**Table 3** and **Figure 1B**). Note that at the beginning of this period, a temporary stop of the feeding was necessary due to a temperature problem in one of the reactors. This stop was applied to both CSTR 3 and 4 to preserve a correct basis for comparison. After restarting the feeding process,

the methane content was rather constant with values ranging from 56 to 64% (**Supplementary Figure B.3**). At the end of period 2a, the digester was completely run through with manure. A steady state should thus be reached if operation is maintained under the same conditions. **Supplementary Figure B.3** shows indeed that methane production decreased gradually tending to go to one value, namely 160 L CH_4 kg^{-1} oDM. This value was only 53% of the methane potential (**Table 2**), thus indicating process inhibition. The TAN and ammonia concentration were high with values up to 5.4 g N kg^{-1} and 2.2 g NH_3-N kg^{-1}, respectively, at the end of period 2a and mainly caused this inhibition. H_2S concentrations in the gas remained within an acceptable range (<1,700 ppm). The OLR reached values up to 4 g oDM L^{-1} d^{-1} (**Supplementary Figure B.3**), which should still be manageable for a microbiology adapted to thermophilic conditions according to Liu et al. (2017).

Despite some inhibition during period 2a, there were no specific signs of instability when assessing the change in methane content and individual VFA concentrations. The methanogenic community seemed to work properly as was demonstrated by the relatively constant methane content and both the rather low acetic acid (<1,000 mg kg^{-1}) and butyric acid concentrations (<20 mg kg^{-1}) at the end of period 2a. However, propionic acid accumulated to values up to 3,700 mg kg^{-1} (**Supplementary Figure B.3**). Propionic acid will more likely accumulate at higher DM contents, even though no inhibition due to ammonia or sulfur-containing components takes place, because the hydrogen partial pressure will increase due to the higher resistance to H_2-release (Corijn, 2017). The low acetic acid concentration and methane production could thus be the result of less propionic acid conversion. Despite the high VFA concentration, acidification did not occur, shown by the rather constant pH (**Supplementary Figure B.3**). This phenomenon is common for digestion of nitrogen-rich substrates such as pig manure, since ammonia serves as a strong buffer (Angelidaki and Ahring, 1994; Garcia and Angenent, 2009).

Around the moment of transition from an HRT of 60 days (period 2a) to an HRT of 45 days (period 2b), methane production values and relative efficiencies started to deviate from the steadily decreasing trend, suggesting some process instability (**Figure 1B** and **Supplementary Figure B.3**). Due to the set-up of the experiments, it was however not possible to identify with certainty whether instability occurred at the end of period 2a, during digestion at an HRT of 60 days, or at the start of period 2b, when the shift was made to an HRT of 45 days. During period 2b, digestion only yielded an average methane production of 58 L CH_4 kg^{-1} oDM. The average relative efficiency was 19% (**Figure 1B** and **Table 3**). The methane content started to decrease once an HRT of 45 days was reached (**Supplementary Figure B.3**). The increase in OLR up to 5.3 g oDM L^{-1} d^{-1} caused overloading of the system, inducing an increase in VFAs. Overloading was confirmed by the FOS/TAC ratio reaching values up to 0.84 (**Table 4**). The increase in VFAs resulted in acidification, shown by the decrease in pH from the start of period 2b (**Supplementary Figure B.3**). Methanogenic activity became inhibited by this low pH, demonstrated by the fast increase in acetic acid and butyric acid concentration (**Supplementary Figure B.3**), leading to even more acidification and ultimately extreme process disturbance. Although during period 2b the digestion process was mainly affected by a pH decrease, ammonia (< 2.2 g NH_3-N kg^{-1}) (**Table 4**) and H_2S (<2,100 ppm) (**Table 3**) also (in)directly contributed.

Effect of Thermal Pre-Treatment

Fresh Liquid Pig Manure

Figure 1A demonstrates that the same trend in relative efficiency was obtained for LPM A and LPM A_p over the two periods (experiment 1). This could be expected, as the composition of the not pre-treated and pre-treated manure was similar (**Table 2**). Instability occurred at the same moments (**Figure 1A** and **Supplementary Figures B.1, B.2**), more specifically after an operational period of 1/3–1/2 of the HRT. During period 2b, a slightly higher relative efficiency was obtained for the pre-treated sample (**Table 3** and **Figure 1A**). The change in ammonia and H_2S concentration over time was comparable for LPM A and LPM A_p (**Supplementary Figures B.1, B.2**). For LPM A_p, TAN and ammonia concentrations up to 4.3 g N kg^{-1} and 2.2 g NH_3-N kg^{-1} (**Table 4**), respectively, and H_2S concentrations close to 4,000 ppm (**Table 3**) were reached, both suggesting the occurrence of inhibition. After instability at the end of period 2a, a temporary stop of the feeding was sufficient for recovery of the microbiology digesting LPM A_p, while for the case of LPM A addition of inoculum was necessary.

Methane production values and relative efficiencies obtained for LPM A_p were similar to somewhat higher than those for LPM A (**Figure 1A**). This observation was in agreement with the results found by Appels et al. (2010), who investigated the influence of thermal pre-treatment at for example 70°C on mesophilic anaerobic digestion of sludge from a waste water treatment plant. Via batch anaerobic tests, Bonmatí et al. (2001) examined the effect of thermal pre-treatment at 80°C for 3 h on mesophilic digestion of pig slurry with a low (1.3 g N kg^{-1}) and high (3.7 g N kg^{-1}) TAN concentration. In the case of a low TAN concentration, methane production values were 45% higher upon thermal pre-treatment. Pre-treatment of pig slurry with a high TAN concentration showed to have a negative effect on methane production as ammonia inhibition occurred. Carrère et al. (2009) thermally pre-treated liquid pig manure at 70°C for 3 h, resulting in an increase in methane potential of the soluble fraction up to 70%. At 20 h of pre-treatment instead of 3 h, a 10% increase in methane production was found by Sutaryo et al. (2014) after 11 days of mesophilic digestion. However, the methane potential of the total fraction did not increase in both studies. González-Fernández et al. (2008) obtained a 35% increase in methane production after pre-treatment of pig slurry at 170°C for 30 min. It is clear that the possible increase in methane production by thermal treatment prior to digestion depends on the treatment duration, the applied temperature and the nitrogen content of the substrate. The aim of this study was to improve the process stability by thermal pre-treatment, and not necessarily the methane production. Nonetheless, the performed thermal pre-treatment did not succeed in advancing the LPM digestion stability.

Fresh Separated Pig Manure

Methane production values and relative efficiencies of SPM B_{p1} digestion at an HRT of 60 days (experiment 2, period 2a) were similar to those of SPM B_1 (**Figure 1B** and **Supplementary Figures B.3, B.4**). This is in agreement with the results of Rafique et al. (2010) who did not find an increase in methane production after thermally pre-treating the solid fraction of pig manure for 1 h at 70°C. According to Sutaryo et al. (2014), prolonging this pre-treatment time to 20 h results in an 11% increased methane production after 11 days of mesophilic digestion. Raju et al. (2013) achieved a 29% increase after 27 days of mesophilic digestion by thermal pre-treatment for 15 min at 200°C. Nonetheless, the observed values in the experiment with thermal pre-treatment decreased more steadily with less variation (**Figure 1B** and **Supplementary Figures B.3, B.4**). The steady state value was lower than the methane potential (**Table 2**) due to propionic acid accumulation and inhibition mainly by ammonia (<2.3 g NH_3-N kg^{-1}) (**Table 4**), as was also the case for SPM B_1. Some foam was formed during digestion of SPM B_1, however not to such extent that it affected the process. Almost no foam was observed when digesting SPM B_{p1}. Furthermore, values of 4,100 and 930 mPa s were obtained for the digestate viscosity of SPM B_1 and SPM B_{p1}, respectively, implying that digestate becomes less viscous when SPM is thermally pre-treated.

The digestion process with SPM B_{p1} was relatively stable and close to the steady state value during the first 2 weeks of period 2b, after transition to an HRT of 45 days and a short adaptation period (**Figure 1B** and **Supplementary Figure B.4**). The methane content remained rather constant up to 3 weeks. The buffer capacity was sufficient to cope with the increasing amount of VFAs, reaching values up to 12.5 g kg^{-1}. However, due to the need for such a high buffer capacity, ammonia concentrations remained high (**Table 4**) leading to further inhibition. In general, a more stable digestion process was observed upon thermal pre-treatment, as this may have induced the higher resistance to inhibiting factors, such as ammonia and sulfur-containing components.

Although there are signs that instability only occurred multiple days after the transition to an HRT of 45 days, some uncertainty remains as the HRT was adapted not long after the reactor was completely run through with SPM B_{p1}. To elucidate the effect of the HRT, an additional experiment (experiment 3) was conducted in which pre-treated SPM from farm B (SPM B_{p2}) was again digested at an HRT of 60 days, however over a longer time period. Parallel to this, the pre-treated SPM from another farm with a similar pig housing construction (SPM C_p) was digested. Experiment 3 only focused on pre-treated SPM, as this induced the most promising results in experiment 2.

An average methane production of 226 and 280 L CH_4 kg^{-1} oDM was obtained during digestion of SPM B_{p2} and SPM C_p, respectively (**Table 3**). The average relative efficiency was respectively, 74 and 95% (**Figure 1C** and **Table 3**). The former was equal to the value obtained during experiment 2 with manure from the same farm. The lowest methane production values were mostly reached after a non-feeding period of a few days (e.g., weekend). The methane content remained rather constant (**Supplementary Figures B.5, B.6**).

In general, a gradually decreasing methane production and relative efficiency, with the tendency to go to one value, were observed for both SPM B_{p2} and SPM C_p until about one HRT (**Figure 1C** and **Supplementary Figures B.5, B.6**). In the case of SPM C_p, a steady-state value of 220 L CH_4 kg^{-1} oDM or 40 L CH_4 kg^{-1} manure (**Supplementary Figure B.6**) was ultimately reached, indicating a relatively stable digestion of SPM C_p. If the obtained value would be the actual methane production in a farm-scale digester, assuming that the transfer of this fresh manure to the digester is technically feasible, about 17 kWe could be generated given a daily feeding amount of 5 tons, a conversion factor of 10 kWh m^{-3} methane (Banks, 2009) and an electrical efficiency of 21%. In this experiment, the steady-state value corresponded to a relative efficiency of 75% (**Figure 1C**), indicating some inhibition. High ammonia levels (>2 g NH_3-N kg^{-1}) (**Table 4**) were the predominant cause of this inhibition. The H_2S content in the gas stayed below 900 ppm (**Table 3**). In the case of SPM B_{p2}, the methane production decreased further without reaching a clear steady-state value. Ammonia and H_2S levels were slightly higher during digestion of SPM B_{p2} as well as the OLR, reaching values of 3.6 instead of 3.0 g oDM L^{-1} d^{-1} (**Supplementary Figures B.5, B.6**). The higher OLR caused some overloading of the reactor, shown by a FOS/TAC ratio of 0.63 at the end of the experimental period (**Table 4**).

VFAs accumulated strongly, especially during digestion of SPM B_{p2} (**Table 4**). Propionic acid concentrations were higher compared to the other measured VFAs due to the high DM content of manure (**Supplementary Figures B.5, B.6**). The pH decrease by the end of the experiment with SPM B_{p2} demonstrated the occurrence of acidification due to VFA accumulation. No significant pH decrease was detected for SPM C_p. Viscosity measurements showed that the digestate resulting from digestion of SPM C_p was less viscous, 550 instead of 1,550 mPa s, thus leading to better H_2-release and less propionic acid accumulation. In general, almost no foam was detected during digestion of both pre-treated substrates.

Effect of Separation

Figure 2 shows the effect of DM content, H_2S concentration in the gas and ammonia concentration on the methane production during LPM and SPM digestion. The average values were derived from the experiments performed at an HRT of 60 days. Additional values observed after recovery and continuation of the digestion process with (pre-treated) LPM A (experiment 1) and SPM B_1 (experiment 2) were included, however were not previously described as they did not provide new perspectives on the digestion stability. Methane production on oDM base by SPM digestion, including results for not pre-treated and pre-treated substrates, was on average 42% higher than by LPM digestion (**Figure 2A**). Conversion to mass base showed that methane production by SPM digestion was on average over three times higher, indicating the effect of partial removal of the low energy liquid fraction (Asam et al., 2011; Deng et al., 2014), which was in this case mainly urine.

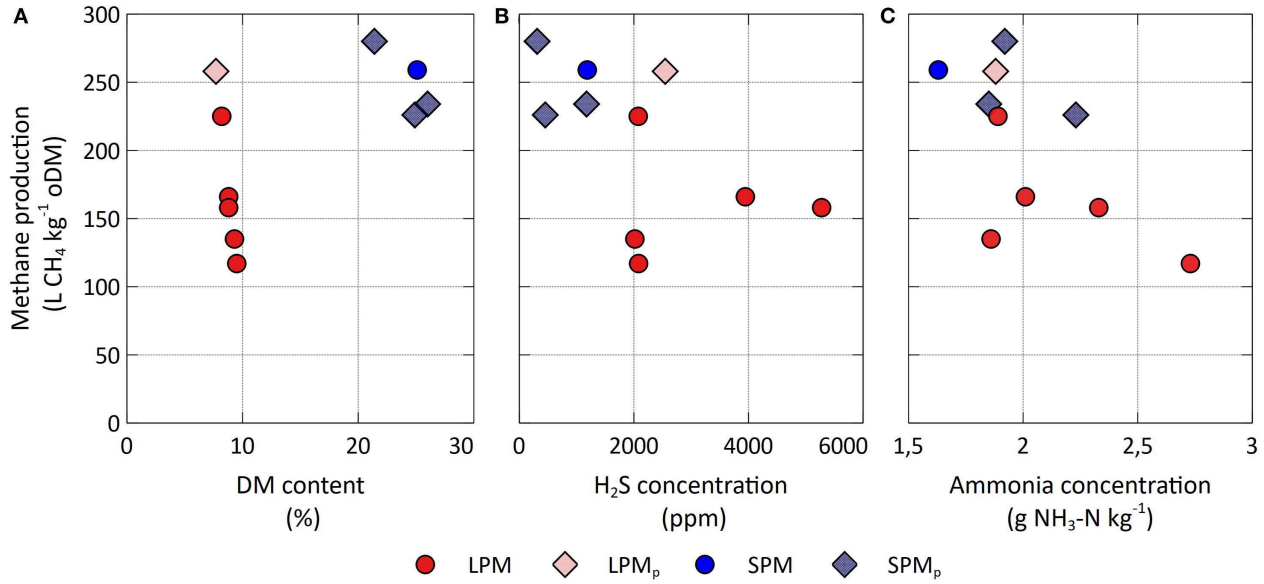

FIGURE 2 | The effect of **(A)** average DM content (%), **(B)** H_2S concentration in the gas (ppm) and **(C)** ammonia concentration (g NH_3-N kg^{-1}) on the average methane production obtained during thermophilic digestion of (not) pre-treated fresh liquid pig manure (LPM) and of the (not) pre-treated fresh fecal fraction from source separation by a specific pig housing construction (SPM), at an HRT of 60 days. Note that the OLR varied between the experiments. The figure did not include period 1a for LPM A and LPM A_p (experiment 1) due to the effect of the inoculum. The results of all other experimental periods at an HRT of 60 days were shown, including some values observed after continuation of the experiments with (pre-treated) LPM A and SPM B_1, which were not specifically mentioned in the main article.

The digestion process proved to be more stable for separated substrates. This is in accordance with previous research which reported (extreme) inhibition and/or instability when the liquid fraction of manure was still present during digestion and when initial TAN and sulfide concentrations were high (Hashimoto, 1983, 1986; Sutaryo et al., 2013). In contrast, Møller et al. (2007) achieved a stable process when liquid pig manure, with or without being partly substituted by its solid fraction (up to 60% on mass base), was digested. In general, the methane production decreased when the concentration of ammonia or H_2S in the gas increased (**Figure 2**). The lower H_2S concentrations in the gas when digesting SPM instead of LPM (**Figure 2B**) were in line with the statement of Deublein and Steinhauser (2009), that the H_2S content will be higher when digesting liquid substrates, and indicated the occurrence of less sulfide inhibition during SPM digestion. The ammonia concentration was in general only slightly lower for SPM than LPM substrates (**Figure 2C**). These findings suggest that the main cause of instability was the excess of sulfur-containing components. High concentrations of ammonia seem to have resulted in inhibition, but not necessarily in instability.

For the case of SPM, the digestion stability seemed to be affected by the (organic) DM content. The most stable digestion process was observed for the thermally pre-treated fecal fraction from farm C, having a DM content of 21% (experiment 3). At DM contents up to 26%, some instability occurred (experiment 2 and 3). In general, a higher OLR and more propionic acid accumulation during digestion were induced for substrates with a higher (organic) DM content and resulted in lower methane production values (**Supplementary Figures B.3, B.6**). The (organic) DM content of separated manure is directly related to the extent of separation, and more specifically to the remaining fraction of urine in the manure. Besides the (organic) DM content, farm-specific properties could also have contributed to a change in digestion stability.

Perspectives

Liquid Pig Manure Digestion

The experiment with LPM showed that stable thermophilic mono-digestion will be a challenge as inhibition and intoxication by ammonia and sulfur-containing components is facilitated. In the case of mono-digestion, some strategies to reduce ammonia inhibition during digestion are controlling the pH or temperature (Rajagopal et al., 2013), as at lower values, less ammonia is formed (Equation 4). Tackling sulfur issues is not only related to process stability but also to avoiding corrosion of equipment, such as the combustion engine and piping (Wellinger and Lindberg, 2005). In practice, H_2S is often dealt with, during or after digestion, through biological desulfurization by air (microaeration) or oxygen dosing, through adsorption on activated carbon or through precipitation by addition of iron salts (Wellinger and Lindberg, 2005; Deublein and Steinhauser, 2009).

Research on substrate pre-treatment aimed at (partial) removal of nitrogen and sulfur-containing components is limited. In the case of sulfur, it could however eliminate undesirable side effects of (partial) removal techniques, which are applied during or after the digestion process. Side effects may be: process disturbance by too much air or oxygen dosing, damage of the equipment by insufficient replacement of the activated carbon or formation of impregnable phosphate components

after digestate fertilization. Ammonia could be removed prior to digestion by means of a stripping and scrubbing process (Ghyselbrecht et al., 2018; Bijnagte, 2019) or through gas-permeable membranes (Filho et al., 2018). At this moment, such techniques still come at a high cost. In view of future farm-scale implementations, attention should be given to low-cost inhibitor removal techniques prior to digestion. Besides, the single and combined effect of (partial) removal or avoidance of these inhibitors on the digestion stability as well as the necessary extent of inhibitor removal needs further elaboration.

This study focused on mono-digestion because of its link to decentralized digestion on farms. Pig farmers often have no other agricultural by-products for digestion apart from pig manure. Besides, Flemish legislation does not promote co-digestion of manure and agro-residues at this moment, as the resulting digestate is completely categorized as animal manure, while part originates from agro-residues (Vlaamse Overheid, 2019). However, co-digestion of pig manure with carbon-rich agro-residues could increase the C:N ratio of the digested substrate, thereby lowering the risk for ammonia inhibition (Rajagopal et al., 2013). Co-digestion of pig manure, whether or not combined with a sulfur removal process, could thus possibly induce a (more) stable LPM digestion. However, research should be conducted on which and how much co-substrates should be added in proportion to manure.

In this study, instability of LPM digestion occurred after specific operational periods. Regular addition of inoculum or a regular stop of the feeding could ensure preservation of an active microbiology that can cope with inhibiting and limiting factors under the investigated conditions. In practice, the application of this approach will be difficult, due to the related economic losses and additional work load. Adaptation of the microbiology to its inhibitors can be a solution to some extent (Deublein and Steinhauser, 2009; Chen et al., 2014). However, practical implementation of microbial adaptation before digestion should be evaluated.

Separated Pig Manure Digestion

The experiments with SPM demonstrated the potential for stable thermophilic mono-digestion at an HRT of 60 days. The most stable digestion process was observed for the thermally pre-treated fecal fraction with a DM content of 21%. At higher DM contents, some instability occurred due to an increase in OLR and propionic acid accumulation, suggesting an effect of the (organic) DM content on the digestion stability. Further research, focusing on the 15 to 25% DM range, could explore whether an optimal (organic) DM content for stable thermophilic digestion of SPM with a high nitrogen content exists. Based on the outcome of this research, the required extent of separation can be determined, thereby evaluating if it can be accomplished by both source separation by an animal housing construction and mechanical separation.

Thermal Pre-Treatment

A thermal pre-treatment for 1 h at 70°C was chosen to keep the total thermal demand of decentralized digestion on farms as low as possible, although increased treatment times or temperatures could improve methane production (Wang et al., 1997; Valo et al., 2004; Appels et al., 2010; Rafique et al., 2010; Raju et al., 2013; Sutaryo et al., 2014). Moreover, from practical point of view, a thermal treatment for 1 h at 70°C ensures pasteurization of manure, i.e., the destruction of harmful bacteria and germs (FAVV, 2017), making export possible (European Commission, 2009).

Heat is not only necessary for thermal pre-treatment but also to keep the manure in the digester on temperature (De Dobbelaere et al., 2015; Paterson, 2015). The heat demand will be higher for LPM due to its higher water content (Asam et al., 2011). In this study, the water content of LPM was over 90% of the total mass, for SPM this was up to 79% (**Table 2**). Excess heat from the combined heat and power unit could be used to perform the thermal pre-treatment. The degree of excess depends on the heat demand of the farm and the digester implementation, and is also directly related to the prevailing outside air temperature. The heat requirement of a well-insulated digester is expected to be low, because heated substrate will be fed daily. Due to the lower water content of SPM, less heat will probably be necessary to cover the demand for pre-treatment and digester, thus making implementation more feasible.

Furthermore, thermal pre-treatment positively affected the digestion stability of the investigated SPM, especially at lower HRTs. Additional experiments are needed, simultaneous to the suggested ones for the determination of an optimal (organic) DM content, to discover whether thermal pre-treatment is always necessary for process stability in that DM range.

Operational Restrictions

The use of fresh pig manure is essential in view of maximizing methane formation and thus renewable energy production through anaerobic digestion. de Buisonjé and Verheijen (2014) found that the biogas potential of liquid pig manure reduces by more than 30% after pre-storage for 1 month. The current standard pig farms, consisting of a manure pit below the slatted floor of the animal housing, do not allow for collection of fresh pig manure. The fecal fraction, resulting from source separation by a specific pig housing construction with manure scrapers, can be collected freshly. Nonetheless, under the current conditions, investments in such pig housing constructions will probably remain limited in Flanders, especially if no stable digestion process can be guaranteed, as long as end-of-pipe techniques (such as air scrubbers) are sufficient for reduction of ammonia emissions and no additional standards are imposed on greenhouse gas emission reduction. Both fresh pig manure collection and stable digestion are thus crucial toward practical implementation and require further investigation.

Besides fresh pig manure collection, attention should be given to the transfer of manure from animal housings to the digester. If digestion takes place in a CSTR, keeping the manure pumpable is recommended to limit costs. No problems in terms of pumpability are expected with liquid pig manure. However, the investigated fecal fractions (SPM B and C), which proved to be more promising in terms of digestion stability, had a DM content up to 26%, suggesting that transfer through piping

will be difficult. In the context of practical implementation, this manure-specific property will thus have to be taken into account.

The HRT maintained in the digester is directly related to the digester volume. If long HRTs are required, a larger digester can be implemented. Due to the digester volume increase, the OLR will decrease if the daily feeding amount remains constant (Equation 5). However, a larger digester will induce higher investment costs. Promising results in terms of stability were obtained during the digestion experiments with SPM at an HRT of 60 days. At an HRT of 45 days, methane production values were low. In practice, the HRT of farm-scale mesophilic digesters is recommended to be 30 days (De Dobbelaere and Verleden, 2018). HRTs of thermophilic digesters are expected to be even lower (Al Seadi et al., 2008). In view of cost reduction, achieving stable digestion at lower HRTs seems necessary. Nonetheless, the HRT should be kept high enough, so that the residual methane potential of digestate remains limited (Vergote et al., 2019).

Moreover, this study focused on thermophilic digestion of pig manure. Under thermophilic conditions, the growth rate of the microbiology will increase. Furthermore, the digestibility is enhanced (Al Seadi et al., 2008), which is important for substrates such as manure, mainly consisting of non-readily biodegradable compounds (Vavilin et al., 1996). However, at thermophilic temperatures, the risk for inhibition may be higher than at mesophilic temperatures, if no substrate pre-treatment takes place or under other specific conditions (Al Seadi et al., 2008; Chen et al., 2014). A techno-economic assessment would be valuable to find the most optimal farm-scale implementation taking into account digestion of pig manure at these two temperature regimes.

CONCLUSIONS

No stable thermophilic mono-digestion of fresh liquid pig manure was observed at an HRT of 60 days, due to too high concentrations of ammonia and sulfur-containing components. Thermophilic mono-digestion of the fresh fecal fraction from source separation by a specific pig housing construction was more stable, if allowed sufficient time for digestion. The H_2S concentration in the gas was much lower when mono-digesting the fecal fraction instead of liquid pig manure, suggesting the excess of sulfur-containing components to be the main driver for instability. The stability of the digestion process with the fecal fraction further improved by thermal pre-treatment at 70°C for 1 h, though seemed to be affected by the (organic) dry matter content. No improvement was noted for liquid pig manure.

In general, (source) separation, possibly followed by a thermal pre-treatment, appeared to be a promising strategy in view of thermophilic pig manure mono-digestion, since it improved the process stability and increased the energy content on mass base. However, toward practical implementation, further elaboration or research is required on the extent of separation, the necessity for thermal pre-treatment and its techno-economic evaluation, (partial) inhibitor removal prior to digestion, fresh manure collection, and manure transfer to the digester.

DATA AVAILABILITY STATEMENT

The datasets generated for this study are available on request to the corresponding author.

AUTHOR CONTRIBUTIONS

TV, BW, AD, JL, and EM developed the experimental set-up. TV, BW, and AD took care of substrate and inoculum collection. TV and BW were involved in the execution of the experiments with input from AD, JL, and EM. BW supervised the chemical analyses. TV conducted data processing and wrote the manuscript. TV, BW, AD, JL, and EM discussed the results. AD, JL, JB, EV, and EM read and commented on the manuscript.

FUNDING

This work was supported by the LA project Pocket Power (150913), funded by Flanders Innovation and Entrepreneurship (VLAIO, http://www.vlaio.be).

ACKNOWLEDGMENTS

The authors thank Innolab for the opportunity to perform experiments at the facility, for the technical support and for sharing knowledge. The owners of the pig farms are acknowledged for giving access to their facility for manure collection.

SUPPLEMENTARY MATERIAL

The Supplementary Material for this article can be found online at: https://www.frontiersin.org/articles/10.3389/fenrg.2020.00040/full#supplementary-material

REFERENCES

Ahmed, J., Ramaswamy, H. S., Alli, I., Raghavan, V. G. S., Ahmed, J., Ramaswamy, H. S., et al. (2007). Protein denaturation, rheology, and gelation characteristics of radio-frequency heated egg white dispersions. *Int. J. Food Prop.* 10, 145–161. doi: 10.1080/10942910600986970

Al Seadi, T., Rutz, D., Prassl, H., Köttner, M., Finsterwalder, T., Volk, S., et al. (2008). *Biogas Handbook*. Esbjerg: University of Southern Denmark Esbjerg. doi: 10.1533/9780857097415.1.85

Angelidaki, I., and Ahring, B. K. (1994). Anaerobic thermophilic digestion of manure at different ammonia loads: effect of temperature. *Water Res.* 28, 727–731.

Appels, L., Degrève, J., Van der Bruggen, B., Van Impe, J., and Dewil, R. (2010). Influence of low temperature thermal pre-treatment on sludge solubilisation, heavy metal release and anaerobic digestion. *Bioresour.Technol.* 101, 5743–5748. doi: 10.1016/j.biortech.2010.02.068

Asam, Z.-Z., Poulsen, T. G., Nizami, A.-S., Rafique, R., Kiely, G., and Murphy, J. D. (2011). How can we improve biomethane production per unit of feedstock

in biogas plants? *Appl. Energy* 88, 2013–2018. doi: 10.1016/j.apenergy.2010.12.036

Banks, C. (2009). *Optimising Anaerobic Digestion - Evaluating the Potential for Anaerobic Digestion to Provide Energy and Soil Amendment*. University of Reading.

Bijnagte, J. W. (2019). POULAR - Poultry *Manure De-ammonification* as *Pre*-treatment for *Anaerobic Digestion*.

Bonmatí, A., Flotats, X., Mateu, L., and Campos, E. (2001). Study of thermal hydrolysis as a pretreatment to mesophilic anaerobic digestion of pig slurry. *Water Sci. Technol.* 44, 109–116. doi: 10.2166/wst.2001.0193

Calli, B., Mertoglu, B., Inanc, B., and Yenigun, O. (2005). Effects of high free ammonia concentrations on the performances of anaerobic bioreactors. *Proc. Biochem.* 40, 1285–1292. doi: 10.1016/j.procbio.2004.05.008

Carrère, H., Sialve, B., and Bernet, N. (2009). Improving pig manure conversion into biogas by thermal and thermo-chemical pretreatments. *Bioresour. Technol.* 100, 3690–3694. doi: 10.1016/j.biortech.2009.01.015

Chen, J. L., Ortiz, R., Steele, T. W. J., and Stuckey, D. C. (2014). Toxicants inhibiting anaerobic digestion: a review. *Biotechnol. Adv.* 32, 1523–1534. doi: 10.1016/j.biotechadv.2014.10.005

Chen, Y., Cheng, J. J., and Creamer, K. S. (2008). Inhibition of anaerobic digestion process: a review. *Bioresour. Technol.* 99, 4044–4064. doi: 10.1016/j.biortech.2007.01.057

Climent, M., Ferrer, I., Baeza, M., del, M., Artola, A., Vázquez, F., et al. (2007). Effects of thermal and mechanical pretreatments of secondary sludge on biogas production under thermophilic conditions. *Chem. Eng. J.* 133, 335–342. doi: 10.1016/j.cej.2007.02.020

Coppens, G. (2009). Overzicht van 15 *Jaar Mestanalyse Door* de *Bodemkundige Dienst* van *België*.

Corijn, S. (2017). *Accumulatie van Propionzuur en het Biologisch Herstel Ervan Door Sulfaat*.

de Buisonjé, F., and Verheijen, R. (2014). *Drijfmest Verliest Snel Zijn Waarde Voor Biogas*. V-Focus; Rubriek Onderzoek & Beleid.

De Dobbelaere, A., De Mey, J., Lebuf, V., Ryckaert, B., Schollier, C., and Van Driessche, J. (2015). *Kleinschalige vergisting: Praktijkvoorbeelden uit binnen- & buitenland*. Inagro.

De Dobbelaere, A., and Verleden, I. (2018). *Enquête project Pocketboer - Impact van reactorinstellingen op energieproductie*. Unpublished data. Inagro.

de Haan, J., van Geel, W., Paauw, J., van der Burgt, G.-J., Hospers, M., Venhuizen, A., et al. (2013). *Databank Organische Meststoffen*. Retrieved from: https://www.researchgate.net/publication/289128391_Databank_organische_meststoffen (accessed November 22, 2019).

Decorte, M., Tessens, S., and Winternitz, K. (2019). *De Vlaamse biogassector in 2018*. Voortgangsrapport Biogas-E.

Deng, L., Li, Y., Chen, Z., Liu, G., and Yang, H. (2014). Separation of swine slurry into different concentration fractions and its influence on biogas fermentation. *Appl. Energy*. 114, 504–511. doi: 10.1016/j.apenergy.2013.10.018

Deublein, D., and Steinhauser, A. (2009). *Biogas From Waste and Renewable Resources (2nd Edn)*. Weinheim: WILEY-VCH Verlag GmbH & Co. KGaA.

Drosg, B. (2013). *Process Monitoring in Biogas Plants*. IEA Bioenergy.

European Commission (2009). *Verordening (EG) nr. 1069/2009 van het Europees Parlement en de Raad van 21 Oktober 2009 tot Vaststelling van Gezondheidsvoorschriften Inzake Niet Voor Menselijke Consumptie Bestemde Dierlijke Bijproducten en Afgeleide Producten en Tot Intrekking van Vero*. Publicatieblad van de Europese Unie, nr. L 300. Available online at: https://eur-lex.europa.eu/legal-content/NL/ALL/?uri=CELEX%3A32009R1069

FAVV (2017). Risico van de *Verspreiding* van *Mest* en *Mestdigestaten Gecontamineerd Door Clostridium botulinum*. FAVV.

Filho, J., de, S. O., Daguerre-Martini, S., Vanotti, M. B., Saez-Tovar, J., Rosal, A., et al. (2018). Recovery of ammonia in raw and co-digested swine manure using gas-permeable membrane technology. *Front. Sustain. Food Syst.* 2, 1–9. doi: 10.3389/fsufs.2018.00030

Garcia, M. L., and Angenent, L. T. (2009). Interaction between temperature and ammonia in mesophilic digesters for animal waste treatment. *Water Res.* 43, 2373–2382. doi: 10.1016/j.watres.2009.02.036

Gavala, H. N., Yenal, U., Skiadas, I. V., Westermann, P., and Ahring, B. K. (2003). Mesophilic and thermophilic anaerobic digestion of primary and secondary sludge. Effect of pre-treatment at elevated temperature. *Water Res.* 37, 4561–4572. doi: 10.1016/S0043-1354(03)00401-9

Ghyselbrecht, K., Monballiu, A., Somers, M. H., Sigurnjak, I., Meers, E., Appels, L., et al. (2018). Stripping and scrubbing of ammonium using common fractionating columns to prove ammonium inhibition during anaerobic digestion. *Int. J. Energy Environ. Eng.* 9, 447–455. doi: 10.1007/s40095-018-0283-7

González-Fernández, C., León-Cofreces, C., and García-Encina, P. A. (2008). Different pretreatments for increasing the anaerobic biodegradability in swine manure. *Bioresour. Technol.* 99, 8710–8714. doi: 10.1016/j.biortech.2008.04.020

Hansen, K. H., Angelidaki, I., and Ahring, B. K. (1998). Anaerobic digestion of swine manure: inhibition by ammonia. *Water Res.* 32, 5–12. doi: 10.1016/S0043-1354(97)00201-7

Hashimoto, A. G. (1983). Thermophilic and mesophilic anaerobic fermentation of swine manure. *Agr. Wastes* 6, 175–191.

Hashimoto, A. G. (1986). Ammonia inhibition of methanogenesis from cattle wastes. *Agr Wastes* 17, 241–261. doi: 10.1016/0141-4607(86)90133-2

Henneberg, W., and Stohman, F. (1860). *Begründung einer rationellen Ftterung der Wiederkäuer. Vol. 1*. Braunschweig: Schwetschtke u. Sohn.

Hjorth, M., Christensen, K. V., Christensen, M. L., and Sommer, S. G. (2010). Solid-liquid separation of animal slurry in theory and practice. A review. *Agron. Sustain. Dev.*30, 153–180.

Ichimura, Y. (1991). *Thermal Denaturation of Proteins II*. Tokyo: Hitachi High-Tech Science Corporation.

Jain, S., Newman, D., Nzihou, A., Dekker, H., Le Feuvre, P., Richter, H., et al. (2019). *Global Potential of Biogas*. World Biogas Association.

Koster, I. W., Rinzema, A., De Vegt, A. L., and Lettinga, G. (1986). Sulfide inhibition of the methanogenic activity of granular sludge at various pH-levels. *Water Res.* 20, 1561–1567. doi: 10.1016/0043-1354(86)90121-1

Krayzelova, L., Bartacek, J., Díaz, I., Jeison, D., Volcke, E. I. P., and Jenicek, P. (2015). Microaeration for hydrogen sulfide removal during anaerobic treatment: a review. *Rev. Environ. Sci. Bio/Technol.* 14, 703–725. doi: 10.1007/s11157-015-9386-2

Liebetrau, J., Sträuber, H., Kretzschmar, J., Denysenko, V., and Nelles, M. (2019). Anaerobic Digestion. *Adv. Biochem. Eng. Biotechnol.* 166, 281–300. doi: 10.1007/10

Lindorfer, H., and Demmig, C. (2016). Foam formation in biogas plants–a survey on causes and control strategies. *Chem. Eng. Technol.* 39, 620–626. doi: 10.1002/ceat.201500297

Liu, C., Wang, W., Anwar, N., Ma, Z., Liu, G., and Zhang, R. (2017). Effect of organic loading rate on anaerobic digestion of food waste under mesophilic and thermophilic conditions. *Energy Fuels* 31, 2976–2984. doi: 10.1021/acs.energyfuels.7b00018

Matulaitis, R., Juškien,e, V., and Juška, R. (2015). Measurement of methane production from pig and cattle manure in Lithuania. *Zemdirbyste-Agr.* 102, 103–110. doi: 10.13080/z-a.2015.102.013

McCarty, P. L., and Smith, D. P. (1986). Anaerobic wastewater treatment. *Environ. Sci. Technol.* 20, 1200–1206. doi: 10.1021/es00154a002

Møller, H. B., Nielsen, A. M., Nakakubo, R., and Olsen, H. J. (2007). Process performance of biogas digesters incorporating pre-separated manure. *Livest. Sci.* 112, 217–223. doi: 10.1016/j.livsci.2007.09.014

Møller, H. B., Sommer, S. G., and Ahring, B. K. (2004). Methane productivity of manure, straw and solid fractions of manure. *Biomass Bioenergy*. 26, 485–495. doi: 10.1016/j.biombioe.2003.08.008

Nordmann, W. (1977). *Die Überwachung der Schlammfaulung*. KA-Informationen für das Betriebspersonal, Beilage zur Korrespondenz Abwasser, 3/77.

Parkin, G. F., and Owen, W. F. (1986). Fundamentals of Anaerobic Digestion of Wastewater Sludges. *J. Environ. Eng.* 112, 867–920. doi: 10.1061/(ASCE)0733-9372(1986)112:5(867)

Paterson, M. (2015). *Kleinschalige Vergisting in de Praktijk - Handboek Voor Landbouwers*. BioEnergy Farm II Publication; KTBL.

Pavlostathis, S. G., and Giraldo-Gomez, E. (1991). Kinetics of anaerobic treatment: a critical review. *Crit. Rev. Environ. Contr.* 21, 411–490. doi: 10.1080/10643389109388424

Rafique, R., Poulson, T. G., Nizami, A., Asam, Z., Murphy, J. D., and Kiely, G. (2010). Effect of thermal, chemical and thermo-chemical pre-treatments to enhance methane production. *Energy* 35, 4556–4561. doi: 10.1016/j.energy.2010.07.011

Rajagopal, R., Massé, D. I., and Singh, G. (2013). A critical review on inhibition of anaerobic digestion process by excess ammonia.

Bioresour. Technol. 143, 632–641. doi: 10.1016/j.biortech.2013.06.030

Raju, C. S., Sutaryo, S., and Ward, A. J. (2013). Effects of high-temperature isochoric pre- treatment on the methane yields of cattle, pig and chicken manure. *Environ. Technol.* 34, 239–244. doi: 10.1080/09593330.2012.689482

Scarlat, N., Fahl, F., Dallemand, J.-F., Monforti, F., and Motola, V. (2018). A spatial analysis of biogas potential from manure in Europe. *Renew. Sustain. Energy Rev.* 94, 915–930. doi: 10.1016/j.rser.2018.06.035

Shah, F. A., Mahmood, Q., Shah, M. M., Pervez, A., and Asad, S. A. (2014). Microbial ecology of anaerobic digesters: the key players of anaerobiosis. *Sci. World J.* 2014:183752. doi: 10.1155/2014/183752

Skiadas, I. V., Gavala, H. N., Lu, J., and Ahring, B. K. (2005). Thermal pre-treatment of primary and secondary sludge at 70°C prior to anaerobic digestion. *Water Res.* 52, 161–166.

Smets, S., Palmans, S., and Luys, L. (2018). *Dikke Fractie: Praktijkgids Voor Productie en Aanwending*. Uitgegeven door PIBO-Campus vzw; PVL Bocholt vzw en VCM vzw.

Sommer, S. G., Christensen, M. L., Schmidt, T., and Jensen, L. S. (2013). *Animal Manure Recycling: Treatment and Management*. John Wiley & Sons Ltd.

Sommer, S. G., Hjorth, M., Leahy, J. J., Zhu, K., Christel, W., Sørensen, C. G., et al. (2015). Pig slurry characteristics, nutrient balance and biogas production as affected by separation and acidification. *J. Agr. Sci.* 153, 177–191. doi: 10.1017/S0021859614000367

Sutaryo, S., Ward, A. J., and Møller, H. B. (2013). Anaerobic digestion of acidified slurry fractions derived from different solid–liquid separation methods. *Bioresour. Technol.* 130, 495–501. doi: 10.1016/j.biortech.2012.12.037

Sutaryo, S., Ward, A. J., and Møller, H. B. (2014). The effect of low-temperature thermal pre-treatment on methane yield of pig manure fractions. *Anim. Prod.* 16, 55–62.

Trabue, S. L., Kerr, B. J., and Scoggin, K. D. (2019). Swine diets impact manure characteristics and gas emissions : Part I sulfur level. *Sci. Total Environ.* 687, 800–807. doi: 10.1016/j.scitotenv.2019.06.130

Valo, A., Carrère, H., and Delgenès, J. P. (2004). Thermal, chemical and thermo-chemical pre-treatment of waste activated sludge. *J. Chem. Technol. Biotechnol.* 79, 1197–1203. doi: 10.1002/jctb.1106

van Lier, J. B. (1995). *Thermophilic anaerobic wastewater treatment; Temperature aspects and process stability* (Ph.D. thesis), Wageningen Agricultural University, Wageningen, The Netherlands.

Van Overbeke, P., D'Hoop, M., Van Ransbeeck, N., and Demeyer, P. (2010). *Code van Goede Praktijk Voor Emissiearme Stalsystemen in de Varkenshouderij*. ILVO.

Van Ranst, E., Verloo, M., Demeyer, A., and Pauwels, J. M. (1999). *Manual for the Soil Chemistry and Fertility Laboratory: Analytical Methods of Soils and Plants Equipment and Management of Consumables*. Ghent: University of Ghent, International Training Centre for Post-Graduate Soil Scientists.

Vannecke, T., Gorissen, A., and Vanrespaille, H. (2018). *Literatuurstudie: Waarde van de Dikke Fractie na Mestscheiding als Bron van Organische stof*. Uitgegeven door het Vlaams Coördinatiecentrum voor Mestverwerking vzw te Brugge.

Vavilin, V. A., Rytov, S. V., and Lokshina, L. Y. (1996). A description of hydrolysis kinetics in anaerobic degradation of particulate organic matter. *Biores. Technol.* 56, 229–237. doi: 10.1016/0960-8524(96)00034-X

Verdoes, N. (2013). *Mestbewerking en Mestproducten*. Wageningen: Wageningen UR Livestock Research.

Vergote, T. L. I., Vanrolleghem, W. J. C., Van der Heyden, C., De Dobbelaere, A. E. J., Buysse, J., Meers, E., et al. (2019). Model-based analysis of greenhouse gas emission reduction potential through farm-scale digestion. *Biosyst. Eng.* 181, 157–172. doi: 10.1016/j.biosystemseng.2019.02.005

Vermeulen, G. (2019). *Voorstel VeDoWS Vermeulen Dobbelaere Welfare System Duurzaam Emissiearm Systeem*. Koplopersbijeenkomst: milieu- en kringloopeconomie in de varkenshouderij.

Vlaamse Overheid (2019). *6de Actieprogramma in Uitvoering van de Nitraatrichtlijn* 2019–2022.

VLM (2019a). *Lijst van Ammoniak-Emissiearme Stalsytemen (AEA-lijst) - Stikstofverliezen en Ammoniakemissiefactor Varkens*. Vlaamse Landmaatschappij.

VLM (2019b). *Mestrapport 2019*. Vlaamse Landmaatschappij.

VLM (2019c). *Normen en Richtwaarden 2019. Versie juli 2019 - MAP6*. Vlaamse Landmaatschappij.

Wang, Q., Noguchi, C., Hara, Y., Sharon, C., Kakimoto, K., and Kato, Y. (1997). Studies on anaerobic digestion mechanism: influence of pretreatment temperature on biodegradation of waste activated sludge. *Environ. Technol.* 18, 999–1008. doi: 10.1080/09593331808616619

Weinrich, S. (2019). Predicting BMP from substrate composition. In: *Workshop "Start!", 16th IWA World Conference on Anaerobic Digestion*.

Wellinger, A., and Lindberg, A. (2005). Biogas upgrading and utilisation. In: *IEA Bioenergy Task 24: Energy Form Biological Conversion of Organic Waste*.

Wiese, J., and König, R. (2007). *Procesbewaking van Vergisters in Biogasinstallaties*. Hach Lange.

Conflict of Interest: AD and JL were employed by the company Inagro. BW was employed by the company Innolab.

The remaining authors declare that the research was conducted in the absence of any commercial or financial relationships that could be construed as a potential conflict of interest.

frontiers in Energy Research

ORIGINAL RESEARCH
published: 16 April 2020
doi: 10.3389/fenrg.2020.00050

The Mixed Fermentation Technology of Solid Wastes of Agricultural Biomass

Feng Zhang, Wei Yu, Wenhe Liu and Zhanyang Xu*

College of Water Conservancy, Shenyang Agricultural University, Shenyang, China

Due to the large quantity and wide range of solid wastes of the biomass, and the dual characteristics of pollution and resource utilization, the energy utilization of anaerobic fermentation can promote its pollution control, so the mixed fermentation technology of solid wastes of agricultural biomass was studied. Corn straw, pig manure, and kitchen waste were selected as solid wastes of agricultural biomass. A system including a temperature control device, a fermentation device and a gas gathering device is used to measure the content and pH value of biogas and methane. Physical, chemical, and biological pretreatment methods were used to strengthen the anaerobic reference of biomass, and the mixed fermentation of different biomass was used to complete the anaerobic fermentation of a variety of solid wastes of agricultural biomass. The results showed that pig manure and corn straw were suitable for medium temperature fermentation at 30°C, while cow manure and corn straw were suitable for high temperature fermentation at 60°C. In the process of anaerobic fertilization, when the ratio of cow dung to sludge is 2:1, 3:1, and 4:1 respectively, the methane content is shown as follows: (1) The first 130 days are relatively stable and then slowly decreased; (2) The first 120 days are slowly increased, and then it rises to the maximum value at 140 days and then remains unchanged; (3) It remains at 2% all the time. After the mixture of cow manure and sludge, the higher the proportion of cow manure is, the higher the pH value in the initial stage of anaerobic fertilization is. The higher the basicity of methanogens in the fermentation liquid inside the fermentation tank is, the higher the pH value of the system is, and the basicity of methanogens has a significant positive correlation with the crude protein content of biomass.

Keywords: agricultural biomass, solid waste, mixed fermentation, anaerobic fermentation, pH value

OPEN ACCESS

Edited by:
Su Shiung Lam,
University of Malaysia Terengganu, Malaysia

Reviewed by:
Rock Keey Liew,
Universiti Malaysia Terengganu, Malaysia
Peter Nai Yuh Yek,
University College of Technology Sarawak, Malaysia
Changlei Xia,
Nanjing Forestry University, China

****Correspondence:***
Wei Yu
yuwei067@126.com

Specialty section:
This article was submitted to Bioenergy and Biofuels, a section of the journal Frontiers in Energy Research

Received: *20 December 2019*
Accepted: *12 March 2020*
Published: *16 April 2020*

Citation:
Zhang F, Yu W, Liu W and Xu Z (2020) The Mixed Fermentation Technology of Solid Wastes of Agricultural Biomass. Front. Energy Res. 8:50. doi: 10.3389/fenrg.2020.00050

INTRODUCTION

With the rapid development of China's economy, the living standards and lifestyle in rural areas have also undergone significant changes, which have broken the waste recycling system in traditional agricultural society, and the types and quantity of waste in rural areas have also begun to rise sharply (Natalia et al., 2019). Previously, the domestic waste in rural areas was mainly kitchen waste, and the surplus kitchen waste was used to raise livestock, and the manure produced by livestock was mostly returned to the field as organic fertilizer (Xu et al., 2017). The construction of new socialist countryside has changed the traditional life mode in the countryside, and the amount

of solid wastes such as livestock manure, domestic garbage, crop straw has also increased greatly. In recent years, with the improvement of farmers' living standards, the consumption structure has been constantly changed. For example, the large-scale use of chemical fertilizer makes the manure and domestic garbage of livestock be discarded at will. The original firewood energy has been replaced by electric energy and natural gas, and the utilization rate of rice straw is low (Zhang Q. et al., 2017). The random stacking of organic solid wastes will cause the pollution of rivers, groundwater, and other water sources in rural areas, which directly threatens the drinking water safety and health of farmers. Therefore, rural organic solid waste not only causes land occupation and pollution, but also affects human health and environmental health (Zhang et al., 2018). There are four disposal methods of organic solid wastes in rural areas, which are incineration, sanitary landfill, aerobic composting, and anaerobic fertilization. Among them, the water demand of anaerobic fertilization treatment technology is small, without power consumption, low cost, small floor area, which can recover biogas energy, and reduce pollution load. And the filtrate can be used as the additive or fertilizer of soil, which can increase the economic benefits. It is gradually becoming an important choice for countries around the world to deal with organic solid waste and produce new energy (Jongkeun et al., 2018).

Biomass refers to various organisms formed through photosynthesis, including all animals, plants, and microorganisms. Compared with traditional fossil fuels, biomass resources have the advantages of renewability and cleanness (Hong et al., 2017). Biomass resources are the basis for the development of biomass energy industry. Although there are abundant biomass resources in the world and more and more researches on biomass, most of them are still in the experimental stage and have not been widely used (Lam et al., 2018).

According to the latest statistical data, the annual output of crop waste is 6.88 × 108 t, and the total amount of resources and energy is 8.89 × 1,015 kj, equivalent to 3.04 × 108 t standard coal. Biomass solid waste has the dual characteristics of pollution and resource reuse. A large number of biomass are stacked randomly or burned in the open air, which not only causes waste of resources, but also affects the environment. However, by strengthening energy and resource utilization, pollution control can be promoted (Luc et al., 2017; Ojha et al., 2017). Acquiring bioenergy by anaerobic fertilization is one of the important ways to promote the transformation of biomass solid waste from pollution characteristics to energy. In this method, biomass solid waste is fermented under controlled conditions to produce biogas and organic fertilizer without oxygen and energy supply. Although solid wastes of agricultural biomass were fermented in the research of anaerobic fertilization by agidxis and devid, the waste used for fermentation was single, the amount of biogas entangled was small, and the effect was not ideal. In the study of anaerobic fertilization, hifinger only selected plant-based raw materials, without considering that animal manure is an important factor to promote the effect of mixed fermentation, so the fermentation technology studied is not comprehensive. In the study of anaerobic fermentation, the fermentation technology used by Qian is aerobic fermentation technology. A large number of studies show that anaerobic fertilization technology is one of the effective ways to realize the resource utilization of biomass waste (Ahamed et al., 2018; Pivoto et al., 2018; Sawan, 2018). Therefore, the solid wastes of agricultural biomass mixed fermentation technology studied in this paper are mainly composed of anaerobic fermentation. Biomass anaerobic fertilization is to effectively transform the organic matter in biomass under the assimilation of anaerobic bacteria, and finally generate methane and a small amount of carbon dioxide with economic value. It can be used for combustion and power generation, and biogas residue can be used as animal feed or land fertilizer, and biogas slurry can also be used as nutrient solution of crops. In this paper, the research results of the utilization of biomass waste resource anaerobic fermentation are reviewed, and the progress of the enhancement of biomass anaerobic fermentation by means of pretreatment, mixed fermentation of different biomass, and the addition of exogenous catalyst is also reviewed.

MATERIALS AND METHODS

Test Materials

The agricultural wastes involved in this experiment include corn straw, wheat straw, rice straw, pig manure, cow manure, chicken manure, kitchen waste, and cassava residue. Among them, wheat straw and corn straw were obtained from the experimental field in the North Campus of Shaanxi recycling agricultural engineering technology center of northwest agricultural and Forestry University in the previous year; rice straw was stored by farmers near the University for nearly one year. All straws are dried in the air before being put into the fermentation tank, crushed to about 2 mm in diameter, and put into a cool and ventilated place after being screened and bagged. Pig manure, cattle manure, and chicken manure are from the farms near the North Campus of Northwest University of agriculture and forestry technology, and no antibiotics have been used in the farms in the near future (Girotto et al., 2017). The biogas slurry is taken from the biogas digester which is normally used by the farmers in Cuixigou, Yangling, Shaanxi Province as the inoculum. When the inoculum is selected, the suspended matter in the upper part of the biogas slurry is removed, and the mature biogas slurry without obvious rotten odor in the lower part is evenly mixed.

Test Equipment and Design

Test Equipment

The device system used in the experiment is designed by the laboratory of Shaanxi recycling agricultural engineering technology research center. The whole system includes temperature control device, fermentation device, and gas gathering device. The relay in the temperature control device is used to display the temperature, the fermentation device is placed in the constant temperature water tank, and the heating temperature in the water tank is controlled by the temperature controller. The temperature fluctuation range of the whole temperature control device is ± 1°C. The fermentation device

and the gas gathering device are composed of a plurality of conical bottles with a volume of 1l, which are sealed with rubber plugs. Each part is connected with the rubber pipe through a glass conduit, and the discharged water is collected with a plastic pot with a capacity of 2.5 L, and the displacement is measured with a measuring cylinder. Liquictoc analyzer, Beijing Science, and Technology Development Co., Ltd.; pH detector, Shanghai Shifa science and Technology Co., Ltd.; TGL-16g high-speed desktop centrifuge, Shanghai Anting science instrument factory. In the experiment, the total solid mass fraction (TS) of all fermentation materials was 8%, the volume of fermentation bottle was 1 L, and the effective volume was 0.7 L. During the test, each treatment was set with 3 repetitions. The pH value and alkalinity content of in the erobic reference process were measured every 5 days. Solid waste anaerobic fermentation period can be divided into multiple stages, because this article study period is longer, as long as 170 days, set the test time interval is short, can cause workload, if the test time interval, the greater the cannot get representative as a result, after comprehensive consideration, this paper measured once every 5 day pH value, in order to get the typical experimental data. The daily gas production is measured at 17:00 p.m. every day after shaking the fermentation tank manually.

Experimental Reagents

Acid and alkali regulators: hydrochloric acid (HCl), sodium hydroxide (NaOH), calcium hydroxide [$Ca(OH)_2$], sodium carbonate (Na_2CO_3).

Test Design

Daily biogas production (DBP).

The fermentation materials were pig manure, cow manure, and corn straw. After manual screening, the feces are put into the plastic bucket after removing the sundries, sealed and retreaded, and stirred every three days, the total retreading time is 7 days. After air drying, the straw is cut to about 1cm in length and put in a cool and ventilated place for standby. Add a little cow dung into the biogas slurry 2 days in advance, mix and seal, domesticate, and reserve. Pig manure/corn straw and cow manure/corn straw are respectively set with five levels: 1:9, 3:7, 5:5, 7:3, 9:1. The total solid content of fermentation substrate was maintained at 8%. 560g of fermentation raw materials and 140 g of acclimated biogas slurry inoculum were put into 1 L triangular glass bottle. Each treatment test is set with three repetitions. After checking the air tightness of the device, the fermentation tank is placed in a constant temperature water tank with set temperature for heating. The test temperature is 30° and 60°C, respectively. During the experiment, the fermentation raw materials and inoculum were put into the fermentation tank, and the fermentation tank was placed in the constant temperature water bath culture tank, the devices were connected, the temperature was set, and the biogas output was measured by the drainage method. The measurement time is set at 17:00 p.m. every day, shake the fermentation tank manually for 30 s to break the crust on the surface of fermentation raw materials in the fermentation tank and release the generated gas. The volume of water in the water collecting barrel was measured with the cylinder, which is the biogas output of the day.

Methane content, MC

The liquid TOC analyzer (Beijing Science and Technology Development Co., Ltd.) was used to measure methane content in gas before measuring DBP every day.

PH value

Measure the pH value of the mixed fermentation substrate every 5 days with a pH detector.

Determination of total alkalinity

Determine the total alkalinity by potentiometric titration. Potentiometric titration is based on the sudden jump of potentiometric titration curve at the end point to determine the alkalinity at a specific pH, which is not affected by the turbidity and chroma of water samples, and has a wide range of application. The specific determination steps are as follows:

(a) Accurately prepare HCl standard solution with concentration of about 0.1 mol/L, and calibrate it with reference Na_2CO_3 solution.
(b) Install and calibrate the potentiometer according to the instructions, and clean the electrode with distilled water.
(c) According to the above method, the water sample is centrifuged or filtered (5,000 r/min, 10 min), and 2 mL of filtrate is sucked into a 50 mL beaker with a pipette. The amount of sample should be able to consume 2–8 mL of HCl (0.1 mol/L) standard solution. The same volume of distilled water was used as blank control.
(d) The water temperature of the sample is 25 ± 2°C, the 50 mL beaker containing the sample is placed on the titration table, and a magnetic stirring rod about 1.5 cm long is put in. Stir it with a certain intensity. Note that the glass electrode needs to be placed below the calomel electrode in the beaker. Turn on the automatic titration switch and set the end point to ph3.7, and the automatic titration process starts. After the titration stops automatically, record the volume of HCl standard solution consumed in titration.

The formula for determination of total alkalinity can be expressed as follows:

$$\text{alkalinity}\left(\text{mgCa}CO_3/L\right) = \frac{(V_1 - V_0) \times c \times 50}{V_2} \times 1000 \quad (1)$$

Where V_1 is the volume of HCl standard solution consumed by sample, ml; V_2 is the volume of sample, ml; V_0 is the volume of HCl standard solution consumed by titration blank control, ml; C is the accurate concentration of HCl standard solution, mol/L.

Strengthening Methods

The effect of anaerobic fertilization is not ideal when the substances (straw, energy crops, etc.) containing a large amount of cellulose and lignin are directly used, but the fermentation effect can be improved by pretreating the raw materials rich in such ingredients or mixing several raw materials (Paulina et al., 2018). In the same way, better gas production effect can be obtained by using catalyst. The enhancement of biomass anaerobic fertilization is a hot topic in the research of biomass anaerobic fertilization (Wang et al., 2017).

Pretreatment

The physical pretreatment method uses heat energy, mechanical energy, electromagnetic radiation energy, and other energy to act on the refractory biomass and release the intracellular material by destroying the cell wall. Finally, the utilization difficulty of the refractory biomass is reduced (Alarcon et al., 2017; Steven et al., 2017). Physical pretreatment mainly includes heat pretreatment, microwave pretreatment, and ultrasonic pretreatment. Heat pretreatment can destroy the cell wall of biomass, release the organic matter in the cell, and transform the insoluble organic matter into soluble organic matter, which greatly shortens the hydrolysis time and improves the biogas production efficiency. After heat treatment of food waste for 1.5 h at 80°C, anaerobic fertilization was carried out. The methane content in the gas production was 647.5 ± 10.6 $mL{\cdot}g^{-1}VS$, which was 52% higher than that of untreated. There are two mechanisms for microwave pretreatment to destroy the cell wall of biomass: (1) microwave causes molecular oscillation, which causes the temperature of biomass to rise and leads to the heating effect (Jia et al., 2018); (2) the alternating electric field generated by microwave breaks the hydrogen bond of macromolecules in the cell wall, thus damaging the cell wall structure. Different microwave intensity was used to treat straw, and then it was used for anaerobic fertilization. It was found that microwave treatment significantly promoted the anaerobic fertilization of straw. The average daily gas production of pretreated straw increased from 6.21 to 8.16 $mL{\cdot}g^{-1}VS$, which increased by 31.33%; the average concentration of methane increased from 50 to 62%. The researchers also studied the effect of microwave irradiation on the performance of anaerobic fertilization of energy, and obtained 345.16 $mg{\cdot}g^{-1}TS$ gas production. The role of ultrasound is to use the whole effect in low frequency and the chemical effect in high frequency. The effect of ultrasonic pretreatment on the anaerobic fertilization of cattle manure was also studied. The results showed that the ultrasonic pretreatment with appropriate intensity had a certain promoting effect on it. After pretreatment with 250 W ultrasonic for 40 min, the gas production rate reached the optimum, which was 297.78 $mL{\cdot}g^{-1}TS$. After the sludge of paper mill was pretreated by ultrasound, its anaerobic fertilization was studied (Ling et al., 2018). The results showed that 1250 W ultrasonic pretreatment could promote the fermentation (Marzieh and Andrew, 2018; Yu et al., 2018), and the mixture of the by-product of the meat processing factory and the cow manure was pretreated by ultrasonic. The result of the anaerobic fertilization showed that the biogas production increased obviously after the ultrasonic pretreatment.

Chemical Pretreatment

Chemical pretreatment is to use some corrosive chemicals (strong acid, strong alkali, and strong oxidant, etc.) to destroy the cell wall structure and extracellular polymer of biomass. Chemicals even react with extracellular macromolecular organics to promote their degradation (Pujaningsih et al., 2017). Chemical pretreatment includes alkali pretreatment, acid treatment, and ozone pretreatment. After pretreatment of banana stem with 6% NaOH, the researchers found that the gas production of biogas increased to 357.90 $mL{\cdot}g^{-1}VS$. The researchers also pretreated wheat straw anaerobic fertilization with 4% ammonia water, and found that the removal rate of hemicellulose and cellulose can reach 42 and 20% respectively, and under the load rate of 65 $g{\cdot}L^{-1}$, the maximum biogas output of 377 $mL{\cdot}g^{-1}$ can be obtained through anaerobic fertilization. Corn straw was treated with dilute acid and then used in anaerobic dry fermentation. After 60 h of treatment, the total gas production rate is 4.76 $m^3{\cdot}m^{-3}$, and the maximum methane content is 82.90%. In this paper, acid and alkali pretreatment was used to treat lemongrass and reed. The results showed that the accumulated gas production and methane content of anaerobic fertilization were significantly increased after acid-base pretreatment, and the effect of acid treatment was better than that of alkali treatment. After straw was treated with alkaline ozone, lignin was oxidized, and decomposed into small molecular organic acids, which improved the efficiency of anaerobic fertilization of straw (Yu et al., 2017).

Biological Pretreatment

The biological pretreatment of fermentation raw materials is to use microbial community to degrade lignin in straw and change the structure of lignin. The researchers domesticated a group of cellulose decomposing complex bacteria with high enzyme activity and stability, and used them to pretreat straw for anaerobic fertilization. Its gas production is 33.3% higher than that of untreated group. The results of anaerobic fertilization showed that the cumulative gas production of pretreated rape straw was 17.8% higher than that of untreated. When testing the effect of white rot fungus pretreatment on biogas production of sugarcane leaves, it was found that adding white rot fungus can accelerate the start-up rate and peak gas production of anaerobic fertilization (Zhang C. H. et al., 2017; Hu et al., 2018). With the above-mentioned pretreatment methods, the gas production effect of biomass feedstock in the anaerobic fertilization process has been improved to some extent.'

Mixed Fermentation of Different Biomass

Due to the differences in the composition of various biomass, the effect of single biomass fermentation is not ideal, and the mixed fermentation of different biomass can effectively improve the gas production effect of anaerobic fertilization. The sludge contains a large number of anaerobic microorganisms but lacks nutrients, so the sludge can be used as inoculum or raw material for mixed fermentation with other biomass (Qu, 2017; Tang et al., 2019). The researchers used a mixture of dewatered sludge and Canadian goldenrod, an imported ornamental plant, for anaerobic fertilization. The results showed that the methane production per unit volume increased by 79.5% compared with anaerobic fertilization alone. Anaerobic granular sludge, digested sludge, and excess sludge were mixed with cyanobacteria respectively, and they can effectively promote the anaerobic fertilization process. When the ratio of cyanobacteria to anaerobic granular sludge is 6:1, the gas production rate is 73 $mL{\cdot}g^{-1}VS$. When the mixed fermentation of solid wastes of the biomass with different proportion and sludge is adopted, the gas production effect is significantly improved (Liu et al.,

2017). When the bean curd dregs are mixed with the digested sludge, the fermentation effect of bean curd dregs is good. When rice straw was used as the fermentation base, the fermented cow manure, pig manure, chicken manure, sludge, and anaerobic granular sludge were inoculated respectively, it was found that the above five inoculants effectively improved the gas production rate of rice straw anaerobic fertilization. In the process of anaerobic fertilization, different proportion of mixture will affect biogas quantity, methane content, pH value and alkali concentration.

When the carbon rich food waste and nitrogen rich piggery wastewater are mixed and fermented, the biogas output is 396 $mL \cdot g^{-1}VS$. When solid wastes of the biomass and glycerin were mixed at 50°C, anaerobic fertilization was carried out. It was found that the biogas production increased with different proportion of mixed fermentation, and the highest methane production was 640 $L \cdot kg^{-1}VS$. After mixing the grass and pig manure, different inoculums were added for anaerobic fertilization. The results showed that the highest methane production was 521.9 $mL \cdot g^{-1}TS$. When the cow manure and pear were mixed for fermentation, the biogas production was increased in different proportion, and the maximum gas production was 390.0 ± 2.0 $mL \cdot g^{-1}VS$. After mixing chicken manure with rice straw, it was found that the methane production was 223 ± 7 $mL \cdot g^{-1}VS$ in the stable fermentation environment.

Different kinds of biomass are mixed for fermentation, which can make up for the shortage of single substance and create a good living environment for microorganisms. Finally, the resource utilization of biomass waste is realized.

RESULTS

The changes of biogas amount, methane content, pH value, and alkalinity of fermentation liquid in the mixed fermentation process of solid wastes of agricultural biomass were studied in the laboratory of an Agricultural University of science and technology. A variety of solid wastes are collected in the nearby city farms. The anaerobic fertilization process was completed in the fermentation tank of the laboratory, and the multi-level treatment test under single condition was carried out. Through the gas production (the most intuitive test index), the optimal fermentation temperature, methane content, and initial pH value of each single raw material were determined. Then a variety of solid wastes of the biomass were placed in the fermentation tank respectively, and the influence of the components of biomass on the alkalinity of the fermentation liquid was analyzed in the anaerobic fertilization process.

Effect of Medium Temperature (30°C) and High Temperature (60°C) on Biogas Production of Mixed Anaerobic Fertilization

Under medium and high temperature, the unit biogas output of pig manure/corn straw, cow manure/corn straw with multi ratio for anaerobic fertilization is shown in **Table 1**.

TABLE 1 | Biogas output per unit with different substrate ratio under medium and high temperature conditions (mL/g TS).

Raw material	Pig manure/corn straw		Cow manure/corn straw	
Fermentation temperature	**30°C**	**60°C**	**30°C**	**60°C**
1:9	153.15	303.57	227.43	380.93
3:7	193.40	375.82	155.70	411.74
5:5	249.65	390.47	174.86	318.16
7:3	241.09	212.99	121.59	315.27
9:1	283.74	284.13	160.65	252.31

TABLE 2 | Two factor variance analysis of unit biogas output.

Source	Model	Error	Correction totaling
Freedom	20	36	55
Sum of squares	295484.45	215.963	295699.3
Mean square	15078.129	7.2497	
F value	2549.28		
Pr > F	< 0.0001		
R^2R-Square	Coefficient of variation	Root mean square error	Mean value of dependent variable
0.999356	1.085747	2.588736	230.5560

At medium temperature, the biogas output per unit of pig manure/corn straw is better than that of cow manure/corn straw. When the ratio of pig manure to corn straw is 9:1, the maximum gas production is 283.74 mL/g TS; when the ratio of cow manure to corn straw is 7:3, the minimum gas production is 121.59 mL/g TS. Under high temperature, the biogas yield of cow manure/corn straw is better than that of pig manure/corn straw. When the ratio of cow manure to corn straw is 3:7, the maximum gas production is 411.74 mL/g TS; when the ratio of pig manure to corn straw is 7:3, the minimum gas production is 212.99 mL/g TS.

The analysis of variance of unit biogas output of two mixtures with different proportions under medium and high temperature conditions is shown in **Table 2**.

It can be concluded that the biogas output per unit of anaerobic fertilization is significantly different at medium and high temperature, and the high temperature fermentation is significantly higher than the medium temperature fermentation. The biogas output of pig manure/corn straw is significantly different from that of cow manure/corn straw, the former is better. When the ratio of feces to straw was 1:9, 5:5, 9:1, and 3:7, there was significant difference between the two groups. There were significant differences among the other groups.

By comparing the biogas production of pig manure/corn straw with each ratio in the middle temperature and high temperature, it can be concluded that the difference of biogas production in the middle temperature is greater than that in the high temperature. However, the biogas production per unit of cow manure/corn straw was significantly higher than that of medium temperature at high temperature, which indicated that the mixed fermentation of cow manure/corn straw was more suitable for high temperature. However, the linear relationship

between the unit gas production and the ratio of each treatment is not obvious, which needs further test to verify. By comparing the methane production of mixed raw materials under the conditions of medium temperature and high temperature, it can be concluded that the type and proportion of fermentation raw materials will affect the biogas production under the same temperature. In the medium temperature condition, the mixed fermentation effect of pig manure and corn straw is quite different, and the stability of fermentation process is general; in the high temperature condition, although the gas production is improved, the fermentation starts late, and the stagnation period is prolonged. Cow dung/corn straw showed better stability, especially at high temperature, gas production, and stagnation time were significantly optimized. The results showed that the fermentation effect of pig manure/corn straw was better at medium temperature, while that of cow manure/corn straw was better at high temperature.

Methane Production of Mixture in Anaerobic Fertilization Process

When the ratio of cow manure with sludge is 2:0, 2:1, 3:1, and 4:1, respectively, the methane content changes with the increase of fermentation time, as shown in **Figure 1**. It is assumed that the fermentation tanks with four proportions of cow manure and sludge are U1, U2, U3, and U4 respectively.

The methane content increased from 17.54 to 51.4% in the first 20 days after U2 feeding, which indicated that acid production was dominant in the early stage of fermentation. At the 20–130th day, the methane content increased very slowly and remained stable between 45 and 51.4% for a long time. After 131 days, it began to decline slowly, from 49.1 to 35.45%, indicating that the reaction began to enter the aging period, and methanogens began to fail. U1 and U3 were similar in the first 22 days, but U1 experienced two peaks of methane content in the whole 170 days of fermentation time, which were 33.2% at 40 days and 47.31% at 140 days. Since then, it began to decline rapidly, characterized by short peak holding time and inactive methanogenesis, which was in line with the characteristics of its non-inoculated mud. U3 experienced a relatively stagnant period from 70 to 100 days, and the methane content remained between 9.8 and 22.28%, and then began to increase rapidly, and the growth rate was much higher than that of other fermentation tanks in the same period. By the end of the experiment, the content reached 55.11%, which was the highest among the four fermentation tanks. It can be concluded that the methanogenic activity in U3 is still in a vigorous breeding period, which may be due to the addition of NaOH in the fermentation tank to regulate the pH value so that the final methanogenic bacteria in the fermentation tank is more than the acid producing bacteria. In the long process of competition between acidogenic bacteria and methanogens, more excellent methanogens were screened out, which can be obtained from the highest methane content of U2 and U3 (51.48 and 55.11%). Therefore, if no sludge is added to the anaerobic fertilization process, the methane content will slowly increase in the first half of anaerobic fertilization process, and then slowly decrease in the second half. When the ratio of cattle manure to sludge is 2:1, the methane content will be stable between 45 and 51.4% in the first 130 days, and then slowly decrease. When the ratio of cattle manure to sludge is 3:1, the methane content will

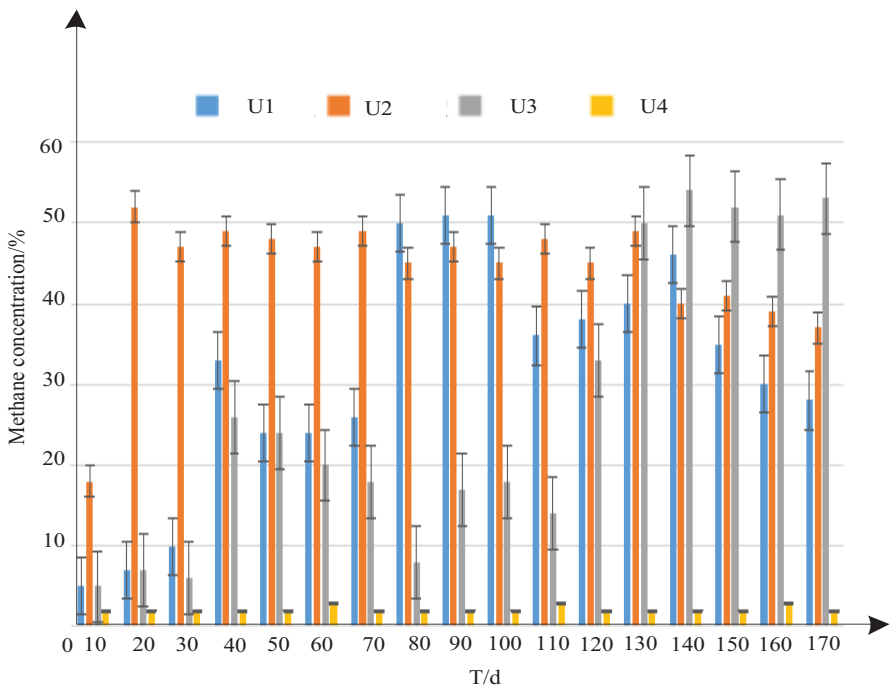

FIGURE 1 | Change of methane content in biogas.

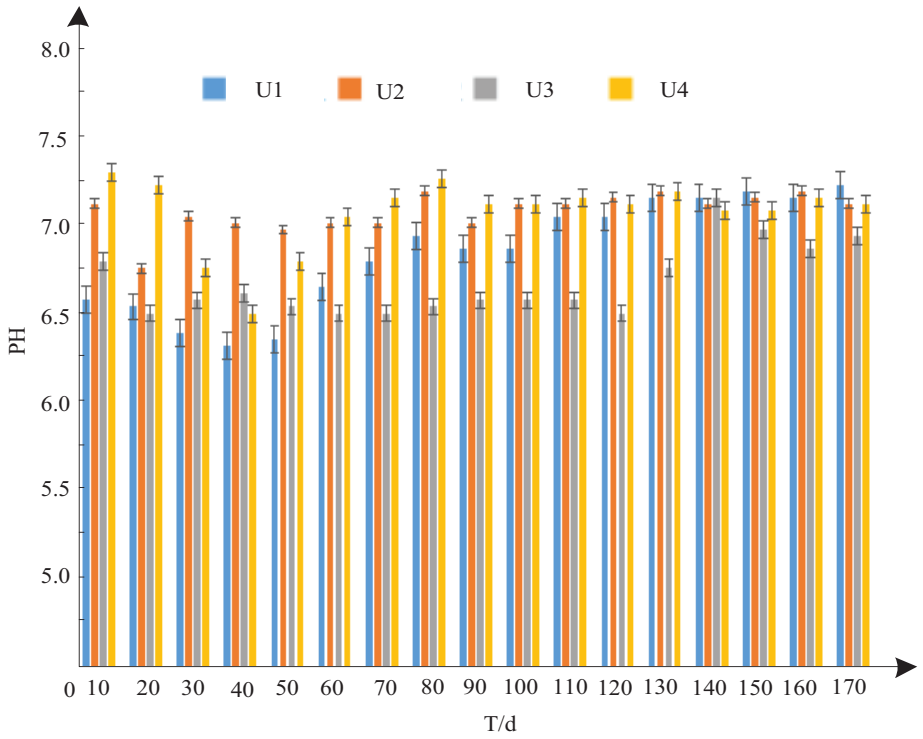

FIGURE 2 | Change of pH value in anaerobic fermentation process.

rise slowly in the first 120 days, and reach the maximum value of 55% on the 140th day, and then keep stable. When the ratio of cattle manure to sludge is 4:1, the methane content will be kept at 2%, and the methane production is the least.

The Change of pH Value in Anaerobic Fermentation Process

The change of pH value in anaerobic fermentation process is shown in **Figure 2**.

It can be seen from **Figure 2** that when U3 is used to complete anaerobic fermentation, acidification occurs in anaerobic fermentation tank, and the pH of the produced leachate drops to about 5.5 in the early stage. The results showed that the acidification of straw could not be prevented at the initial stage of leachate reflux, and the microorganisms in solid phase only hydrolyzed the organic matters in leachate. A large number of acid producing bacteria increased the organic acids and decreased the pH value in the leachate, which destroyed the ecological balance of the microbial community in the solid layer. After anaerobic fertilization in U3, the leachate produced reached the highest value of 7.25 at 140 days, and then began to decline, and the hydrolysis reaction began to be active again. However, this does not affect its gas production, and after 140 days pH has been maintained above 6.5, methanogens have gradually adapted to the slightly acidic environment and can smoothly produce gas.

The pH value of the leachate produced after anaerobic fertilization in U2 is always above 7.0, and it is close to 7.25 at the end of the test. This may be due to the high water content will dilute the acid produced by hydrolysis, and alleviate the impact of acid production reaction on methanogens. In addition, high inoculation amount also has a certain ability to prevent acidification. It was found that the pH value of the leachate after U1 anaerobic fertilization decreased in the initial 40 days, which was similar to the leachate after U4 anaerobic fertilization. Then, the pH of U1 permeate began to increase suddenly within 50 days, and gradually approached to neutral. Therefore, in the mixture of cow dung and sludge, the higher the proportion of cow dung is, the higher the pH value at the beginning of anaerobic fertilization is, and in the early stage of anaerobic fertilization, the higher the proportion of cow dung will lead to the rapid decline of pH value, and then it will slowly rise to about 7.25. When the proportion of cow dung is relatively low, the pH value tends to be stable and keeps around 7.25 all the time; the pH value of cow dung without sludge is the lowest at the beginning of anaerobic fertilization, and slowly rises to about 7.25 after the initial pH value keeps stable for a period of time.

Effect of pH on the Alkalinity of Fermentation Liquid

Alkalinity is not alkali. In a broad sense, alkalinity refers to the concentration of strong alkali and weak acid salt in water. It has different forms of existence under different pH values (different number of H on weak acid roots), and can release or absorb H ions according to the environment, thus playing the role of pH change in buffer solution and reducing the pH fluctuation in the system. Alkalinity is not directly involved in the reaction.

TABLE 3 | Daily average alkalinity value of each fermenter at the later stage of fermentation.

Fermentation tank No	**U5 (Cow dung)**		**U7 (Chicken manure)**		**U8 (Goat manure)**		**U9 (Food waste)**	
Entry name	Basicity of methanogen	Methyl orange alkalinity	Basicity of methanogen	Methyl orange alkalinity	Basicity of methanogen	Methyl orange alkalinity	Basicity of methanogen	Methyl orange alkalinity
Total alkalinity ($mgCaCO_2/L$)	5411	4095	9090	6641	4274	2837	2353	1192
Fermentation tank No	**U10 (Cassava residue)**		**U12 (Corn stalk)**		**U13 (wheat stalk)**		**U14 (Rice straw)**	
Entry name	Basicity of methanogen	Methyl orange alkalinity	Basicity of methanogen	Methyl orange alkalinity	Basicity of methanogen	Methyl orange alkalinity	Basicity of methanogen	Methyl orange alkalinity
Total alkalinity ($mgCaCO_2/L$)	3,353	3,192	3,276	1,966	4,285	3,848	4,274	2,837

Alkalinity is an important index to measure the buffering capacity of anaerobic system, and it is also a standard to measure the pH impact resistance of the system.

In the determination of alkalinity, according to the titration end point, it can be divided into phenolphthalein alkalinity and methyl orange alkalinity. The former has a pH value of 8.3, which indicates the end point of neutralization of hydroxide in water sample and conversion of carbonate to bicarbonate; the latter has a pH value of 4.4–4.5, which indicates that the end point of neutralization of bicarbonate in water (including original bicarbonate and bicarbonate converted from carbonate) is equivalent to the pH value of just turning methyl orange into orange red. Industrial waste water or water with complex components can be used with pH = 3.7 to indicate the titration end point of total acidity.

In the continuous anaerobic fertilization process, the suitable pH range for methanogens is 6.8–7.8, and the broader pH range is 6.5–8.2. Therefore, in this experiment, as a new definition, the basicity of methanogens is used, that is, in the titration measurement process of total basicity, when the pH displayed by the potential titrator reaches 6.5, the calculated basicity value. Different from phenolphthalein alkalinity and methyl orange alkalinity, methanogen alkalinity can reflect the ability to maintain the pH of the system above 6.5 in the sample to be tested, that is, the buffering ability to absorb hydrogen ions to maintain the pH of the system above 6.5. Therefore, the basicity of methanogens can better serve the experiment and production of anaerobic biogas production than that of methyl orange. **Table 3** shows the daily average alkalinity value of each fermentation tank in the later stage of fermentation.

Table 3 shows that the daily average methyl orange alkalinity and methane bacteria alkalinity between the fermentation tanks are quite different. Among them, the methane bacteria alkalinity of U5, U6, and U7 were above 3,900 mg $CaCO_3$/L, significantly higher than other fermentation tanks. This shows that the three groups of materials in the fermentation tank have strong buffer capacity and can withstand higher organic load, which is also an important reason for their pH above 7.5. There are only the fermentor with methane bacteria alkalinity above 2,800 mg $CaCO_3$/L in U8, U10, U13, and U14. The other fermentation tanks have a $CaCO_3$/L of 1,000–2,000 mg, of which the lowest is U9, 1,192 mg. This indicated that its buffering capacity was the weakest among 10 groups of fermentation tanks.

TABLE 4 | Average basicity of methane bacteria in fermentation tank at later stage of experiment.

Project type	**Basicity of methanogenmg $CaCO_3$/L**	**Reactor no**	**Corresponding material**
1	> 3,900	2,800–3,900	1,000–2,800
2	U5, U6, U7	U8, U10, U13, U14	U9, U11, U12
3	Cow dung, Pig manure, Chicken manure	Goat manure, Cassava residue, Wheat stalk, Rice straw	Food waste, Chinese medicine residue, Corn stalk

In addition, **Table 3** also shows that the total alkalinity of the internal fermentation liquid of each group of fermentation tanks is significantly higher than their methane bacteria alkalinity. The difference amplitude between two alkalinity of each material is different. Therefore, methane bacteria alkalinity is not the direct "reduced version" of the total alkalinity, but the independent index that can truly react to the starting enzyme and stabilize the pH above 6.5. According to the methane bacteria alkalinity, 10 groups of fermentation tanks can be divided into three groups: high, medium and low, as shown in **Table 4**.

It can be seen from **Tables 3**, **4** that the higher the methane bacteria alkalinity of the fermentation liquid is, the higher the pH of the system is.

The pH can reflect the ability of the starting fermentation liquid to neutralize organic acids. Therefore, we can continue to increase the organic load of the fermentation tank to improve the production efficiency of methane in the anaerobic fermentation; on the contrary, the internal fermentation liquid of the fermentation tank has a low methane bacteria alkalinity, and its pH also decreases. This indicates that the ability of neutralizing organic acids in fermentation broth is weakening at this time. If the organic load is not reduced, it may go to rancidity, and finally lead to the failure of methane production by anaerobic fertilization. Therefore, according to the pH value and methane bacteria alkalinity of the fermentation tank, the

TABLE 5 | Correlation analysis of biomass components and alkalinity in fermentation broth.

Entry name	Relevance	Saliency	*N*
Crude protein	0.898	0.123	9
Crude fat	0.186	0.958	9
Total sugar	−0.712	0.198	9
Crude fiber	0.157	0.998	9
Hemicellulose	0.425	0.522	9
Cellulose	−0.115	0.997	9
Lignin	0.330	0.683	9

top three groups of fermentation tanks perform best, which can continue to increase the organic load.

Although the pH of U8 showed the downward trend, it was relatively slow as a whole, so it was not suitable to continue to increase the organic load; the pH of u9, U10, and U11 showed the significant decline in the later stage of the test, so they were not suitable to continue to increase the organic load. In particular, U9 with cassava residue as the substrate has the lowest methane bacteria alkalinity, which is 1,192 mg $CaCO_3$/L, and the pH has dropped below 7.0 at the end of the experiment. According to the above analysis, the PH value of U5 (cow dung) and U6 (pig dung) were the most stable in 10 groups of fermentation tanks.

Table 5 shows the correlation between the composition of biomass and the alkalinity of fermentation liquid.

As shown in **Table 5**, there is only a significant positive correlation between the content of crude protein in biomass and the methane bacteria alkalinity. The results show that the higher the content of protein compounds in biomass is, the higher the alkalinity of biomass after anaerobic fertilization is.

DISCUSSION

(1) Temperature effect. At medium temperature, the biogas output per unit of the mixture of pig manure and corn straw is higher than that of the mixture of cow manure and corn straw, and the higher the content of pig manure and corn straw is, the higher the gas production is. At high temperature, the biogas production of cow manure and corn straw is higher than that of pig manure and corn straw. When the ratio of cow manure to corn straw is 3:7, the gas production is the highest. According to the analysis of variance of unit biogas output of two different mixtures at medium and high temperature, it can be seen that the unit biogas output of pig manure/corn straw at medium temperature is significantly higher than that at high temperature, while the unit biogas output of cow manure/corn straw at high temperature is significantly higher than that at medium temperature. The results showed that the mixture of pig manure and corn straw was suitable for medium temperature fermentation, while the mixture of cow manure and corn straw was suitable for high temperature fermentation. Therefore, the medium temperature fermentation effect of pig manure/corn straw is better, and the high temperature fermentation effect of cow manure/corn straw is better. Therefore, in order to get more biogas, according to the above research, the biogas amount can be increased by increasing the fecal content under the appropriate fermentation temperature.

(2) Changes in methane content. If no sludge is added to the anaerobic fertilization process, the methane content will slowly increase in the first half of anaerobic fertilization process, and then slowly decrease in the second half. When the ratio of cattle manure to sludge is 2:1, the methane content will be stable between 45 and 51.4% in the first 130 days, and then slowly decrease. When the ratio of cattle manure to sludge is 3:1, the methane content will rise slowly in the first 120 days, and reach the maximum value of 55% on the 140th day, and then keep stable. When the ratio of cattle manure to sludge is 4:1, the methane content will be kept at 2%, and the methane production is the least. Therefore, in order to improve the methane content, based on the premise of its own fermentation time limit, choose the appropriate proportion of manure and sludge to complete the anaerobic fertilization, so as to achieve the purpose of increasing the methane content. Li Xuebing's research on the optimization of solid waste fermentation of agricultural biomass shows that the proper pretreatment of agricultural waste can significantly improve the gas production efficiency and organic load of CO fermentation. Through response surface optimization analysis, the optimal temperature conditions of CO fermentation of cow manure and sludge are obtained. At the same time, the influence degree of different factors on the load methane production rate is analyzed. It is the initial organic load and pretreatment temperature, but this method does not study the gas production under the different mixing ratio of cow manure and sludge. The research is shallow and not deep enough. This method makes up for this very well.

(3) Change in the PH value. When the ratio of cattle manure to sludge is 3:1, the anaerobic fermentation tank is acidified. A large number of acid producing bacteria increased the organic acids and decreased the pH value in the leachate, which destroyed the ecological balance of the microbial community in the solid layer. After 140 days pH has been maintained above 6.5, methanogens have gradually adapted to the slightly acidic environment and can smoothly produce gas. When the ratio of cattle manure to sludge is 2:1, the pH value of leachate is stable and keeps above 7.0. When the ratio of cow dung to sludge is 2:0, the pH value will first slowly decrease, then suddenly increase, and finally gradually approach to neutral. Therefore, in the mixture of cow dung and sludge, the higher the proportion of cow dung is, the higher the pH value at the beginning of anaerobic fertilization is, and in the early stage of anaerobic fertilization, the higher the proportion of cow dung will lead to the rapid decline of pH value, and then it will slowly rise to about 7.25. When the proportion of cow dung is relatively low, the pH value tends to be stable and keeps around 7.25 all the time; the pH value of cow dung without sludge is the lowest at the beginning of anaerobic fertilization, and slowly rises to about 7.25 after the initial pH value keeps stable for a period of time. Therefore, in order to control the pH value in the anaerobic fermentation process, we can select the appropriate solid wastes of the biomass

ratio according to the characteristics of the above pH value changes. Fang Shaohui, a Chinese scholar, conducted a study on the characteristics of biomass energy conversion by slant dry-type anaerobic fermentation of rural mixtures. During the experiment, the rural biomass waste was used as raw material for biogas dry-type anaerobic fermentation. Based on the previous research results, a small-scale orthogonal experiment was conducted with three factors, namely temperature, inoculation amount, and total solid matter content (TS). The experimental results showed that the gas production increased significantly at high temperature (50°C), the gas production quality was good, and the utilization rate of raw materials was high; the gas production increased more obviously at the inoculation rate of 10–20%. The pH change in the dry anaerobic fermentation process generally showed a trend of "first decreased and then increased, and finally tended to be stable," and the change trend was in line with the three-stage theory. The change of pH is consistent with the results of this study, so the validity of the experimental results is verified.

(4) Alkalinity of fermentation liquid. In the detection of the alkalinity of the fermentation liquid, the concept of the alkalinity is proposed for the first time, that is, the alkalinity value calculated when the pH value drops to 6.5 in the traditional alkalinity measurement process. Compared with the traditional total alkalinity (methyl orange alkalinity), the ability of starting enzyme to stabilize the pH above 6.5 (the lowest pH tolerance line of methanogens) can be effectively reflected, which can better serve the anaerobic fertilization test. In the analysis of the correlation between the composition of biomass and the methane bacteria alkalinity, the results showed that there was only a significant correlation between the content of crude protein and methane bacteria alkalinity, that is to say, with the increase of protein compounds in biomass, the methane bacteria alkalinity in fermentation broth also increased.

CONCLUSION

With the continuous development of agricultural production, a large number of agricultural biomass solid wastes are generated. In order to reduce the pollution of these solid wastes to the environment and turn them into available energy, a new mixed fermentation technology of agricultural biomass solid wastes was studied in this paper. The changes of methane content and pH value, the influence of temperature on biogas production and the influence of anaerobic reference liquid on the alkalinity of fermentation liquid were analyzed when agricultural biomass solid waste was mixed in different proportion. The results showed that the mixture of pig manure and corn straw was suitable for medium temperature fermentation, and the mixture of cow manure and corn straw was suitable for high temperature fermentation. If no sludge is added in the process of anaerobic fertilization, the methane content in the first half of anaerobic fertilization will increase slowly, and the methane content in the second half will decrease slowly. When the ratio of feces to sludge is 2:1, the methane content is stable between 45 and 51.4% in 130 days, and then slowly decreases. When the ratio of cow manure to sludge was 3:1, the methane content increased slowly in the first 120 days, reached the maximum value of 55% on the 140th day, and then kept stable. When the ratio of cow manure to sludge is 4:1, the methane content is kept at about 2%, and the methane production is the least. In the mixture of cow manure and sludge, the higher the proportion of cow manure is, the higher the pH value is in the early stage of anaerobic fertilization. In the early stage of anaerobic fertilization, the higher the proportion of cow manure is, the lower the pH value will be. There was only a significant correlation between crude protein content and basicity of methanogens, that is, with the increase of protein compounds in biomass, the basicity of methanogens in fermentation broth also increased. On the basis of this study, the following suggestions are proposed:

By adjusting the proportion of agricultural biomass solid waste, the amount of biogas and methane content produced in the process of mixed fermentation can be controlled. By adjusting the proportion of agricultural biomass solid waste, the pH value of leachate and the basicity of fermentation liquid can be controlled, so that the mixed fermentation process is more smooth and the fermentation effect is more ideal.

DATA AVAILABILITY STATEMENT

All datasets generated for this study are included in the article/supplementary material.

ETHICS STATEMENT

The study was approved by Shenyang Agricultural University. All authors provided written informed consent.

AUTHOR CONTRIBUTIONS

FZ and WY studied the mixed fermentation technology of solid wastes of agricultural biomass and selected corn straw, pig manure, and kitchen waste as solid wastes of agricultural biomass. WL and ZX did the experiments, used physical, chemical, and biological pretreatment methods to strengthen the anaerobic reference of biomass, and the mixed fermentation of different biomass to complete the anaerobic fermentation of a variety of solid wastes of agricultural biomass. FZ wrote the manuscript.

FUNDING

This research was supported by The National Natural Science Foundation of China-Outstanding agricultural research talents and Innovation Team Project of the Ministry of Agriculture (No. 31570706).

REFERENCES

Ahamed, M. S., Guo, H., and Tanino, K. (2018). A quasi-steady state model for predicting the heating requirements of conventional greenhouses in cold regions. *Inform. Process.Agric.* 5, 33–46. doi: 10.1016/j.inpa.2017.12.003

Alarcon, M., Santos, C., and Cevallos, M. (2017). Study of the mechanical and energetic properties of pellets produce from agricultural biomass of quinoa, beans, oat, cattail and wheat. *Waste Biomass Valorization* 8, 1–8.

Girotto, F., Lavagnolo, M. C., Pivato, A., and Cossu, R. (2017). Acidogenic fermentation of the organic fraction of municipal solid waste and cheese whey for bio-plastic precursors recovery – Effects of process conditions during batch tests. *Waste Manag.* 70:71. doi: 10.1016/j.wasman.2017.09.015

Hong, M. Z., Xue, L. Z., and Shi, C. Z. (2017). Effects of agricultural biomass burning on regional haze in China: a review. *Atmosphere* 8, 15–17.

Hu, N. J., Zhou, W., and Zheng, J. L. (2018). Preparation and electrochemical performance of porous V2O5 microspheres. *CJPS* 42, 108–116.

Jia, W. H., Jian, W. Z., and Dong, B. W. (2018). Effect of diclofenac on the production of volatile fatty acids from anaerobic fermentation of waste activated sludge. *Bioresour. Technol.* 254, 7–15. doi: 10.1016/j.biortech.2018.01.059

Jongkeun, L., Kwanyong, L., Donghwan, S., Young Mo, K., Ki Young, P., et al. (2018). Hydrothermal carbonization of lipid extracted algae for hydrochar production and feasibility of using hydrochar as a solid fuel. *Energy* 153, 2957–2965.

Lam, S. S., Lee, X. Y., Nam, W. L., Phang, X. Y., Liew, R. K., Yek, P. N. Y., et al. (2018). Microwave vacuum pyrolysis conversion of waste mushroom substrate into biochar for use as growth medium in mushroom cultivation. *J. Chem. Technol. Biotechnol.* 12, 78–89.

Ling, L., Xiao, P. G., and Cheng, L. Z. (2018). Adsorption behaviors and mechanisms of heavy methane ions on municipal waste composts with different degree of maturity. *Environ. Technol.* 40, 1–43.

Liu, W., Xu, C. H., and Chen, Z. Y. (2017). Simulation of adaptive filtering method for target image data. *CS* 34, 260–263.

Luc, D. V., Simon, V. K., and Frédéric, L. (2017). Microbial ecology and process technology of sourdough fermentation. *Adv. Appl. Microbiol.* 100, 49–160. doi: 10.1016/bs.aambs.2017.02.003

Marzieh, G., and Andrew, A. R. (2018). The effect of mixing on fermentation of primary solids, glycerol, and biodiesel waste. *Water Sci. Technol.* 77, 180–196. doi: 10.2166/wst.2018.015

Natalia, H. G., Manuel, B., and Davi, B. (2019). Effects of enzymes addition on biogas production from anaerobic fermentation of agricultural biomasses. *Waste Biomass Valorization* 3, 1–12. doi: 10.1016/j.watres.2009.11.048

Ojha, K. S., Mason, T. J., and O'Donnell, C. P. (2017). ultrasound technology for food fermentation applications. *Ultrason. Sonochem.* 34, 410–417. doi: 10.1016/j.ultsonch.2016.06.001

Paulina, K., Aleksander, H., and Krzysztof, F. (2018). The study on application of biopolyols obtained by cellulose biomass liquefaction performed with crude glycerol for the synthesis of rigid polyurethane foams. *J. Polym. Environ.* 26, 2546–2554. doi: 10.1007/s10924-017-1145-8

Pivoto, D., Waquil, P. D., Talamini, E., Finocchio, C. P. S., Dalla Corte, V. F., and de Vargas Mores, G. (2018). Scientific development of smart farming technologies and their application in Brazil. *Inform. Process. Agric.* 5, 21–32. doi: 10.1016/j.inpa.2017.12.002

Pujaningsih, R. I., Mukodiningsih, S., and Pakpahan, I. (2017). Cassava waste processing technology to support the provision of alternative feed on zero waste management system of livestock. *Adv. Sci. Lett.* 23, 2595–2597. doi: 10.1166/asl.2017.8727

Qu, J. J. (2017). Research on the function of electronic medical record and related problems in hospital informatization management. *AI* 15, 226–227.

Sawan, Z. M. (2018). Climatic variables: evaporation, sunshine, relative humidity, soil and air temperature and its adverse effects on cotton production. *Inform. Process. Agric.* 5, 134–148. doi: 10.1016/j.inpa.2017.09.006

Steven, W., Ilona, S. H., Mohammad, J., and Taherzadeh, M. J. (2017). Biochemicals from food waste and recalcitrant biomass via syngas fermentation: a review. *Bioresour. Technol.* 248, 113–117. doi: 10.1016/j.biortech.2017.06.075

Tang, M., Yang, Y., and Li, X. F. (2019). Two-grid finite element discretization methods for a class of poisson-nernst-planck equations. *J. Jilin Univ.* 57, 71–77.

Wang, S. Q., Li, Z. H., and Wu, H. K. (2017). Design and experiment on solid heat carrier heating device heated by high temperature flue gas for pyrolysis of biomass. *Trans. Chin. Soc. Agric. Eng.* 6, 47–49.

Xu, H., Liang, C. Y., and Xu, J. L. (2017). Study on One-step ethanol production from CO by cautoethanogenum. *Trans. Chin. Soc. Agric. Eng* 18, 76–78.

Yu, L., Gordeeva, A. V., Borodin, L., and Gordeev, S. (2018). Estimating the limiting rate of dilution in technology for lactic acid production by continuous fermentation. *Theor. Found. Chem. Eng.* 52, 64–66. doi: 10.1134/s0040579518010050

Yu, X. L., Xu, Y. J., and Zhou, Z. X. (2017). Sparse event detection based on parallel discrete social spider optimization algorithm and compressed sensing in wireless sensor networks. *JCAEIT* 12, 202–208.

Zhang, C. H., Zhou, J. W., and Du, C. S. (2017). Review of control strategies of single-phase cascaded H-bridge multilevel inverter for grid-connected photovoltaic systems. *JPS* 15, 1–8.

Zhang, Q., Liu, H., and Hu, J. (2017). Effects of phosphate and carbonate on photo-fermentative hydrogen production of biomass straw. *Trans. Chin. Soc. Agric. Eng.* 33, 251–257.

Zhang, P., Shen, Y. J., and Zhao, L. X. (2018). Study on control of alkyl sulfide in the aerobic fermentation of pig manure by biochar. *EST* 21, 132–135.

Conflict of Interest: The authors declare that the research was conducted in the absence of any commercial or financial relationships that could be construed as a potential conflict of interest.

frontiers in Energy Research

ORIGINAL RESEARCH
published: 23 April 2020
doi: 10.3389/fenrg.2020.00055

Multi-Scale Variability Analysis of Wheat Straw-Based Ethanol Biorefineries Identifies Bioprocess Designs Robust Against Process Input Variations

David Benjamin Nickel[1], *Rickard Fornell*[2]*, *Matty Janssen*[3] and *Carl Johan Franzén*[1]*

[1] Division of Industrial Biotechnology, Department of Biology and Biological Engineering, Chalmers University of Technology, Gothenburg, Sweden, [2] Division of Built Environment, Department of Energy and Resources, RISE Research Institutes of Sweden, Gothenburg, Sweden, [3] Division of Environmental Systems Analysis, Department of Technology Management and Economics, Chalmers University of Technology, Gothenburg, Sweden

OPEN ACCESS

Edited by:
Su Shiung Lam,
University of Malaysia
Terengganu, Malaysia

Reviewed by:
Zhi-Hua Liu,
Texas A&M University, United States
Sarma V. R. K. Mutturi,
Central Food Technological Research
Institute (CSIR), India

***Correspondence:**
Rickard Fornell
rickard.fornell@ri.se
Carl Johan Franzén
franzen@chalmers.se

Specialty section:
This article was submitted to
Bioenergy and Biofuels,
a section of the journal
Frontiers in Energy Research

Received: 26 September 2019
Accepted: 17 March 2020
Published: 23 April 2020

Citation:
Nickel DB, Fornell R, Janssen M and
Franzén CJ (2020) Multi-Scale
Variability Analysis of Wheat
Straw-Based Ethanol Biorefineries
Identifies Bioprocess Designs Robust
Against Process Input Variations.
Front. Energy Res. 8:55.
doi: 10.3389/fenrg.2020.00055

Bioprocesses based on (ligno-)cellulosic biomass are highly prone to batch-to-batch variations. Varying raw material compositions and enzyme activities hamper the prediction of process yields, economic feasibility and environmental impacts. Commonly, these performance indicators are averaged over several experiments to select suitable process designs. The variabilities in performance indicators resulting from variable process inputs are often neglected, causing a risk for faulty performance predictions and poor process design choices during scale-up. In this paper, a multi-scale variability analysis framework is presented that quantifies the effects of process input variations on performance indicators. Using the framework, a kinetic model describing simultaneous saccharification and ethanol fermentation was integrated with a flowsheet process model, techno-economic analysis and life cycle assessment in order to evaluate a wheat straw-based ethanol biorefinery. Hydrolytic activities reported in the literature for the enzyme cocktail Cellic® CTec2, ranging from 62 to 266 FPU·mL^{-1}, were used as inputs to the multi-scale model to compare the variability in performance indicators under batch and multi-feed operation for simultaneous saccharification and fermentation. Bioprocess simulations were stopped at ethanol productivities $\leq$0.1 g·L^{-1}·h^{-1}. The resulting spreads in process times, hydrolysis yields, and fermentation yields were incorporated into flowsheet, techno-economic and life cycle scales. At median enzymatic activities the payback time was 7%, equal to 0.6 years, shorter under multi-feed conditions. All other performance indicators showed insignificant differences. However, batch operation is simpler to control and well-established in industry. Thus, an analysis at median conditions might favor batch conditions despite the disadvantage in payback time. Contrary to median conditions, analyzing the input variability favored multi-feed operation due to a lower variability in all performance indicators. Variabilities in performance indicators were at least 50% lower under multi-feed operation. Counteracting the variability in enzymatic activities by adjusting the amount of added enzyme instead resulted in

higher uncertainties in environmental impacts. The results show that the robustness of performance indicators against input variations must be considered during process development. Based on the multi-scale variability analysis process designs can be selected which deliver more precise performance indicators at multiple system levels.

Keywords: multi-scale model, variability analysis, biorefinery, bioethanol, uncertainty analysis, techno-economic analysis, life cycle assessment, system analysis

INTRODUCTION

Ethanol derived from lignocellulosic biomass is regarded to be a sustainable replacement of fossil fuels in the transport sector. Compared to gasoline, bioethanol has the potential to significantly reduce greenhouse gas emissions (Muñoz et al., 2014) and provide energy security (Uría-Martínez et al., 2018). Lignocellulosic ethanol production utilizes agricultural and forestry waste, amongst others wheat straw (Erdei et al., 2013; Westman et al., 2017), corn (Öhgren et al., 2006; Uppugundla et al., 2014), and wood (Wang et al., 2014).

The utilization of lignocellulosic materials and hydrolytic enzymes poses several challenges at different system scales, e.g., the optimal choice of products, seasonal availability of raw materials with their inherent compositional variation (Collins et al., 2014), and the inhibitory action of pretreated raw materials on fermentation (Horváth et al., 2003; Bellido et al., 2011). During process development, variations in raw material types and compositions or enzymatic activities can influence decisions on the process design. In simultaneous saccharification and fermentation (SSF) processes for example, the hydrolysis rate, with which polysaccharides are broken down into fermentable sugars, is typically the overall rate limiting step. Changes in enzymatic activities result in different saccharification yields and rates which determine the amount of sugars that can undergo ethanol fermentation, with subsequent impacts on techno-economic analysis (TEA) and life cycle assessment (LCA) performance indicators. Thereby, uncertainties in process inputs can result in process designs that eventually fail to meet set production and cost targets.

TEAs and LCAs commonly incorporate uncertainties in performance indicators based on rough estimates of increasing or decreasing performance (Olofsson et al., 2017). Very few studies have based their uncertainty estimates on laboratory data (Vicari et al., 2012). Still, these studies investigate the impacts of uncertainties on single system level. However, data presented in these studies indicate that changes in process inputs affect process indicators at multiple system levels. Changing the amount of added enzyme will for example influence hydrolysis yields. Moreover, the energy-intense off-site production of hydrolytic enzymes, especially the concentration and purification of the enzyme product which is typically driven by fossil energy, contributes significantly to the climate impact of the overall ethanol production process (MacLean and Spatari, 2009; Janssen et al., 2014, 2016). Hence, changing the amount of added enzyme will affect both the bioprocess and the LCA as increased hydrolysis yields will likely result in improved ethanol yields while the climate impact might also increase. In this example, a single level analysis will not enable prediction of the multi-level, diverging outcomes of the overall process. It is therefore necessary to assess the impacts of the variability in process inputs on all important performance indicators across multiple system scales at once.

For a systematic analysis of variations across system scales, multi-scale models are inevitable. Multi-scale models integrate several models at different scales and allow precise descriptions and analyses of each scale by collaborating experts. Multiscale models have been established in various disciplines, e.g., in fluid phase and wastewater treatment research (Deen et al., 2004; Xavier et al., 2007; Ofiteru et al., 2014), metabolic engineering (Dada and Mendes, 2011; Bogart and Myers, 2016), and biomass pretreatment (Hosseini and Shah, 2009). Zhuang and Herrgård (2015) proposed a biorefinery multi-scale model to describe the impacts different microbial strains, products and raw materials have on process economics and environmental impacts by connecting dynamic flux balance analysis to TEA and LCA. The authors used the model to guide strain development from an economic and environmental perspective in early process development stages. However, a systematic assessment of the effects of process input variations across system scales in early process development stages is still missing in the field of lignocellulosic biorefineries.

In this study, we developed a multi-scale variability analysis framework which integrates bioprocess, flowsheet, TEA and LCA scales. The framework was developed with the objective to systematically assess the effects of input variations on the performance indicators of a wheat straw-based ethanol biorefinery. A previously published bioprocess model describing simultaneous saccharification and fermentation to ethanol (Wang et al., 2016) was integrated with flowsheet, TEA and LCA models to form a multi-scale model describing the biorefinery. The validity of the simulated results at bioprocess scale was analyzed by local sensitivity and uncertainty analyses. In a case study the variability in reported hydrolytic, specifically cellulolytic, enzymatic activities was propagated through the multi-scale model to compare two alternative modes of operation, batch and multi-feed. With the help of the multi-scale model the effects of the input variability on the performance indicators were determined and compared between the two modes of operation, and the mode most robust against the input variations was identified.

Abbreviations: AD, Anaerobic digestion; EP, Eutrophication potential; FPU, Filter paper units; IRR, Internal rate of return; LCA, Life cycle assessment; LHV, Lower heating value; PBT, Payback time; SSF, Simultaneous Saccharification and Fermentation; TEA, Techno-Economic Analysis; WIS, Water Insoluble Solids.

SYSTEM DESCRIPTION

The developed multi-scale variability analysis framework covers a multi-scale model describing a wheat straw-based ethanol biorefinery. The biorefinery was assumed to be situated in the south of Sweden. Wheat is cultivated and harvested (**Figure 1**). It was assumed that wheat straw is available at an average distance of 45 km from the biorefinery plant. The straw is transported to the biorefinery and pretreated by H_2SO_4-catalyzed steam explosion. The resulting slurry is pH-adjusted with NaOH and separated by a filter press into a solid fraction and a liquid fraction, referred to as hydrolysate. The hydrolysate is added to molasses medium used in the on-site propagation of *Saccharomyces cerevisiae* to adapt the yeast cells to the lignocellulose-derived inhibitory compounds. The yeast and the solid fraction are added to the simultaneous saccharification and fermentation (SSF) process in which hydrolytic enzymes depolymerize polysaccharides into fermentable sugars. The sugars are taken up by the yeast which convert them into ethanol. After the SSF, ethanol is purified from the bioreactor content through distillation and molecular sieves. The residual slurry is filtered, and the solids are burned in a boiler to generate process steam. Electricity is produced from the excess steam. The process has a net surplus of produced electricity. The liquid fraction of the distillation residues is mixed with residual streams from pretreatment and propagation and sent to anaerobic digestion (AD) to produce biogas from remaining sugar and protein sources. After AD, the liquid is sent to a waste water treatment plant including aerobic bio-oxidation and filtration. Solid residues from AD are dewatered and sent to the boiler for steam production. A detailed description of the modeled biorefinery can be found in section The Flowsheet Model. In the LCA model, upstream activities include the production of H_2SO_4 for pretreatment, NaOH for pH adjustment after pretreatment, glucose as carbon source in yeast propagation, hydrolytic enzymes for the SSF, non-ionic surfactant used in waste water treatment, and all fuel and electricity requirements. The three products of the biorefinery system are ethanol, biogas and electricity.

METHODS

The Multi-Scale Variability Analysis Framework

The multi-scale variability analysis framework was developed with the objective to quantify the variation of performance indicators in response to varying process inputs. The framework consists of three phases: (1) The collection of variable process input data, (2) the use of these data in a multi-scale model, and (3) a statistical analysis of the resulting variability in performance indicators (**Figure 2**).

Within the framework, variable process inputs are defined based on laboratory measurement or literature data. These data can either be direct inputs to the developed multi-scale model, or, in case of a sufficiently large dataset, serve as basis for fitting distributions to be used in Monte-Carlo simulations.

The established multi-scale model simulates a wheat straw-based ethanol biorefinery. A macro-kinetic bioprocess model was connected to flowsheet, TEA and LCA models. The multi-scale model is characterized as a serial-integrated, scale-connecting multi-scale model (Yang and Marquardt, 2009). The data collected in phase (1) are inputs to a bioprocess model covering simultaneous saccharification and ethanol fermentation. The differential equation system of the bioprocess model is solved with the ode15s solver for stiff problems in MATLAB R2016b (The MathWorks Inc., Nattick, USA). The resulting spreads in the bioprocess model outputs hydrolysis yield, fermentation yield and process time are, after a statistical analysis, automatically stored in a .xlsx-file using a component object model. To ensure a feasible number of simulations at flowsheet scale, the 5th, 25th, 50th, 75th, and 95th percentile of each bioprocess model output are automatically retrieved and used as inputs to flowsheet simulations in SuperPro Designer (Intelligen Inc., Scotch Plains, USA). Iterations over the varying inputs are run through an MS Excel-based dashboard. The flowsheet model solves the plant-wide mass and energy balances. The economic performance of each iteration of the biorefinery is determined using the TEA model as defined in SuperPro Designer. Relevant flows and emission data are exported to a .csv-file and transferred to the LCA software openLCA version 1.7 (Ciroth, 2007). To enable a feasible amount of simulations, variabilities in the LCA input data were restricted to the 5th, 50th, and 95th percentiles. At LCA scale the environmental impacts of the produced ethanol are assessed from the cultivation and harvesting of the wheat straw to the gate of the biorefinery (cradle-to-gate). The performance indicators analyzed in this study can be found in **Table 1**.

The Multi-Scale Model

The Bioprocess Model

A macro-kinetic model was used to describe the bioprocess. The model was developed and validated by Wang et al. (2016) to simulate batch and multi-feed SSF processes based on steam pretreated wheat straw at 5–15 filter paper units (FPU)·g_{WIS}^{-1} and 0.02 $g_{Cells}\cdot g_{WIS}^{-1}$ at maximally 13% water insoluble solids (WIS). Multi-feed SSF processes enable efficient mixing and high cell viabilities as solids and cells are added at discrete times with sufficient liquefaction in between. Due to the solid additions and their subsequent hydrolysis, the cumulative WIS is higher than the 13% maximum operating WIS. In the case study the simulated multi-feed process conditions resembled the experimental conditions of a demo plant run at an enzyme activity of 9.3 FPU·g_{WIS}^{-1}, a cell load of 0.02 $g_{Cells}\cdot g_{WIS}^{-1}$ and a final cumulative WIS of 21.85%, with cell additions at 0, 12, 24, 48, and 72 h and solid additions at 0, 4, 12, 24, 48, and 72 h (Wang et al., 2016, **Figure 6**). Batch processes were simulated at identical relative cell and enzymatic activity loadings, but at 13% final WIS, all of which was added initially. The total added enzyme activity was relative to the final cumulative WIS of the process.

The bioprocess model covers the progress of the concentrations of solids, cellulose, xylan, adsorbed hydrolytic enzymes, glucose, xylose, ethanol, cells and the volume in the SSF process. A boundary condition was added to the model to avoid further enzyme adsorption after reaching equilibrium state. Multi-feed SSF processes were modeled as repeated, piece-wise batch processes.

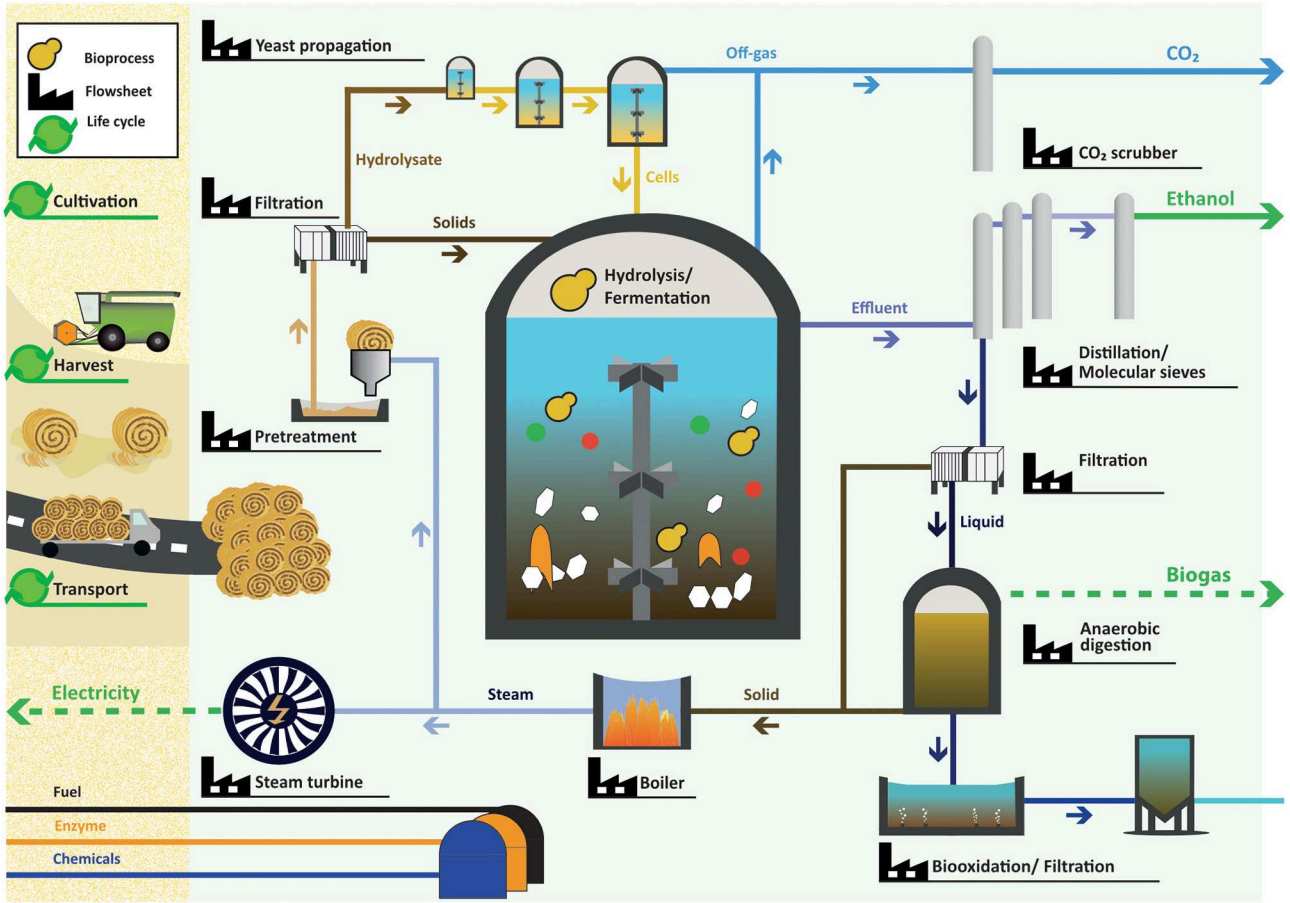

FIGURE 1 | The wheat straw-based ethanol biorefinery system. Wheat straw is cultivated, harvested and transported to the factory. The pretreatment of wheat straw is followed by filtration. The hydrolysate is used for cell propagation while the solid phase is added together with the propagated cells into the bioreactor in which the hydrolysis of the solids into monosaccharides and fermentation to ethanol take place. CO_2 is extracted from the exhaust gas of all bioreactors. After fermentation the bioreactor content is sent to distillation columns and molecular sieves to reach ethanol concentrations ≥ 99%. The remainder of the first distillation column is filtered. The liquid fraction undergoes AD, aerobic bio-oxidation and filtration while the solids are burned together with the solid leftovers after AD in a boiler, generating steam for pretreatment. The excess steam is used in a backpressure turbine to produce power. The biorefinery products are ethanol, biogas, and electricity.

Uncertainty and sensitivity analysis of bioprocess model

Uncertainty and sensitivity analyses were performed based on the methods described by Sin et al. (Sin et al., 2009; Sin and Gernaey, 2016). The uncertainty analysis comprised the following steps:

(1) Process and model definition

The process was defined to be a 96 h SSF batch process under previously described conditions. The model structure was represented by:

$$\frac{dx(t)}{dt} = f(x(t), t, \theta);\ y(t) = g(x(t));\ x(t_0) = x_0 \qquad (1)$$

where $x(t) \in \mathbb{R}^n$ are the state variables, $t \in [t_0\ t_{end}]$ is the process time, $\theta \in \mathbb{R}^n$ the model parameters, and $y(t) \in \mathbb{R}^n$ the model outputs.

(2) Uncertainty definition

The input uncertainties for the estimated parameters k, k_G, γ, k_{ad}, and K_{iEtOH} were defined based on published confidence intervals (**Table 2**). As the parameters k, k_G, K_{iEtOH}, and γ were log-transformed before parameter estimation, they were as well log-transformed before sampling from the input domain. Based on experience, uncorrelated uniform distributions with a low uncertainty of ± 10% for Y_{EtOH} and a medium one of ± 25% for K_S, q_G, α, and β around the mean parameter value were assumed (**Table 2**).

(3) Sampling from uncertainty input domain

For each of the 10 parameters, 1,000 probabilistic samples were taken generating pseudo-random numbers from the specified normal and uniform distributions.

(4) Propagation of uncertainties through Monte-Carlo simulations

The parameter uncertainties were propagated through the bioprocess model, obtaining 1,000 simulation results for each simulated state variable and time point.

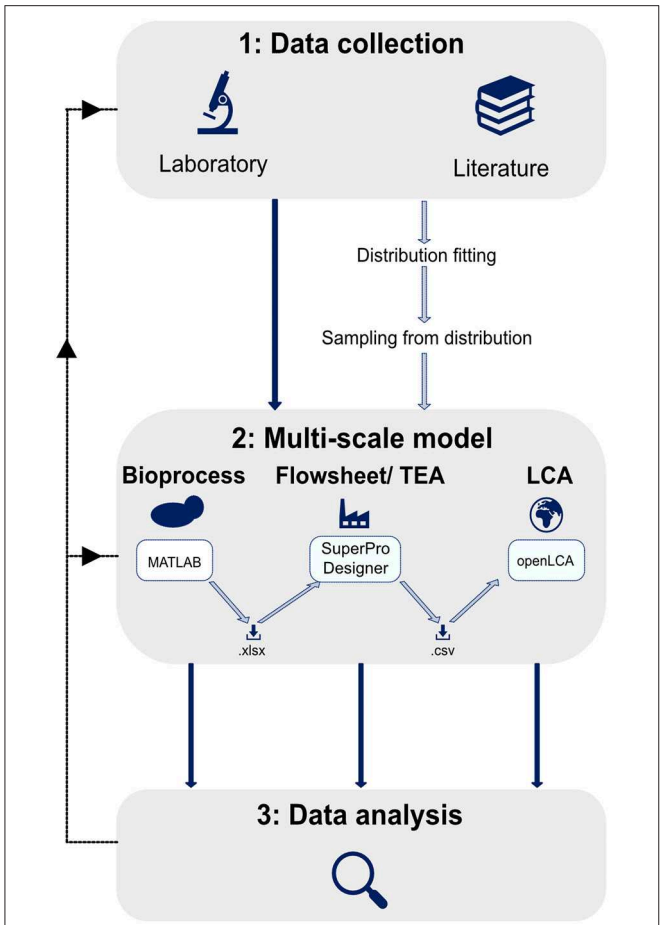

FIGURE 2 | Schematic description of multi-scale variability analysis framework. First, data on the variability of a process input are collected in laboratories or through literature search. The data can be used as direct inputs to the multi-scale model. If enough datapoints are collected, a distribution can be fitted to the data. Samples from the distribution are then inputs to the multi-scale model, following the Monte-Carlo approach. In step 2 the collected data are inputs to the multi-scale model which consists of a bioprocess model in MATLAB, a flowsheet model and TEA in SuperPro Designer, and an LCA in openLCA. The different models are connected via .xlsx- and .csv-files. The resulting variabilities in performance indicators are analyzed statistically in a third step.

(5) Statistical analysis of simulation results

The obtained cumulative distribution functions were analyzed with respect to their mean, 5 and 95% confidence intervals.

Local sensitivity analysis was performed using the finite difference method, specifically the central difference between backward and forward perturbations, to analyze the effect of a change in each parameter θ_i on the model output $y_j(t)$ under the same process conditions as for the uncertainty analysis. The relative sensitivity function $rs_{i,j}$ (Equation 2) was computed by multiplying the first order derivative of y_j with regards to θ_i with the ratio of scaling factors sc_i and sc_j.

TABLE 1 | Analyzed performance indicators.

Scale	Performance indicator	Unit
Bioprocess	Final process time	[h]
	Final ethanol concentration	[$g \cdot L^{-1}$]
	Cellulose hydrolysis yield	[$kg_{Released\ glucose} \cdot kg^{-1}_{Cellulose}$]
	Fermentation yield	[$kg_{EtOH} \cdot kg^{-1}_{WIS}$]
Flowsheet/TEA	Ethyl alcohol production	[MW]
	Methane production	[MW_{LHV}]
	Net electricity production	[MW]
	Size of SSF reactors	[m^3]
	Total equipment cost	[MEUR]
	Pretreatment	[MEUR]
	Bioreactor	[MEUR]
	Product upgrading	[MEUR]
	Waste water treatment plant	[MEUR]
	Utilities	[MEUR]
	Total operating cost	[$MEUR \cdot year^{-1}$]
	Revenues	[$MEUR \cdot year^{-1}$]
	Internal rate of return	[%]
	Payback time	[year]
LCA	Climate impact	[$kg_{CO2eq} \cdot L^{-1}_{EtOH}$]
	Eutrophication potential	[$kg_{PO4eq} \cdot L^{-1}_{EtOH}$]

The table lists all performance indicators analyzed in the case study with the help of the multi-scale model.

$$rs_{i,j}(t) = \frac{\partial y_j(t)}{\partial \theta_i} \frac{sc_i}{sc_j} \tag{2}$$

To assess the importance of each parameter on the variance in model outputs, parameters were ranked as proposed by Sin and Gernaey (2016) according to the δ^{msqr} measure (Equation 3) which summarizes the influence of each parameter θ_i on a model output y_j over process time.

$$\delta^{msqr}_{i,j} = \sqrt{\frac{1}{N} \sum_{i=1}^{N} rs^2_{i,j}} \tag{3}$$

The Flowsheet Model

The flowsheet model was developed in SuperPro Designer with the objective to assess the preliminary design in early process development of a typical wheat straw-based biorefinery with ethanol, biogas and electricity as products. Variations of process inputs were analyzed at a fixed flowrate of wheat straw into the process. The flowrate was determined by setting the ethanol output to 100,000 m^3 per year for a 96 h multi-feed process under conditions described in 3.2.1. The flowsheet model was fitted to data obtained from lab- (1–2.5 L), pilot-, and demo scale (10 m^3) experiments and to the bioprocess model outputs: hydrolysis yield, ethanol yield, and process time.

The flowsheet starts with a one-step steam explosion pretreatment. Wheat straw is first heated by recycled flash steam followed by an addition of 0.2% H_2SO_4 and pretreatment at 188°C for 7 min. The pretreatment temperature is reached by direct steam injection with steam at 12.3 bar. After pretreatment

TABLE 2 | Model parameter values with published confidence intervals or assumed parameter limits.

Parameters	Parameter value	Confidence interval/Parameter limits	Distribution	Parameter description
k	0.016	[0.009, 0.03][a]	Lognormal	Hydrolysis rate constant
K_G	6.13	[2.7, 13.8][a]	Lognormal	Glucose inhibition constant on cellulose hydrolysis
K_{iEtOH}	16.6	[14.4, 19.1][b]	Lognormal	Ethanol inhibition constant on cellulose hydrolysis
γ	0.028	[0.01, 0.08][a]	Lognormal	Proportionality constant between cellulose and xylan hydrolysis
k_{ad}	0.27	[0.03, 0.5][a]	Normal	Adsorption rate constant
K_S	0.01	[0.0075, 0.0125]	Uniform	Saturation constant of glucose uptake
q_G	1.6	[1.2, 2]	Uniform	Specific glucose uptake rate
Y_{EtOH}	0.42	[0.378, 0.462]	Uniform	Ethanol yield on glucose
α	0.026	[0.0195, 0.0325]	Uniform	Pre-exponential factor on ethanol-induced cell death rate
β	0.0037	[0.0028, 0.0046]	Uniform	Exponential factor on ethanol-induced cell death rate

[a]*Wang et al. (2016)*, [b]*Wang et al. (2014).*
In case of assumed parameters values, the specified intervals are the limits of a uniform distribution for Monte-Carlo simulations.

one flash drum lowers the pressure. Thereby, water and a fraction of the volatile compounds generated during pretreatment, mainly furfural and acetic acid, are removed. The flash steam was assumed to be recycled to the pre-steaming reactor, thus reducing energy and water demands. The pretreatment and the concentrations of total organic carbon, total sulfur and furfural in the flash steam were based on experiments conducted in the Biorefinery Demo Plant at RISE Processum (Örnsköldsvik, Sweden) (Fornell et al., 2016).

The slurry resulting from pretreatment is cooled and separated in a filter press into a solid fraction and a hydrolysate. The hydrolysate with a total (soluble) solids concentration of 85 $g{\cdot}L^{-1}$ is sent to the SSF bioreactors, the yeast propagation and AD. The solid fraction with a total solids concentration of 440 $g{\cdot}L^{-1}$ (WIS: 385 $g{\cdot}L^{-1}$) is sent to the SSF bioreactor. The solid fraction is diluted to a WIS concentration resulting in the same final ethanol concentrations and yields (based on the solid fraction after pretreatment and filtration) as in the bioprocess model. The WIS contents differ between the bioprocess and flowsheet model due to additional reactions and literature estimates included in the flowsheet model for the SSF description in order to close the mass balances.

The yeast propagation is designed as a series of five propagation reactors, and two parallel trains (Humbird et al., 2011). The carbon sources for yeast propagation consist of 50% molasses (containing sucrose, modeled as glucose) and 50% hydrolysate (containing glucose and xylose). The stoichiometries for glucose and xylose conversion were experimentally determined and 100% conversion was assumed:

$$1\,\text{kg Glucose} + 0.6\,\text{kgO}_2 \rightarrow 0.6\,\text{kg CO}_2 + 0.68\,\text{kg H}_2\text{O} + 0.3\,\text{kg Biomass} + 0.02\,\text{kg Ethanol} \quad (4)$$

$$1\,\text{kg Xylose} + 0.7\,\text{kg O}_2 \rightarrow 0.7\,\text{kg CO}_2 + 0.78\,\text{kg H}_2\text{O} + 0.2\,\text{kg Biomass} + 0.02\,\text{kg Ethanol} \quad (5)$$

After cell propagation the yeast cells are separated by centrifugation.

To start the SSF, hydrolytic enzymes and propagated yeast cells are added to the solids in the SSF bioreactor. The SSF reactor system was designed as a set of 12 parallel reactors (Humbird et al., 2011). The stoichiometries of the SSF reactions are based on moles except for the conversion of cellulose to glucose. The conversion yields from cellulose to glucose and glucose to ethanol varies based on the outputs from the bioprocess model (**Appendix 1**), while other yields did not change. The reactions defined in SuperPro Designer are the following:

$$\text{Cellulose} + \text{H}_2\text{O} \rightarrow \text{Glucose} \quad \text{Varying conversion} \quad (6)$$

$$\text{Glucose} \rightarrow 2\text{CO}_2 + 2\text{Ethanol} \quad \text{Varying conversion} \quad (7)$$

$$\text{Glucose} \rightarrow 2\text{Glycerol} \quad 0.74\%\ \text{based on glucose} \quad (8)$$

$$\text{Xylose} \rightarrow \text{Xylitol} \quad 14\%\text{based on xylose} \quad (9)$$

$$3\text{Xylose} \rightarrow 5\text{Glycerol} \quad 20.2\%\text{based on xylose} \quad (10)$$

The hydrolysis of galactan, mannan, and arabinan is excluded from the model due to their low content in the solids added to the SSF. The flowsheet model excludes xylose to ethanol conversion based on experimental data and in accordance with the bioprocess model.

In the distillation sequence three heat-integrated columns are used. The first two columns are parallel strippers. The crude ethanol from the strippers is purified in a rectification column to near azeotropic concentrations while the bottom slurry is separated in a filter press into solids mainly consisting of lignin and a filtrate. To minimize potential fouling in the strippers, the highest pressure is applied to the rectification column. After distillation the crude ethanol at >90% purity is dehydrated in a set of molecular sieves. The molecular sieves and the filter press are designed according to Humbird et al. (2011).

The modeled biorefinery has its own waste water treatment. The filtrate from the strippers, the centrifuge water from yeast propagation, and excess hydrolysate are mixed and cooled to 32°C. In subsequent AD organic compounds are converted to CH_4. Conversions are simulated based on chemical oxygen demands according to reference literature values (Barta et al.,

2010; Humbird et al., 2011; Petersson, 2012). The waste water from AD is treated by aerobic bio-oxidation and filtration to decrease the concentration of relevant substances to acceptable levels before being released to the recipient.

The solids from the AD are centrifuged and combined with the solids from the filtration of the stripper bottoms. These solids are sent to the steam boiler which produces steam at 90 bar and 470°C with an excess oxygen input of 10% and overall heat losses of 5%. The boiler was designed based on reference literature (Humbird et al., 2011; Fornell and Berntsson, 2012; Fornell et al., 2012). The blow-down of boiler feed water was set to 5% of the total steam production. The 90 bar pressure steam is sent to a backpressure turbine with steam extractions at 12.3 bar for the pretreatment reactor and 4.5 bar for other process demands, e.g., distillation and preheating, and a condensing tail with an exhaust pressure of 0.1 bar. The cold utility in the process is based on the cooling demand as calculated by SuperPro Designer. A cooling tower is used for the cooling water system. The cooling water system is designed based on information found in Perry's Chemical Engineers' Handbook (Humbird et al., 2011; Ahmetović et al., 2014).

The heat exchangers in the process simulation model were integrated based on a pinch analysis. The analysis is an important part of the assessment since the energy integration might affect both TEA and LCA. The heat exchanger network was designed in order to be well-integrated and practically feasible, and the different heat exchangers needed were designed and included in the simulation model. In this heat exchanger network the distillation section is internally integrated, i.e., the distillation bottoms are used to preheat the column feeds. The 4.5 bar steam condensate in the boiler section is heat exchanged with the makeup boiler water and the condensate from the turbine while the flash steam from pretreatment is directly recycled in that section.

The flowsheet modeling software SuperPro Designer includes the capacity to conduct TEAs based on data and information generated by the performed flowsheet simulations. Different costs for design and operation of a lignocellulosic ethanol biorefinery were manually adjusted in the software, and a TEA was performed in order to study the propagation of variability from the bioprocess model to the flowsheet model and TEA. Since the focus of this TEA was to assess the effect of variations in input data to the bioprocess model on the economic performance, no statistical analysis of the input data specific for the TEA (e.g., costs for raw material and market price of products) was performed. In the TEA the yearly revenues, operating cost, internal rate of return (IRR), and payback time (PBT) were calculated. All equipment cost correlations, operating costs, and product values (including references), and model inputs and outputs are presented in **Appendix 1**.

The Life Cycle Assessment

The LCA was defined as a cradle-to-gate system, from the cultivation of wheat (to obtain the wheat straw) until the gate of the ethanol biorefinery (**Figure 3**). The functional unit in this LCA was the amount of ethanol produced from a fixed input of wheat straw into the biorefinery. This functional unit was chosen because the primary function of the analyzed system was to produce bioethanol and not to process wheat straw. Furthermore, the biorefinery flowsheet model was simulated with a fixed input of wheat straw. The LCA results are, however, given per liter of ethanol produced.

The LCA was carried out using an attributional approach (Baumann and Tillman, 2004) since the focus of this study lay on the variability of process inputs and parameters in the production process, and its impact on the LCA results. The life cycle impact assessment was conducted using the CML characterization method (Gorrée et al., 2002). The climate impact and eutrophication potential (EP) were used as impact categories for the evaluation of the system. These two impact categories were chosen since a reduction of fossil-based fuel use is the main goal of biofuel production, and fertilizer and nutrients are used in the production of straw-based ethanol, respectively. The need for allocation of the environmental burden of the system to the main product (ethanol) and its by-products (biogas and electricity) was avoided, thanks to the available data and information, and sufficient detail from the process flowsheet model that was used to define the LCA model.

The LCA model was implemented and run in openLCA version 1.7 for batch and multi-feed processes at variable process times, with median inventory values, and with 5 and 95% confidence interval inventory values for the different process flows (both foreground and background) that were part of the model. These values, except for those for the cultivation and harvesting of the wheat straw and the straw preparation, were delivered by the process simulations done in SuperPro Designer. The following choices were made for modeling the wheat cultivation and harvesting, straw preparation, and enzymes and chemicals needed in the process:

1. Cultivation and harvesting were modeled using the inventory data for wheat production compiled by Röös, Sundberg, and Hansson (Röös et al., 2011). It was assumed that 15% of the harvested wheat straw was lost due to its transportation and preparation for the pretreatment.
2. In the straw preparation to cut the straw in sufficiently small chips, $3.6{\cdot}10^{-3}$ $kWh_{electricity}{\cdot}kg^{-1}$ of wheat straw was needed. Electricity use was modeled with the ecoinvent process "market for electricity, medium voltage" for Sweden (Frischknecht et al., 2007).
3. Enzyme production was modeled using inventory data compiled by Liptow et al. (2013) and was assumed to take place in Kalundborg, Denmark.
4. Use of NaOH, H_2SO_4, glucose and non-ionic surfactant were modeled with the ecoinvent processes "market for sodium hydroxide, without water, in 50% solution state," "market for sulfuric acid," "glucose production," and "market for non-ionic surfactant," respectively (Althaus et al., 2007).

Case Study—Impact of Variable Enzymatic Activities of Cellic® CTec2

Lignocellulosic bioprocesses rely on saccharification to obtain monosaccharides for the microbial conversion into desired products. Therefore, SSF process development focuses both

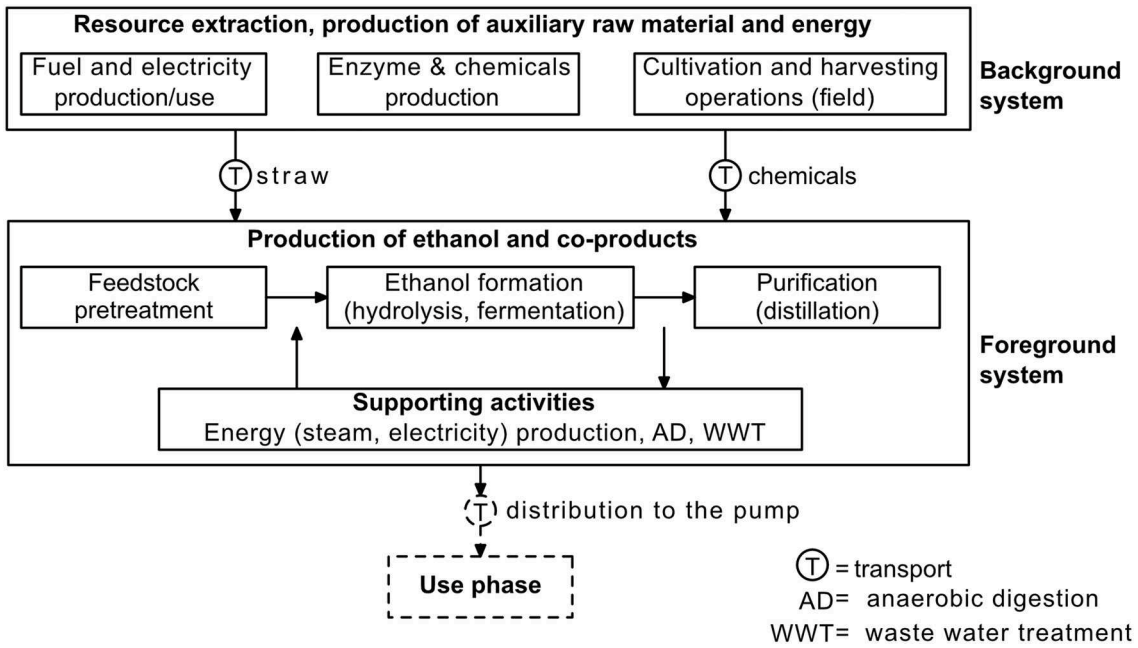

FIGURE 3 | System boundaries of the life cycle assessment. The dashed lines indicate processes and flows that are outside of the scope of this study.

on hydrolysability and fermentability of pretreated materials. This case study has the objective to analyze with the help of the developed multi-scale variability analysis framework, how robust performance indicators of a projected wheat straw-based biorefinery are against variations in enzymatic activities under batch and multi-feed operation. The case study specifically reflects conditions at early process development stages to illustrate the use of the multiscale variability analysis as a help for stakeholders to decide on projected process designs given the reliability of the performance indicators.

Phase 1: Data Collection

The Cellic® CTec2 enzyme cocktail (Novozymes A/S, Denmark) has been widely used in research. Hence, many publications report enzymatic activity measurements for Cellic® CTec2, allowing for a systematic assessment of enzymatic variability from literature data. To obtain an unbiased selection of publications, a literature search with the search terms "Cellic," "CTec2," and "CTec 2" was performed in SciFinder (CAS Chemical Abstracts Service, Columbus, USA) on 2018-01-23. The results (**Appendix 1**) were statistically analyzed as described in **Appendix 2** and a final dataset for the variability analysis was retrieved.

Phase 2: Application of Multi-Scale Model

The impact of the variability in enzymatic activities on the choice of process design based on metrics obtained from the multi-scale model was evaluated for batch and multi-feed SSF processes under previously described conditions at variable process times. Two scenarios were simulated:

(1) The variability in enzymatic activities was unknown *a priori* and a fixed amount of Cellic® CTec2 was added to the reactor. The scenario was simulated for batch and multi-feed operation. The scenario reflects a single activity measurement which is then used as input for several experiments with one or several batches of the enzyme cocktail.

(2) The variability in enzymatic activity was known *a priori*. To compensate for the variability in generated products, the amount of added Cellic® CTec2 was adjusted to reach the same enzymatic activity in the reactor. This scenario was simulated for multi-feed operation at all system levels and for batch processes at TEA level. The scenario reflects the unbiased measurement of enzymatic activities before each laboratory experiment.

For simulations of scenario (1) the dataset on the variability in enzymatic activities was directly used as input to the bioprocess model. For scenario (2), the amount of enzyme to be added to reach the nominal activity was calculated and used as input to the simulations. The total volume was balanced by modulating the addition of process water.

Phase 3: Statistical Analysis

Basic statistical entities including mean, and 5th, 25th, 50th, 75th, and 95th percentiles were determined for all performance indicators at bioprocess, flowsheet and TEA scales. At the LCA scale, the 5th, 50th, and 95th percentiles were determined for all performance indicators.

RESULTS AND DISCUSSION

Uncertainty and Sensitivity Analysis of the Bioprocess Model

The developed multi-scale model relies on a serial connection of models at different scales. To assess the validity of the

bioprocess model under the chosen process conditions prior to its integration into the multi-scale model, an uncertainty and sensitivity analysis was performed on a 96 h batch process. Hydrolytic enzymes were simulated to adsorb to the solids, leading to cellulose and xylan degradation and a release of glucose and xylose. As glucose uptake was limited by the maximal glucose uptake rate of the yeast cells, glucose accumulated (**Figure 4**). Eventually, the hydrolysis rate decreased due to glucose feed-back inhibition and depletion of available substrate, after which an equilibrium between glucose release and uptake was established, reflected in glucose concentrations close to 0 $g{\cdot}L^{-1}$. According to the model, the yeast cells converted the released glucose directly into ethanol. When both the solid cellulose and the dissolved glucose were depleted, the ethanol production stopped due to a lack of substrate.

In the first 40 h, uncertainties in model parameter estimates led to a spread in glucose concentrations of up to 26 $g{\cdot}L^{-1}$ (**Figure 4**). The large spread indicates that the bioprocess model has difficulties to precisely predict the shift in the overall rate limiting step from fermentation to hydrolysis. Limitations in glucose uptake and ethanol conversion capacities result in glucose accumulation, whereas a limited hydrolysis capacity results in low glucose concentrations. Accordingly, sensitivity analysis showed that glucose concentrations were most influenced by the hydrolysis rate constant k, the glucose uptake rate q_G, and the cell death rate α (**Figure 5**). Increases in q_G led to lower glucose concentrations, thereby relieving feed-back inhibition of hydrolysis. In contrast, increases in k or α caused glucose accumulation because the glucose consumption rate became the overall limiting step. Under glucose-limited conditions after 40 h, the influence of q_G and k declined.

Final ethanol concentrations were mainly influenced by the ethanol yield on glucose, Y_{EtOH}. Ultimately, variations in final ethanol concentrations would only stem from Y_{EtOH} if operating the process infinitely long time. The other model parameters affected the dynamic changes in ethanol concentrations. The parameter-related uncertainty was low when stopping the process at ethanol productivities lower than 0.1 $g{\cdot}L^{-1}{\cdot}h^{-1}$.

Case Study: The Impact of Variable Enzymatic Activities on Performance Indicators of an Ethanol Biorefinery

The Reported Variability in the Enzymatic Activity of Cellic® CTec2

A literature search on the enzymatic activity of Cellic® CTec2 resulted in 476 hits. Forty nine hits contained measurements of the protein content, and 81 presented the cellulose hydrolysis activity expressed in $FPU{\cdot}mL^{-1}$. Because the protein content had a higher standard deviation of 72 $mg{\cdot}mL^{-1}$ around a mean of 150 $mg{\cdot}mL^{-1}$, and the lower number of hits, the cellulose hydrolysis activity was used as a direct measure for enzymatic activity. After statistical analysis 70 hits representing the variability in the enzymatic activity of Cellic® CTec2 remained. The average activity was 146 $FPU{\cdot}mL^{-1}$, the median activity 139 $FPU{\cdot}mL^{-1}$, and the standard deviation was 41 $FPU{\cdot}mL^{-1}$. The distribution of enzymatic activities was negatively skewed, reflected in a maximum activity of 266 $FPU{\cdot}mL^{-1}$ vs. a minimum of 62 $FPU{\cdot}mL^{-1}$.

The high spread in measured activities is very problematic during process development at laboratory scale and scale-up. Commonly, the amount of added enzyme is stated as hydrolytic activity relative to the WIS, total solid or cellulose content to enable comparisons of experiments across scales and laboratories. Failures to measure enzymatic activities accurately and precisely could therefore lead to suboptimal process designs and the exclusion of better process alternatives.

The collected enzyme activity data include both measurement variability and the actual enzyme product variability. It is likely that measurement variability contributes more to the overall variability, as the FPU assay has been reported to be difficult to reproduce (Dashtban et al., 2010).

Scenario 1: Fixed Addition of Enzymatic Cocktail With Unknown Activity

In the first case study scenario batch and multi-feed operations were analyzed under the assumption that actual enzymatic activities were unknown. Thus, in simulations a fixed amount of enzyme, calculated from the median activity, was added to the bioreactors, resulting in variations in the actual added enzymatic activity per WIS.

Bioprocess model

Variations in enzymatic activities had no effect on final ethanol concentrations when running batch processes for 10,000 h. Instead, the variability affected the time it took to reach the final ethanol concentrations. These findings are in agreement with uncertainty analysis and confirm that variation or improvements in enzymatic activities affect process dynamics but not final titers. To further investigate these dynamic effects a stop criterion was applied. The stop criterion resulted in a spread in final process times from 31.6 h (5th percentile) to 46.2 h (95th percentile) at a median of 36.6 h. Ethanol concentrations ranged from 23.6 to 25.4 $g{\cdot}L^{-1}$ (**Figure 6**).

Variations in process times were highly dependent on the inoculum size. Large inocula led to immediate glucose consumption. Therefore, hydrolysis became rate-limiting and variations in hydrolysis rates had a direct effect on the process time. With small inocula instead, glucose accumulated as the hydrolysis rate exceeded the fermentative capacity of the cells. Hence, these conditions minimized process time variations at the expense of overall longer process times. Given the high model uncertainty around the shift between hydrolysis and fermentation as rate-limiting steps, the predictive quality of the model would need improvements to infer exact inoculum sizes to restrict process time variations under batch operation.

Under multi-feed operation, frequent solid additions resulted in an accumulated solid load of 21.85% WIS, 68% higher than under batch operation. In the simulations, the higher solid loadings led on average to 2.6 times longer process times than in the batch operation (5th percentile: 89.7 h; 50th percentile:

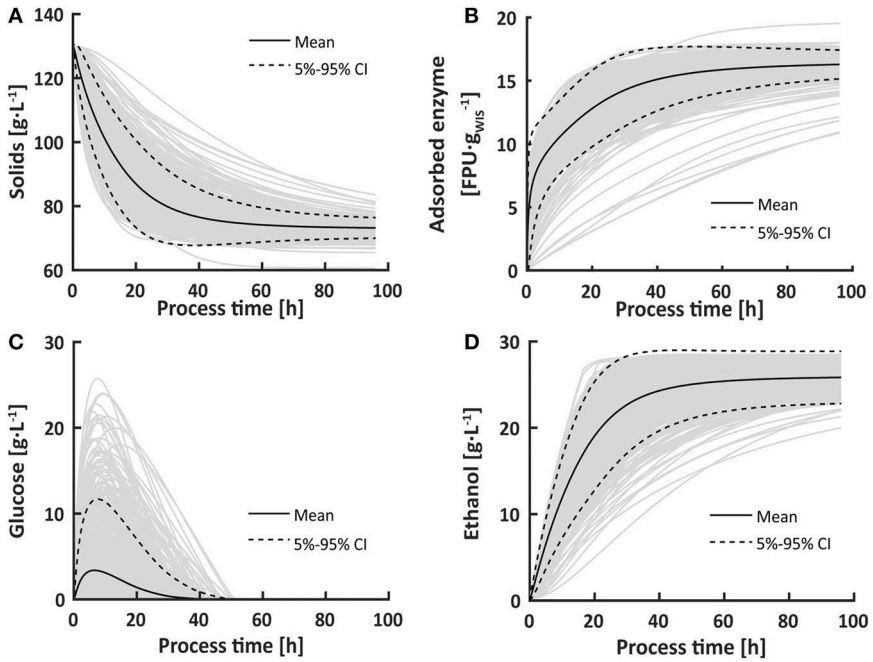

FIGURE 4 | Uncertainty in the modeled solids **(A)**, adsorbed enzyme **(B)**, glucose **(C)** and ethanol **(D)** concentrations for a 96 h SSF batch process. The uncertainty in model parameters, evaluated in 1,000 Monte-Carlo simulations, lead to a high spread in glucose concentration in the first 40 h of the bioprocess due to a shifting balance between hydrolysis and fermentation. The dashed lines indicate the 5 to 95% confidence intervals in each set of 1,000 results.

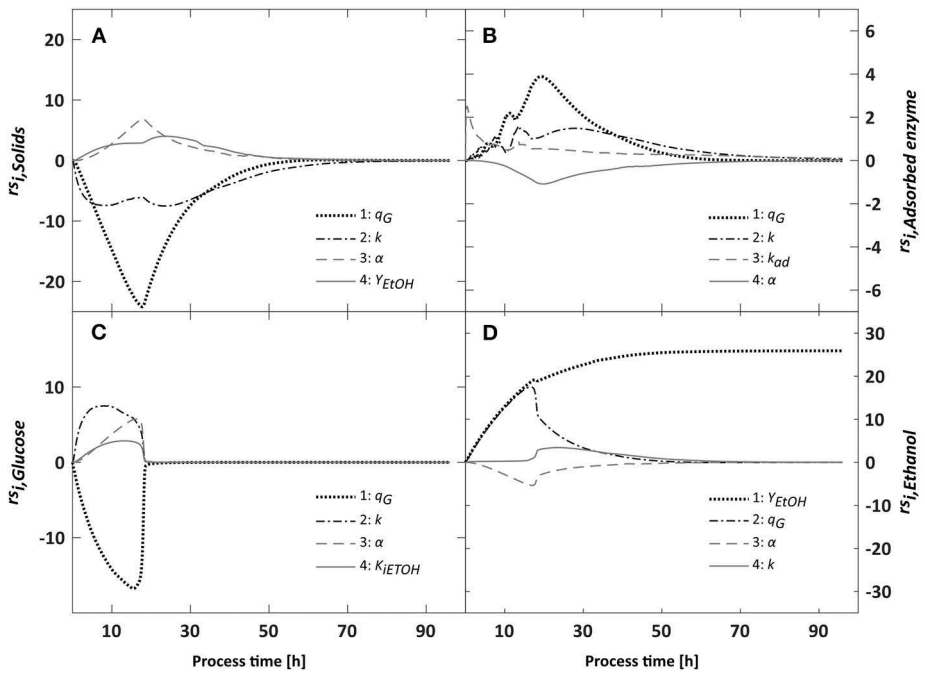

FIGURE 5 | Relative sensitivities of the modeled solids **(A)**, adsorbed enzyme **(B)**, glucose **(C)** and ethanol **(D)** concentrations toward changes in their four most influential model parameters. The overall influence of parameters on each output was computed using the δ^{msqr} measure for a 96 h batch process. Overall, the hydrolysis rate k and the glucose uptake rate q_G influenced the model most, especially during the first 40 h of the process.

95.1 h; 95th percentile: 102.7 h) and final ethanol concentrations between 41.9 and 43.6 $g \cdot L^{-1}$. The spread in final process times relative to the median was 65% lower than in batch operation. The standard deviation in final ethanol concentrations and the variation in the ethanol yield [$g_{EtOH} \cdot g_{WIS}^{-1}$] decreased compared to batch operation.

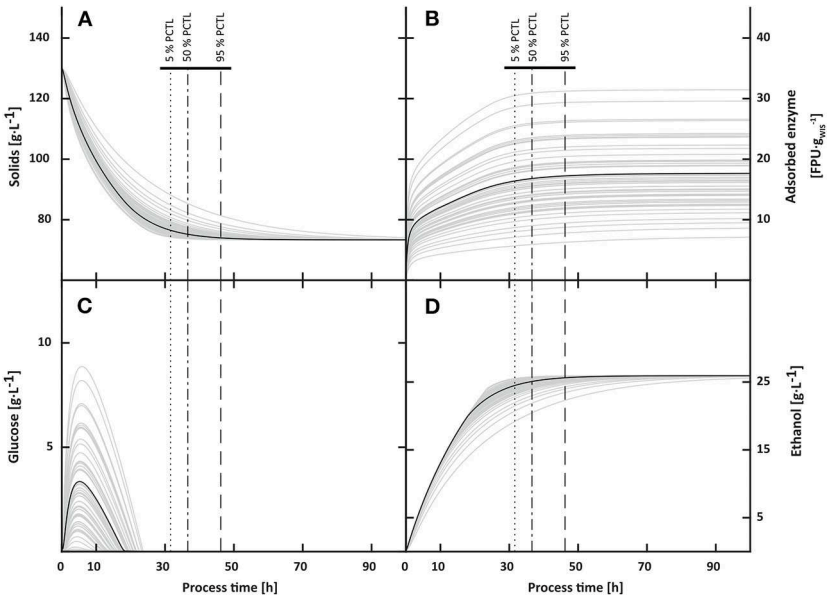

FIGURE 6 | Impact of variability in enzymatic activities on solids **(A)**, adsorbed enzyme **(B)**, glucose **(C)** and ethanol **(D)** concentrations in batch process. Final ethanol concentrations were not affected by the variable input. Instead, the variability in enzymatic activities affected the time to completely deplete glucose and thereby the final process time. When applying a process stop criterion at ethanol productivities ≤ 0.1 g·L^{-1}, the final process time varied between 31.6 h (5th percentile) and 46.2 h (95th percentile).

The simulations indicate that the multi-feed operation could be further improved. As **Figure 7** shows, ethanol concentrations stabilized after each solids and cell addition while maintaining enough cell viability for ethanol production, indicating cellulose depletion. With the proposed stop criterion and online ethanol measurements, feeding events could be triggered, thereby achieving a higher productivity while decreasing the process time. However, as feeding events would be triggered by decrements in fermentation rates caused by decreasing hydrolysis rates due to cellulose depletion, the hydrolysis rate would ultimately be the overall rate limiting step. Hence, such an adaptive strategy might be highly susceptible to varying enzymatic activities.

The performance indicator most affected by varying enzymatic activities at bioprocess scale was the final process time. Hydrolysis and fermentation yields showed low variation. Therefore, the variation in final process times was integrated into higher system scales. Batch and multi-feed operations were analyzed when 5, 25, 50, 75, and 95% of all bioprocesses were stopped according to the stop criterion.

Flowsheet model and techno-economic analysis

Variation in enzymatic activities affected ethanol, methane and electricity production in the biorefinery under batch and multi-feed operation. At median enzymatic activities and median process times approximately 72 MW_{LHV} (LHV = lower heating value) of the main product ethanol were produced in both modes of operation. However, at median final process times, the variability in produced ethanol was 65% higher under batch than under multi-feed conditions (**Figure 8**). The difference in variabilities decreased with increasing final process times as maximum final ethanol concentrations were reached even at lower enzymatic activities. Under batch operation, ethanol production ranged from 70 to 74 MW_{LHV} across the analyzed process times at median enzymatic activities, under multi-feed operation from 71 to 73 MW_{LHV}.

At median final process times and nominal enzyme activity approximately 42 MW_{LHV} of methane were produced in AD under batch and multi-feed operation. The AD process seemed to be nearly independent of the variation in enzymatic activities. The small variations in the range of 1–3% of the solids content sent to AD, caused by different hydrolysis and fermentation yields, were smaller than the variations inherent in model calculations. To investigate these differences, a more detailed model would be required. The low variability in biogas production can on the one hand be attributed to the constant flow of hydrolysate from pretreatment to AD, in all cases corresponding to >50% of the total feed, which is independent of the hydrolysis efficiency. On the other hand, differences in the hydrolysis efficiency affected ethanol production rather than AD as >90% of the sugars released during hydrolysis were converted to ethanol. Therefore, the feed from the distillation columns to AD varied only by a few percent under all investigated conditions.

Electric power generation, however, was affected by enzymatic variabilities to the same extent as ethanol production, suggesting that there is a counterbalance between ethanol production and electric power generation via the left-over cellulose that instead can be burnt for steam generation. This hypothesis was substantiated by the observation that the minimum enzymatic activity caused the highest electric power generation in both process configurations. In short, lower hydrolysis yields increased the amounts of solids (cellulose) remaining after SSF and thereby

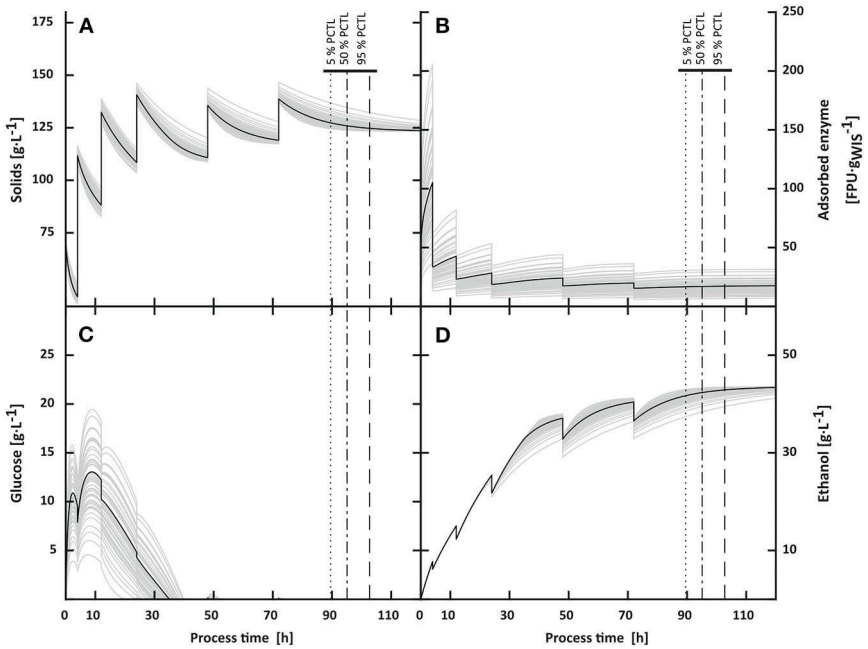

FIGURE 7 | Impact of variability in enzymatic activities on solids **(A)**, adsorbed enzyme **(B)**, glucose **(C)** and ethanol **(D)** concentrations in multi-feed process. At solid additions ethanol was diluted and increased afterwards due to cellulose hydrolysis and fermentation. The final process time ranged from 89.7 h (5th percentile) to 102.7 h (95th percentile). Final ethanol concentrations varied by 2%.

the amount of fuel sent to the boiler. Accordingly, less electricity was produced at longer process times as more cellulose was hydrolyzed and subsequently converted into ethanol.

The amount of electricity produced from steam generated in the boiler was higher under multi-feed operation (**Figure 8**). The underlying reasons for the lower electricity production under batch operation were the higher flow rates and the substantially lower final ethanol concentrations after SSF. The lower ethanol concentrations in batch processes increased the steam demand for distillation, thereby lowering the capacity in the steam turbine for electricity production.

With the assumptions made in the TEA, the variability in enzymatic activities caused no significant changes (<2%) in the equipment costs under both modes of operation. However, the costs for the bioreactors varied by 20% across the different process times under batch and by 8% under multi-feed operation (**Figure 9A**). The lower variation in bioreactor costs under multi-feed operation was a result of the lower variation in final bioprocess times. The cost for the SSF bioreactors accounted for 10% of the total equipment cost in multi-feed processes. Due to longer residence times in response to higher cumulative WIS content, the bioreactor equipment costs were higher in multi-feed processes, whereas the equipment costs for product upgrading and waste water treatment were lower due to decreased flow rates in response to the higher cumulative WIS contents.

Contrary to the equipment and operating costs which were almost constant under all investigated conditions given the assumptions made in the TEA model, the yearly revenues were significantly affected by variations in enzymatic activities (**Figure 9B**). The responses to the variation followed the same trend as the ethanol production, with higher variances caused under batch operation. As ethanol production increased across process times, the yearly revenues increased. The median yearly revenues of 79.3 MEUR·year^{-1} under batch and 80 MEUR·year^{-1} under multi-feed operation differed only by 0.7 MEUR·year^{-1}. Since the economic results followed the trend of produced ethanol, the data indicate that ethanol production affects the economic profitability of the biorefinery system the most even though increased ethanol production is counterbalanced by reduced electricity production and, under batch operation, by increased equipment cost.

The variance in the internal rate of return (IRR) was at median process times 56% higher under batch operation (**Figure 9C**), and in the payback time (PBT) 81% higher (**Figure 9D**). Furthermore, the median IRR was lower under batch operation, leading to 7% longer median PBT. Across process times the IRRs increased, following the trend in ethanol production, and the payback times decreased. The TEA results indicate that the TEA performance indicators are more robust under multi-feed operation against variations in enzymatic activities. Taking the IRR and PBT into account, the multi-feed process was economically more favorable than batch operation.

In order to draw conclusions regarding the economic feasibility of batch and multi-feed operation, more detailed assessments are required. These assessments include the scheduling of the bioreactor system including yeast propagation and SSF, and different utilizations of excess hydrolysate after pretreatment. For example, sending the hydrolysate to the SSF and yeast propagation bioreactors instead of the biogas plant

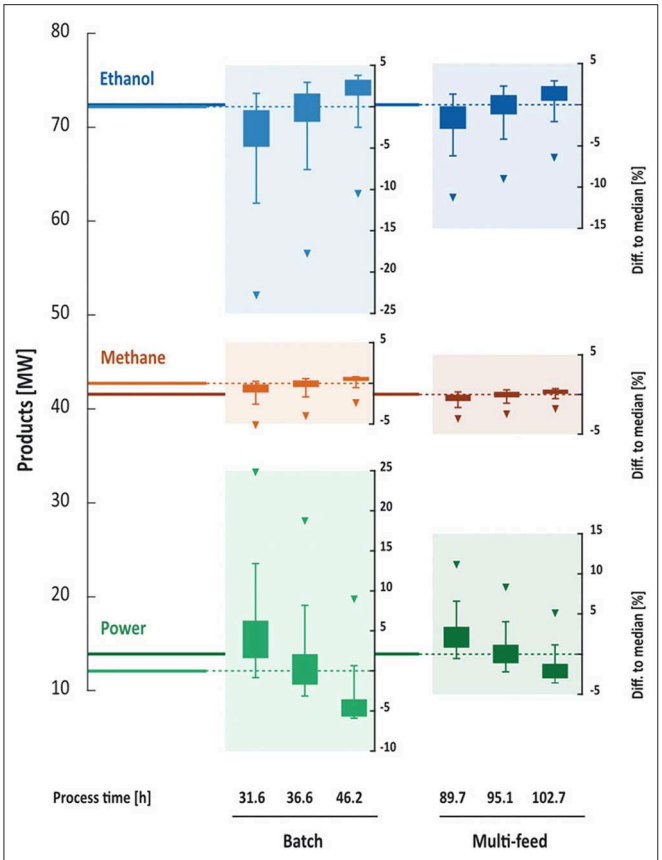

FIGURE 8 | Median product generation and variability in products. Under batch conditions less power and more methane are produced due to a less complete cellulose conversion compared to multi-feed conditions. The variability in generated products as response to variance in enzymatic activities is larger under batch conditions. The least affected product is methane. Longer process times reduce the variability as more processes at different hydrolysis efficiency reach full conversion of cellulose to ethanol. The triangles indicate the minimum enzymatic activity, box limits 25th and 75th percentiles, and error bar limits the 95th and 5th percentiles in enzymatic activities. The left axis relates to the median values under investigated conditions, the right axes to the variability expressed as percentage of the median.

directly might affect both the TEA results and the sensitivity to variations in process parameters.

Life cycle assessment

At median enzyme activities and median process times the climate impact under batch operation was equal to that of the multi-feed operation (0.869 and 0.864 $kg_{CO2eq} \cdot L_{EtOH}^{-1}$, respectively). However, as observed for the economic measures, the variation under batch operation was 70% higher (**Figure 10A**). The climate impact decreased with increasing final process times due to higher ethanol yields relating to a more complete raw material utilization. The contribution of enzyme production to the climate impact was stable at 43% for all investigated cases as the same amount of enzyme was added. The EP followed the same trends as the climate impact (**Appendix 1**). As these findings also follow the trends for the ethanol production, it supports the hypothesis that the variability in climate impact is directly related to the variability in produced ethanol as a response to variances in enzymatic activities.

Summary of scenario 1

Scenario 1 shows that multi-scale variability analysis can have a strong influence on the process design of projected biorefineries. Considering only the mean or median values for enzymatic activity, batch and multi-feed operations have the same yearly revenues. Although performance indicators such as the IRR and PBT indicate slight advantages of multi-feed operations, process designers might tend more toward choosing batch operation due to its wide application and simpler operability and controllability, contrary to multi-feed operation. However, multi-scale variability analysis shows that under multi-feed operation, all performance indicators are more robust against variations in enzymatic activities. Therefore, performance indicators retrieved from multi-feed experiments at laboratory and demo plant scale are more reliable when coping with variations in hydrolysis rates. Variations in hydrolysis rates could also stem from variations in the amount of added enzyme due to the high viscosity of enzyme preparations. The analyzed scenario shows that the developed multi-scale variability analysis framework can pinpoint bottlenecks in the process which are not robust against input variations. In contrast to an analysis at median conditions, the framework delivers a measure of the reliability in performance indicators and provides stakeholders with valuable information on how to proceed in process development. Compared to Vicari et al. (2012), the framework not only considers the lower uncertainties in yields but also takes the process dynamics into account. Specifically, the spread in process times at bioprocess scale is transformed in a spread in yearly material flows at flowsheet, TEA and LCA scales. The performed analysis shows that this spread in process times affects performance indicators at higher system scales more than variabilities in hydrolysis or fermentation yields.

Another advantage of the variability analysis approach shown by scenario 1 is the consistent evaluation of variability effects on all system levels. Thereby, process dynamics of the biorefinery can be reflected in greater detail and be introduced to non-dynamic models at flowsheet, TEA and LCA levels. Furthermore, the variabilities derived from measurement data could potentially be used as inputs to uncertainty and sensitivity analysis at the TEA and LCA levels. The variabilities could improve assumptions on step changes or distributions in input variables and flowsheet model or LCA parameters, and their dynamic effects on the bioethanol plant.

Scenario 2: Varying Addition of Enzyme Cocktail With Unknown Activity

The second scenario covered an *a priori* knowledge of the actual enzyme activity and adjustment of the added amount of enzyme to reach the target activity of 9.3 $FPU \cdot g_{WIS}^{-1}$ under multi-feed operation. Since the amount of added enzyme changed, the same activity was added to the bioreactors, resulting in identical final ethanol concentrations and process times for all simulations. The differences in the added amount of enzyme

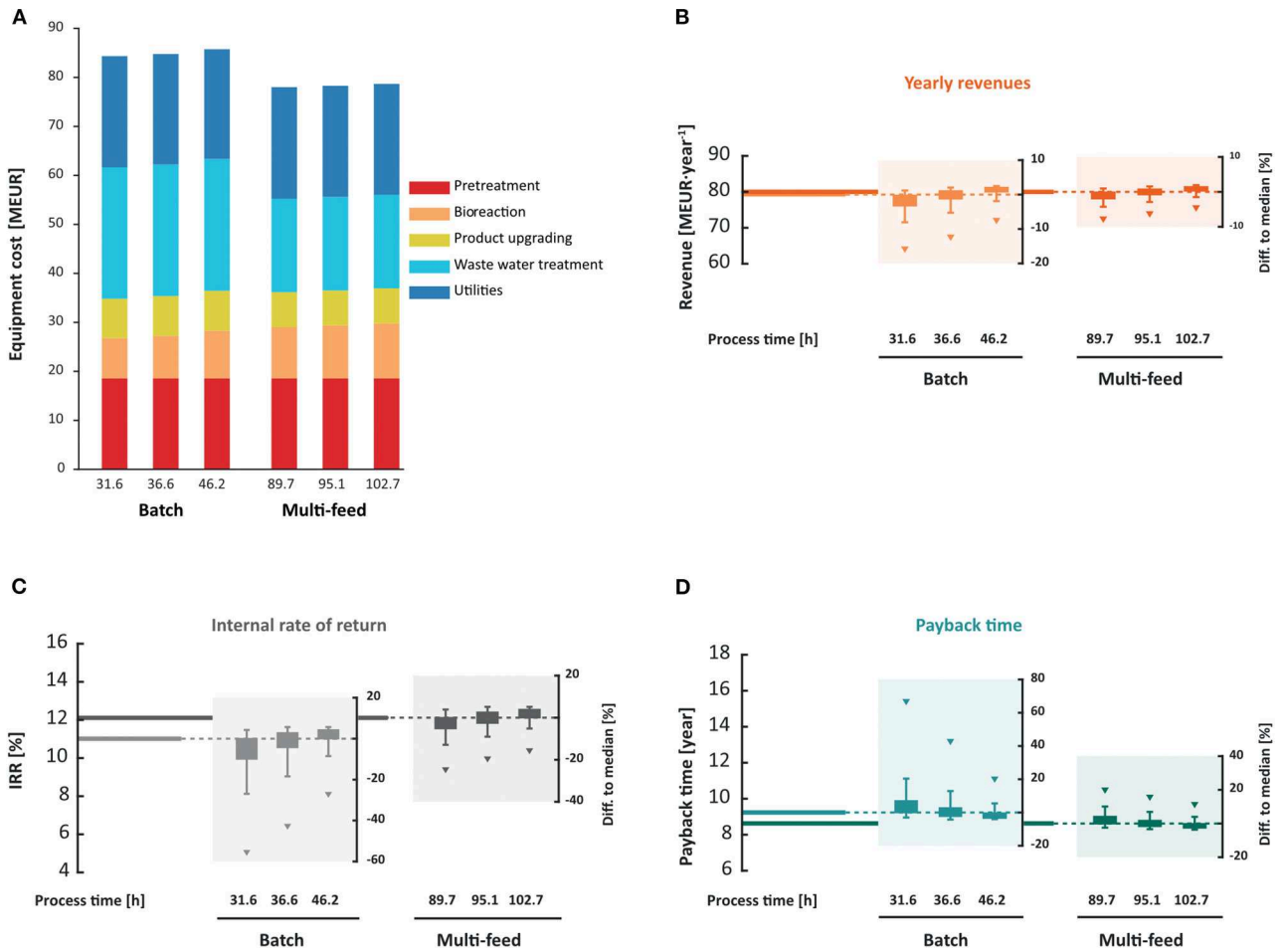

FIGURE 9 | Impact of variability in enzymatic activity on techno-economic parameters under batch and multi-feed conditions. The variability in enzymatic activities had no effect on equipment cost **(A)**. Batch and multi-feed conditions affected the cost for the bioreaction, product upgrading and waste water treatment section. The yearly revenues were significantly influenced by the variability in enzymatic activities, with a higher variability under batch conditions **(B)**. The variability in yearly revenues propagated to the IRR **(C)** and PBT **(D)**. The triangles indicate the minimum enzymatic activity, box limits 25th and 75th percentiles, and error bar limits the 95th and 5th percentiles in enzymatic activities. The left axis relates to the median values under investigated conditions, the right axes to the variability expressed as percentage of the median.

resulted in differing process costs, emissions and resources related to enzyme production.

Under the assumptions made in this case study, for multi-feed operation a constant addition of enzyme (scenario 1) would be preferable over adjusting the amount of added enzyme to varying activities (scenario 2). Variations in the enzyme prices due to changed amounts of added volume would have a larger effect on the process economics (scenario 2) than the variation in process performance (scenario 1). Under batch conditions adjusting the amount of added enzyme to varying activities (scenario 2) would be preferable except for process times longer than 46.2 h (95th percentile). In the case of longer process times the variation in process performance is decreased in scenario 1 to an extent that the variation in enzyme prices due to varying amounts of added enzyme (scenario 2) is higher.

The climate impact was significantly affected by changes in the added enzyme volume. Contrary to the situation in scenario 1, the contribution of the enzymes on the climate impact and EP varied in scenario 2 for multi-feed operation. The contribution of enzyme addition to the climate impact ranged from 33 to 54%, and to the EP from 20 to 37%. The high contribution of enzymes produced off-site to the climate impact is in agreement with other LCA studies on second generation bioethanol production (Janssen et al., 2014, 2016; Olofsson et al., 2017). Moreover, the variability in climate impact was 588% higher in scenario 2 compared to scenario 1 (**Figure 10B**).

For batch operation scenario 2 seems favorable due to a high stability in generated products and techno-economic parameters. However, the improvements in process robustness are counterbalanced by the increased variability in climate impact. For multi-feed operation both the techno-economic

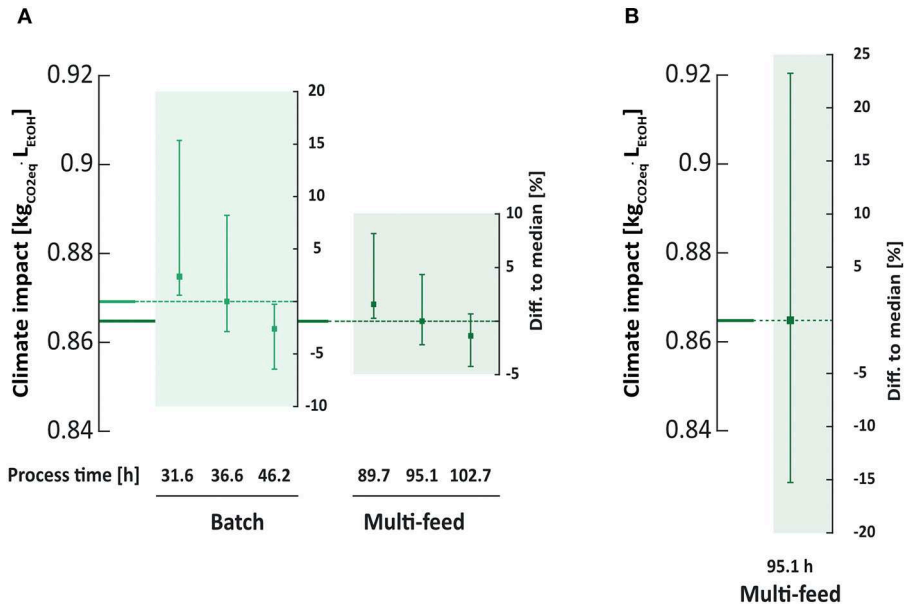

FIGURE 10 | Variation in climate impact as response to variation in enzymatic activities. In scenario 1 the variability in enzymatic activities affects the global warming potential significantly more under batch than under multi-feed conditions as response to changing saccharification efficiency **(A)**. Changing the amount of added enzyme as response to variation in enzymatic activities (scenario 2) results in a spread between the 5th and 95th percentile of 39% around the median for the multi-feed process running 95.1 h **(B)**, almost six times higher than in scenario 1. The error bar limits indicate the 95th and 5th percentiles in enzymatic activities. The left axis relates to the median values under investigated conditions, the right axes to the variability expressed as percentage of the median.

parameters and the climate impact show higher variation in scenario 2 compared to scenario 1, favoring the addition of a defined amount of enzyme regardless of varying activities. This indicates that there might be potential for aligning environmental and economic goals with design strategies for ethanol-based biorefineries, if the process is designed to be robust against variations in performance. In case of a process sensitive to variations in process inputs, such as the batch process in this study, the environmental and economic goals will be contradictive.

CONCLUSIONS

A multi-scale variability analysis framework was developed to quantify variances in performance indicators resulting from process input variations. The framework was applied to evaluate a wheat straw-based ethanol biorefinery. An application to different raw materials and products requires the integration of other validated bioprocess models into the framework. With the existing serial structure, new models can be easily integrated at bioprocess scale. Therefore, the framework could also be extended to compare the predictions based on different models describing the same bioprocess at different system scales. Another extension to the developed framework could include the analysis of one or more process inputs different to the enzymatic activity. Therefore, the model structure at flowsheet scale might need adjustments to call the necessary variables from bioprocess scale. Furthermore, future work should aim to directly link the different model environments to reduce the complexity in data transfer and remove potential error sources.

In the presented multi-scale variability analysis framework input variations were propagated through a multi-scale model describing a wheat straw-based biorefinery. Thereby, the robustness of performance indicators against these variations could be quantified at multiple system scales for different process operations and designs.

Case study scenario 1 illustrated that analyses of median or average process inputs lead to different conclusions than using the full variability in process inputs. The developed framework enables the assessment of the reliability of performance indicators whereas an analysis at median levels provides single values without an uncertainty estimate. The results of scenario 1 showed that performance indicators are more reliable under multi-feed than under batch operation. Furthermore, the analysis revealed that only a specific group of performance indicators is affected by variations in enzymatic activities. While equipment and operating costs remained almost constant, the yearly revenues, for example, were significantly affected within this analysis.

A key advantage over single-scale assessments is the integration of process dynamics into static TEA and LCA models. Until now, uncertainty and variability assessments at TEA scale were restricted to changes in yields or raw material compositions. As the uncertainty analysis of the bioprocess model showed, the variation in process times is higher than the variation in hydrolysis and fermentation yields, unless a large part of the cellulose remains unconverted, which in any case would result in a non-viable process. The results of case study scenario 1

illustrated that process time evaluation is key to predict process designs with favorable economics and environmental impact as time-dependent trends can be identified. Furthermore, the multi-scale approach allows for the inclusion of multiple criteria for process evaluation. As such, multi-scale variability analysis could be used for multi-objective optimization under variable process inputs.

The uncertainty estimates of performance indicators are very important in a biorefinery context as process development is confronted with multiple design choices under varying process inputs, e.g., varying raw material compositions, supply chains or process portfolios. The framework developed in this study offers a methodology for performing such investigations.

DATA AVAILABILITY STATEMENT

The original literature dataset, the output datasets from each model scale as well as the statistical analysis of raw data are available in **Appendix 1**. The models in MATLAB, SuperPro Designer, and openLCA are available from the corresponding authors on reasonable request.

AUTHOR CONTRIBUTIONS

DN performed the search and statistical analyses of literature data, the mathematical modeling, and uncertainty analysis of the fermentation process. RF designed and performed the process simulations and techno-economic analysis. MJ performed the life cycle assessment. DN and RF designed and programmed the automated data exchange between fermentation simulations, process system simulations, and techno-economic analyses. DN, RF, and MJ drafted the manuscript. All authors analyzed, interpreted, integrated the results, edited the manuscript, read and approved the final manuscript, and conceived and designed the study.

FUNDING

This research was funded by the Swedish Energy Agency (P41272-1) and the Area of Advance Energy at Chalmers University of Technology. The funding bodies had no influence on the design of the study and were involved neither in the collection, analysis and interpretation of data, nor in the writing of the manuscript.

ACKNOWLEDGMENTS

The authors thank Ruifei Wang for providing raw data from laboratory and demo scale experiments.

SUPPLEMENTARY MATERIAL

The Supplementary Material for this article can be found online at: https://www.frontiersin.org/articles/10.3389/fenrg.2020.00055/full#supplementary-material

REFERENCES

Ahmetović, E., Ibrić, N., and Kravanja, Z. (2014). Optimal design for heat-integrated water-using and wastewater treatment networks. *Appl. Energy* 135, 791–808. doi: 10.1016/j.apenergy.2014.04.063

Althaus, H.-J., Chudacoff, M., Hischier, R., Jungbluth, N., Osses, M., and Primas, A. (2007). *Life Cycle Inventories of Chemicals*. Ecoinvent Report No 8., v2.0. Dübendorf: EMPA Dübendorf, Swiss Centre for Life Cycle Inventories.

Barta, Z., Reczey, K., and Zacchi, G. (2010). Techno-economic evaluation of stillage treatment with anaerobic digestion in a softwood-to-ethanol process. *Biotechnol. Biofuels* 3:21. doi: 10.1186/1754-6834-3-21

Baumann, H., and Tillman, A.-M. (2004). *The Hitch Hiker's Guide to LCA: An Orientation in Life Cycle Assessment Methodology and Application*. Lund: Studentlitteratur AB.

Bellido, C., Bolado, S., Coca, M., Lucas, S., González-Benito, G., and García-Cubero, M. T. (2011). Effect of inhibitors formed during wheat straw pretreatment on ethanol fermentation by *Pichia stipitis*. *Bioresour. Technol.* 102, 10868–10874. doi: 10.1016/j.biortech.2011.08.128

Bogart, E., and Myers, C. R. (2016). Multiscale metabolic modeling of C4 plants: connecting nonlinear genome-scale models to leaf-scale metabolism in developing maize leaves. *PLoS ONE* 11:e0151722. doi: 10.1371/journal.pone.0151722

Ciroth, A. (2007). ICT for environment in life cycle applications openLCA – a new open source software for life cycle assessment. *Int. J. Life Cycle Assess.* 12:209. doi: 10.1065/lca2007.06.337

Collins, S. R., Wellner, N., Bordonado, I. M., Harper, A. L., Miller, C. N., Bancroft, I., et al. (2014). Variation in the chemical composition of wheat straw: the role of tissue ratio and composition. *Biotechnol. Biofuels* 7:121. doi: 10.1186/s13068-014-0121-y

Dada, J. O., and Mendes, P. (2011). Multi-scale modelling and simulation in systems biology. *Integr. Biol.* 3, 86–96. doi: 10.1039/c0ib00075b

Dashtban, M., Maki, M., Leung, K. T., Mao, C., and Qin, W. (2010). Cellulase activities in biomass conversion: measurement methods and comparison. *Crit. Rev. Biotechnol.* 30, 302–309. doi: 10.3109/07388551.2010.490938

Deen, N. G., van Sint Annaland, M., and Kuipers, J. A. M. (2004). Multi-scale modeling of dispersed gas–liquid two-phase flow. *Chem. Eng. Sci.* 59, 1853–1861. doi: 10.1016/j.ces.2004.01.038

Erdei, B., Hancz, D., Galbe, M., and Zacchi, G. (2013). SSF of steam-pretreated wheat straw with the addition of saccharified or fermented wheat meal in integrated bioethanol production. *Biotech. Biofuels* 6:169. doi: 10.1186/1754-6834-6-169

Fornell, R., and Berntsson, T. (2012). Process integration study of a kraft pulp mill converted to an ethanol production plant – Part A: Potential for heat integration of thermal separation units. *Appl. Therm. Eng.* 35, 81–90. doi: 10.1016/j.applthermaleng.2011.10.010

Fornell, R., Berntsson, T., and Åsblad, A. (2012). Process integration study of a kraft pulp mill converted to an ethanol production plant – part B: Techno-economic analysis. *Appl. Therm. Eng.* 42, 179–190. doi: 10.1016/j.applthermaleng.2012.02.043

Fornell, R., Willquist, K., Petersson, A., and Franzén, C. J. (2016). Water management in lignocellulosic ethanol production – a case study and comparative analysis from a Swedish perspective. *Chem. Eng. Trans.* 52, 703–708. doi: 10.3303/CET1652118

Frischknecht, R., Tuchschmid, M., Faist Emmenegger, M., Bauer, C., and Dones, R. (2007). *Strommix und Stromnetz. Sachbilanzen von Energiesystemen: Grundlagen für den Ökologischen Vergleich von Energiesystemen und den Einbezug von Energiesystemen in Ökobilanzen für die Schweiz*. Dübendorf: Swiss Centre for Life Cycle Inventories.

Gorrée, M., Heijungs, R., Huppes, G., Kleijn, R., de Koning, A., Van Oers, L., et al. (2002). *Handbook on Life Cycle Assessment: Operational Guide to the ISO Standards*. Dordrecht: Kluwer Academic Publishers.

Horváth, I. S., Franzén, C. J., Taherzadeh, M. J., Niklasson, C., and Lidén, G. (2003). Effects of furfural on the respiratory metabolism of *Saccharomyces cerevisiae* in glucose-limited chemostats. *Appl. Environ. Microbiol.* 69, 4076–4086. doi: 10.1128/AEM.69.7.4076-4086.2003

Hosseini, S. A., and Shah, N. (2009). Multiscale modelling of hydrothermal biomass pretreatment for chip size optimization. *Bioresour. Technol.* 100, 2621–2628. doi: 10.1016/j.biortech.2008.11.030

Humbird, D., Davis, R., Tao, L., Kinchin, C., Hsu, D., Aden, A., et al. (2011). *Process Design and Economics for Biochemical Conversion of Lignocellulosic Biomass to Ethanol: Dilute-Acid Pretreatment and Enzymatic Hydrolysis of Corn Stover*. Technical Report NREL/TP-5100-477642011. Golden: National Renewable Energy Laboratory (NREL).

Janssen, M., Tillman, A.-M., Cannella, D., and Jørgensen, H. (2014). Influence of high gravity process conditions on the environmental impact of ethanol production from wheat straw. *Bioresour. Technol.* 173, 148–158. doi: 10.1016/j.biortech.2014.09.044

Janssen, M., Xiros, C., and Tillman, A.-M. (2016). Life cycle impacts of ethanol production from spruce wood chips under high-gravity conditions. *Biotechnol. Biofuels* 9:53. doi: 10.1186/s13068-016-0468-3

Liptow, C., Tillman, A.-M., Janssen, M., Wallberg, O., and Taylor, G. A. (2013). Ethylene based on woody biomass – what are environmental key issues of a possible future Swedish production on industrial scale. *Int. J. Life Cycle Assess.* 18, 1071–1081. doi: 10.1007/s11367-013-0564-6

MacLean, H. L., and Spatari, S. (2009). The contribution of enzymes and process chemicals to the life cycle of ethanol. *Environ. Res. Lett.* 4:014001. doi: 10.1088/1748-9326/4/1/014001

Muñoz, I., Flury, K., Jungbluth, N., Rigarlsford, G., i Canals, L. M., and King, H. (2014). Life cycle assessment of bio-based ethanol produced from different agricultural feedstocks. *Int. J. Life Cycle Assess.* 19, 109–119. doi: 10.1007/s11367-013-0613-1

Ofiteru, I. D., Bellucci, M., Picioreanu, C., Lavric, V., and Curtis, T. P. (2014). Multi-scale modelling of bioreactor–separator system for wastewater treatment with two-dimensional activated sludge floc dynamics. *Water Res.* 50, 382–395. doi: 10.1016/j.watres.2013.10.053

Öhgren, K., Bengtsson, O., Gorwa-Grauslund, M. F., Galbe, M., Hahn-Hägerdal, B., and Zacchi, G. (2006). Simultaneous saccharification and co-fermentation of glucose and xylose in steam-pretreated corn stover at high fiber content with *Saccharomyces cerevisiae* TMB3400. *J. Biotechnol.* 126, 488–498. doi: 10.1016/j.jbiotec.2006.05.001

Olofsson, J., Barta, Z., Börjesson, P., and Wallberg, O. (2017). Integrating enzyme fermentation in lignocellulosic ethanol production: life-cycle assessment and techno-economic analysis. *Biotechnol. Biofuels* 10:51. doi: 10.1186/s13068-017-0733-0

Petersson, A. (2012). *Basdata Om Biogas*. Sverige: Svenskt Gastekniskt Center.

Röös, E., Sundberg, C., and Hansson, P.-A. (2011). Uncertainties in the carbon footprint of refined wheat products: a case study on Swedish pasta. *Int. J. Life Cycle Assess.* 16, 338–250. doi: 10.1007/s11367-011-0270-1

Sin, G., and Gernaey, K. (2016). "Data handling and parameter estimation", in *Experimental Methods in Wastewater Treatment*, eds M. C. M. van Loosdrecht, P.H. Nielsen, C.M. Lopez-Vazquez, and D. Brdjanovic (London: IWA Publishing), 201–234.

Sin, G., Gernaey, K. V., and Lantz, A. E. (2009). Good modeling practice for PAT applications: propagation of input uncertainty and sensitivity analysis. *Biotechnol. Prog.* 25, 1043–1053. doi: 10.1002/btpr.166

Uppugundla, N., da Costa Sousa, L., Chundawat, S. P., Yu, X., Simmons, B., Singh, S., et al. (2014). A comparative study of ethanol production using dilute acid, ionic liquid and AFEX^{TM} pretreated corn stover. *Biotechnol. Biofuels* 7:72. doi: 10.1186/1754-6834-7-72

Uría-Martínez, R., Leiby, P. N., and Brown, M. L. (2018). Energy security role of biofuels in evolving liquid fuel markets. *Biofuel. Bioprod. Bioref.* 12, 802–814. doi: 10.1002/bbb.1891

Vicari, K. J., Tallam, S. S., Shatova, T., Joo, K. K., Scarlata, C. J., Humbird, D., et al. (2012). Uncertainty in techno-economic estimates of cellulosic ethanol production due to experimental measurement uncertainty. *Biotechnol. Biofuels* 5:23. doi: 10.1186/1754-6834-5-23

Wang, R., Koppram, R., Olsson, L., and Franzén, C. J. (2014). Kinetic modeling of multi-feed simultaneous saccharification and co-fermentation of pretreated birch to ethanol. *Bioresour. Technol.* 172, 303–311. doi: 10.1016/j.biortech.2014.09.028

Wang, R., Unrean, P., and Franzén, C. J. (2016). Model-based optimization and scale-up of multi-feed simultaneous saccharification and co-fermentation of steam pre-treated lignocellulose enables high gravity ethanol production. *Biotechnol. Biofuels* 9:88. doi: 10.1186/s13068-016-0500-7

Westman, J. O., Wang, R., Novy, V., and Franzén, C. J. (2017). Sustaining fermentation in high-gravity ethanol production by feeding yeast to a temperature-profiled multifeed simultaneous saccharification and co-fermentation of wheat straw. *Biotechnol. Biofuels* 10:213. doi: 10.1186/s13068-017-0893-y

Xavier, J. B., De Kreuk, M. K., Picioreanu, C., and van Loosdrecht, M. C. (2007). Multi-scale individual-based model of microbial and bioconversion dynamics in aerobic granular sludge. *Environ. Sci. Technol.* 41, 6410–6417. doi: 10.1021/es070264m

Yang, A., and Marquardt, W. (2009). An ontological conceptualization of multiscale models. *Comput. Chem. Eng.* 33, 822–837. doi: 10.1016/j.compchemeng.2008.11.015

Zhuang, K. H., and Herrgård, M. J. (2015). Multi-scale exploration of the technical, economic, and environmental dimensions of bio-based chemical production. *Metab. Eng.* 31, 1–12. doi: 10.1016/j.ymben.2015.05.007

Conflict of Interest: The authors declare that the research was conducted in the absence of any commercial or financial relationships that could be construed as a potential conflict of interest.

frontiers in Energy Research

ORIGINAL RESEARCH
published: 27 May 2020
doi: 10.3389/fenrg.2020.00090

Efficient Extraction of Bioenergy From *Cinnamomum camphora* Leaves

Zanpei Zhang†, Xuanxuan Wu†, Yong Lai, Ximei Li, Dangquan Zhang and Yuanyuan Chen**

College of Forestry, Henan Agricultural University, Zhengzhou, China

Cinnamomum camphora is an evergreen tree native to China and distributed to some Asian countries. Its leaves are rich in bioactive compounds and their pharmacological effects are well-known. A potent method to extract and preserve the active biological substances is crucial for latter application in bioenergy and as chemical raw material. In this study, the metabolite profiles of *C. camphora* were comprehensively analyzed by using FT-IR and GC-MS after extracted by three type of solvent: ethanol, benzene, and acetone. The identified chemical compounds were then classified into different functional groups based on previous study. Our result proposes the potential application of *C. camphora* into biomedicine, bioenergy, and chemical raw materials industry.

Keywords: renewable biomass, *Cinnamomum camphora* leaves, extract, bioactive components, bioenergy

OPEN ACCESS

Edited by:
Su Shiung Lam,
University of Malaysia Terengganu, Malaysia

Reviewed by:
Peter Nai Yuh Yek,
University College of Technology Sarawak, Malaysia
Chin Fhong Soon,
Universiti Tun Hussein Onn Malaysia, Malaysia

****Correspondence:***
Dangquan Zhang
zhangdangquan@163.com
Yuanyuan Chen
cyuan091@163.com

†These authors have contributed equally to this work

Specialty section:
This article was submitted to Bioenergy and Biofuels, a section of the journal Frontiers in Energy Research

Received: *10 November 2019*
Accepted: *28 April 2020*
Published: *27 May 2020*

Citation:
Zhang Z, Wu X, Lai Y, Li X, Zhang D and Chen Y (2020) Efficient Extraction of Bioenergy From Cinnamomum camphora Leaves. Front. Energy Res. 8:90. doi: 10.3389/fenrg.2020.00090

INTRODUCTION

Increment of human population has huge impact to energy consumption that mainly depends on non-renewable energy such as fossil fuel, oil, coal, and natural gas to sustain the human need. To date, only 11% of energy is generated from renewable energy (https://www.iea.org/weo2018/) due to several shortages such as efficiency and resources. Therefore, researcher started to explore resource like *Cinnamomum camphora* as alternative to fossil fuel.

Cinnamomum camphora (Lauraceae) is commonly known as camphor tree, are widely distributed in subtropical zones, including southeastern China and northeastern Australia (Yakefu et al., 2018). *C. camphora* is famous for its ornamental, economic, and medicinal value (Chen and Dai, 2015). In particular, *C. camphora* contain oil gland cells that can be used to extract camphor oil (Afrin et al., 2019). The essential oil has antifungal activity (Sattar et al., 1991), insecticidal and insect repellent properties (Liu L. et al., 2018), antioxidant (Fu et al., 2016), anti-aging, anti-bacterial, and anti-inflammatory effects (Chen C. et al., 2018; He et al., 2018; Chen et al., 2019). The bark is used in treating limb ulcer and the fruit of *C. camphora* has properties to relieve fever, treat common flu, and dysentery (Satyal et al., 2013). The root of *C. camphora* promote blood circulation, improving rheumatism, treating stomach diseases, and bruises (Jiang et al., 2016; Chen S. et al., 2018; Liu X. et al., 2019).

The application of camphor oil is not limited to medical application but also as flavors, soap, painting materials, mineral processing, plastics polymer, explosives, and as preservative (Guo et al., 2016). The leaf powder of *C. camphora* was reported to absorb and remove dye (Wang et al., 2014), copper (II) ions (Chen et al., 2010a), and Pb (II) (Chen et al., 2010b) from aqueous solution. The broth of *C. camphora* represents new green material in palladium nanoparticles formation to replace synthetic nanoparticles (Yang et al., 2010).

To tackle the problem of resources, supply in application as renewable energy, the large-scale production of *C. camphora* has been established via *in vitro* micropropagation technique (Shi et al., 2016). To fully utilize the resources of *C. camphora,* the biosynthesis pathway of secondary metabolomics production is also well explored (Chen et al., 2017). Volatile constituents from *C. camphora* have been detected and identified such as camphor, eucalyptol, linalool, nerolidol, limonene, β-pinene, -terpineol, and other volatile substances (Yang et al., 2016; Xu Y. et al., 2018). In particular, the biosynthesis pathway of secondary metabolomics production is also well explored (Chen et al., 2017). The constituent of oil composition was also reported (Jiang et al., 2016; Liu Z. et al., 2018). However, there is no complete list of metabolite profile available for different solvent types and hence it is difficult to suggest the optimal extraction method for *C. camphora.* As we know different solvent type has affinity to different type of metabolites and results to the extraction of different functional groups, we tested three types of solvents and listed the metabolite profile from the three solvents.

MATERIALS AND METHODS

Extraction of Leave Sample by Different Types of Solvents

An amount of 500 g of *C. camphora* leaves were cleaned, dried, and crushed into fine powder. The powder is subsequently sieved through a 200 mesh, the sample was divided into three parts and soaked with three types of solvents: ethanol, acetone, and benzene with ratio of material to liquid 1:15 (Xu K. et al., 2018; **Figure 1**). The mixture was boiled in water baths for 4 h and the temperature were set to the boiling point of each solvent. After removal from water bath, the solution were filtered by pump filter and then dried up using rotary evaporator. The solvent was collected once it reach approximately amount of 20 mL (Kumar and Kumari, 2019).

FT-IR Analysis

Solid Sample

After 200 mesh screening, the solid powder was taken as the sample. 0.5–2 mg of sieved powder was mixed with an appropriate amount of potassium bromide. It was then ground into fine and uniform particles in a mortar. A sample of this powder was taken and pressed to flatten the sample into an evenly transparent sheet. This sheet was then dried in an oven.

Liquid Sample

Solvents of ethanol, acetone, and benzene were pipetted out by using manual pipette and dropped evenly in the center of pure potassium bromide thin films. The film was then oven dried before it was measured at 4,000–400 cm^{-1} by Fourier transform infrared spectroscopy (Shimadzu, IR affinity-1) (Wu et al., 2019).

Gas Chromatography-Tandem Mass Spectrometry

GC-MS Determination

The program was set as initial temperature at 5°C without retention, increased and remained from 13 to 18°C, and then

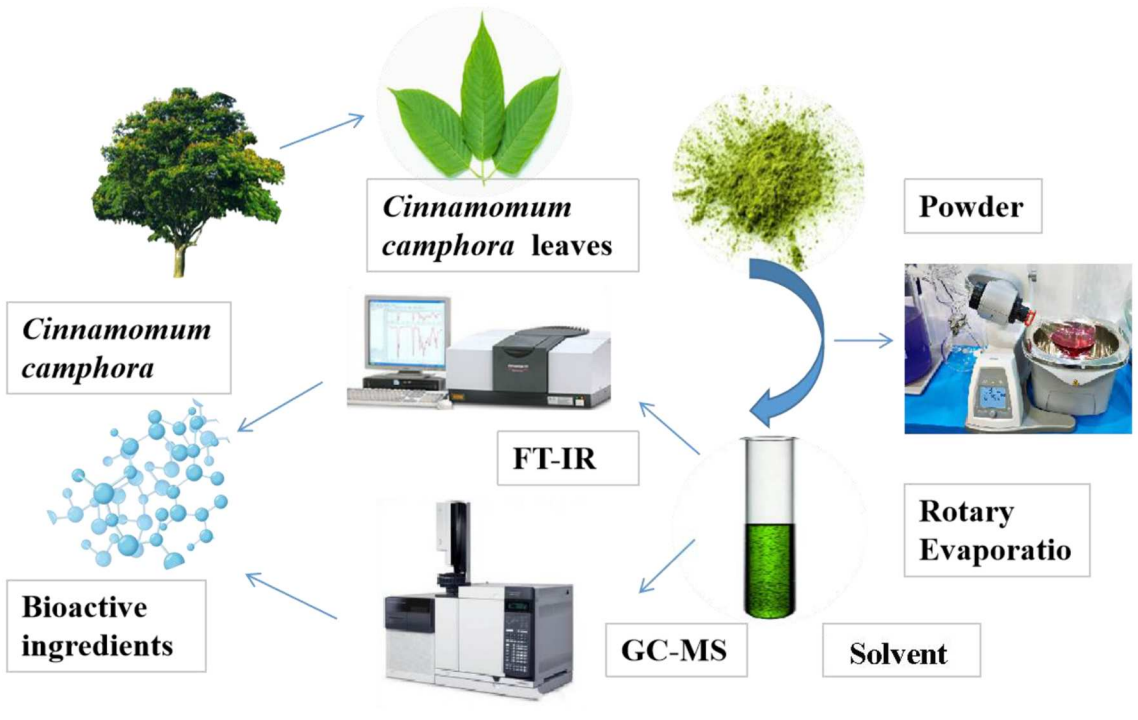

FIGURE 1 | The preparation process of *C. camphora* leaves.

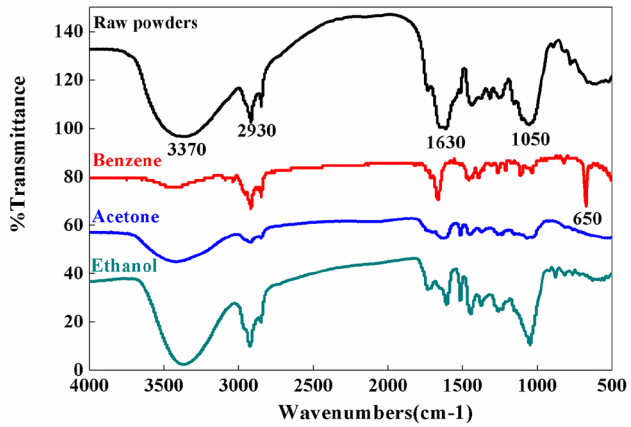

FIGURE 2 | The FTIR results of the raw powder and three solvents from *C. camphora* leaves.

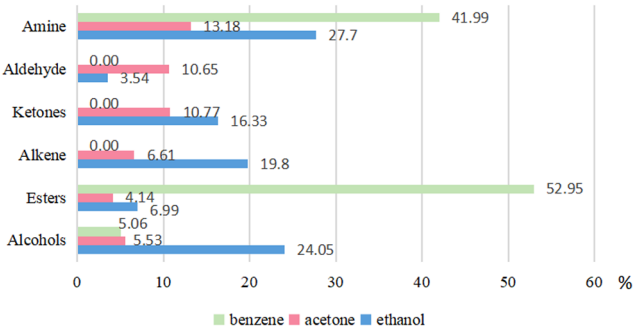

FIGURE 3 | Content percentage of three solvents from *C. camphora* leaves.

rose to 30°C for 5 min. The inlet temperature was set to 28°C with column flow of 1.0 mL/min, and split ratio was 20:1. A fused silica HP-5ms capillary GC column (30 m × 0.25 mm × 0.25 μm) was used. Mass spectrometry proceeded under the following conditions: ionization mode was EI, electron energy of 70 eV, ion source temperature of 23°C, scanning starting point of 30–60°C (Liu Z. et al., 2019; Ma et al., 2019).

Data Processing

The raw MS spectra data were first normalized by peak area and based line corrected. The chemicals composition detected were then identified by in house databased program and were grouped into similar functional groups based on previous study.

RESULTS

Characteristics of Solid and Liquid Extracts of *C. camphora*

The FTIR result of the fine powder sample show peaks and variation observed in the regions of 3,730–3,050 cm^{-1}, 3,050–2,500 cm^{-1}, 2,000–1,500 cm^{-1}, and 1,500–500 cm^{-1} (**Figure 2**). According to the infrared functional group comparison table, there is a strong absorption peak in the region of 1,500–500 cm^{-1} represents to ether bond, which can be identified as aliphatic ether and aromatic ether. The region observed at 3,050–2,500 cm^{-1} represents mainly olefins, alkynes, and aromatic compounds, resulted by the stretching vibration absorption of unsaturated carbon C-H.

Benzene solvent causing a sharp peak observed at 650 cm^{-1}. The presence of organic halides could be determined due to the expansion and contraction of aliphatic C-Br. In the 2,000–1,500 cm^{-1} region, there are olefins due to the vibrations of the bonds of unsaturated carbon, which are consistent with the compounds predicted in the same interval of raw powder sample. In the acetone solvent, the region around 1,500–500 cm^{-1} may represent alcohol, phenol, aromatic ether, and ester. Finally, the solvents of ethanol may contain functional group of olefins and amines as shown in the region 1,500–500 cm^{-1} and aromatic ethers as observed at region 1,050 cm^{-1}.

These results show that the infrared spectra of the ethanol as solvent are similar to those of raw powder, indicating that ethanol is a better solvent for extracting bioactive components from *C. camphora* leaves than benzene and acetone.

Volatile Components of the Three Extracts

A total of 120 compounds were detected from the acetone solvent by GC-MS (**Appendix Figure 1**, **Appendix Table 1**). Amongst them, 94 were identified and group into functional groups of amines (13.18%), ketone (10.77%), alkenes (6.61%), alcohol (5.53%), and esters (4.14%) (**Figure 3**). There are 58 of chemical compound were detected in ethanol solvent, in which 48 are organic compounds (**Appendix Figure 2**, **Appendix Table 2**). These compounds were classified into amines group (27.70%), Tetrazol-5-amine and N-(3, 4-dimethoxybenzyl) (25.44%), alcohols (24.05%), alkenes (19.80%), ketones (16.33%), and esters (6.99%). In benzene solvent, only 12 chemical compounds were detected and 4 substances were identified and classified into esters (52.95%), amines (41.99%), and alcohols (5.06%) (**Appendix Figure 3**, **Appendix Table 3**).

The results showed that the three solvents for *C. camphora* leaves have outstanding functional properties that serve as chemical raw materials for different green application including cosmetics, spices, food additives, chemicals raw materials, and biomedicine. The percentage of the bioactive components detected are highest in benzene solvent (41.99%), followed by ethanol solvent (33.53%), and acetone solvent (28.23%). For cosmetics and food additives application, the best extraction method is ethanol as solvent which enables recovery of 2 and 10.44% of active compounds, respectively. The functional content of spices was highest when acetone as solvent (15.51%) (**Figure 4**).

CONCLUSION

In order to enhance the application value of *C. camphora* leaves, the effects of different extraction methods on the bioactive substances in *C. camphora* leaves were investigated. Three common solutions of ethanol, acetone, and benzene were used to extract the substances in *C. camphora* leaves. There were significant differences in the types and proportions of bioactive

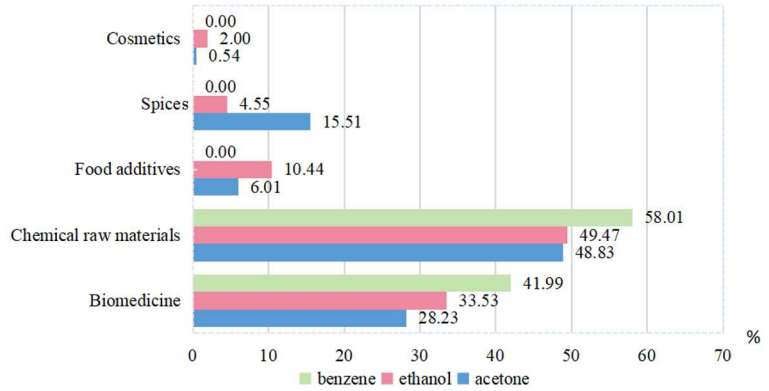

FIGURE 4 | Potential application based on thefunctional groups constitute of three solvents from *C. camphora* leaves.

compounds obtained by the three extraction methods. The FT-IR results showed that ethanol can effectively extract the bioactive compounds in *C. camphora* leaves. The GC-MS results indicated that more amines and alcohols were obtained from *C. camphora* using ethanol as solvent. The amines can be used in cosmetics and biomedicine, and the alcohols can be widely used in industrial fields. Aldehyde, ketones, alkene, and esters in ethanol solvent can also be applied in the fields of chemical raw materials, biomedicine, bioenergy, and spices.

DATA AVAILABILITY STATEMENT

All datasets generated for this study are included in the article/**Supplementary Material**.

AUTHOR CONTRIBUTIONS

DZ contributed to the integrity of the entire research, research concepts, and research design. YC contributed to the literature research, manuscript editing, and critically revision. ZZ and XW did the experimental studies, data acquisition, data analysis, and manuscript preparation. YL and XL gave guidance and participated in the experiments.

FUNDING

This project was supported by the talent project (DZ) of Henan Agricultural University, China, and the Project of Henan Provincial Science Research, China (192102110174).

SUPPLEMENTARY MATERIAL

The Supplementary Material for this article can be found online at: https://www.frontiersin.org/articles/10.3389/fenrg.2020.00090/full#supplementary-material

REFERENCES

Afrin, F., Chouhan, G., Islamuddin, M., Want, M. Y., Ozbak, H. A., and Hemeg, H. A. (2019). *Cinnamomum cassia* exhibits antileishmanial activity against *Leishmania donovani* infection *in vitro* and *in vivo*. *PLoS Negl. Trop. Dis.* 13: e0007227. doi: 10.1371/journal.pntd.0007227

Chen, C., Zheng, Y., Liu, S., Zhong, Y., Wu, Y., Li, J., et al. (2017). The complete chloroplast genome of *Cinnamomum camphora* and its comparison with related *Lauraceae species*. *Peer J.* 5:e3820. doi: 10.7717/peerj.3820

Chen, C., Zheng, Y., Zhong, Y., Wu, Y., Li, Z., Xu, L. A., et al. (2018). Transcriptome analysis and identification of genes related to terpenoid biosynthesis in *Cinnamomum camphora*. *BMC Genomics*. 19:550. doi: 10.1186/s12864-018-4941-1

Chen, H., Dai, G., Zhao, J., Zhong, A., Wu, J., and Yan, H. (2010a). Removal of copper (II) ions by a biosorbent—*Cinnamomum camphora* leaves powder. *J. Hazardous Mater.* 177, 228–236. doi: 10.1016/j.jhazmat.2009.12.022

Chen, H., Zhao, J., Dai, G., Wu, J., and Yan, H. (2010b). Adsorption characteristics of Pb (II) from aqueous solution onto a natural biosorbent, fallen *Cinnamomum camphora* leaves. *Desalination* 262, 174–182. doi: 10.1016/j.desal.2010.06.006

Chen, S., Zheng, T., Ye, C., Huannixi, W., Yakefu, Z., Meng, Y., et al. (2018). Algicidal properties of extracts from *Cinnamomum camphora* fresh leaves and their main compounds. *Ecotoxicol. Environ. Saf.* 163, 594–603. doi: 10.1016/j.ecoenv.2018.07.115

Chen, Y., and Dai, G. (2015). Acaricidal activity of compounds from *Cinnamomum camphora* (L.) Presl against the carmine spider mite, *Tetranychus cinnabarinus*. *Pest Manage. Sci.* 71, 1561–1571. doi: 10.1002/ps.3961

Chen, Y., Weng, Y., Zhou, M., Meng, Y., Liu, J., Yang, L., et al. (2019). Linalool-and α-terpineol-induced programmed cell death in *Chlamydomonas reinhardtii*. *Ecotoxicol. Environ. Saf.* 167, 435–440. doi: 10.1016/j.ecoenv.2018.10.062

Fu, J., Zeng, C., Zeng, Z., Wang, B., and Gong, D. (2016). *Cinnamomum camphora* seed kernel oil ameliorates oxidative stress and inflammation in diet-induced obese rats. *J. Food Sci.* 81, H1295–H1300. doi: 10.1111/1750-3841.13271

Guo, S., Geng, Z., Zhang, W., Liang, J., Wang, C., Deng, Z., et al. (2016). The chemical composition of essential oils from *Cinnamomum camphora* and their insecticidal activity against the stored product pests. *Int. J. Mol. Sci.* 17:1836. doi: 10.3390/ijms17111836

He, H., Qin, J., Cheng, X., Xu, K., Teng, L., and Zhang, D. (2018). Effects of exogenous 6-BA and NAA on growth and contents of medicinal ingredient of *Phellodendron chinense* seedlings. *Saudi J. Biol. Sci.* 25, 1189–1195. doi: 10.1016/j.sjbs.2017.11.037

Jiang, H., Wang, J., Song, L., Cao, X., Yao, X., Tang, F., et al. (2016). GC× GC-TOFMS analysis of essential oils composition from leaves, twigs and seeds of *Cinnamomum camphora* L. Presl and their insecticidal and repellent activities. *Molecules* 21:423. doi: 10.3390/molecules21040423

Kumar, S., and Kumari, R. (2019). Cinnamomum: review article of essential oil compounds, ethnobotany, antifungal and antibacterial effects. *Open Access J. Sci.* 3, 13–16. doi: 10.15406/oajs.2019.03.00121

Liu, L., Cheng, X., Zhao, W. W., Wang, Y. H., Dong, X., Chen, L., et al. (2018). Systematic characterization of volatile organic components and pyrolyzates from *Camellia oleifera* seed cake for developing high value-added products. *Arab. J. Chem.* 6, 802–814. doi: 10.1016/j.arabjc.2017.12.031

Liu, X., Meng, Y., Zhang, Z., Wang, Y., Geng, X., Li, M., et al. (2019). Functional nano-catalyzed pyrolyzates from branch of *Cinnamomum camphora*. *Saudi J. Biol. Sci.* 26, 1227–1246. doi: 10.1016/j.sjbs.2019.06.003

Liu, Z., Deng, B., Li, S., and Zou, Z. (2018). Optimization of solvent-free microwave assisted extraction of essential oil from *Cinnamomum camphora* leaves. *Industr. Crops Products* 124, 353–362.

Liu, Z., Kong, L., Lu, S., and Zou, Z. (2019). Application of a combined homogenate and ultrasonic cavitation system for the efficient extraction of flavonoids from *Cinnamomum camphora* leaves and evaluation of their antioxidant activity *in vitro*. *J. Analyt. Methods Chem.* 2019:4892635. doi: 10.1155/2019/4892635

Ma, X., Hu, Z., Mao, J., Xu, Y., Zhu, X., and Xiong, H. (2019). Synthesis of cocoa butter substitutes from *Cinnamomum camphora* seed oil and fully hydrogenated palm oil by enzymatic interesterification. *J. Food Sci. Technol.* 56, 835–845. doi: 10.1007/s13197-018-3543-x

Sattar, A., Gilani, A. M., and Saeed, M. A. (1991). Gas chromatographic examination of the essential oil of cinnamomum camphora. *Pak. J. Sci. Ind. Res.* 34, 135–136.

Satyal, P., Paudel, P., Poudel, A., Dosoky, N. S., Pokharel, K. K., and Setzer, W. N. (2013). Bioactivities and compositional analyses of Cinnamomum essential oils from Nepal: C. *camphora, C. tamala,* and *C. glaucescens*. *Natural Product Commun.* 8, 1777–1784. doi: 10.1177/1934578x1300801232

Shi, X., Zhang, C., Liu, Q., Zhang, Z., Zheng, B., and Bao, M. (2016). *De novo* comparative transcriptome analysis provides new insights into sucrose induced somatic embryogenesis in camphor tree (*Cinnamomum camphora L.*). *BMC Genomics*. 17:26. doi: 10.1186/s12864-015-2357-8

Wang, H., Yuan, X., Wu, Z., Wang, L., Peng, X., Leng, L., et al. (2014). Removal of basic dye from aqueous solution using *Cinnamomum camphora* sawdust: kinetics, isotherms, thermodynamics, and mass-transfer processes. *Separ. Sci. Technol.* 49, 2689–2699. doi: 10.1080/01496395.2014.940590

Wu, L., Xiong, W., Hu, J. W., Wu, J., Li, Z. J., Gao, Y., et al. (2019). Secondary metabolites from the twigs of *Cinnamomum camphora*. *Chem. Natural Comp.* 55, 345–347. doi: 10.1007/s10600-019-02686-8

Xu, K., He, G., Qin, J., Cheng, X., He, H., Zhang, D., et al. (2018). High-efficient extraction of principal medicinal components from fresh Phellodendron bark (*Cortex phellodendri*). *Saudi J. Biol. Sci.* 25, 811–815. doi: 10.1016/j.sjbs.2017.10.008

Xu, Y., Xiao, H., Guan, H., and Long, C. (2018). Monitoring atmospheric nitrogen pollution in Guiyang (SW China) by contrasting use of *Cinnamomum Camphora* leaves, branch bark and bark as biomonitors. *Environ. Pollut.* 233, 1037–1048. doi: 10.1016/j.envpol.2017.10.005

Yakefu, Z., Huannixi, W., Ye, C., Zheng, T., Chen, S., Peng, X., et al. (2018). Inhibitory effects of extracts from *Cinnamomum camphora* fallen leaves on algae. *Water Sci. Technol.* 77, 2545–2554. doi: 10.2166/wst.2018.199

Yang, D., Zhang, H., Peng, K., Chen, L., He, H., Huang, X., et al. (2016). Differential gene regulation of lipid synthesis in the developing seeds of two biodiesel tree species, Jatropha and Vernicia. *Int. J. Agric. Biol.* 18, 1143–1152. doi: 10.17957/IJAB/15.0218

Yang, X., Li, Q., Wang, H., Huang, J., Lin, L., Wang, W., et al. (2010). Green synthesis of palladium nanoparticles using broth of *Cinnamomum camphora* leaf. *J. Nanopart. Res.* 12, 1589–1598. doi: 10.1007/s11051-009-9675-1

Conflict of Interest: The authors declare that the research was conducted in the absence of any commercial or financial relationships that could be construed as a potential conflict of interest.

frontiers in Energy Research

ORIGINAL RESEARCH
published: 08 July 2020
doi: 10.3389/fenrg.2020.00136

Development and Performance of a Multi-Fuel Residential Boiler Burning Agricultural Residues

Despina Vamvuka[1]*, *Dimitrios Loukeris*[1], *Evaggelos Stamou*[1], *Aristotelis Vlasiadis*[1], *Stelios Sfakiotakis*[1] and *Grigorios Bandelis*[2]

[1] School of Mineral Resources Engineering, Technical University of Crete, Chania, Greece, [2] Energy Mechanical of Crete S.A., Chania, Greece

The combustion behavior of selected agricultural residues (olive and peach kernels, almond and walnut shells) and their blends was investigated in a prototype low-investment combustion unit of nominal capacity 65 $kW_{th.}$ Blending ratio for olive kernel was 50 or 70%, while for the rest of the residues 30 or 50%. Flue gas temperatures, inlet and outlet water temperatures of the boiler and gaseous emissions were measured at specific feed and air flow rates and combustion and boiler efficiencies were determined. CO and NO_x emissions from all fuels during the whole operation of the unit were below legislation limits, while SO_2 emissions were negligible. Combustion efficiencies were satisfactory, ranging between 84 and 86%. Peach kernels burned with the highest efficiency. By blending olive kernels with peach kernels, almond or walnut shells at percentages up to 50%, the overall efficiency of the system in terms of emissions and degree of combustion was improved, achieving the best performance with olive kernels/peach kernels 50:50 blend. Co-combustion of unpelletized materials could be predicted to a great extent from the combustion of component fuels, offering apart from environmental and economic benefits.

Keywords: agricultural residues, blends, combustion, stoker burner, emissions, efficiency

OPEN ACCESS

Edited by:
Su Shiung Lam,
University of Malaysia Terengganu, Malaysia

Reviewed by:
Fehmi Akgun,
TUBITAK Marmara Research Centre Energy Institute, Turkey
Peter Nai Yuh Yek,
University College of Technology Sarawak, Malaysia

***Correspondence:**
Despina Vamvuka
vamvuka@mred.tuc.gr

Specialty section:
This article was submitted to Bioenergy and Biofuels, a section of the journal Frontiers in Energy Research

Received: *27 August 2019*
Accepted: *04 June 2020*
Published: *08 July 2020*

Citation:
Vamvuka D, Loukeris D, Stamou E, Vlasiadis A, Sfakiotakis S and Bandelis G (2020) Development and Performance of a Multi-Fuel Residential Boiler Burning Agricultural Residues. Front. Energy Res. 8:136. doi: 10.3389/fenrg.2020.00136

INTRODUCTION

Population growth, depletion and rising cost of fossil fuels and climate crisis across the world require rapid development of renewable energy technologies, with minimum environmental impact. Biomass fuels have a remarkable potential in meeting these needs, due to their abundance, low cost and reduction of greenhouse emissions. Up to 33–50% of the world's current consumption could be met by biomass by 2050 (McKendry, 2002).

EU has set the target to increase the share of renewable energy in its total energy consumption to 27% by the year 2030 (EU, 2014). Woody fuels have been predominantly used for both large and small scale systems, for heat or power production. However, the increasing competition for such fuels in the heating sector, sawmills and paper industries, as well as the increase in wood pellet production, have raised the price of wood and resulted in raw material shortage (Uslo et al., 2010). Thus, to fulfill the goal of growth of biomass utilization, a wider assortment of raw materials will be required (Carvalho et al., 2013; Cardozo et al., 2014; Zeng et al., 2018), creating a further need for fuel processing and emission control technologies.

For South European countries, where residential heating with biomass fuels as a cheaper alternative is growing, agricultural and agro-industrial residues are the feedstock of choice. They are readily available in large quantities and they have a high energy potential, reducing by combustion the volume of wastes and increasing economic returns to rural communities. In Greece, about 4 million tons/year are available and equivalent to approximately 50% of the gross energy consumption (Vamvuka and Tsoutsos, 2002; Vamvuka, 2009).

The common types of residential combustion devices are wood stoves, wood log boilers, wood pellet stoves and wood chip appliances. Apart from wood stoves and conventional boilers with endless screws, mixed combustion boilers are being used, featuring automation add-ons, storing solutions and a variety of feeding mechanisms (Vamvuka, 2009; Sutar et al., 2015; Ahn and Jang, 2018). Past studies have investigated flue gas emissions, efficiency and ash related problems, during combustion of agricultural residues. Large scale units or small pellet appliances for domestic or residential central heating, some using top feeding, rotary or moving grates (Vamvuka, 2009; Carvalho et al., 2013; Rabacal et al., 2013; Garcia-Maraver et al., 2014; Pizzi et al., 2018; Zeng et al., 2018; Nizetic et al., 2019), have been extensively investigated. However, there is still not enough information on the performance of unpelletized raw materials in terms of efficiency and pollutant emissions according to threshold values, as a function of different small system designs and operating conditions. Wood chips have been principally used (Kortelainen et al., 2015; Caposciutti and Antonelli, 2018), whereas the development of boilers in Mediterranean countries is slow.

Small scale biomass systems have been proved to significantly contribute to local air quality through emissions of pollutants, such as CO, SO_2, NO_x, polyaromatic hydrocarbons and particulate matter, which can seriously affect human health and climate. These emissions depend on fuel properties, technology implemented and process conditions and their monitoring and controlling is very important in order to meet environmental limits and cost-effectiveness of market demands. CO emissions have been found to vary between 600 and 680 ppm_v for peach pits (Rabacal et al., 2013), 50–400 ppm_v for Brazilian nut shells and 100–400 ppm_v for sunflower husks (Cardozo et al., 2014). NO_x emissions have been shown to range between 300-600 mg/m^3 for peach pits (Rabacal et al., 2013), 180–270 mg/m^3 for Brazilian nut shells and 50–720 mg/m^3 for sunflower husks (Cardozo et al., 2014). For the latter, SO_2 emissions varied between 78 and 150 mg/m^3. Boiler efficiency has been reported (Rabacal et al., 2013; Fournel et al., 2015) to range between 63 and 83%, depending on fuel type.

As agricultural residues are available only in limited periods throughout a year, mixtures of them would increase supply options for operating plants. However, when mixtures are used as feedstock the compatibility of the fuels with respect to combustion performance has to be properly evaluated, for the effective design and operation of the combustion units. The variable composition of these materials implies a thorough knowledge of their behavior in thermal systems, in order to avoid fuel combinations with unwanted properties. To authors' knowledge, blends of such wastes found at low or no cost have not been investigated in residential appliances. Only pellets of woody fuels or energy crops have been used to determine particulate emissions and slag formation (Carroll and Finnan, 2015; Sippula et al., 2017; Zeng et al., 2018).

Based on the above, the aim of present study was to compare the combustion behavior of selected unpelletized agricultural residue materials, which are abundant in South European countries and mixtures of them, in order to investigate any additivity or synergy effects among component fuels and gain knowledge about the use of such blends in small scale boilers. The objective was to evaluate the performance of a prototype low-investment combustion unit, allowing pre-drying of fuels and combustion air by exhaust fumes, for the production of thermal energy in buildings, farms, small enterprises and green houses, in terms of important parameters, such as combustion and boiler efficiency, flue gas temperature and environmental emissions.

EXPERIMENTAL SECTION

Fuels and Characterization

The agricultural residues of this study were selected on the basis of their abundance and availability in Greece and Mediterranean countries, in general. These were olive kernels (OK) provided by AVEA Chania Oil Cooperatives (S. Greece), peach kernels (PK) provided by the Union of Agricultural Cooperatives of Giannitsa (N. Greece), almond shells (AS) provided by a private company (Agrinio, C. Greece) and walnut shells (WS) provided by Hohlios company (N. Greece).

After air drying, homogenization and riffling the materials were ground to a particle size <6 mm, using a jaw crusher and vibrative dry sieving. Representative samples were ground to a particle size of −425 μm by a cutting mill and characterized by proximate analysis, ultimate analysis and calorific value, according to the European standards CEN/TC335. Volatiles content was measured by thermogravimetric analysis, using a TGA-6/DTG system, in the range of 25–900°C, under a flow of nitrogen of 45 ml/min and at a linear heating rate of 10°C/min. Chemical analysis of ashes was performed by an X-ray fluorescence spectrophotometer (XRF), type Bruker AXS S2 Ranger (anode Pd, 50 Watt, 50 kV, 2 mA). Deposition tendency of ashes was predicted through the use of empirical indices. These indices, despite their shortcomings due to the complex conditions, which arise in boilers and their associated heat transfer equipment, are widely used and probably remain the most secure basis for decision making, if used in conjunction with pilot plant testing.

The base-to-acid ratio (Equation 1) is a useful index, since typically a high percentage of basic oxides lowers the melting temperature, while acidic oxides increase it. This takes the form (Vamvuka et al., 2017):

$$R_{b/a} = \frac{\%\left(Fe_2O_3 + CaO + MgO + K_2O + Na_2O\right)}{\%\left(SiO_2 + TiO_2 + Al_2O_3\right)} \quad (1)$$

where the label for each compound makes reference to its weight concentration in the ash. When $R_{b/a}$ <0.5 deposition tendency

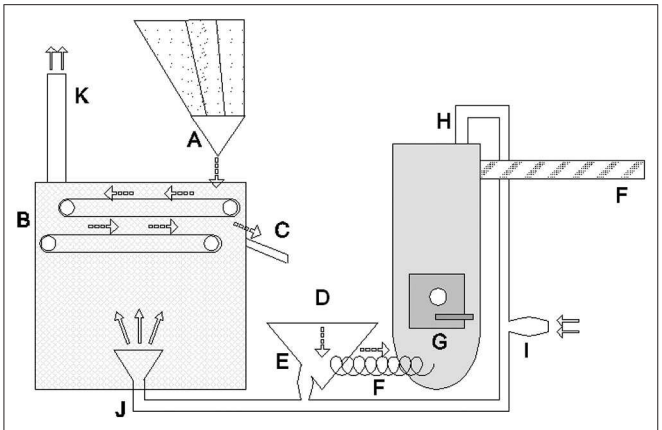

FIGURE 1 | Schematic diagram of multi-fuel boiler (solid arrows show air flow direction, while dotted arrows show biomass flow direction).

is low, when $0.5 < R_{b/a} < 1$ deposition tendency is medium and when $R_{b/a} > 1$ deposition tendency is high. For $R_{b/a}$ values >2, this index cannot be used safely without additional information.

The influence of the alkalis in the slagging/fouling tendency of the biomass ashes is critical, due to their tendency to lower the ash melting temperature. One simple index, the alkali index (Equation 2), expresses the quantity of alkali oxides in the fuel per unit of fuel energy in GJ (Vamvuka et al., 2017):

$$\mathrm{AI} = \frac{\mathrm{kg}\,(K_2O + Na_2O)}{\mathrm{GJ}} \quad (2)$$

When AI values are in the range 0.17–0.34 kg/GJ fouling or slagging is probable, while when these values are >0.34 fouling or slagging is virtually certain to occur.

For combustion tests, mixtures of above materials with blending ratios up to 50% by weight were prepared with the most abundant agricultural waste in Greece, olive kernels.

Description of Prototype Combustion System

The combustion unit is illustrated schematically in **Figure 1**. The main parts are two silos, a desiccator, a continuous feedstock supply system and a cross flow boiler. The nominal capacity is 65 kW_{th}.

The fuel is stored in a main silo (A), the side surfaces of which are perforated, to dry the fuel physically. According to the availability of the biomass and the special energy needs, a regulating valve is opened and the system is fed with the appropriate fuel. The biomass is then transferred from the silo to the desiccator through an inclined rack with tracks, with a speed that is controlled according to the needs of the boiler. The hot air is provided by the exhaust fumes, through a feedback system (H,J). The dryer hosts two inner conveyor belts (B) consisted of perforated slow-turning rollers with steel netting, enabling hot air to travel thought it in a bottom-up flow direction. The dryer (B) has several compartments, so as to allow the air to travel and eventually lose a part of its temperature, thus creating a temperature difference. The special steel netting has high endurance and it can handle the extreme temperature variances quite efficiently. The speed of the rollers is closely connected to the humidity of the biomass and can vary according to the needs of the automatic control. The dry biomass is then transferred (C) to a temporary silo (D) and mixed with warm air coming from the feedback system (E), before it is led to the burner and the combustion area of the boiler. Using a horizontal warm screw, 1&1/2 inch in diameter, the processed biomass is fed into the burner (G). The feed rate is controlled via two electronic dimmers. The first dimmer corresponds to the time that the feeding system is operating, while the second dimmer corresponds to the delay time (screw is off). In this way, the feedstock supply follows a semi-batch process. Primary combustion air is introduced through a pipe in the front of the furnace and it is controlled with a blower. The ratio of primary to secondary air is adjusted by use of a regulator installed in the exhaust flue (K), with a mechanic regulator that permits variations of the chimney draft. The boiler (G) is hydraulic and it primarily produces hot water in a closed-loop circulating system (F). This system has security arrangements, to keep the water pressure constant and transports hot water to high efficiency fan coils for space heating. Pt temperature sensors are used for measurement of the water temperatures of the forward and return flow, as well as of the flow inside the boiler. A calorific value meter is measuring the flow of water and the useful energy picked up by the water. The exhaust fumes of the boiler are driven through a heat exchanger before they go to the chimney. The heat exchanger (I) uses the exhaust fumes to warm-up air, which is then used for the drying of the wet biomass.

The novelty of this prototype unit is the design of the desiccator fed with exhaust fumes, handling extreme temperature variances and running according to boiler needs, the heat exchanger also fed with exhaust fumes, as well as the temperature sensors and calorific value meter enclosed. Because all main parts of the unit are conventional, the manufacturing cost of such installation is kept low. The analog sensors and parts already installed will be replaced with digital sensors and mechanical parts with digital inputs and outputs, according to the results of the unit response experiments. A limitation of the system is the inability to adjust an optimal excess air ratio, so that there is a need for robust control of combustion air supplied. Determination of optimal parameters of a custom automatic control system should be adopted, to allow the unit to run autonomously.

Experimental Procedure and Data Measurements

The experiments were structured in such way, so that an analytical profile of each material could be built and also the behavior of fuel type during the different stages of the process could be investigated. Two series of experiments were conducted, in order to study the behavior and response of each residue to the processing chain of the unit. During the first series of tests, a calibration of the feeding rate vs. the dimmer switches was carried out for each biofuel. The feed rate was determined

by the on-off delay interval sequences, of the first and second dimmer, respectively. The flow rate of flue gases, for each feedstock supply, was determined by measuring the speed of the fan at the gas exit installed in position (K), by an anemometer. Consequently, each biofuel was tested in the combustion unit in order to optimize the thermal efficiency by tuning its special parameters, taking into account the quality of the emissions. Important independent variables were the feedstock supply rate, the speed of the fan controlling the air flow of the boiler and the boiler inner temperature. Present study reports the results for one set of these parameters, aiming to compare the combustion performance between the agricultural residues tested, as well as of their blends, under constant operating conditions. The parametric study for the optimization of the process will be presented in a following report.

To start up the boiler, the fuel was ignited and the solid feeder and air lines were turned on and set to the desired values (on/off 10/30 s/s). The furnace was allowed to run for 30 min before the first readings were taken. The hot water circulating system was adjusted to operate, once the temperature was ≥55°C. When water temperature exceeded 70°C, the supply of feedstock was temporarily stopped.

Flue gas composition was continuously monitored during the tests, by a multi-component gas analyzer, model Madur GA-40 plus of Maihak, equipped with double-in-line filter and dryer. The sampling was achieved using a heating line with a probe, according to the ELOT 896 Greek standards. The analyzer uses electrochemical sensors for the measurement of gas concentrations. The CO_2, CO, O_2, SO_2, NO_x contents in the exhaust gas stream, the soot index, the heat losses of the fumes, the flue gas temperature and the excess air coefficient (λ) were continuously recorded by the analyzer. The analog output of the analyzer was transmitted to a computer, where the signals were processed and the mean values computed over a sampling period of 0.5 min.

After taking measurements at steady operating conditions and allowing the furnace to run for about 3 h, the fuel feeder and air line were turned off, the view port was opened and the exhaust fan was set on high to cool the unit. Bottom ash was drained, weighed and analyzed for combustion losses due to unburned carbon. The experiments were replicated twice to determine their reproducibility, which was found to be good.

The thermal efficiency of the system was defined as the proportion of the useful energy picked up by the water of the boiler, to the input energy produced by the fuel:

$$\eta_t = \frac{Q_{out}}{Q_{in}} = \frac{q_w c_{pw} \Delta T_w \Delta t}{m_f Q_f} (\%) \quad (3)$$

where, q_w: mass flow of water (kg/h), c_{pw}: thermal capacity of water (MJ/kgK), ΔT_w: temperature difference of the forward and return flow of water (°K), Δt: total combustion time at water temperature 70°C, m_f: mass of fuel/mixture burned (kg), Q_f: calorific value of fuel/mixture (MJ/kg).

Combustion efficiency was defined as follows:

$$\eta_c = 100 - SL - IL - L_a (\%) \quad (4)$$

where,

$$SL = (T_f - T_{amb})\left(\frac{A}{[CO_2]} + B\right) \quad (5)$$

$$IL = \frac{a[CO]}{[CO] + [CO_2]} \quad (6)$$

$$L_a = 100 - \frac{m_o - m_a}{m_o} \quad (7)$$

where: T_f: temperature of flue gases (°C), T_{amb}: temperature of ambient air (°C), [CO] and [CO_2]: concentrations of CO and CO_2 in flue gases (%), A, B, a: combustion parameters characteristic for each type of fuel (given by the analyzer), m_o: total mass of organic matter of fuel burned (kg), m_a: mass of organic matter in ash (kg).

For each experimental test it was examined whether the available heat of the flue gas was enough to preheat the inlet air for the combustion of the fuel to 70°C and also to dry the biomass in the system dessicator:

$$Q_{fl} \geq Q_{amb} + Q_d \quad (8)$$

or

$$m_{fl} c_{pfl} \Delta T_f \geq m_{amb} c_{pamb} \Delta T_{amb} + Q_d \quad (9)$$

where: m_{fl}, m_{amb}: mass of flue gases and air per kg of biomass burned (kg), c_{pfl}, c_{pamb}: specific heat of flue gas and air (kJ/kg°K), ΔT_f, ΔT_{amb}: temperature difference of flue gases at the exit and inlet of the chimney and of preheated air and ambient air, respectively (°K), Q_d: heat of biomass drying (Moyers and Baldwin, 1997). According to the results which follow, the above inequality always held.

RESULTS AND DISCUSSION

Raw Fuel Analyses

Table 1 indicates the proximate and ultimate analyses of the agricultural residues studied. As can be observed, all samples were rich in volatile matter and had low ash contents. Almond shells presented the highest percentage of volatiles, whereas walnut shells the lowest percentage of ash. The concentration of oxygen was significant for all samples and the calorific value, ranging between 17.5 and 20.4 MJ/kg, was comparable to the upper limit of low rank coals. The sulfur content of all residues was practically null, revealing that SO_2 emissions are not of concern for these biofuels. On the other hand, the nitrogen content of almond shells was considerable, which might be a problem during thermal processing, in terms of NO_x emissions.

The chemical analysis of ashes, expressed in the usual way for fuels as oxides, is compared in **Table 2**, together with the slagging/fouling indices and deposition tendency. The common feature of these ash materials is that they were rich in Ca and K and to a lesser extent in P and Mg. The base-to-acid ratio was far >2, due to the low silica and alumina content of these ashes, so that no definite guidelines for slagging bahavior can be drawn. The alkali induced slagging/fouling potential can be

TABLE 1 | Proximate and ultimate analyses and calorific value of the samples (% dry weight).

Sample	Volatile matter	Fixed carbon	Ash	C	H	N	O	S	GCV[a] (MJ/kg)
Olive kernels (OK)	78.2	14.5	7.3	49.5	6.3	0.9	36.0	<0.05	20.4
Peach kernels (PK)	76.2	19.4	4.4	48.0	5.9	–	41.7	<0.05	18.9
Almond shells (AS)	81.4	13.1	5.5	46.5	5.7	2.2	40.1	<0.05	17.5
Walnut shells (WS)	72.1	26.5	1.4	48.5	6.3	0.8	43.0	<0.05	19.5

[a]*Gross calorific value.*

TABLE 2 | Chemical analysis of raw material ashes and slagging/fouling tendency.

Sample	Ash composition (%)									Base-to-acid ratio $R_{b/a}$	Alkali index AI	Slagging/fouling tendency
	SiO_2	Al_2O_3	Fe_2O_3	MgO	CaO	Na_2O	K_2O	P_2O_5	SO_3			
OK	4.5	1.4	1.9	4.9	26.7	2.7	28.9	6.6	5.9	11.0	1.17	High
PK	2.6	2.6	4.7	3.7	27.6	0.4	4.6	1.8	3.7	7.8	0.15	Low
AS	6.2	1.4	1.5	4.5	14.7	0.8	27.2	3.8	1.7	6.4	0.56	High
WS	2.2	0.6	1.4	6.2	49.6	0.6	16.3	7.4	2.6	26.4	0.12	Low
OK/PK 70:30	3.9	1.8	2.7	4.5	27.0	2.1	21.7	5.2	5.2	10.2	0.72	High
OK/PK 50:50	3.6	2.0	3.3	4.3	27.1	1.5	16.5	4.2	4.8	9.4	0.49	High
OK/AS 70:30	5.0	1.4	1.8	4.8	23.1	2.0	28.2	5.8	4.6	9.3	0.96	High
OK/AS 50:50	5.3	1.4	1.7	4.7	20.7	1.6	27.8	5.2	3.8	8.4	0.95	High
OK/WS 70:30	3.7	1.1	1.7	5.1	33.0	1.9	24.8	6.7	5.1	13.8	0.74	High
OK/WS 50:50	3.2	1.0	1.6	5.4	37.7	1.6	22.1	6.9	4.4	21.4	0.52	High

predicted more accurately by the alkali index. Thus, according to the AI values, for olive kernels and almond shells the fouling propensity is certain to occur, due to the high amounts of alkali with respect to unit of fuel energy they contain (for almond shells the propensity is much lower), while for peach kernels and walnut shells no fouling is expected in boilers. When olive kernels were mixed with the other residues at blending ratios up to 50%, **Table 2** shows that the AI values were significantly lowered. It must be mentioned however, that for small systems, such as the one used in this work, operating below 1,000°C and for a relatively short period of time, slagging or fouling phenomena due to ashes were not observed.

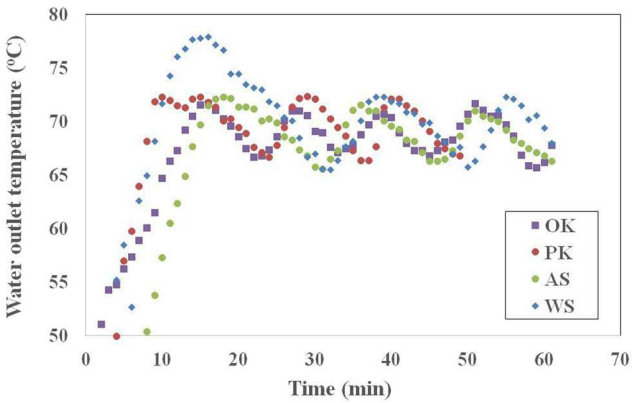

FIGURE 2 | Evolution of boiler water outlet temperature for raw fuels during full operation of the unit.

Combustion Performance of Agricultural Residues Biofuels

Boiler Water Temperature

The variation of water outlet temperature of the boiler, during full operation of the combustion unit, is illustrated in **Figure 2**. It is clear that peach kernels and walnut shells started burning earlier than the other two residues, offering their thermal energy to water about 6 min earlier than olive kernels for rising the temperature from 25 to 70°C. The behavior of walnut shells, however, was quite different. Water temperature during the start up phase rose up to 78°C (second dimmer at off), so that for three full cycles (on/off) combustion time was extended by about 20 min, as compared to olive kernels. For walnut and almond shells, three cycles under the conditions studied lasted about 1 h.

Flue Gas Temperature and Emissions

Flue gas temperature (**Table 3**) presents a dependence on fuel. Thus, it was higher for almond shells, 267°C, for full boiler operation (at steady state), while lower for peach kernels, 245°C, implying greater and lower heat losses from the furnace, respectively. All flue gas temperature values were high enough to pre-dry the raw materials (Equation 9).

CO concentration in flue gases at steady state operation of the furnace (dimmer at on), for the four residues under study, is

TABLE 3 | Combustion characteristics of the fuels (average values) at steady state.

Sample	Fuel rate (kg/h)	Stoich. air rate per kg fuel (m^3/h)	Excess air ratio λ	CO (ppm_V)	SO_2 (ppm_V)	NO_x (ppm_V)	T_f (°C)	SL (%)	IL (%)	L_a (%)	η_c (%)	η_t (%)
OK	13.5	5.6	1.9	1224.7	3.0	136.1	241.0	14.1	1.0	0.4	84.5	86.3
PK	18.0	4.7	1.5	1014.5	9.2	81.9	245.2	13.2	0.9	0.1	85.8	93.4
AS	15.3	4.5	1.8	1194.4	10.6	81.7	267.6	14.6	1.0	0.2	84.2	90.5
WS	13.8	5.1	1.7	1145.0	12.4	88.0	244.8	13.4	1.0	0.1	85.5	87.4

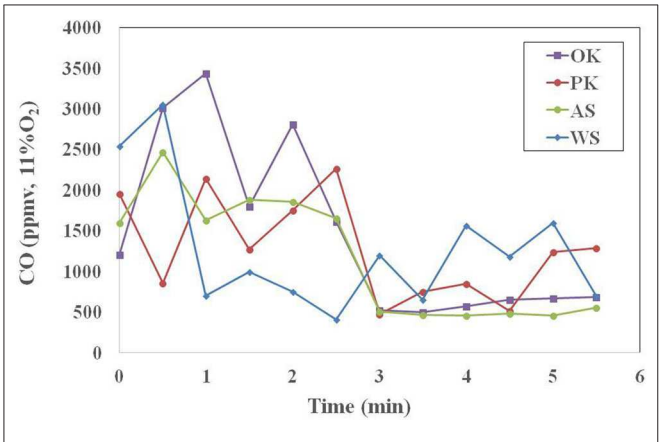

FIGURE 3 | CO concentration in flue gases for raw fuels at steady state.

compared in **Figure 3**. The increased CO levels of olive kernels biofuel were most probably attributed to its great amount of volatiles, which boost hydrocarbons concentration in the reactor, inhibiting further oxidation of CO to CO_2, as well as to a lesser extent the higher ash content of this fuel, which weakened oxygen penetration to the char particles. Nevertheless, all CO values were below legislation limits for small scale systems (ELOT, 2011).

The average pollutant concentrations (± standard error) at steady state and during the whole operation of the unit are represented and compared in **Figures 4A,B**, respectively. SO_2 emissions from all biofuels, being extremely low (0–13 ppm_v), were omitted from the graphs. **Figure 4A** shows that the highest CO emissions were released from olive kernels combustion, while the lowest from peach kernels combustion. However, even though during full boiler operation (including intervals with no fuel feeding, i.e., second dimmer at off) CO values were higher (**Figure 4B**), they did not exceed allowable limits (ELOT, 2011). Furthermore, NO_x emissions from all materials studied were low and according to the guidelines of EU countries (EC, 2001; ELOT, 2011) for small units (200–350 mg/Nm^3). The lower NO_x levels of almond shells, despite their higher fuel-N among the biofuels tested, could be a result of a temporary reducing environment created by the large amount of volatiles of this residue (81.5%), which favored NO_x decomposition.

Present gaseous emission values were comparable to those reported in literature for similar fuels, while those of NO_x were significantly lower. For peach pits CO emissions varied between 600 and 680 ppm_v (Rabacal et al., 2013), for Brazilian nut shells between 50 and 400 ppm_v (Cardozo et al., 2014), for palm kernels between 2,000 and 14,000 ppm_v (Pawlak-Kruczek et al., 2020), for oil cake pellets between 1,900 and 6,500 ppm_v (Kraszkiewicz et al., 2015) and for olive pruning pellets were 1,800 ppm_v (Garcia-Maraver et al., 2014). On the other hand, NO_x emissions were found for peach pits 300–600 mg/m^3 (Rabacal et al., 2013), for Brazilian nut shells 180–270 mg/m^3 (Cardozo et al., 2014), for palm kernels between 90 and 200 ppm_v (Pawlak-Kruczek et al., 2020), for oil cake pellets 230-870 mg/m^3 (Kraszkiewicz et al., 2015) and for olive pruning pellets 680 mg/m^3 (Garcia-Maraver et al., 2014).

Combustion and Thermal Efficiency

The combustion performance of the four residues is represented in **Table 3**. Combustion efficiencies are considered satisfactory for small systems (77% according to European Standards EN 303-5), ranging between 84 and 86%. These values were controlled by the flue gas temperatures, which reflected the sensitive heat losses and the concentration of CO in flue gases, which represented the principal heat losses due to incomplete combustion. Thus, peach kernels, presenting the lowest SL and IL losses, burned with the highest efficiency. It is interesting to note that, the higher amount of air in the case of olive kernels (excess air ratio $\lambda = 1.9$), increasing fumes flow, seemed to somehow reduce fireplace temperature and therefore increase CO level and gaseous heat losses (IL). Moreover, the thermal efficiency of the system, shown in **Table 3**, was affected by the combustion efficiency of the fuel and it was higher for peach kernels, due to improved combustion in the furnace and improved heat recovery in system tubes, by increasing the temperature difference between the forward and return flow of water to the boiler ($\Delta T_w = 26.2°C$). The fluctuations observed in the table are owned to the different amounts of each biofuel burned as a function of time, when the boiler was operated at specific on/off intervals of the feed regulating dimmers. An optimization of fuel rate and excess air ratio toward a lower value could result in higher fireplace temperature (a high flow of air supply cools the furnace), lower CO emissions due to better combustion, lower oxygen and higher CO_2 concentrations in fumes and therefore reduced heat or fuel losses and increased combustion efficiency. This, in turn, would improve heat recovery in tubes and rise thermal efficiency. Furthermore, some modifications in the furnace to increase the residence time of flue gases would lower their temperature at the exhaust and thus sensitive heat losses.

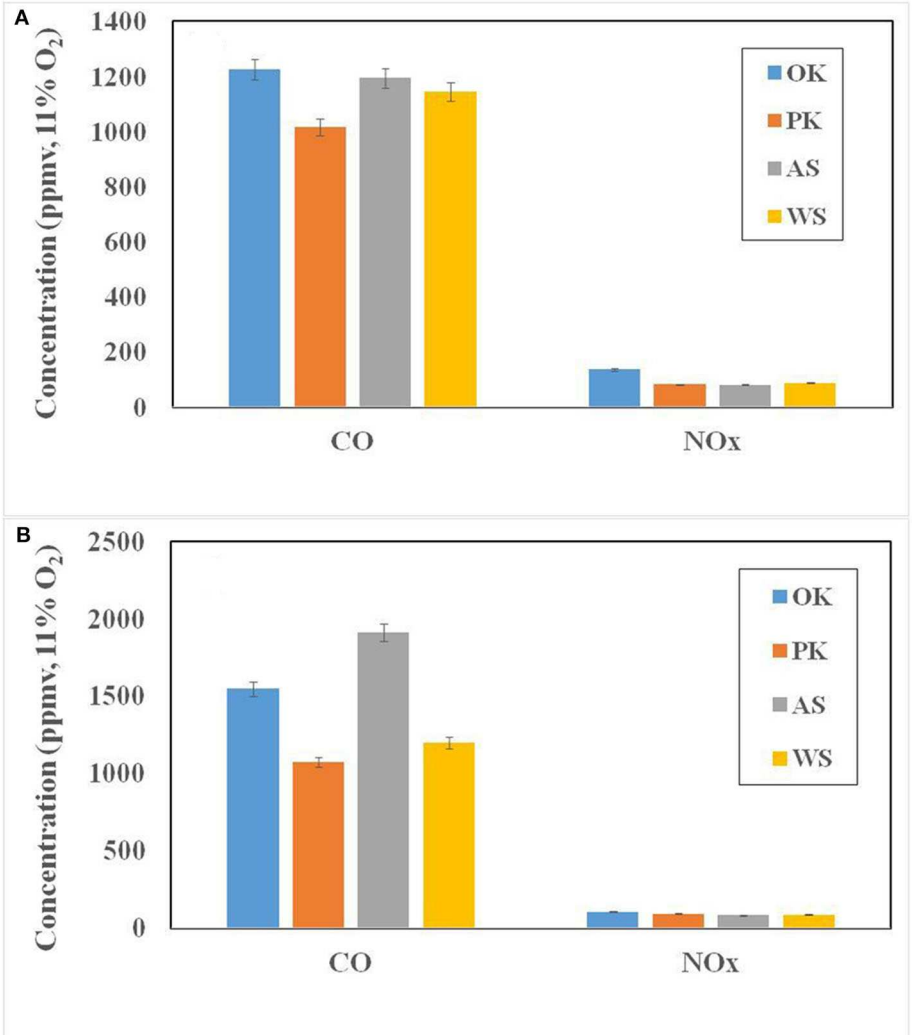

FIGURE 4 | Average pollutant concentrations of gases from raw fuels **(A)** at steady state and **(B)** during whole operation of unit.

Nevertheless, boiler efficiency was in accordance with literature data. Values of 91%, 83–86% and 75–83% have been reported for wood pellets (Kraiem et al., 2016), pine wood and peach pits (Rabacal et al., 2013), respectively. Moreover, for a multi-fuel boiler burning woody materials thermal efficiency was found (Fournel et al., 2015) to be dependent on the ash content of each feedstock, i.e., for ash content 1% the efficiency was 74%, while for ash content 7% it dropped to 63%. In another unit, burning forest residues and energy crops, the efficiency varied between 69 and 75% (Forbes et al., 2014).

Combustion Performance of Agricultural Residues Blends

Boiler Water Temperature

Figures 5A–C represent the evolution of water temperature at the outlet of the boiler as a function of time, during full operation of the furnace, for the mixtures of olive kernels residue with peach kernels, almond and walnut shells. From these figures it can be observed that both the start up phase and the phase when the system was in full operation were delayed when feeding with mixtures of fuels, shifting the curves to higher time values by about 4–6 min. It seems that feeding of blends and consequently burn out were not so homogeneous as theoretically expected.

Flue Gas Temperature and Emissions

Table 4 shows that flue gas temperatures, which affect sensitive heat losses of the fumes, for all blends at steady state, varied between the values of component fuels. This reveals that the combustion performance of the mixtures was dependent on the contribution of each residue in the blend.

The average CO and NO_x emissions (±standard error) at steady state, from all mixtures, are compared with those of raw fuels in **Figures 6A–C**. SO_2 emissions are not presented in the graphs, as they were extremely low (4–20 ppm_v). CO values, ranging between 1,121 and 1,212 ppm_v, were kept between

the values corresponding to component fuels and were within accepted limits for small units (ELOT, 2011). Moreover, NO_x levels (87–129 ppm_v, or 174–258 mg/m^3) followed the same trend and were kept below the threshold limits of EU countries (EC, 2001; ELOT, 2011). The best performance in terms of emissions was achieved by OK/PK 50:50 blend.

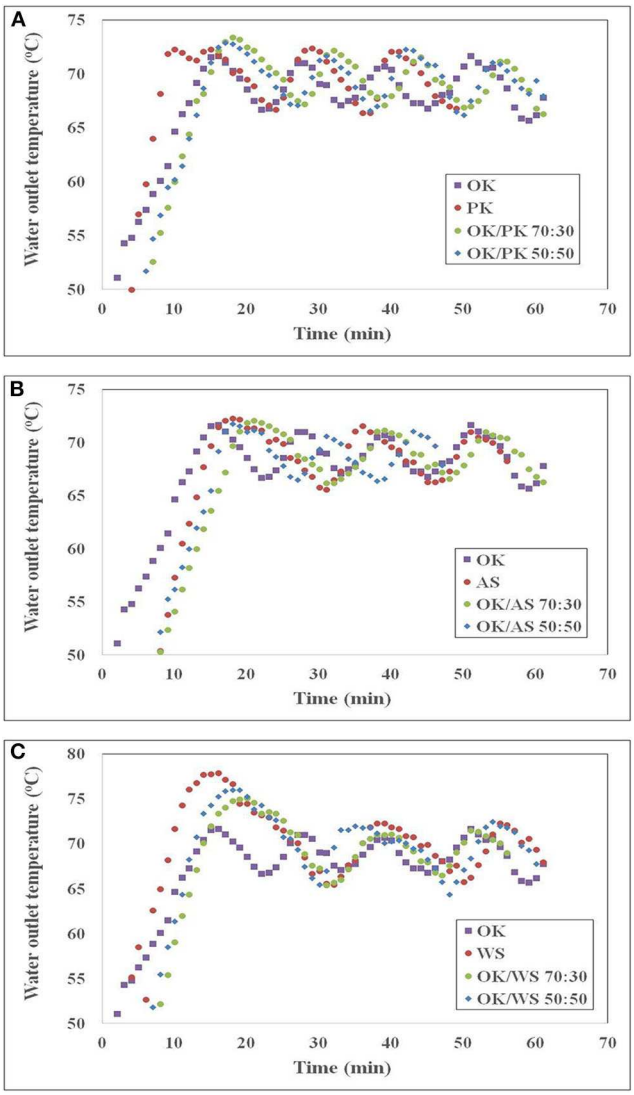

FIGURE 5 | Evolution of boiler water outlet temperature during full operation of the unit for **(A)** OK/PK, **(B)** OK/AS, and **(C)** OK/WS mixtures.

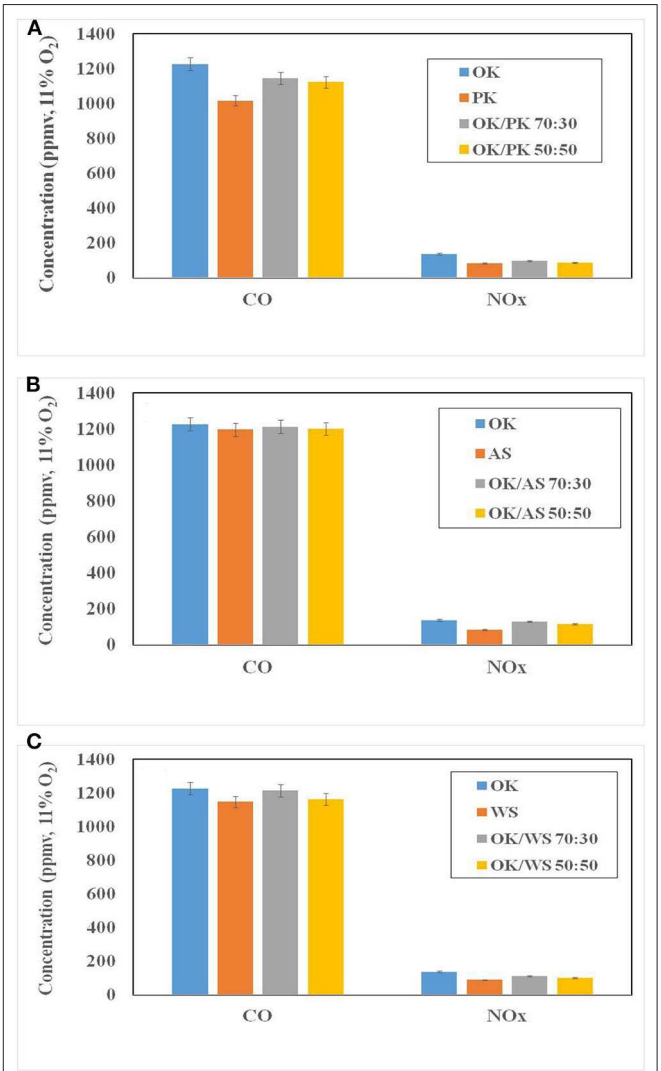

FIGURE 6 | Average CO and NO_x emissions of gases at steady state from **(A)** OK/PK, **(B)** OK/AS, and **(C)** OK/WS mixtures.

TABLE 4 | Combustion characteristics of fuel mixtures (average values) at steady state.

Sample	Fuel rate (kg/h)	Stoich. air rate per kg fuel (m^3/h)	Excess air ratio λ	CO (ppm_V)	SO_2 (ppm_V)	NO_x (ppm_V)	T_f (°C)	SL (%)	IL (%)	L_a (%)	η_c (%)	η_t (%)
OK/PK 70:30	14.8	5.3	1.59	1143.8	3.6	96.5	240.6	13.3	1.0	0.2	85.5	88.8
OK/PK 50:50	15.7	5.1	1.66	1121.3	8.0	86.6	238.7	13.4	0.9	0.1	85.6	91.4
OK/AS 70:30	14.0	5.3	1.85	1210.8	12.5	129.0	255.1	14.3	1.0	0.2	84.5	87.7
OK/AS 50:50	14.4	5.0	2.0	1199.3	19.6	113.1	253.8	14.6	0.9	0.3	84.2	87.2
OK/WS 70:30	13.6	5.4	1.85	1211.6	18.2	109.0	254.1	14.1	1.0	0.2	84.7	81.2
OK/WS 50:50	13.7	5.3	1.80	1161.2	9.9	99.1	242.6	14.1	1.0	0.1	84.8	81.6

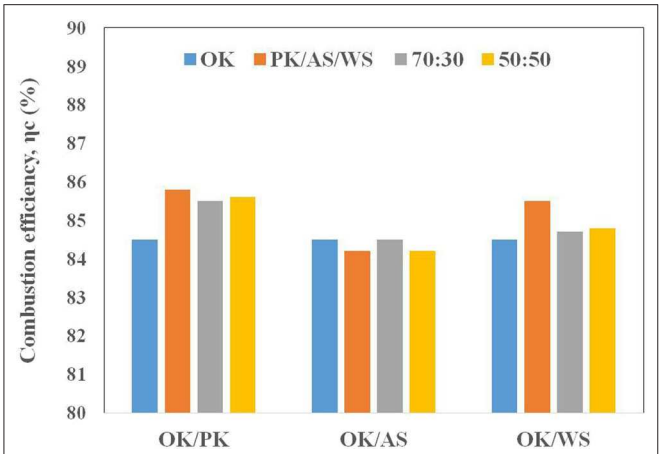

FIGURE 7 | Combustion efficiency of fuel blends.

Combustion and Thermal Efficiency

Combustion efficiencies of olive kernels blends with peach kernels, almond and walnut shells ranged between 84.2 and 85.6%, as indicated in **Figure 7**. These values were between those corresponding to component materials, but not in proportion to the percentage of each residue in the mixture. As shown in **Table 4**, combustion efficiency was a result of feedstock type and mass flow, as well as excess air ratio, which defined fireplace and fumes temperatures and consequently heat losses. The highest efficiency was achieved in the case of OK/PK 50:50 blend, which in turn was reflected in the thermal efficiency of the boiler, by improved heat recovery from the flow of water.

CONCLUSIONS

The agricultural residues studied were characterized by high volatile and low ash contents. Their calorific value was significant ranging between 17.5 and 20.4 MJ/kg. CO and NO_x emissions, from all fuels during the whole operation of the unit under the conditions studied, were below legislation limits, while SO_2 emissions were negligible. Combustion efficiencies were satisfactory, ranging between 84 and 86%. Peach kernels, followed by walnut shells burned with the highest efficiency, due to lower sensitive heat losses and losses from incomplete fuel combustion, emitted lower concentrations of toxic gases and increased boiler efficiency by improving the heat recovery in system tubes.

Co-combustion of the agricultural residues could be predicted to a great extent from the combustion of component fuels, which could offer not only environmental, but also economic benefits. By blending olive kernels with peach kernels, almond or walnut shells at percentages up to 50%, the overall efficiency of the system in terms of emissions and degree of combustion was improved. The pest performance was achieved by olive kernels/peach kernels 50:50 blend.

Combustion efficiency was a result of feedstock type, mass flow and excess air ratio. Robust control of combustion air supply is needed and determination of optimal parameters.

DATA AVAILABILITY STATEMENT

All datasets generated for this study are included in the article/supplementary material.

AUTHOR CONTRIBUTIONS

DV: supervisor, evaluation of results, and paper writing. DL: experiments. ES: experiments. AV: experiments. SS: evaluation of results. GB: technical support and evaluation of results. All authors: contributed to the article and approved the submitted version.

ACKNOWLEDGMENTS

The authors kindly thank AVEA Chania Oil Cooperatives, the Union of Agricultural Cooperatives of Giannitsa and private companies Agrinio and Hohlios for providing the fuels, as well as the laboratories of Hydrocarbons Chemistry and Technology and Inorganic and Organic Geochemistry, of the Technical University of Crete, for the CHNS and XRF analyses.

REFERENCES

Ahn, J., and Jang, J. H. (2018). Combustion characteristics of a 16 step grate-firing wood pellet boiler. *Renew. Energy* 129, 678–685. doi: 10.1016/j.renene.2017.06.015

Caposciutti, G., and Antonelli, M. (2018). Experimental investigation on air displacement and air excess effect on CO, CO_2 and NO_x emissions of a small fixed bed biomass boiler. *Renew. Energy* 116, 795–804. doi: 10.1016/j.renene.2017.10.001

Cardozo, E., Erlich, C., Alejo, L., and Fransson, T. H. (2014). Combustion of agricultural residues: an experimental study for small-scale applications. *Fuel* 115, 778–787. doi: 10.1016/j.fuel.2013.07.054

Carroll, J., and Finnan, J. (2015). The use of additives and fuel blending to reduce emissions from the combustion of agricultural fuels in small scale boilers. *Biosyst. Eng.* 129, 127–133. doi: 10.1016/j.biosystemseng.2014.10.001

Carvalho, L., Wopienka, E., Pointner, C., Lundgren, J., Kumar, V., Haslinger, W., et al. (2013). Performance of a pellet boiler with agricultural fuels. *Appl. Energy* 104, 286–296. doi: 10.1016/j.apenergy.2012.10.058

EC (2001). *Directive 2001/80/EC of the European Parliament and of the Council of 23 October 2001, on the Limitation of Emissions of Certain Pollutants into the Air from Large Combustion Plants.*

ELOT (2011). EN 303.05/1999. *Limit Values for CO and NO_x Emissions for New Thermal Units Using Solid Biofuels*. FEK 2654/B/9-11-2011.

EU (2014). *Leaders Agree 2030 Climate and Energy Goals*. Available online at: http://ec.europa.eu/clima/news/articles/news_2014102401_en.htm

Forbes, E., Easson, D., Lyons, G., and McRoberts, W. (2014). Physico-chemical characteristics of eight different biomass fuels and comparison of combustion and emission results in a small scale multi-fuel boiler. *Energy Conv. Managem.* 87, 1162–1169. doi: 10.1016/j.enconman.2014.06.063

Fournel, S., Palacios, J. H., Morissette, R., Villeneuve, J., Godbout, S., Heitza, M., et al. (2015). Influence of biomass properties on technical and environmental

performance of a multi-fuel boiler during on-farm combustion of energy crops. *Appl. Energy* 141, 247–259. doi: 10.1016/j.apenergy.2014.12.022

Garcia-Maraver, A., Zamorano, M., Fernandes, U., Rabacal, M., and Costa, M. (2014). Relationship between fuel quality and gaseous and particulate matter emissions in a domestic pellet-fired boiler. *Fuel* 119, 141–152. doi: 10.1016/j.fuel.2013.11.037

Kortelainen, M., Jokiniemi, J., Nuutinen, I., Torvela, T., Lamberg, H., Karhunen, T., et al. (2015). Ash behaviour and emission formation in a small-scale reciprocating-grate combustion reactor operated with wood chips, reed canary grass and barley straw. *Fuel* 143, 80–88. doi: 10.1016/j.fuel.2014.11.006

Kraiem, N., Lajili, M., Limousy, L., Said, R., and Jeguirim, M. (2016). Energy recovery from Tunisian agri-food wastes: Evaluation of combustion performance and emissions characteristics of green pellets prepared from tomato residues and grape marc. *Energy* 107, 409–418. doi: 10.1016/j.energy.2016.04.037

Kraszkiewicz, A., Przywara, A., Kachel-Jakubowska, M., and Lorencowicz, E. (2015). Combustion of plant biomass pellets on the grate of a low power boiler. *Agricul. Agricul. Sci. Proc.* 7, 131–138. doi: 10.1016/j.aaspro.2015.12.007

McKendry, P. (2002). Energy production from biomass (part 1): overview of biomass. *Bioresour. Technol.* 83, 37–46. doi: 10.1016/S0960-8524(01)00118-3

Moyers, C. G., and Baldwin, G. W. (1997). "Psychrometry, evaporative cooling and solids drying," in *Perry's Chemical Engineers' Handbook, 7th Edn*, eds R. H. Perry and D. W. Green (New York, NY: Mc Graw Hill).

Nizetic, S., Papadopoulos, A., Radica, G., Zanki, V., and Arici, M. (2019). Using pellet fuels for residential heating: a field study on its efficiency and the users' satisfaction. *Energy Build.* 184, 193–204. doi: 10.1016/j.enbuild.2018.12.007

Pawlak-Kruczek, H., Arora, A., Moscicki, K., Krochmalny, K., Sharma, S., and Niedzwiecki, L. (2020). A transition of a domestic boiler from coal to biomass-Emissions from combustion of raw and torrefied Palm Kernel shells (PKS). *Fuel* 263, 116–124. doi: 10.1016/j.fuel.2019.116718

Pizzi, A., Foppa Pedretti, E., Duca, D., Rossini, G., Mengarelli, C., Ilari, A., et al. (2018). Emissions of heating appliances fuelled with agropellet produced from vine pruning residues and environmental aspects. *Renew. Energy* 121, 513–520. doi: 10.1016/j.renene.2018.01.064

Rabacal, M., Fernandes, U., and Costa, M. (2013). Combustion and emission characteristics of a domestic boiler fired with pellets of pine, industrial wood wastes and peach stones. *Renew. Energy* 51, 220–226. doi: 10.1016/j.renene.2012.09.020

Sippula, O., Lamberg, H., Leskinen, J., Tissari, J., and Jokiniemi, J. (2017). Emissions and ash behaviour in a 500kW pellet boiler operated with various blends of woody biomass and peat. *Fuel* 202, 144–153. doi: 10.1016/j.fuel.2017.04.009

Sutar, K. B., Kohli, S., Ravi, M. R., and Ray, A. (2015). Biomass cookstoves: a review of technical aspects. *Renew. Sustainable Energy Rev.* 41, 1128–1166. doi: 10.1016/j.rser.2014.09.003

Uslo, A., Gomez, N. C., and Belda, M. S. (2010). *Demand for Lignocellulosic Biomass in Europe. Elobio Biofuels Policies for Dynamic Markets*. Available online at: https://www.elobio.eu/fileadmin/elobio/user/docs/Additional_D_to_WP3-Linocellulosic_biomass.pdf

Vamvuka, D. (2009). *Biomass, Bioenergy and the Environment.* Salonica: Tziolas Publications.

Vamvuka, D., Trikouvertis, M., Pentari, D., Alevizos, G., and Stratakis, A. (2017). Characterization and evaluation of fly and bottom ashes from combustion of residues from vineyards and processing industry. *J. Energy Instit.* 90, 574–587. doi: 10.1016/j.joei.2016.05.004

Vamvuka, D., and Tsoutsos, T. (2002). Energy exploitation of agricultural residues in Crete. *Energy Expl. Exploit.* 20, 113–121. doi: 10.1260/014459802760170439

Zeng, T., Pollex, A., Weller, N., Lenz, V., and Nelles, M. (2018). Blended biomass pellets as fuel for small scale combustion appliances: effect of blending on slag formation in the bottom ash and pre-evaluation options. *Fuel* 212, 108–116. doi: 10.1016/j.fuel.2017.10.036

Conflict of Interest: GB was employed by the company Energy Mechanical of Crete S.A.

The remaining authors declare that the research was conducted in the absence of any commercial or financial relationships that could be construed as a potential conflict of interest.

frontiers in Energy Research

ORIGINAL RESEARCH
published: 04 August 2020
doi: 10.3389/fenrg.2020.00166

Enhanced Methanization of Long-Chain Fatty Acid Wastewater at 20°C in the Novel Dynamic Sludge Chamber–Fixed Film Bioreactor

Suniti Singh[1,2,3,4], B. Conall Holohan[2,5], Simon Mills[3], Juan Castilla-Archilla[2], Marika Kokko[1], Jukka Rintala[1], Piet N. L. Lens[1,4], Gavin Collins[3] and Vincent O'Flaherty[2]*

[1] Faculty of Engineering and Natural Sciences, Tampere University, Tampere, Finland, [2] Microbial Ecology Laboratory, School of Natural Sciences, National University of Ireland Galway, Galway, Ireland, [3] Microbial Communities Laboratory, School of Natural Sciences, National University of Ireland Galway, Galway, Ireland, [4] IHE Delft Institute for Water Education, Delft, Netherlands, [5] NVP Energy Ltd., IDA Technology Park, Galway, Ireland

OPEN ACCESS

Edited by:
Su Shiung Lam, University of Malaysia Terengganu, Malaysia

Reviewed by:
Qaisar Mahmood, COMSATS University Islamabad, Pakistan
Francisco Jesus Fernandez Morales, University of Castilla-La Mancha, Spain

***Correspondence:**
Marika Kokko
marika.kokko@tuni.fi

Specialty section:
This article was submitted to Bioenergy and Biofuels, a section of the journal Frontiers in Energy Research

Received: *05 February 2020*
Accepted: *30 June 2020*
Published: *04 August 2020*

Citation:
Singh S, Holohan BC, Mills S, Castilla-Archilla J, Kokko M, Rintala J, Lens PNL, Collins G and O'Flaherty V (2020) Enhanced Methanization of Long-Chain Fatty Acid Wastewater at 20°C in the Novel Dynamic Sludge Chamber–Fixed Film Bioreactor. Front. Energy Res. 8:166. doi: 10.3389/fenrg.2020.00166

Lipid-containing wastewaters, such as those arising from dairy processing, are frequently discharged at temperatures ≤ 20°C. Their valorization at low ambient temperatures offers opportunities to expand the application of high-rate anaerobic wastewater treatment toward achieving energy neutrality by minimizing the energy demand for heating. Lipid hydrolysis generates long-chain fatty acids (LCFAs), which incur operational challenges and hinder stable bioreactor operation by inducing sludge flotation and washout, coupled with the added challenge of treatment at lower temperature (20°C). These challenges are tackled together uniquely during the treatment of LCFA-rich synthetic dairy wastewater (SDW) (33% COD-LCFA) through *de novo* formed microbial granular sludge within the dynamic sludge chamber–fixed film (DSC-FF) reactor. The novel reactor design facilitated sludge retention for the entire operational period of 150 days by containing settled, flotating, and LCFA-encapsulated granular sludge and biofilm within a single module. High COD removal efficiencies (87–98%) were achieved in the three replicated DSC-FF reactors, along with complete LCFA removal at 18–72 h HRT (LCFA loading rate of 220–890 mgCOD-LCFA/L·day) and partial LCFA removal at 12 h HRT (LCFA loading rate of 1333 mgCOD-LCFA/L·day). The high removal efficiencies of unsaturated and saturated LCFAs achieved are reported for the first time during continuous anaerobic wastewater treatment at low temperatures (20°C). Moreover, *de novo* granulation was achieved within 8 days from a combination of inoculum mixtures at a high LCFA concentration (33% COD-LCFA) in SDW. The results demonstrate the feasibility of the DSC-FF reactor for treating LCFA-rich wastewaters at discharge temperatures and offer potential for expanded and more energetically productive anaerobic valorization of lipid-rich wastewater.

Keywords: dynamic sludge chamber fixed film reactor, dairy wastewater, long-chain fatty acid mixture, anaerobic sludge granulation, biofilm formation

INTRODUCTION

The United Nations 2030 Agenda for Sustainable Development necessitates the development of sustainable wastewater treatment and resource recovery systems to successfully attain the goals targeted for the focus areas of clean water and sanitation (SDG 6), renewable energy (SDG 7), sustainable communities (SDG 11), and climate action (SDG 13) (United Nations, 2015). High-rate anaerobic digestion (AD) is a sustainable option for the biological treatment of municipal and industrial wastewaters, and is widely applied in bioreactors under mesophilic (approximately 30–40°C) or thermophilic (approximately 45–60°C) conditions (Batstone and Jensen, 2011). The extension of AD technologies for application at cooler temperatures (≤20°C) is an important innovation in improving the net energy recovery from wastewater treatment, especially in temperate climates where low ambient air temperatures decrease the wastewater temperatures (McHugh et al., 2003). Lipid-containing wastewaters, including a variety of dairy waste streams, are emitted in large quantities at low ambient temperatures and are energy-dense (theoretically, 1.43 L-CH_4/g-lipid); thus, opening opportunities for high-potential valorization through bio-methanization (Alves et al., 2009). Anaerobic treatment of such high-volume wastewaters at discharge temperatures would steer the treatment processes toward the achievement of energy neutrality (Martin et al., 2011; Petropoulos et al., 2019b). Thus, it is important to develop high-rate processes for the anaerobic treatment of fat, oil, and grease (FOG)-rich wastewaters at low ambient temperatures.

However, the anaerobic treatment of lipid-rich streams is problematic, since their hydrolysis produces long-chain fatty acids (LCFAs) that can destabilize anaerobic treatment due to physicochemical and microbial inhibition (Lalman and Bagley, 2002; Zheng et al., 2005; Davidsson et al., 2008; Alves et al., 2009; Desbois and Smith, 2010; Sun et al., 2013; Zhou et al., 2013). In high-rate anaerobic reactors, such as upflow anaerobic sludge bed (UASB) reactors, the accumulation of LCFAs produced from lipid degradation has been associated with operational challenges including the sludge flotation and washout, scum layer formation, and substrate diffusion limitation through LCFA-encapsulated sludge (Rinzema et al., 1994; Pereira et al., 2005). Moreover, LCFAs behave as surfactants at neutral pH (Sam-Soon et al., 1991) and disrupt the structure of the anaerobic granules, consequently aggravating the granular sludge washout. Hence, the anaerobic treatment of lipid- and LCFA-rich wastewaters warrants the development of high microbial activity, stable microbial structures, and enhanced sludge retention in reactors, especially at low temperatures with slow microbial growth rates, along with the characterization of LCFA profiles to assess the efficacy of reactor design in the removal of different LCFAs.

Strategies for improved sludge retention for treating lipid-rich wastewaters have included (i) forming biofilms on support material in anaerobic filters, fixed-bed reactors, anaerobic baffled reactors, and moving-bed biofilm reactors (Alves et al., 2001; Pereira et al., 2002; Kim et al., 2004; Biswas and Turner, 2012; Fujihira et al., 2018); (ii) sludge flotation in specialized reactor designs, such as anaerobic flotation reactor (AFRs; Paques, Netherlands) and inverted anaerobic sludge bed (IASB) reactors (Alves et al., 2007); (iii) application of membrane bioreactor (MBR) systems (Ramos et al., 2014; Dereli et al., 2015; Jensen et al., 2015); and (iv) granular sludge reactors (Hwu et al., 1998a; Saatci et al., 2003; Jeganathan et al., 2006; Leal et al., 2006; Passeggi et al., 2009). Of these reactor designs, indeed, various single- and two-stage reactor systems have been employed to treat dairy wastewaters at lower temperatures (5–20°C) (**Table 1**; Toldrá et al., 1987; Viraraghavan and Kikkeri, 1990; Dague et al., 1998; Ramasamy and Abbasi, 2000; Luostarinen and Rintala, 2005; Park et al., 2012; Buntner et al., 2013; Nikolaeva et al., 2013; Bialek et al., 2014; Zielińska et al., 2018), but these studies used non-fat dry milk substrates (≤3% lipid-COD) which are not representative of the typical dairy wastewaters that have a high lipid content of 0.1–0.5 g/L (28–35% COD basis) (Szabo-Corbacho et al., 2019; Holohan, 2020).

Up until recently, the high-rate anaerobic treatment of LCFAs has been studied extensively at mesophilic or thermophilic conditions (e.g., Hwu et al., 1998a; Kim et al., 2004; Jeganathan et al., 2006; Ramos et al., 2014; Dereli et al., 2015; Cavaleiro et al., 2016; Duarte et al., 2018; Szabo-Corbacho et al., 2019) but not at low ambient temperatures. An evaluation of the anaerobic LCFA treatment at low temperatures will bring new insights into the treatment of lipid-rich wastewaters. We recently showed the feasibility of anaerobic treatment of LCFA-containing wastewater (with 33% LCFA-COD) at 20°C in expanded granular sludge bed (EGSB) reactors (Singh et al., 2019). The process performance was stable for around 60 days, but prolonged operation involved significant sludge flotation and washout in EGSB reactors influenced by the LCFA loading rates and the LCFA concentrations in complex substrate (Singh et al., 2019). High COD removal (>99%) and methane yield efficiencies (MYE) (89–91%) have been achieved during the treatment of lipid-rich dairy wastewater in MBR (HRT = 53 h) at 35°C (Szabo-Corbacho et al., 2019), demonstrating the suitability of MBR for FOG methanization at mesophilic conditions. Conversely, at psychrophilic conditions (15°C), the MBR has been reported to be unsuitable for lipid treatment due to a high accumulation and the fouling propensity of the lipids (Petropoulos et al., 2019b). The hybrid reactor designs combining the sludge retention principles of UASBs or EGSBs with additional features, such as a biofilm compartment, support improved process performance (e.g., at 20°C for digestion of whey wastewater; McHugh et al., 2006) and may be applied to develop innovative reactor configuration for treating LCFA-rich wastewater at discharge temperature.

The objective of this study was to evaluate for the first time the high-rate anaerobic treatment of synthetic dairy wastewater (SDW) rich in mixed-LCFA at 20°C through the dynamic sludge chamber–fixed film (DSC-FF) reactor configuration. The fate of individual LCFAs at high LCFA loading rates was assessed for the first time at discharge temperatures in FOG-rich wastewaters. The reactors were seeded with a mixture of sludges with distinct capability for LCFA degradation and high acetotrophic and methanogenic activities to engineer a microbial consortium suitable for high-rate low-temperature treatment of SDW in the form of a *de novo* granular sludge.

TABLE 1 | Process performance of anaerobic dairy wastewater treatment in adhered-film and granular sludge reactors at psychrophilic and low ambient temperatures.

Substrate	Reactor	Temp (°C)	Influent pH	LCFA loading rate (gCOD/L.day)	OLR (g-COD/L.day)	HRT (h)	sCOD removal (%)	Methane yield at STP (ml/g-COD.day)	References
Non-fat dry milk	ASBR	5–25	7	[a]	0.6–2.4	6-24-1	60–98	95–290	Dague et al., 1998
Dairy processing wastewater	SGBR	10–25	5.8 ± 0.7	NR	0.6–9.7	9	> 90	90–340	Park et al., 2012
Synthetic dairy parlor wastewater	Two-phased UASB septic tank	10–20	6.1 ± 0.4	NR	0.1–0.24	84 + 36 + 1.5	33–62	NR	Luostarinen and Rintala, 2005
Dairy wastewater	UASB-activated sludge	20	7.9 ± 1.2	0.75 ± 0.06 (22%)[b,c]	3.4	24 (+ 1.92)	69	NR	Tawfik et al., 2008
Skim milk	UASB-aerobic MBR	17–25	7	NR	2.4–1.6	10–14 (total 14–19)	95 UASB, 99 total	110–310	Buntner et al., 2013
Dairy wastewater	FBR (support material: sand)	20 (35)	9.05, adjusted to 7	NR	0.6–6	2, 4, 6, 8	20–42	NR	Toldrá et al., 1987
Synthetic skimmed dairy wastewater	IFB (support material: Extendospheres^{TM} made of silica and traces of aluminum)	10	7	[a]	0.5–2	12–48	24–80	107–294	Bialek et al., 2014
Dairy washing wastewater	AFBR (fixed-bed support material: tire rubber and zeolite)	22–26	7.2 ± 0.3	NR	4.4–24	24–132	28–82	70–180	Nikolaeva et al., 2013
Dairy wastewater	AF (support material: plastic)	21	7-7.3	NR	4	24	55	180	Viraraghavan and Kikkeri, 1990
Synthetic dairy wastewater	CSTR (support material: nylon mesh)	Room temp	NR	NR	NR	> 240	46–59	NR	Ramasamy and Abbasi, 2000
Synthetic dairy wastewater	MBBR (support material: metallic iron-PVC plastic)	20		[a]	3.9	132	70–86	103	Zielińska et al., 2018
Synthetic dairy wastewater	EGSB	20	7.1 ± 0.1	0.67	2	24	83–87	172–186	Singh et al., 2019
Synthetic dairy wastewater	DSC-FF (support material in FF: pumice stone)	20	7.1 ± 0.1	0.22–1.33	0.66–4	12-72-3	87–97	24–360	This study

ASBR, Anaerobic sequencing batch reactor; SGBR, Static granular bed reactor; UASB, Upflow anaerobic sludge blanket; MBR, Membrane bioreactor; FBR, Fluidized bed reactor; IFB, Inverted fluidized bed; AFBR, Anaerobic fixed bed reactor; AF, Anaerobic filter; CSTR, Completely stirred tank reactor; MBBR, Moving biofilm bioreactor; EGSB, Expanded granular sludge bed; DSC, Dynamic sludge chamber; FF, Fixed-film; NR, Not reported; GS, Granular sludge. [a] *<1% fat in substrate.* [b] *Oil and grease (mg/L), i.e., 750 ± 66 mgCOD/L (based on 0.8 g-LCFA/L from 1 g/L oil, 2.89 gCOD-FOG/L from 1 g/L LCFA).* [c] *Lipid content (%) in brackets.*

MATERIALS AND METHODS

Inoculum and Synthetic Wastewater

Two anaerobic sludges were sourced, granular sludge from a Lt-AD® reactor (NVP Energy Limited, Galway, Ireland) treating dairy wastewater from Arrabawn Dairies (Kilconnell, Ireland) and flocculent sludge from a ADI-BVF® reactor (ADI Systems, Evoqua) treating FOG-containing dairy effluents from the Dairygold Co-Operative Society (Mitchelstown, Ireland) and stored for 2 weeks at 7°C in a nitrogen-purged atmosphere prior to usage. The sludges were mixed in a 1:1 ratio [by volatile solids (VS)].

SDW (2 gCOD/L) was prepared using skimmed milk powder and a LCFA mixture (palmitate, stearate, oleate, and linoleate in a COD ratio of 3:1.5:4.5:1) in a COD ratio of 2:1. The SDW was supplemented with 2 g/L $NaHCO_3$ and 1 ml/L basal nutrient solution (Singh et al., 2019).

Reactor Design and Experimental Set-Up

Laboratory-scale (7 L) glass reactors (**Figure 1**) are composed of two operational sections, i.e., a dynamic sludge chamber (DSC) consisting of a granular sludge bed (volume 3.65 L) combined with a flotation zone for sludge retention based on granulation and flotation, and a FF compartment for microbial sludge retention by biofilm. A peristaltic pump (Masterflex) was used to recirculate the reactor liquor through an outlet beneath the flotation compartment to maintain an upflow velocity of 2 m/h for the expansion of the granular sludge bed and to improve sludge-feed contact. The flotation zone was designed to accommodate the LCFA-encapsulated granules. The reactors were set up and run as per Keating et al. (2018) and modified as DSC-FF reactors as per Holohan (2020). Three identical DSC-FF reactors were set up, each inoculated with the sludge mixture (10 gVS/L). SDW stored at 7°C was constantly mixed with a mechanical stirrer placed inside the refrigerator and was connected to nitrogen-filled gas bags to maintain anaerobic conditions. SDW was pumped to the reactors through a multi-channel low-flow peristaltic pump (Masterflex), which were maintained at 20°C for the experimental duration (150 days) by recirculating cooled water through an external water jacket. An outlet located above the FF section discharged effluent to a collection tank. The top of the reactor was connected to a 10 L gas bag to collect biogas. The HRT at start-up (72 h) was decreased gradually to 12 h (stepwise through 42.5, 24, 18, and 12 h on days 9, 25, 59, and 103) on reaching steady state, which was defined based on a similar sCOD removal efficiency for operational durations equivalent to at least three consecutive HRTs, except at 72 h HRT where an operational duration equivalent to two consecutive HRTs was used. Null hypothesis was tested on the sCOD removal efficiency using one-way ANOVA, and statistical significance was nullified at $p > 0.01$.

Liquid samples (20 ml) from a port located above the sludge bed, from a port located above the FF compartment, and from effluent (**Figure 1**) were taken three to four times weekly to measure pH, total COD (tCOD) and soluble COD (sCOD), volatile fatty acids (VFA), and individual LCFA concentrations.

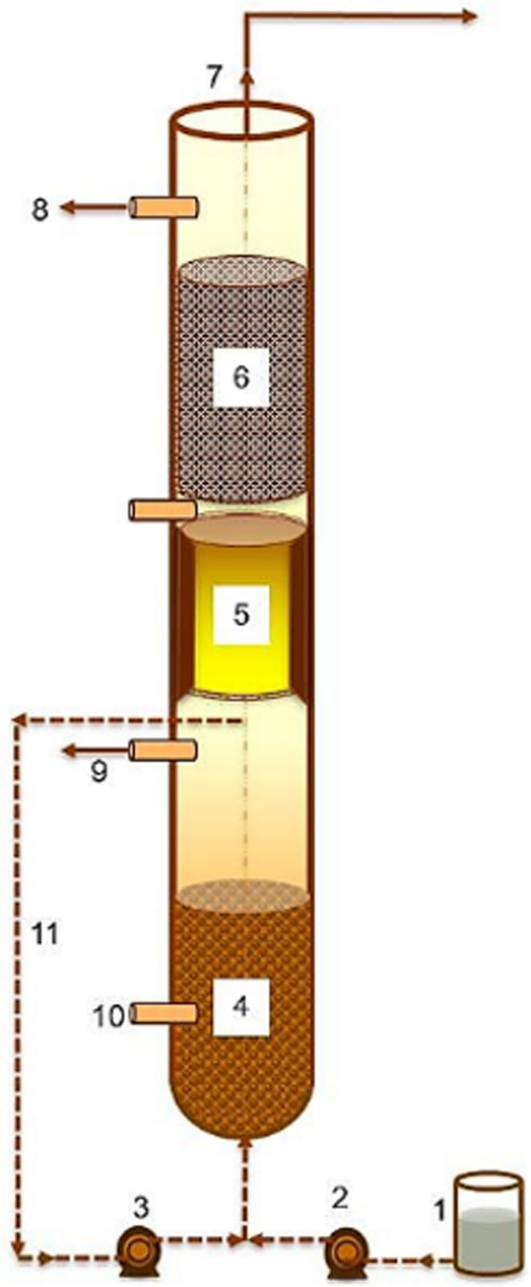

FIGURE 1 | Schematic representation of the components of the dynamic sludge chamber fixed film (DSC-FF) reactor design. (1) Influent tank, (2) peristaltic pump (feed), (3) Peristaltic pump (recirculation), (4) granular sludge bed, (5) anaerobic flotation zone, (6) anaerobic fixed-film (FF) compartment, (7) biogas collection, (8) effluent outlet and sampling, (9) sampling port (for post-granular chamber samples), (10) sampling port (for granular sludge), and (11) liquid recycle.

Analytical Methods

The volume of biogas produced was also determined three to four times weekly, by measuring the biogas volume collected in the gas bag. The methane content of biogas was determined using gas

chromatography (Varian), equipped with a glass column and a flame ionization detector. Nitrogen was used as the mobile phase at a flow rate of 25 ml/min. The biogas volume was measured with the water displacement method and reported at standard temperature and pressure (STP). MYE was calculated from the daily methane production based on the COD added (assuming a maximum of 350 ml-CH_4 per gram of COD at STP). pH was measured with a HI 2210 pH meter. Total solids (TS) and VS were measured gravimetrically using standard methods (APHA, 2005).

Liquid samples were centrifuged at 8000 rpm for 10 min and the supernatant was used for sCOD measurements using the potassium dichromate colorimetric method in commercially procured Hach Lange HR COD digestion tubes and a Hach Lange DR 5000 TM UV-Vis Spectrophotometer. For VFA measurements, the aliquots of supernatants collected after centrifugation were mixed with 50 μl of 30% orthophosphoric acid and then filtered through 0.22 μm Minisart® syringe filters. The VFAs [acetate (C2), propionate (C3), butyrate (C4), valerate (C5), caproate (C6), and caprylate (C8)] were analyzed by gas chromatography on a Varian Saturn 2000 GC with a BP 21 FFAP capillary column (SGE analytical science) and a flame ionization detector (FID) with helium as the carrier gas at a flow rate of 1 ml/min. Injector and FID detector temperatures were 250 and 300°C, respectively. The oven temperature was programmed to heat as follows: held at 60°C for 10 s, heated from 60 to 110°C at 30°C/min, and then heated up to 200°C at 10°C/min after which the temperature was held at 200°C for 2 min. The even-chained LCFAs [myristate (C14:0), palmitate (C16:0), stearate (C18:0), oleate (C18:1), and linoleate (C18:2)] in the liquid samples were measured according to van Gelder (2017) which was a modification of the protocols of Neves et al. (2009) and Ichihara and Fukubayashi (2010).

The development of granules from the sludge mixture was observed visually and under scanning electron microscopy (SEM). Five milliliters of granules was collected from a port located under the sludge bed using tubing connected to a syringe and were anaerobically transferred to a screw cap tube. The granules were incubated overnight at 4°C and then rinsed with a 0.2 M sodium cacodylate buffer solution. Next, samples were dehydrated by treating through an ethanol gradient [30, 50, 70, and 90% (v/v)] and placed onto aluminum stubs before drying with hexamethyldisiloxane (75 μl). Dehydrated samples were coated with a thin layer of gold and viewed using a SEM (Model S-2600 Hitachi, Japan) at 15 kV.

Thermodynamic Calculations

The feasibility of anaerobic conversion of LCFAs to acetate was evaluated at standard condition (25°C), and at temperatures of 20°C, and 37°C based on the standard Gibbs free energy changes for reactions ($\Delta G^{\circ\prime}$). Hydrogenation of the unsaturated LCFAs (linoleate and oleate) and β-oxidation of the saturated (stearate, palmitate) and unsaturated LCFAs (linoleate, oleate) were evaluated using the relationship $\Delta G^{\circ\prime} = \Sigma \Delta G_f^{\circ}$(products) - $\Sigma \Delta G_f^{\circ}$(substrates), where ΔG_f° refers to the standard free energy of formation. Standard Gibbs free energy of formation of LCFA (ΔG_f°) at standard conditions (25°C) was estimated by using the group contribution method (Mavrovouniotis, 1991), and of the other compounds were obtained from Thauer et al. (1977). Standard change in enthalpy for reactions ($\Delta H^{\circ\prime}$) was calculated based on the relationship $\Delta H^{\circ\prime} = \Sigma \Delta H_f^{\circ}$(products) - $\Sigma \Delta H_f^{\circ}$(substrates), where ΔH_f° refers to the standard enthalpy of formation of compounds, obtained from NIST (Linstrom and Mallard, 2014). Standard Gibbs free energy change of reactions ($\Delta G^{\circ\prime}{}_{T^{\circ}C}$) were calculated at 20 and 37°C based on temperature corrections according to the Gibbs-Helmholtz equation (Eq. 1):

$$\Delta G^{\circ\prime}{}_{T^{\circ}C} = \Delta G^{\circ\prime}{}_{25^{\circ}C} \cdot (T/298.5) + \Delta H^{\circ\prime}{}_{T^{\circ}C} \cdot (298.15 - T)/298.15, \quad (1)$$

where $\Delta G_f^{\circ\prime}{}_{T^{\circ}C}$ is the standard Gibbs free energy change of reaction at temperature of interest, $\Delta G_f^{\circ\prime}{}_{25^{\circ}C}$ is the standard Gibbs free energy change for reaction at standard conditions (25°C), T is the temperature of interest in Kelvin, and $\Delta H^{\circ\prime}{}_{T^{\circ}C}$ is the standard change in enthalpy for reaction. All calculation procedures were followed as described by Dolfing (2015).

RESULTS

COD Removal and Methane Production

The sCOD removal efficiency achieved by all three DSC-FF bioreactors was similar during the steady-state periods ($p > 0.01$) (**Supplementary Table S1**) throughout the experiment. The results for only one DSC-FF bioreactor are presented, but the data from all three DSC-FF reactors are provided as supplementary data (**Supplementary Figures S1–S3**). During the first 8 days of operation, when the HRT was 72 h, the tCOD and sCOD removal efficiencies were 88–94% and 96–98%, respectively (**Figure 2**), and the MYE was 5–9%. As the HRT was reduced to 42.5 h, tCOD and sCOD removal efficiencies remained high (94–98% and 97–98%, respectively) and the MYE increased to 26–28% (**Table 2**). After the HRT was reduced further to 24 h, the tCOD removal efficiency fluctuated (82–94%) but the sCOD removal efficiency remained high (90–98%), while the MYE increased further to 49–57% (**Table 2**). After further reducing the HRT to 18 h, the tCOD removal efficiency was 88–91%, the sCOD removal efficiency was 96–98%, and the MYE was 48–62%. Finally, as the HRT was reduced from 18 to 12 h, the removal efficiencies of tCOD and sCOD decreased to 63–72% and 84–89%, respectively (**Figure 2**), but the MYE further improved (up to 103%) (**Table 2**).

Thus, methane production from the DSC-FF reactor increased with the decrease in HRTs. At a HRT of 72 h (OLR of 0.67 gCOD/·day), the methane production was low (24 ± 9 ml-CH_4/$gCOD_{added}$). However, the methane production increased to 95 (± 5), 186 (± 15), and 190 (± 25) ml-CH_4/$gCOD_{added}$ at HRTs of 42.5, 24, and 18 h, respectively, corresponding to the increasing OLRs of 1.13, 2, and 2.67 gCOD/L·day (**Table 2**). A further decrease in the HRT to 12 h (OLR of 4 gCOD/L·day) resulted in a higher methane production of 360 (± 30) ml-CH_4/$gCOD_{added}$ and a MYE of 103%. Although the OLR and LCFA loading rate at the different HRTs were applied consistently, substrate accumulated in the DSC-FF reactor as revealed by the higher tCOD removal than could

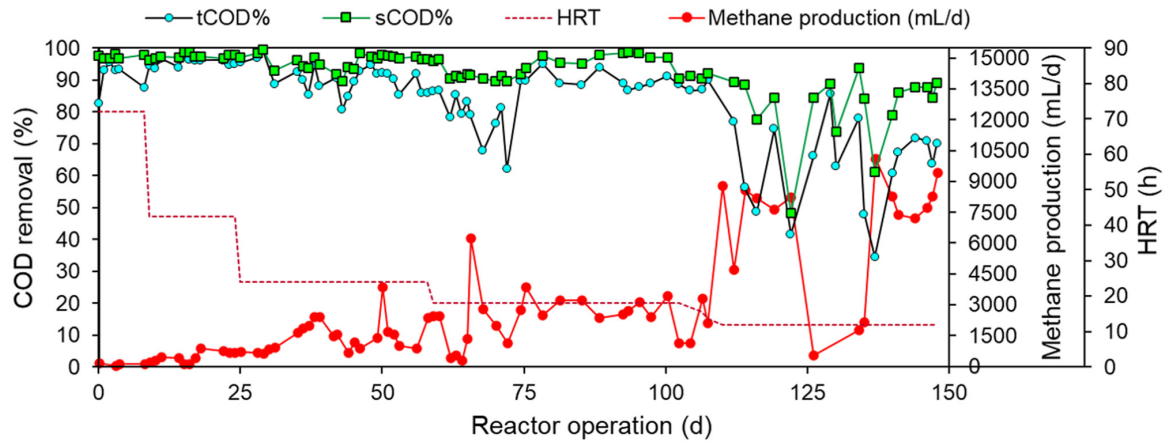

FIGURE 2 | Total COD (tCOD) and soluble COD (sCOD) removals and daily methane production from DSC-FF reactor at the different HRTs of 72, 42.5, 24, 18, and 12 h.

TABLE 2 | Operational conditions and process performance of the DSC-FF reactor and separately of DSC at the different HRTs of 72, 42.5, 24, 18, and 12 h.

Duration (days)	**0–8**	**9–24**	**25–58**	**59–100**	**110–148**
HRT	72	42.5	24	18	12
OLR (gCOD/L.day)	0.66	1.13	2	2.67	4
LCFA loading rate (mgCOD-LCFA/g-VS.day)	41	68	120	180	240
LCFA loading rate (mgCOD/L.day)	220	377	667	890	1333
pH (DSC)	6.9 ± 0.1	6.8 ± 0.1	6.9 ± 0.2	6.8 ± 0.1	6.8 ± 0.1
pH (DSC-FF)	7.9 ± 0.3	7.7 ± 0.5	7.8 ± 0.1	7.2 ± 0.1	6.9 ± 0.1
tCOD removal% (DSC)	81 ± 3	90 ± 2	75 ± 8	76 ± 1	53 ± 3
sCOD removal% (DSC)	95 ± 2	97 ± 1	86 ± 8	95 ± 1	86 ± 4
tCOD removal% (DSC-FF)	93 ± 0.3	95 ± 1	87 ± 3	89 ± 1	68 ± 3
sCOD removal% (DSC-FF)	97 ± 1	97 ± 0.5	97 ± 0.4	98 ± 1	87 ± 2
tCOD (mgCOD/L) (DSC)	406 ± 82	194 ± 30	620 ± 92	469 ± 19	925 ± 82
sCOD (mgCOD/L) (DSC)	97 ± 37	66 ± 20	331 ± 167	93 ± 13	280 ± 64
tCOD (mgCOD/L) (DSC-FF)	142 ± 2	94 ± 12	327 ± 49	207 ± 31	621 ± 27
sCOD (mgCOD/L) (DSC-FF)	57 ± 17	50 ± 9	84 ± 6	48 ± 11	251 ± 25
VFA (mgCOD/L) (DSC)	2 ± 1	43 ± 11	0	3.3 ± 1	100 ± 40
LCFA (mgCOD/L) (DSC)	4 ± 4	0	0	14 ± 14	196 ± 17
VFA (mgCOD/L) (DSC-FF)	32 ± 7	44 ± 6.5	2 ± 2	0 ± 0	208 ± 43
LCFA (mgCOD/L) (DSC-FF)	0	0	21 ± 4	0	183 ± 12
Methane concentration (%)	32 ± 1	62 ± 2	73 ± 2	74 ± 10	75 ± 1
Methane yield (ml-CH_4/$gCOD_{added}$)	24 ± 9	95 ± 5	186 ± 15	190 ± 25	360 ± 30
Methane yield (ml-CH_4/$gCOD_{consumed}$)	25 ± 9	97 ± 5	210 ± 10	200 ± 30	420 ± 30
MYE (%) (based on COD added)	7 ± 2	27 ± 1	53 ± 4	55 ± 7	103 ± 9
MYE (%) (based on COD consumed)	7 ± 2	28 ± 1	60 ± 3	58 ± 8	121 ± 9

be accounted by the methane production and effluent tCOD concentrations (**Figure 3**). The substrate accumulation, as shown by the unaccounted COD, was highest at the HRT of 72 h, and, decreased at the HRTs of 24 and 18 h (**Figure 3**). However, at 12 h HRT, the cumulative COD from the methane production and effluent tCOD concentrations was higher than the influent COD concentration (of 2 gCOD/L equivalent to 100%) (**Figure 3**). This suggests methanization of the accumulated substrates at the 12 h HRT. Moreover, at particular durations observed at 12 h HRT, tCOD removal was low but with a high methane production (e.g., days 113–119), which was followed by higher tCOD removal but with low methane production (e.g., days 126–134), and subsequently again had a lower tCOD removal but increased VFA and methane production (e.g., days 135–140) (**Figure 2**). This trend could be due to the sorption of the substrate during the high COD removal (exerting a substrate overload beyond the intended OLR), followed by methanization of the accumulated substrate in the subsequent duration. Thus, the DSC experienced alternating cycles of organic overloads, particularly when the HRT was 12 h.

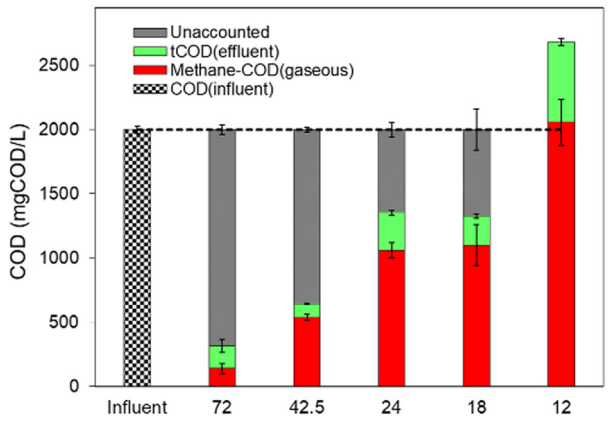

FIGURE 3 | COD balance for the DSC-FF reactor at the different HRTs of 72, 42.5, 24, 18, and 12 h along with the influent COD (equivalent to 2 gCOD/L) shown as reference.

Metabolic Intermediates From LCFA Oxidation

VFAs (C2–C6) and the even-chained LCFAs (C14–C18) in the DSC-FF effluent were analyzed periodically. With HRTs of 72 and 42.5 h, the total VFA concentration of the DSC-FF effluent was 20–120 mgCOD/L, comprising mainly of acetate (C2), propionate (C3), butyrate (C4), and low concentrations of valerate (C5). However, at HRTs of 24 and 18 h, the VFA concentrations were negligible, with only low concentrations of acetate detected (**Figure 4A**). At HRTs of 18–72.5 h, the LCFAs fed to the reactor (palmitate, oleate, and linoleate) were removed completely, and stearate was found at 24 h HRT in low concentrations (>10 mg/L) (**Figure 4B**), though, with the decrease in HRT from 18 to 12 h, the effluent concentration of VFAs increased (up to 190 mg/L) due to marked increases in the concentrations of acetate (60 mg/L) and propionate (130 mg/L). Toward the end of the trial, the VFA concentrations decreased to 97 mg/L (**Figure 4A**). Caproate (C6) that is produced from the β-oxidation of even-chained LCFAs was found only at the 12 h HRT (26–45 mg/L) (**Figure 4A**), along with the saturated LCFAs palmitate (14–40 mg/L) and stearate (20–2 mg/L) (**Figure 4B**), resulting in a LCFA removal efficiency of 71–74%.

Role of FF Compartment in Organics Removal

At 72 and 42.5 HRTs, compared to DSC, the FF contributed to an additional 4–12% tCOD removal (93–96% by DSC-FF vs. 78–92% by DSC alone), and 1% LCFA removal (100% by DSC-FF vs. 99% by DSC alone) (**Figures 5A,B**), whereas the sCOD removal efficiency after treatment by FF remained relatively unchanged

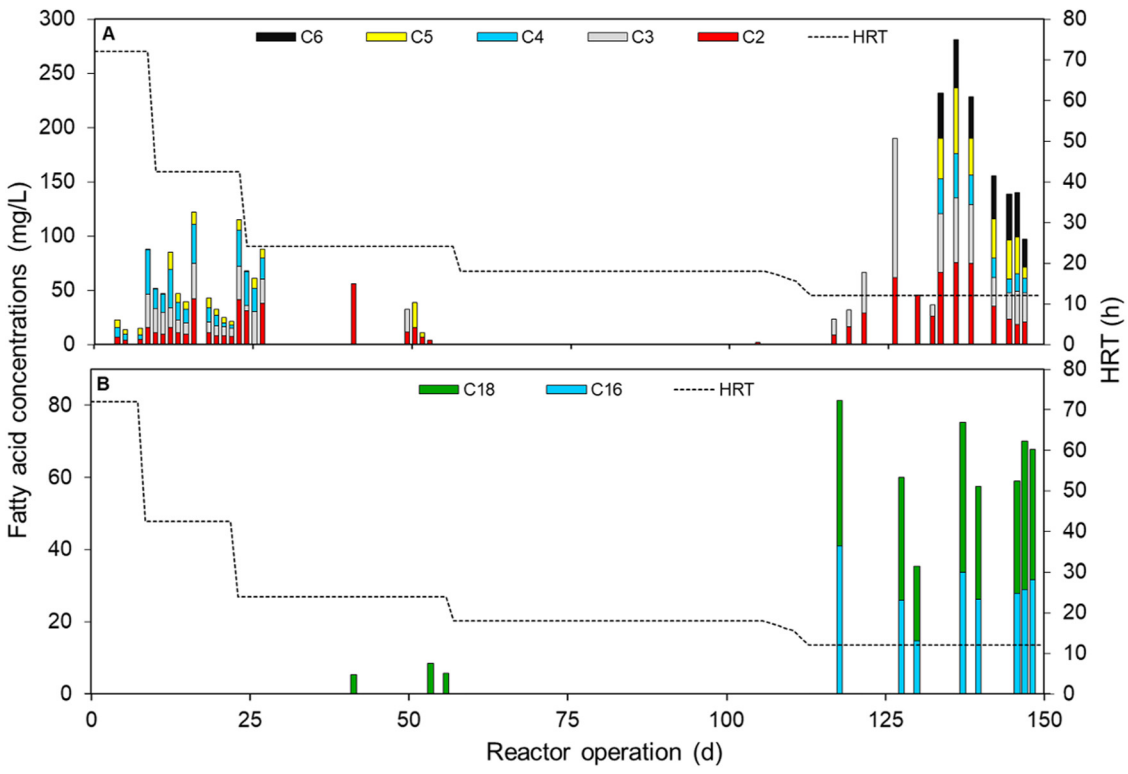

FIGURE 4 | Profiles of **(A)** volatile fatty acids (VFA), i.e. acetate (C2), propionate (C3), butyrate and iso-butyrate (C4), valerate (C5) and caproate (C6), and **(B)** long chain fatty acids (LCFA), i.e. palmitate (C16:0), and stearate (C18:0), in DSC-FF reactor effluent at the different HRTs of 72, 42.5, 24, 18, and 12 h. LCFAs myristate (C14:0), oleate (C18:1), and linoleate (C18:2) were not found in the liquid samples.

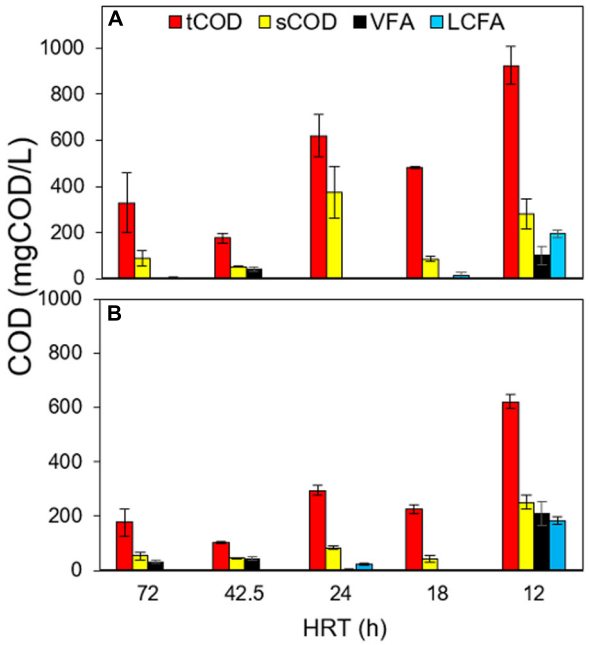

FIGURE 5 | COD fractionation as tCOD, sCOD, VFA-COD and LCFA-COD after treatment by **(A)** the DSC and further by **(B)** the FF at the different HRTs of 72, 42.5, 24, 18, and 12 h.

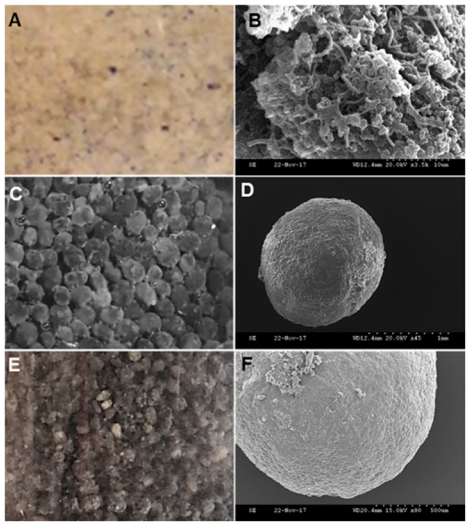

FIGURE 6 | Schematic representation of rapid granulation from inoculum mixture. Sludges prior to inoculation, i.e. flocculent sludge on **(A)** visual observation and **(B)** under Scanning Electron Microscopy (SEM) at 10 μm, and granular sludge on **(C)** visual observation and **(D)** under SEM at 1 mm. *De novo* granulation in the dynamic sludge compartment (DSC) after 8 days on **(E)** visual observation and **(F)** under SEM at 500 μm.

(93–98%) (**Table 2**). At the HRTs of 24 and 18 h, compared to DSC, the FF removed an additional 7–17% tCOD (84–90% by DSC-FF vs. 67–83% by DSC alone), and reduced LCFA concentrations to 25 mgCOD/L (**Supplementary Figure S4**). FF contributed to an additional 3–19% sCOD removal compared to DSC (**Figures 5A,B**), and resulted in overall sCOD removal efficiency of 97–99% by the DSC-FF reactor at 24 and 18 h HRTs (**Table 2**). At 12 h HRT, the tCOD removal by DSC had decreased (50–56%), and FF contributed appreciably (15%) to the tCOD removal, resulting in a tCOD removal efficiency of 65–71% by DSC-FF. Moreover, at 12 h HRT, the LCFA removal efficiency by DSC was 68–73%, wherein FF contributed to an additional 3–4% removal resulting in 71–74% LCFA removal by DSC-FF (**Supplementary Figure S4**). This suggests that FF had an important role in the removal of particulate COD, contingent to the incoming tCOD concentrations from DSC. The tCOD removal by FF was likely due to the entrapment of particulates by the support matrix.

At steady periods of 24 h and 18 h HRT, the VFA concentrations after treatment by DSC were low (<10 mgCOD/L) (**Supplementary Figure S5**). However, at the HRTs of 72 and 12 h, VFA concentrations were higher after treatment by FF (higher by 16- and 2-fold at 72 and 12 h HRT, respectively) than the VFA concentrations after treatment by DSC (**Supplementary Figure S5**), which suggests that acidification occurred in the FF compartment. During the steady state at 12 h HRT, the VFAs propionate, valerate, and caproate were found, whereas after treatment by FF, acetate and butyrate were additionally detected (**Supplementary Figure S5**). This production of acetate and butyrate at 12 h HRT in FF (**Supplementary Figure S5**), along with the simultaneous decrease in palmitate and stearate concentrations in FF (**Supplementary Figure S4**), signifies partial β-oxidation of the saturated LCFAs (stearate and palmitate) in the FF compartment at 12 h HRT.

Overall, the removal of COD and LCFAs by the DSC indicated its importance for the overall anaerobic treatment of SDW, and especially for the removal of saturated and unsaturated LCFAs. Up to the HRT of 18 h (LCFA loading rate of 890 mgCOD/L·day, specific LCFA loading rate 180 mgCOD/gVS·day), DSC achieved a COD removal efficiency exceeding 75% (both tCOD and sCOD). However, the COD removal by DSC decreased upon shortening the HRT to 12 h (LCFA loading rate of 1333 mgCOD/·day, specific LCFA loading rate 240 mgCOD-LCFA/gVS·day), leading to a higher inflow of particulates and saturated LCFAs (stearate and palmitate) into the FF compartment, and consequently a more prominent role of the FF compartment in entrapment and acidification of the SDW.

Sludge Washout and Flotation

No sludge washout was observed at HRTs of 72, 42.5, or 24 h. However, as the HRT was further shortened to 18 and 12 h, the effluent became more turbid (visual observation), though subsequently clarifying after prolonged operation at that particular HRT. The average effluent VS was 0.6 (± 0.1) and 4.5 (± 0.1) gVS/L at HRTs of 18 and 12 h, respectively. The higher sludge washout observed at 12 h HRT presumably resulted from the sloughing from the biofilm at the increased effluent flow rate. Flotation of small broken granules was observed (less than 10% of sludge in the DSC) at HRTs from 42.5 to 12 h.

However, the sludge flotation at these different HRTs did not vary, despite the increase in specific LCFA loading rate, and was accommodated by the DSC.

De novo Granulation in DSC

Initially, the two sludges comprising the inoculum mixture, i.e. the flocculent and granular sludge, were distinguishable visually due to their different colorings in physical formations (**Figures 6a,c**) and under SEM (**Figures 6b,d**). However, over time in the DSC, the two sludges were not visually distinguishable due to continuous mixing of the two inocula and they developed an overall grayish appearance, in contrast to the earlier distinct yellow (**Figure 6a**) and black (**Figure 6c**) respective colors of the inocula. During the continuous mixing, the mixed sludges began to form *de novo* sludge granules. By the end of reactor operation at 72 h HRT (day 8), appearance of distinct rounded granules was observed in the granular sludge bed in the DSC (**Figures 6e,f**).

Thermodynamic Feasibility of Degradation of Saturated and Unsaturated LCFAs

The standard Gibbs free energy changes of reaction ($\Delta G°'$) for the degradation of LCFAs (linoleate, oleate, stearate, and palmitate) present in the feed (SDW) were calculated at 20°C ($\Delta G°'_{20°C}$) (discharge temperature used in this study) and 37°C ($\Delta G°'_{37°C}$) (**Table 3**), as numerous studies evaluating lipid or LCFA degradation at mesophilic conditions have used 37°C as the operational temperature (Ramos et al., 2014; Dereli et al., 2015; Jensen et al., 2015; Cavaleiro et al., 2016).

The analysis of the effect of temperature on the energetic feasibility of hydrogenation revealed that the hydrogenation of linoleate and oleate to stearate was feasible both at 20 and 37°C under standard conditions, however, the hydrogenation reactions had higher free energy at 20°C (−159 and −79.5 kJ/mol) than at 37°C (−153.4 and −76.8 kJ/mol) (**Table 3**). Moreover, the coupling of hydrogenation to one cycle of β-oxidation (producing palmitate) yielded a higher free energy for linoleate **(−104.4 kJ/mol)** than for oleate (-24.9 kJ/mol). In contrast, the fatty acid oxidation of LCFAs (producing equivalent moles of acetate by β-oxidation) was not energetically feasible at either 20 or 37°C, and was more unfavorable at 20°C than at 37°C.

DISCUSSION

Treatment of FOG-Rich Wastewaters at Low-Temperature Through DSC-FF Configuration

This study shows for the first time that high-rate anaerobic treatment is a feasible option for LCFA-rich wastewaters at 20°C, at HRTs as low as 12 h. To the best of the authors' knowledge, many previous studies on anaerobic treatment of dairy wastewaters at lower temperatures (5–20°C) used feed with 1.8–10 times lower lipid or LCFA content (e.g., 3% COD-LCFA) (**Table 1**). While the anaerobic treatment of a similar synthetic dairy wastewater (OLR of 2 gCOD/L·day, 33% COD-LCFA) in lab-scale EGSB reactors at 20°C was feasible for operational durations of 60 days and achieved COD removal efficiencies of 83–87%, the treatment performance deteriorated on prolonged SDW feeding at 24 h HRT and did not recover even after the feeding was stopped (Singh et al., 2019). Contrarily, in this study the DSC-FF reactors achieved stable COD removal (87–97%), despite the application of higher LCFA loading rates. Previous studies reported a lower COD removal efficiency; for example, COD removal efficiency of 46–69% was reported in the anaerobic treatment of lipid-containing dairy wastewater (22% COD-lipid) at 24 h HRT at 20°C (Tawfik et al., 2008), whereas a COD removal efficiency of 38–47% was achieved in the batch treatment of lipid-containing municipal wastewater at 4–15°C at an OLR of 0.29 gCOD/L·day (lipid loading rates of 0.1–0.13 gCOD/L·day, 38–45% lipids) (Petropoulos et al., 2018).

Recently, real municipal wastewater containing 70% lipids (FOG loading rate of 224 mgCOD/L·day) at 15°C was treated in UASB and MBR reactors at short HRTs of 7.7 h with COD removal efficiencies of 79 and 86% and MYE of 17 and 23%, respectively (Petropoulos et al., 2019b). The presence of unhydrolyzed COD (Petropoulos et al., 2018, 2019b) suggested a low anaerobic conversion of the accumulated lipids. Real wastewaters are rich in particulate COD, which often is

TABLE 3 | Change in Gibbs free energy values of reactions ($\Delta G°'$) involved in hydrogenation and oxidation of selected LCFAs at standard conditions[#].

Reactions	$\Delta G°'_{25°C}$ (kJ/reaction)	$\Delta G°'_{20°C}$ (kJ/reaction)	$\Delta G°'_{37°C}$ (kJ/reaction)
Hydrogenation of unsaturated LCFAs			
$Linoleate^- + 2\ H_2 \rightarrow stearate^-$	−157.3	−159	−153.4
$Oleate^- + 1.5\ H_2 \rightarrow stearate^-$	−78.6	−79.5	−76.8
$Linoleate^- + 2\ H_2O \rightarrow palmitate^- + acetate^- + H^+$	−103.9	−104.4	−103.0
$Oleate^- + 2\ H_2O \rightarrow palmitate^- + acetate^- + H_2 + H^+$	−25.4	−24.9	−26.4
Fatty acid oxidation by β-oxidation			
$Linoleate^- + 16\ H_2O \rightarrow 9\ acetate^- + 14\ H_2 + 8H^+$	247.1	257.1	223.8
$Oleate^- + 16\ H_2O \rightarrow 9\ acetate^- + 15\ H_2 + 8H^+$	325.6	336.6	300.4
$Stearate^- + 16\ H_2O \rightarrow 9\ acetate^- + 16\ H_2 + 8H^+$	404.3	416.1	377.2
$Palmitate^- + 14\ H_2O \rightarrow 8\ acetate^- + 14\ H_2 + 7H^+$	353.5	363.9	329.4

[#]*Data for standard conditions (T = 25°C, pH 7, solute concentrations of 1 M, and gas partial pressure of 1 atm).*

challenging to hydrolyze at lower temperatures, more so for lipids than carbohydrates and proteins (Pavlostathis and Giraldo-Gomez, 1991; Perle et al., 1995; Vidal et al., 2000). There is a lack of consensus regarding the main bottleneck in lipid methanization, with both lipolysis and LCFA degradation being reported as the rate-limiting step (Hanaki et al., 1981; Pavlostathis and Giraldo-Gomez, 1991; Petropoulos et al., 2019a). In this study, the accumulated substrates were methanized at 12 h HRT in DSC-FF reactors (**Figure 3**), demonstrating the anaerobic degradation of mixed LCFAs at 20°C at LCFA loading rates up to 890 mgCOD-LCFA/L·day (**Figure 4B** and **Supplementary Figures S3, S4**). It is recommended for future studies discerning the rate-limiting step in low-temperature anaerobic lipid degradation to evaluate lipolysis and LCFA degradation at LCFA loading rates ≥ 1333 mgCOD-LCFA/L·day.

Furthermore, in this study, the MYE increased from 7 to 103% over the 150-day operational duration (**Table 2**), whereas a MYE of ∼80% is typical of high-performing mesophilic reactors (van Lier et al., 2015). The MYE at 20°C in the DSC-FF reactor at 72–18 h HRT was low (7–55%), likely due to accumulation of substrate (in DSC and FF). At 12 h HRT, the high MYE (>100%) resulted from the conversion of substrate that had accumulated in the DSC or in the FF section. The cyclical alternating organic loads experienced by the DSC at 12 h HRT was presumably due to the LCFA accumulation on granular sludge, as LCFAs have a high sorption propensity. Cavaleiro et al. (2009) overloaded sludge with a LCFA-rich feed at 37°C in feed cycles (20–30 days) followed by react cycles (no feeding) for methanization of the accumulated substrates. This strategy of alternating organic loads had enhanced the MYE from 67 to 91% wherein LCFA accumulation increased in the reactor up to 60 days (2 feed cycles), but was subsequently methanized due to specialization of the microbial community (Cavaleiro et al., 2009). In our study, the alternating organic loads likely enriched the LCFA degraders and could be employed as a strategy to improve methanization of LCFA-rich wastewater at 20°C, as previously demonstrated at 35–37°C for oleate treatment (Cavaleiro et al., 2009; Ziels et al., 2017). Tawfik et al. (2008) prevented sludge washout by maintaining a regular sludge discharge (20% of total influent COD) at a LCFA loading rate of 0.75 gCOD-LCFA/L·day (specific LCFA loading rate 95.4 mgCOD-LCFA/gVS·day) while treating dairy wastewater in a UASB reactor at 20°C, though such daily sludge disposal means a loss of the energy-rich organic fraction from the reactor. In comparison, the non-requirement of sludge disposal from the DSC-FF reactors resulted in an efficient containment of the energy-rich LCFAs, which were subsequently converted to methane in the reactors. Overall, the process performance of the DSC-FF reactors during the 150-day trials demonstrates the suitability of this reactor design for the methanization of LCFA-rich dairy wastewater at discharge temperature.

The DSC-FF reactor design facilitated a high contact between the sludge and substrate, and yet prevented suction of the floating granules by the recycle pump (**Figure 1**), which sometimes is the reason for process failure in laboratory scale studies due to increased sludge washout (Yoda and Nishimura, 1997). The upflow velocity of 2 m/h was high enough to effectuate the separation of gas bubbles from the surface of anaerobic granules, thus preventing an incidental lifting of the sludge bed. The anaerobic flotation compartment in the DSC could accommodate the flotation of LCFA-encapsulated granules, although minimal flotation (<10%) was observed even at the LCFA loading rate of 1333 mgCOD-LCFA/L·day (specific LCFA loading rate of 240 mgCOD-LCFA/gVS·day). Indeed, sludge flotation has previously been reported at lower LCFA loading rate of 86–203 mgCOD-LCFA/gVS·day (Hwu et al., 1998b) or 80 mgCOD-FOG/gTS·day (Macarie et al., 2018), wherein flotation of the entire sludge bed resulted in reactor failure. The anaerobic flotation compartment enabled the slow degradation of LCFA from the floating LCFA-encapsulated granules, followed by settling of the granules to the sludge bed. This dynamic behavior allowed for an increased microbial activity in the DSC, while ensuring continuous treatment of the LCFA-rich wastewater at low ambient temperature, and distinguishes the reactor design from the well-known reactor configurations, viz., UASB, EGSB, AFR, and anaerobic filter. Due to the anaerobic treatment achieved in the DSC (by tCOD and LCFA removal), the FF received wastewater with relatively low concentrations of particulate matter and LCFA. Consequently, the potential challenges associated with high lipid concentrations, such as biofilm-thinning or filter clogging, previously observed in anaerobic filters treating oleate (Alves et al., 2001) were prevented in this study. However, the application of LCFA loading rates higher than 1333 mgCOD-LCFA/L·day in the DSC-FF reactors needs to be further evaluated at low or psychrophilic temperatures.

Anaerobic Degradation of Saturated and Unsaturated LCFAs at 20°C

The DSC-FF reactors consistently removed the saturated and unsaturated LCFAs in SDW to concentrations below 50 mg/L in the effluent, at HRTs as short as 18 h. The saturated LCFAs, palmitate and stearate, were partially removed at 12 h. During treatment of wastewaters with high lipid loads, LCFA accumulation constituting of palmitate or stearate has often been encountered in various reactor types (Pereira et al., 2005; Cavaleiro et al., 2009; Dereli et al., 2015; Ziels et al., 2015, 2017; Duarte et al., 2018) due to the fast conversion of unsaturated LCFAs (linoleate and oleate) to palmitate (Cavaleiro et al., 2016).

The degradation of LCFA proceeds sequentially, with an initial sorption to the cell surface, followed by the activation of saturated and unsaturated LCFAs, facilitating their transport into the cytosol of bacteria. The unsaturated LCFAs are hydrogenated to their saturated counterpart, and are subsequently degraded by β-oxidation (Sousa et al., 2009). Subsequently, during each cycle of β-oxidation, the LCFAs are shortened by two carbons in chain length, producing one fatty acid molecule with smaller chain length and one acetate molecule, wherein the LCFA degradation to lower molecular weight C_{n-2} fatty acid proceeds cyclically up until the production of an equivalent number of acetate or propionate molecules from the LCFA is achieved (Alves et al., 2009). The change in Gibb's free energy for the hydrogenation reactions are favorable at 20°C, whereas the β-oxidation reactions are not (**Table 3**). At HRTs of 18–72 h, both hydrogenation and

β-oxidation reactions proceeded in the DSC and FF, resulting in complete removal of the unsaturated LCFAs and high removal of the saturated LCFAs (**Table 3**). In comparison, at 12 h HRT, the complete removal of the unsaturated LCFAs, oleate and linoleate, proceeded due to the increased energetic favorability of the hydrogenation reactions at 20°C than at mesophilic conditions. However, the saturated LCFAs, palmitate and stearate were only removed partially at 12 h HRT, presumably due to the limitations in LCFA uptake at the higher LCFA loading rate (1333 mgCOD-LCFA/L·day). Further studies evaluating the uptake and degradation of individual LCFAs, saturated as well as unsaturated, are needed at temperatures below 20°C to comprehend the temperature dependence of mechanisms involved in the methanization of LCFAs.

CONCLUSION

This study evaluated the anaerobic treatment of mixed LCFA-containing dairy wastewater at low temperature (20°C) by using a novel DSC-FF reactor design. High sCOD removal efficiencies (85–89%) and methane production (360 ± 30 ml-CH_4/gCOD_{added}) were achieved with mixed LCFA-containing dairy wastewater at 20°C up to an OLR of 4 gCOD/L·day (LCFA loading rate 1333 mgCOD-LCFA/L·day, HRT 12 h). The complete removal of the unsaturated LCFAs (oleate and linoleate) was achieved due to the thermodynamic feasibility of hydrogenation of these LCFAs at 20°C, whereas the saturated LCFAs (palmitate and stearate) were removed partially due to the thermodynamic limitations in the β-oxidation of palmitate and stearate at 20°C. Rapid sludge granulation from an inoculum mixture of granular and flocculent sludges in DSC, and the formation of biofilm in FF were achieved during the treatment of mixed-LCFA wastewater even with high LCFA concentration (33% COD basis) and LCFA loading rates of 220–1333 mgCOD-LCFA/·day to allow successful treatment of LCFA-containing wastewater at 20°C. The results from this study demonstrate that the high-rate treatment of LCFA-containing industrial wastewater is feasible at discharge temperature due to sludge retention by granulation, flotation, and biofilm formation in the novel DSC-FF reactor configuration.

DATA AVAILABILITY STATEMENT

All datasets analyzed for this study are included in the article/**Supplementary Material**.

AUTHOR CONTRIBUTIONS

SS and VO'F were involved in the planning of experiments and designing of reactors. SS performed the experiments, the related physico-chemical and data analysis, and wrote the manuscript. BH and JC-A helped in the setup of reactors. SM helped in reactor operation. VO'F, JR, MK, PL, BH, and GC participated in the preparation and correction of the manuscript. All authors contributed to the article and approved the submitted version.

FUNDING

This project has received funding from the European Union's Horizon 2020 research and innovation programme under the Marie Skłodowska–Curie European Joint Doctorate (EJD) in Advanced Biological Waste-To-Energy Technologies (ABWET), under grant agreement No. 643071. This research was also supported through VO'F through the Irish Dairy Processing Technology Centre through the Enterprise Ireland Technology Centres Programme (TC/2014/0016) and Science Foundation Ireland (14/IA/2371 and 16/RC/3889). Financial supported to BH through Irish Research Council Employment Based Postgraduation Scheme with NVP Energy Ltd. is gratefully acknowledged. Financial supported to SM through College of Science Scholarship, NUI Galway, and to GC through Science Foundation Ireland Career Development Award is also gratefully acknowledged.

ACKNOWLEDGMENTS

We are grateful to Arrabawn Dairies (Kilconnell, Ireland) and NVP Energy Limited (Galway, Ireland) for providing the granular sludge. We would also like to thank Dairygold Co-Operative Society (Mitchelstown, Ireland) and ADI Systems (Evoqua Water Technologies, Ireland) for providing the flocculent sludge.

SUPPLEMENTARY MATERIAL

The Supplementary Material for this article can be found online at: https://www.frontiersin.org/articles/10.3389/fenrg.2020.00166/full#supplementary-material

REFERENCES

Alves, M. M., Pereira, M. A., Sousa, D. Z., Cavaleiro, A. J., Picavet, M., Smidt, H., et al. (2009). Waste lipids to energy: how to optimize methane production from long-chain fatty acids (LCFA). *Microb. Biotechnol.* 2, 538–550. doi: 10.1111/j.1751-7915.2009.00100.x

Alves, M. M., Picavet, M. A., Pereira, M. A., Cavaleiro, A. J., and Sousa, D. Z. (2007). Novel anaerobic reactor for the removal of long chain fatty acids from fat containing wastewater. WO Patent No. WO/2007/058,557. Braga: University of Minho.

Alves, M. M., Vieira, M. J. A., Pereira, Á. R. M., Pereira, M. A., and Mota, M. E. (2001). Effects of lipids and oleic acid on biomass development in anaerobic fixed bed reactors. Part I: biofilm growth and activity. *Water Res.* 35, 1264–1270.

APHA (2005). *Standard Methods for the Examination of Water and Wastewater*, Vol. 79. (Washington, DC: APHA), 453–456.

Batstone, D. J., and Jensen, P. D. (2011). "Anaerobic processes," in *Treatise on Water Science*, ed. P. Wilderer (Oxford: Academic Press), 615–639.

Bialek, K., Cysneiros, D., and O'Flaherty, V. (2014). Hydrolysis, acidification and methanogenesis during low-temperature anaerobic digestion of dilute dairy

wastewater in an inverted fluidised bioreactor. *Appl. Microbiol. Biotechnol.* 98, 8737–8750. doi: 10.1007/s00253-014-5864-7

Biswas, K., and Turner, S. J. (2012). Microbial community composition and dynamics of moving bed biofilm reactor systems treating municipal sewage. *Appl. Environ. Microbiol.* 78, 855–864. doi: 10.1128/AEM.06570-11

Buntner, D., Sanchez, A., and Garrido, J. M. (2013). Feasibility of combined UASB and MBR system in dairy wastewater treatment at ambient temperatures. *Chem. Eng. J.* 230, 475–481. doi: 10.1016/j.cej.2013.06.043

Cavaleiro, A. J., Pereira, M. A., Guedes, A. P., Stams, A. J. M., Alves, M. M., and Sousa, D. Z. (2016). Conversion of Cn-Unsaturated into Cn-2-Saturated LCFA Can Occur Uncoupled from Methanogenesis in Anaerobic Bioreactors. *Environ. Sci. Technol.* 50, 3082–3090. doi: 10.1021/acs.est.5b03204

Cavaleiro, A. J., Salvador, A. F., Alves, J. I., and Alves, M. (2009). Continuous high rate anaerobic treatment of oleic acid based wastewater is possible after a step feeding start-up. *Environ. Sci. Technol.* 43, 2931–2936. doi: 10.1021/es8031264

Dague, R. R., Banik, G. C., and Ellis, T. G. (1998). Anaerobic sequencing batch reactor treatment of dilute wastewater at psychrophilic temperatures. *Water Environ. Res.* 70, 155–160.

Davidsson, Å., Lövstedt, C., la Cour Jansen, J., Gruvberger, C., and Aspegren, H. (2008). Co-digestion of grease trap sludge and sewage sludge. *Waste Manag.* 28, 986–992. doi: 10.1016/j.wasman.2007.03.024

Dereli, R. K., Heffernan, B., Grelot, A., van der Zee, F. P., and van Lier, J. B. (2015). Influence of high lipid containing wastewater on filtration performance and fouling in AnMBRs operated at different solids retention times. *Sep. Purif. Technol.* 139, 43–52. doi: 10.1016/j.seppur.2014.10.029

Desbois, A. P., and Smith, V. J. (2010). Antibacterial free fatty acids: activities, mechanisms of action and biotechnological potential. *Appl. Microbiol. Biotechnol.* 85, 1629–1642. doi: 10.1007/s00253-009-2355-3

Dolfing, J. (2015). "Protocols for calculating reaction kinetics and thermodynamics," in *Hydrocarbon and Lipid Microbiology Protocols: Springer Protocols Handbooks*, eds T. J. McGenity, K. N. Timmis, and B. Nogales (Berlin: Springer-Verlag), 155–163. doi: 10.1007/8623

Duarte, M. S., Silva, S. A., Salvador, A. F., Cavaleiro, A. J., Stams, A. J. M., Alves, M. M., et al. (2018). Insight into the role of facultative bacteria stimulated by micro-aeration in continuous bioreactors converting LCFA to methane. *Environ. Sci. Technol.* 52, 6947–6507. doi: 10.1021/acs.est.8b00894

Fujihira, T., Seo, S., Yamaguchi, T., Hatamoto, M., and Tanikawa, D. (2018). High-rate anaerobic treatment system for solid/lipid-rich wastewater using anaerobic baffled reactor with scum recovery. *Bioresour. Technol.* 263, 145–152. doi: 10.1016/j.biortech.2018.04.091

Hanaki, K., Matsuo, T., and Nagase, M. (1981). Mechanism of inhibition caused by long-chain fatty acids in anaerobic digestion process. *Biotechnol. Bioeng.* 23, 1591–1610. doi: 10.1002/bit.260230717

Holohan, B. C. (2020). *High-Rate Anaerobic Treatment of Lipid-Rich Wastewater*. Ph.D. thesis, National University of Ireland Galway, Galway.

Hwu, C. S., Lier, J. B., and Lettinga, G. (1998a). Physicochemical and biological performance of expanded granular sludge bed reactors treating long-chain fatty acids. *Process Biochem.* 33, 75–81.

Hwu, C. S., Tseng, S. K., Yuan, C. Y., Kulik, Z., and Lettinga, G. (1998b). Biosorption of long-chain fatty acids in UASB treatment process. *Water Res.* 32, 1571–1579. doi: 10.1016/S0043-1354(97)00352-7

Ichihara, K., and Fukubayashi, Y. (2010). Preparation of fatty acid methyl esters for gas-liquid chromatography. *J. Lipid Res.* 51, 635–640. doi: 10.1194/jlr.d001065

Jeganathan, J., Nakhla, G., and Bassi, A. (2006). Long-term performance of high-rate anaerobic reactors for the treatment of oily wastewater. *Environ. Sci. Technol.* 40, 6466–6472. doi: 10.1021/es061071m

Jensen, P. D., Yap, S. D., Boyle-Gotla, A., Janoschka, J., Carney, C., Pidou, M., et al. (2015). Anaerobic membrane bioreactors enable high rate treatment of slaughterhouse wastewater. *Biochem. Eng. J.* 97, 132–141. doi: 10.1016/j.bej.2015.02.009

Keating, C., Hughes, D., Mahony, T., Cysneiros, D., Ijaz, U. Z., Smith, C. J., et al. (2018). Cold adaptation and replicable microbial community development during long-term low-temperature anaerobic digestion treatment of synthetic sewage. *FEMS Microbiol. Ecol.* 94:fiy095. doi: 10.1093/femsec/fiy095

Kim, S. H., Han, S. K., and Shin, H. S. (2004). Two-phase anaerobic treatment system for fat-containing wastewater. *J. Chem. Technol. Biotechnol.* 79, 63–71. doi: 10.1002/jctb.939

Lalman, J., and Bagley, D. M. (2002). Effects of C18 long chain fatty acids on glucose, butyrate and hydrogen degradation. *Water Res.* 36, 3307–3313. doi: 10.1016/S0043-1354(02)00014-3

Leal, C. M. R. M., Freire, D. M. G., Cammarota, M. C., and Sant'Anna, G. L. Jr. (2006). Effect of enzymatic hydrolysis on anaerobic treatment of dairy wastewater. *Process Biochem.* 41, 1173–1178. doi: 10.1016/j.procbio.2005.12.014

Linstrom, P. J., and Mallard, W. G. (2014). *NIST Chemistry webBook, NIST Standard Reference Database Number 69*. Gaithersburg, MD: National Institute of Standards and Technology.

Luostarinen, S. A., and Rintala, J. A. (2005). Anaerobic on-site treatment of black water and dairy parlour wastewater in UASB-septic tanks at low temperatures. *Water Res.* 39, 436–448. doi: 10.1016/j.watres.2004.10.006

Macarie, H., Esquivel, M., Laguna, A., Baron, O., El Mamouni, R., Guiot, S. R., et al. (2018). Strategy to identify the causes and to solve a sludge granulation problem in methanogenic reactors: application to a full-scale plant treating cheese wastewater. *Environ. Sci. Pollut. Res.* 25, 21318–21331. doi: 10.1007/s11356-017-9818-3

Martin, I., Pidou, M., Soares, A., Judd, S., and Jefferson, B. (2011). Modelling the energy demands of aerobic and anaerobic membrane bioreactors for wastewater treatment. *Environ. Technol.* 32, 921–932. doi: 10.1080/09593330.2011.565806

Mavrovouniotis, M. L. (1991). Estimation of standard Gibbs energy changes of biotransformations. *J. Biol. Chem.* 266, 14440–14445.

McHugh, S., Collins, G., and O'Flaherty, V. (2006). Long-term, high-rate anaerobic biological treatment of whey wastewaters at psychrophilic temperatures. *Bioresour. Technol.* 97, 1669–1678. doi: 10.1016/j.biortech.2005.07.020

McHugh, S., O'Reilly, C., Mahony, T., Colleran, E., and O'Flaherty, V. (2003). Anaerobic granular sludge bioreactor technology. *Rev. Environ. Sci. Biotechnol.* 2, 225–245. doi: 10.1023/B:RESB.0000040465.45300.97

Neves, L., Pereira, M. A., Mota, M., and Alves, M. M. (2009). Detection and quantification of long chain fatty acids in liquid and solid samples and its relevance to understand anaerobic digestion of lipids. *Bioresour. Technol.* 100, 91–96. doi: 10.1016/j.biortech.2008.06.018

Nikolaeva, S., Sanchez, E., and Borja, R. (2013). Dairy wastewater treatment by anaerobic fixed bed reactors from laboratory to pilot-scale plant:a case study in Costa Rica operating at ambient temperature. *Int. J. Environ. Res.* 7, 759–766. doi: 10.22059/IJER.2013.655

Park, J., Oh, J. H., Evans, E. A., Lally, M. F., Hobson, K. L., and Ellis, T. G. (2012). Industrial wastewater treatment by on-site pilot static granular bed reactor (SGBR). *Water Pract. Technol.* 7:2166. doi: 10.2166/wpt.2012.006

Passeggi, M., López, I., and Borzacconi, L. (2009). Integrated anaerobic treatment of dairy industrial wastewater and sludge. *Water Sci. Technol.* 59, 501–506. doi: 10.2166/wst.2009.010

Pavlostathis, S. G., and Giraldo-Gomez, E. (1991). Kinetics of anaerobic treatment – a critical review. *CRC Crit. Rev. Environ. Control* 21, 411–490. doi: 10.1080/10643389109388424

Pereira, M. A., Pires, O. C., Mota, M., and Alves, M. M. (2002). Anaerobic degradation of oleic acid by suspended and granular sludge: identification of palmitic acid as a key intermediate. *Water Sci. Technolgy* 45, 139–144.

Pereira, M. A., Pires, O. C., Mota, M., and Alves, M. M. (2005). Anaerobic biodegradation of oleic and palmitic acids: evidence of mass transfer limitations caused by long chain fatty acid accumulation onto the anaerobic sludge. *Biotechnol. Bioeng.* 92, 15–23. doi: 10.1002/bit.20548

Perle, M., Kimchie, S., and Shelef, G. (1995). Some biochemical aspects of the anaerobic degradation of dairy wastewater. *Water Res.* 29, 1549–1554. doi: 10.1016/0043-1354(94)00248-6

Petropoulos, E., Dolfing, J., Yu, Y., Wade, M. J., Bowen, E. J., Davenport, R. J., et al. (2018). Lipolysis of domestic wastewater in anaerobic reactors operating at low temperatures. *Environ. Sci. Water Res. Technol.* 4, 1002–1013. doi: 10.1039/c8ew00156a

Petropoulos, E., Shamurad, B., Acharya, K., and Tabraiz, S. (2019a). Domestic wastewater hydrolysis and lipolysis during start-up in anaerobic digesters and microbial fuel cells at moderate temperatures. *Int. J. Environ. Sci. Technol.* 17, 27–38. doi: 10.1007/s13762-019-02426-z

Petropoulos, E., Yu, Y., Tabraiz, S., Yakubu, A., Curtis, T. P., and Dolfing, J. (2019b). High rate domestic wastewater treatment at 15°C using anaerobic reactors inoculated with cold-adapted sediments/soils-shaping robust methanogenic

communities. *Environ. Sci. Water Res. Technol.* 5, 70–82. doi: 10.1039/c8ew00410b

Ramasamy, E. V., and Abbasi, S. A. (2000). Energy recovery from dairy wastewaters: impacts of biofilm support systems on anaerobic CST reactors. *Appl. Energy* 65, 91–98. doi: 10.1016/S0306-2619(99)00079-3

Ramos, C., García, A., and Diez, V. (2014). Performance of an AnMBR pilot plant treating high-strength lipid wastewater: biological and filtration processes. *Water Res.* 67, 203–215. doi: 10.1016/j.watres.2014.09.021

Rinzema, A., Boone, M., van Knippenberg, K., and Lettinga, G. (1994). Bactericidal effect of long chain fatty acids in anaerobic digestion. *Water Environ. Res.* 66, 40–49. doi: 10.2175/WER.66.1.7

Saatci, Y., Arslan, E. I., and Konar, V. (2003). Removal of total lipids and fatty acids from sunflower oil factory effluent by UASB reactor. *Bioresour. Technol.* 87, 269–272. doi: 10.1016/S0960-8524(02)00255-9

Sam-Soon, P., Loewenthal, R. E., Wentzel, M. C., and Marais, G. V. R. (1991). A long-chain fatty acid, oleate, as sole substrate in upflow anaerobic sludge bed (UASB) reactor systems. *Water S. Afr.* 17, 31–36.

Singh, S., Rinta-Kanto, J. M., Kettunen, R., Tolvanen, H., Lens, P., Collins, G., et al. (2019). Anaerobic treatment of LCFA-containing synthetic dairy wastewater at 20°C: process performance and microbial community dynamics. *Sci. Total Environ.* 691, 960–968. doi: 10.1016/j.scitotenv.2019.07.136

Sousa, D. Z., Smidt, H., Alves, M. M., and Stams, A. J. M. (2009). Ecophysiology of syntrophic communities that degrade saturated and unsaturated long-chain fatty acids. *FEMS Microbiol. Ecol.* 68, 257–272. doi: 10.1111/j.1574-6941.2009.00680.x

Sun, Y., Wang, D., Qiao, W., Wang, W., and Zhu, T. (2013). Anaerobic co-digestion of municipal biomass wastes and waste activated sludge: dynamic model and material balances. *J. Environ. Sci.* 25, 2112–2122. doi: 10.1016/s1001-0742(12)60236-8

Szabo-Corbacho, M. A., Pacheco-Ruiz, S., Míguez, D., Hooijmans, C. M., García, H. A., Brdjanovic, D., et al. (2019). Impact of solids retention time on the biological performance of an AnMBR treating lipid-rich synthetic dairy wastewater. *Environ. Technol.* 1–12. doi: 10.1080/09593330.2019.1639829 [Epub ahead of print].

Tawfik, A., Sobhey, M., and Badawy, M. (2008). Treatment of a combined dairy and domestic wastewater in an up-flow anaerobic sludge blanket (UASB) reactor followed by activated sludge (AS system). *Desalination* 227, 167–177. doi: 10.1016/j.desal.2007.06.023

Thauer, R. K., Jungermann, K., and Decker, K. (1977). Energy conservation in chemotrophic anaerobic bacteria. *Bacteriol. Rev.* 40, 100–181. doi: 10.1108/eb027807

Toldrá, F., Flors, A., Lequerica, J. L., and Vallés, S. (1987). Fluidized bed anaerobic biodegradation of food industry wastewaters. *Biol. Wastes* 21, 55–61. doi: 10.1016/0269-7483(87)90146-7

United Nations (2015). *United Nations General Assembly Resolution A/Res/70/1: Transforming Our World: the 2030 Agenda for Sustainable Development*. New York, NY: United Nations.

van Gelder, T. (2017). *Quantification of LCFA Profiles*. Wageningen: Wageningen University & Research.

van Lier, J. B., van der Zee, F. P., Frijters, C. T. M. J., and Ersahin, M. E. (2015). Celebrating 40 years anaerobic sludge bed reactors for industrial wastewater treatment. *Rev. Environ. Sci. Biotechnol.* 14, 681–702. doi: 10.1007/s11157-015-9375-5

Vidal, G., Carvalho, A., Méndez, R., and Lema, J. M. (2000). Influence of the content in fats and proteins on the anaerobic biodegradability of dairy wastewaters. *Bioresour. Technol.* 74, 231–239. doi: 10.1016/S0960-8524(00)00015-8

Viraraghavan, T., and Kikkeri, S. R. (1990). Dairy wastewater treatment using anaerobic filters. *Can. Agric. Eng.* 33, 143–149.

Yoda, M., and Nishimura, S. (1997). Controlling granular sludge floatation in UASB reactors. *Water Sci. Technol.* 36, 165–173. doi: 10.1016/S0273-1223(97)00520-9

Zheng, C. J., Yoo, J. S., Lee, T. G., Cho, H. Y., Kim, Y. H., and Kim, W. G. (2005). Fatty acid synthesis is a target for antibacterial activity of unsaturated fatty acids. *FEBS Lett.* 579, 5157–5162. doi: 10.1016/j.febslet.2005.08.028

Zhou, X., Meile, L., Kreuzer, M., and Zeitz, J. O. (2013). The effect of saturated fatty acids on methanogenesis and cell viability of *Methanobrevibacter ruminantium*. *Archaea* 2103:106916. doi: 10.1155/2013/106916

Zielińska, M., Zieliński, M., and Dębowski, M. (2018). Organic compounds and phosphorus removal from dairy wastewater by biofilm on iron-containing supports. *J. Environ. Eng.* 144:04017087. doi: 10.1061/(ASCE)EE.1943-7870.0001309

Ziels, R. M., Beck, D. A. C., Marti, M., Gough, H. L., Stensel, H. D., and Svensson, B. H. (2015). Monitoring the dynamics of syntrophic β-oxidizing bacteria during anaerobic degradation of oleic acid by quantitative PCR. *FEMS Microbiol. Ecol.* 91:fiv028. doi: 10.1093/femsec/fiv028

Ziels, R. M., Beck, D. A. C., and Stensel, H. D. (2017). Long-chain fatty acid feeding frequency in anaerobic codigestion impacts syntrophic community structure and biokinetics. *Water Res.* 117, 218–229. doi: 10.1016/j.watres.2017.03.060

Conflict of Interest: BH was employed by the company NVP Energy Ltd.

The remaining authors declare that the research was conducted in the absence of any commercial or financial relationships that could be construed as a potential conflict of interest.

frontiers in Energy Research

ORIGINAL RESEARCH
published: 27 November 2020
doi: 10.3389/fenrg.2020.541535

Effect of Temperature on Pyrolysis Oil Using High-Density Polyethylene and Polyethylene Terephthalate Sources From Mobile Pyrolysis Plant

Ruktai Prurapark, Kittwat Owjaraen, Bordin Saengphrom, Inpitcha Limthongtip and Nopparat Tongam*

Faculty of Engineering, Srinakharinwirot University, Nakhon Nayok, Thailand

This research aims to study the effect of temperature, collecting time, and condensers on properties of pyrolysis oil. The research was done be analyzing viscosity, density, proportion of pyrolysis products and performance of each condenser towers for the pyrolysis of high-density polyethylene (HDPE) and polyethylene terephthalate (PET) in the mobile pyrolysis plant. Results showed that the main product of HDPE resin was liquid, and the main product of PET resin was solid. Since the pyrolysis of PET results in mostly solid which blocked up the pipe, the analysis of pyrolysis oil would be from the use of HDPE as a raw material. The pyrolysis of HDPE resin in the amount of 100 kg at 400, 425, and 450°C produced the amount of oil 22.5, 27, and 40.5 L, respectively. The study found that 450°C was the temperature that gives the highest amount of pyrolysis oil in the experiment. The viscosity was in the range of 3.287–4.850 cSt. The density was in the range of 0.668–0.740 kg/L. The viscosity and density were increased according to three factors: high pyrolysis temperature, number of condensers and longer sampling time. From the distillation at temperatures below 65, 65–170, 170–250, and above 250°C, all refined products in each temperature range had the carbon number according to their boiling points. The distillation of pyrolysis oil in this experiment provided high amount of kerosene, followed by gasoline and diesel.

Keywords: index terms-pyrolysis, high density polyethylene, polyethylene terephthalate, energy, environmental

OPEN ACCESS

Edited by:
Su Shiung Lam,
University of Malaysia Terengganu, Malaysia

Reviewed by:
Reynaldo Palacios-Bereche,
Federal University of ABC, Brazil
Rafeah Wahi,
Universiti Malaysia Sarawak, Malaysia

****Correspondence:***
Ruktai Prurapark
ruktai@g.swu.ac.th

Specialty section:
This article was submitted to Process and Energy Systems Engineering, a section of the journal Frontiers in Energy Research

Received: *09 March 2020*
Accepted: *23 October 2020*
Published: *27 November 2020*

Citation:
Prurapark R, Owjaraen K, Saengphrom B, Limthongtip I and Tongam N (2020) Effect of Temperature on Pyrolysis Oil Using High-Density Polyethylene and Polyethylene Terephthalate Sources From Mobile Pyrolysis Plant. Front. Energy Res. 8:541535. doi: 10.3389/fenrg.2020.541535

INTRODUCTION

Energy is important to life and is one of the economic drivers. At present, Thailand has faced with energy problems because Thailand imports energy mainly oil from middle east which affects the way of life and the overall economy of the country. Therefore, energy sustainability is one of Thai society's problems that urgently need solutions. The utilization of energy from waste is an option that has been promoted by the government which has both direct and indirect benefits.

From the Pollution Control Department's pollution quantity survey in 2014, the amount of solid municipal waste in Thailand is 26.17 million tons per year. There is only 19% correct disposal, resulting in accumulated waste up to 19.9 million tons per year. There is also an amount of landfill waste accumulated more than 300 million tons and continuously increase every year. Considering the waste composition, there are generally about 18% of plastic waste, equivalent to 3.75 million tons

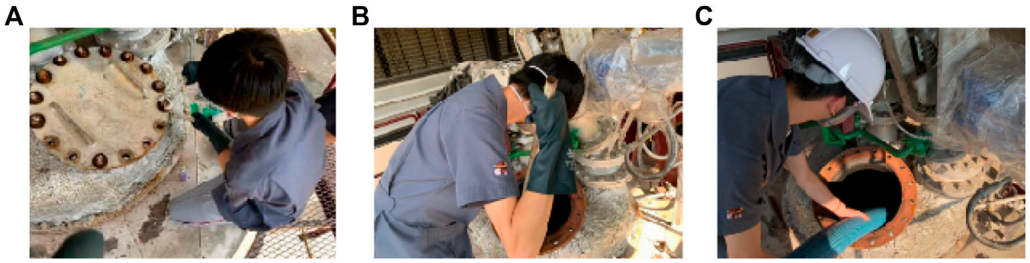

FIGURE 1 | Preparation of pyrolysis reactor **(A)** Opening the lid of a pyrolysis reactor **(B)** Using metal spade to scrape off any remaining sediments and **(C)** Extracting excess sediments and any remaining solid from previous operating sessions using Cyclone machine.

per year and another 25.79 million tons from accumulated waste, which can be processed into pyrolysis oil.

Pyrolysis oil is the oil obtained from biomass, however in this project we use the plastic waste for raw material due to plastic is a main municipal waste in Thailand. The processing rate is 500 L per ton of plastic waste and the oil produced can be used to replace fuel oil and low cycle diesel which our researchers already test in laboratory and confirmed. For this engineering project, we study the temperature of the pyrolysis process to produce oil from plastic pellets, testing the properties of oil obtained at each temperature, and increasing the purity of pyrolysis oil.

The objective of this research is to 1) study the proportion of final pyrolysis oil products in each temperature, 2) study the properties of pyrolysis oil obtained at each temperature, and 3) study the performance of each condensate tower.

THEORIES AND RELATED RESEARCHES

Plastic

Plastics are synthetic organic compounds that are used to replace certain natural materials. The plastic is divided into two types: thermoplastic and thermosetting plastics. There are many types of thermoplastics, such as high density polyethylene (HDPE) with specific gravity values of 0.941–0.965 g/cm^3. HDPE has a melting point temperature of about 135°C, with a linear molecular structure. There are also many types of thermosetting plastics. Polyethylene terephthalate (PET) is the one of them.

Pyrolysis Process

The pyrolysis process is the process of decomposition of various compounds or materials with thermal decomposition at temperatures around 400–800°C in an oxygen-free atmosphere or contain very small amount of oxygen.

In general, the products obtained from the pyrolysis process can be divided into three types according to the condition. The primary product can be gas, liquid (which has oil-like properties) and char. The ratio of obtained products depends on the processing conditions, such as temperature, heat rate, etc. The most preferred product is liquid or oil.

Oil Specifications and Testing

There are few characteristics of the oil that can be directly tested by the instrument, such as sulfur content, viscosity values, etc. In addition, most values are measured by using certain tests that use standards to determine, such as using the standards of ASTM (American Society for Testing and Material) or IP (Institute of Petroleum), etc. The properties tested are 1) flash point 2) viscosity 3) heating value and 4) specific gravity.

CHEMICALS, EQUIPMENT AND METHODS

Chemicals

Chemicals used in this study were HDPE resin from IRPC Company Limited, PET from Thai Chin Kong Industry Corporation Limited, liquefied petroleum gas, and liquid fuel.

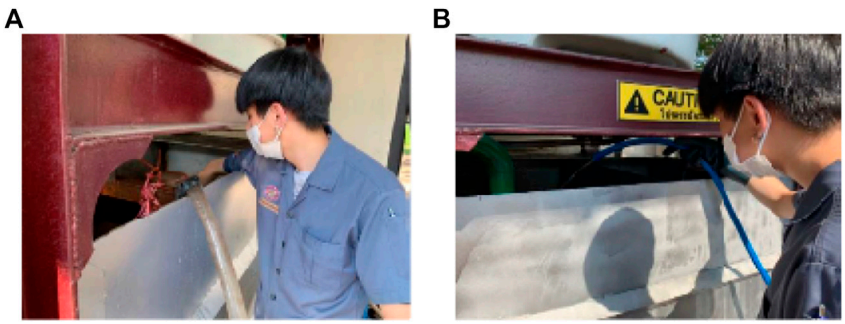

FIGURE 2 | Preparation of the coolant **(A)** Taking remain water out of the coolant tank and **(B)** Adding new water into the tank.

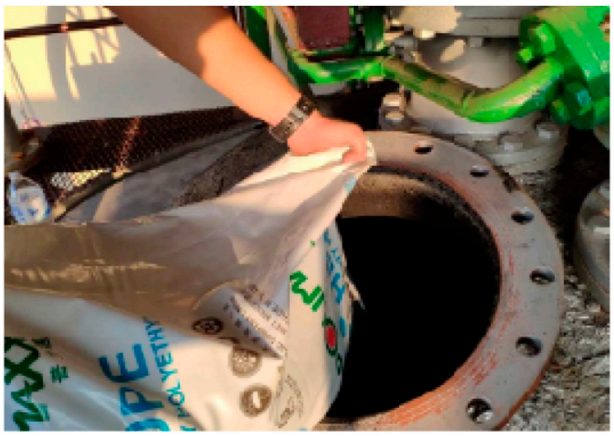

FIGURE 3 | Adding raw materials.

Equipment

Equipment used in this study were mobile pyrolysis system kit, gallon volume 4.5 L, cyclone machine, two 12-inch wrench, diameter ½ inch hose (3 m long), long spade, rice sacks, Brookfield viscometer DV-I+, pure distillation unit, and 3-position weighing scales.

Experimental Methods

Preparation of Pyrolysis Reactor

Preparation of pyrolysis reactors by cleaning the machine from sediment trapped inside. Opening the lid of the pyrolysis reactor from above with a wrench (**Figure 1A**), then use a long spade to scrape off the sediment trapped inside the reactor (**Figure 1B**). After that, use a cyclone to remove all sediment (**Figure 1C**).

Preparation of the Coolant

Water preparation for use in coolers by taking the remaining water out of the coolant tank **Figure 2A** and add the new one into the tank **Figure 2B** to be ready to use the coolant for mobile pyrolysis systems.

Adding Raw Materials

The plastic pellets used in the experiment are fed into the pyrolysis reactor as shown in **Figure 3**.

Collecting Pyrolysis Oil Samples

After the pyrolysis process is complete, oil samples will be collected at the first, second, third, and fourth condensers respectively, as shown in **Figure 4A**, by opening the valve of the bottom filter of each condenser, in order to bring the pyrolysis oil that is condensed at that condenser in the pyrolysis oil refining process (**Figure 4B**).

Mobile Type Pyrolysis Equipment

Three-dimensional model of mobile type pyrolysis equipment shown in **Figures 5A,B** conveying plastic waste by waste conveyor (6) into the raw material shredding machine and into (15) pyrolysis reactor heating by using (13) heating furnace to system at a temperature of 400°C. Over time, the plastic granules will become liquid and evaporate into gas flowing into (3) gas separator to enter (1) the main condenser and enter in (1) condense the first, second, third, and fourth units and collect the oil samples at the exit of the four solid filters at the bottom of each condenser, keeping the temperature to 400°C as For 10 min, then collect the oil samples again until complete three times every 10 min. After that, increase the temperature at the reactor to 425 and 450°C. Experimenting the same method at the temperature of 400°C (**Figures 6** and 7).

FIGURE 4 | Collecting pyrolysis oil samples **(A)** four collecting areas and **(B)** Collecting the condensed pyrolysis oil.

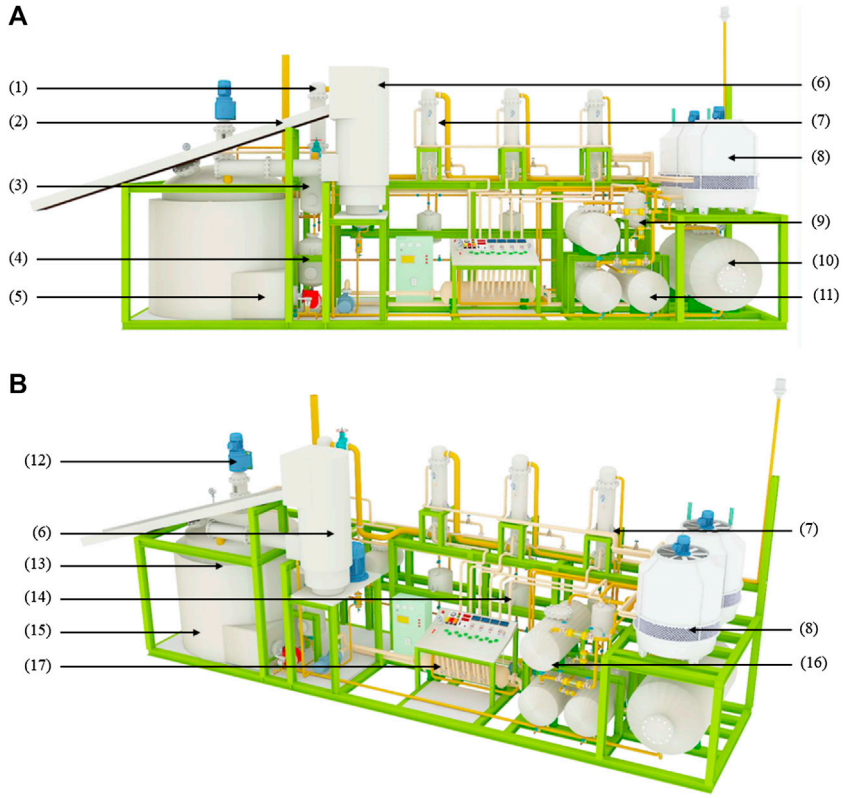

FIGURE 5 | Three-dimensional model of the mobile pyrolysis equipment set Three-dimensional model of the mobile pyrolysis equipment set when **(A,B)** consists of (1) Cyclone, (2) Waste conveyor belt, (3) First gas separator, (4) Gas storage tank, (5) Burner, (6) Sub-machine feeder, (7) Condenser, (8) Cooling machine, (9) Second gas separator, (10) Cooling water tank, (11) Pyrolysis oil storage tank, (12) Gear motor stirring set, (13) Kilns, (14) Product filters, (15) Reactor, (16) Pyrolysis oil storage tanks, and (17) Coolant.

Analysis

Oil Refining Set

The liquid product obtained from pyrolysis of HDPE and PET distilled by the oil distillation kit as shown in **Figure 8** consists of 1) thermometer 2) three-way joints 3) round bottom bottles 4) heating furnaces 5) condensers 6) vacuum joints 7) apple shaped bottles that are distilled at low temperature ranges of lower than 65, 65–170, 170–250, and over 250°C.

Viscosity Analysis

Viscosity analysis was accomplished with Brookfield viscometer DV-I+ at 40°C by adding 1 ml of sample into the sample cup and returning to the viscometer. Adjust the cone with the adjustment ring to contact the liquid surface, and adjust the rotation of the machine to 20 RPM to measure viscosity. The result was reported on screen in centipoise (cP), then convert the unit to centistoke (cSt) from **Eq. 1**.

$$\mu_{cSt} = \frac{\mu_{cP}}{\rho \times 1000} \quad (1)$$

where,

μ_{cP} is the viscosity in centipoise (cP)

μ_{cSt} is the viscosity in centistoke (cSt)

ρ is the density of oil sample in Gram per cubic meter (g/cm^3)

Analysis of Hydrocarbon Compounds

Analysis of various hydrocarbon compounds in the pyrolysis oil by fractional distillation with 300 ml volume purity distillation equipment at temperature ranges of lower than 65, 65–170, 170–250, and more than 250°C. These are standard fractional distillation temperature ranges that use in normal petrochemical process which we have adapted in laboratory scale. The petrochemical products were found from this experiment.

RESULTS AND DISCUSSION

Effect of Raw Materials on Products

From the experiment, it was found that products obtained from the pyrolysis of HDPE were liquid with brown color, which is shown in **Figure 9**. On the other hand, the pyrolysis of PET resulted in gas and solid (**Figure 10**). While gas could be recycled in the process as fuel, solid blocked up the pipe resulting in the termination of process. This corresponds to the study from Williams and Slaney (2007) which stated that the pyrolysis of polyethylene, polypropylene, and polystyrene mostly yield oil products, while the pyrolysis of PET results in mostly solid

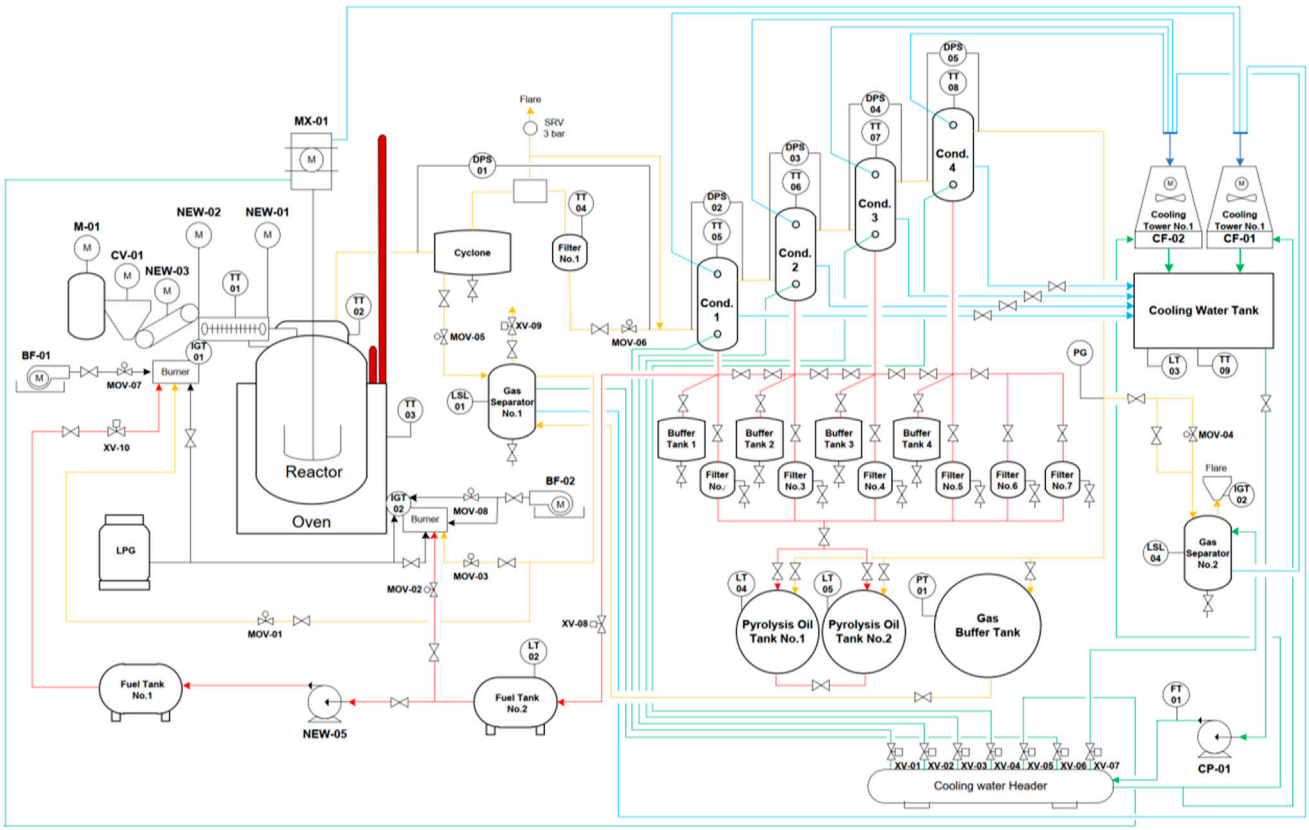

FIGURE 6 | Mobile pyrolysis process flow diagram.

FIGURE 7 | Mobile type pyrolysis equipment set.

products. Also, Encinar and Gonzalez (2008) reported that the pyrolysis of PET yields high amount of carbon monoxide and carbon dioxide since the plastic contains high amount of oxygen. Since the pyrolysis of PET could not produce oil, the analysis in the following section would be from the use of HDPE as a raw material only (**Figure 10**).

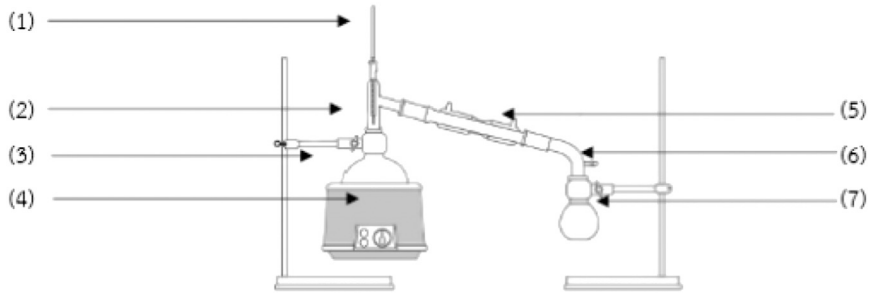

FIGURE 8 | The distillation unit consists of (1) thermometer (2) three-way joint (3) round bottom bottle (4) heating furnace (5) condenser (6) vacuum coupling and (7) Erlenmeyer flask.

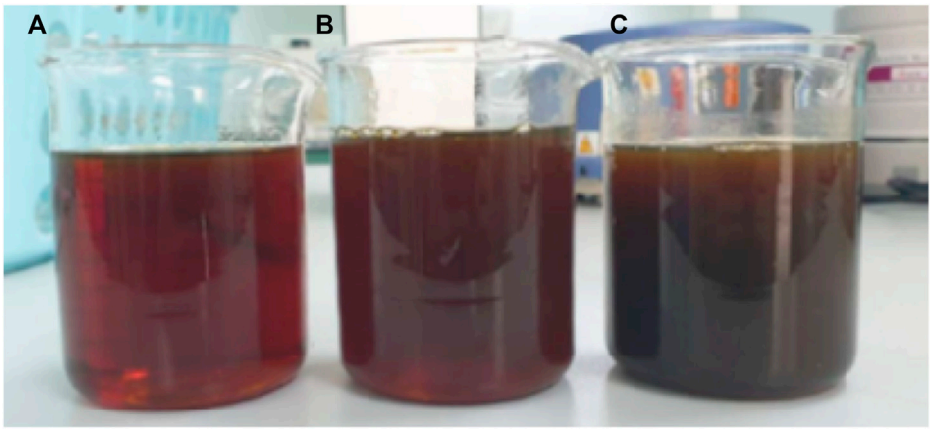

FIGURE 9 | Products obtained from the pyrolysis of HDPE pellets **(A)** first sample collection **(B)** second sample collection (10 min after first collection), and **(C)** the third sample collection (20 min after first collection).

FIGURE 10 | Products obtained from the pyrolysis of PET pellets.

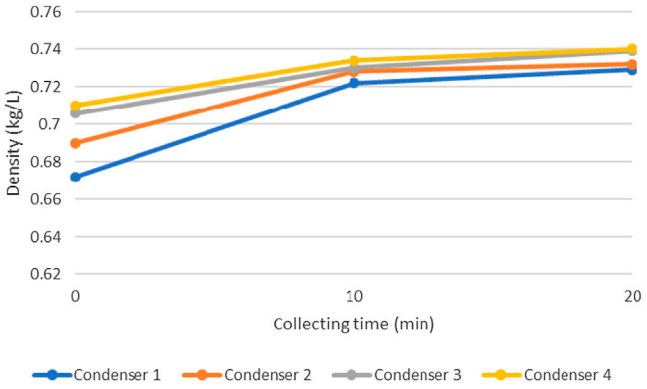

FIGURE 11 | Densities of products from each condenser at different collecting time (pyrolysis temperature = 450°C).

Effect of Pyrolysis Temperature on Product Properties

The pyrolysis of HDPE at the reactor temperature of 400, 425, and 450°C produced oil with the total amount of 22.5, 27, and 40.5 L per 100 kg of HDPE, respectively. This shows that 450°C is the temperature that produce the highest amount of pyrolysis oil from the experiment. The result corresponds to the study from Kumar and Singh (2013) which reported that the highest liquid yield for HDPE pyrolysis was at 450°C. Furthermore, pyrolysis oil products were measured for density and viscosity at 40°C standard room temperature. It was found that densities of products from the first condenser at the pyrolysis temperature of 400, 425, and 450°C were 0.668, 0.67, and 0.672 kg/L, respectively, while viscosities were 3.287, 3.289, and 3.297 cSt, respectively. It could be seen that density and viscosity increase with the pyrolysis temperature. This is

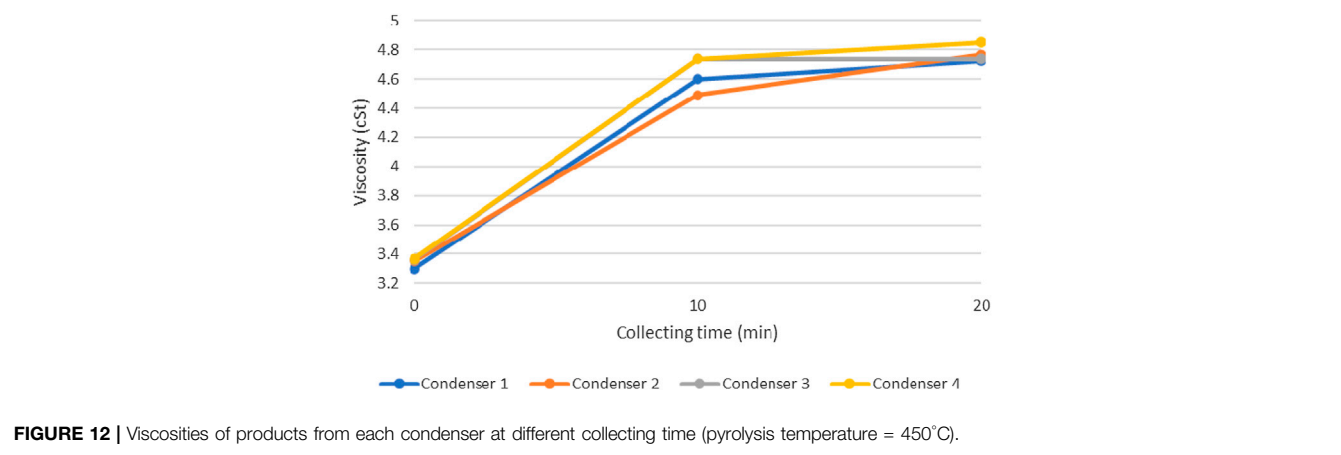

FIGURE 12 | Viscosities of products from each condenser at different collecting time (pyrolysis temperature = 450°C).

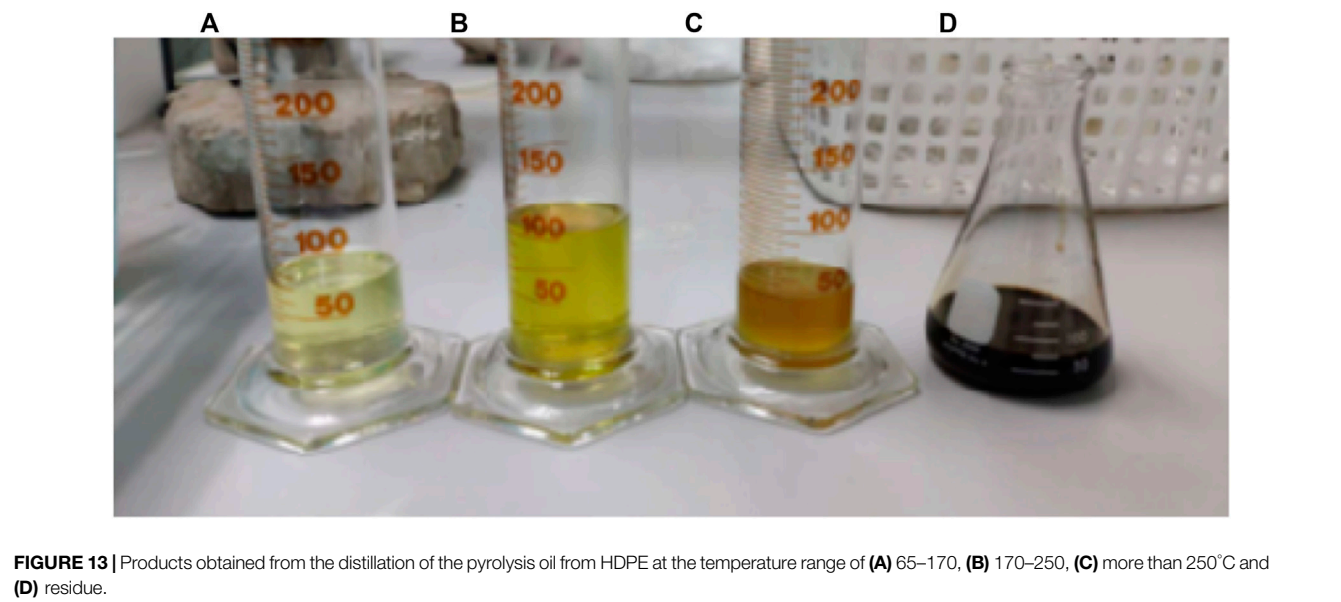

FIGURE 13 | Products obtained from the distillation of the pyrolysis oil from HDPE at the temperature range of **(A)** 65–170, **(B)** 170–250, **(C)** more than 250°C and **(D)** residue.

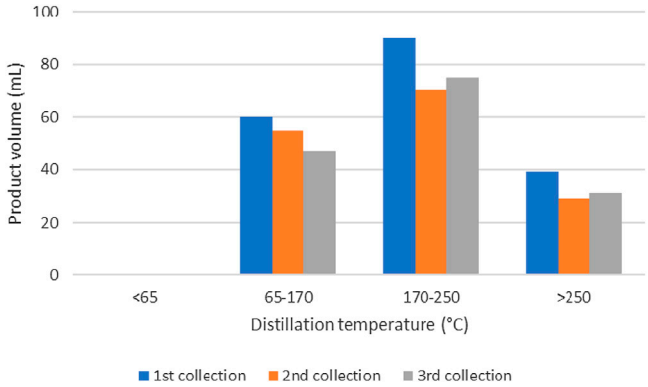

FIGURE 14 | Amount of pyrolysis oil from HDPE at different distillation temperature ranges and different collection periods.

TABLE 1 | Fuel properties compared with standard values.

Properties/Fuels	95 gasoline		Kerosene		Diesel	
	Measured	Standard value	Measured	Standard value	Measured	Standard value
Density (40°C, kg/L)	0.730	0.741[a]	0.800	0.807[a]	0.814	0.837[a]
Viscosity (40°C, cSt)	0.72	0.40–0.80[b]	1.19	1.24[c]	3.44	1.80–4.10[d]

[a]*The Energy And Fuel And Data Sheet.*
[b]*Specific Gravity and Viscosity of Liquids.*
[c]*Analysis of Adulterant Kerosene in Diesel by Kinematic Viscosity Measurement.* (More et al., 2012)
[d]*Department of Energy Business, Ministry of Energy.*

because higher reaction temperature results in product with longer chain of molecules.

Effect of Collecting Time and Condensers on Product Properties

Liquid products from the pyrolysis of HDPE were collected from each condenser for three times: 1) when the system reached the target temperature, 2) 10 min after the first collection, and 3) 20 min after the first collection. Densities and viscosities of these products were illustrated in **Figures 11** and **12**.

These figures show the density and viscosity of product at the pyrolysis temperature of 450°C. It could be seen that the density and viscosity of pyrolysis oil increases as the collecting time increases. This is because hydrocarbons with shorter molecular chain could condense earlier than that of the longer chain (Lee and Shin, 2007). Also, the condenser at which the product was collected also affect product properties. Pyrolysis oil tends to have higher density and viscosity as it passes through number of condensers, which is due to the different time of condensation as explained. For other pyrolysis temperatures (400 and 425°C), product yields were low so that no additional oil could be obtained at the time of the second and third collection periods.

Results of Purification by Distillation

To improve the purity of liquid products obtained from the pyrolysis of HDPE and PET, simple distillations were conducted at various temperature ranges (Demirbas, 2004). Theoretically, hydrocarbon compounds with C5–C7 (naphtha) would be found at distillation temperature lower than 65°C, C6–C12 (gasoline) in the range of 65–170°C, C10–C14 (kerosene) in the range of 170–250°C, and C14–C19 (diesel) would be found above the distillation temperature of 250°C. Example of products from the distillation were shown in **Figure 13** for HDPE as raw material. The amount of pyrolysis oil from HDPE at different distillation temperature ranges and different collection periods was shown in **Figure 14**.

It could be seen that no product was obtained at the distillation temperature below 65°C which could be interpreted that there was no naphtha in this experiment. Kerosene was obtained with highest amount in the temperature range of 170–250°C, followed by gasoline in the range of 65–170°C and diesel at the temperature above 250°C. Also, the first product collection provided the best distillation yield for all temperature ranges since it gave the highest amount of the distillation product.

Fuel Properties

Different types of fuel obtained from the pyrolysis process followed by distillation were measured for densities and viscosities. These are compared with their standard values and can be shown in **Table 1**.

It could be seen that densities of pyrolysis fuels were slightly lower than standard values (0.9–2.7% difference), while

viscosities are mostly in range. The result shows the quality of products obtained from the pyrolysis process which were close to conventional fuels. With further refining process, these fuels could certainly be used as an alternative source of energy.

CONCLUSION

Main product for the pyrolysis of HDPE resin was liquid and PET resin was solid. 450°C was the temperature that gives the highest amount of pyrolysis oil in the experiment. The viscosity and density were increased according to three factors: high pyrolysis temperature, the number of condensers and longer collecting time. All refined products in each temperature range had the carbon number according to their boiling points. The distillation of pyrolysis oil in this experiment provided high amount of kerosene, followed by gasoline and diesel.

DATA AVAILABILITY STATEMENT

All datasets analyzed for this study are included in the article/ supplementary material.

AUTHOR CONTRIBUTIONS

All authors listed have made a substantial, direct, and intellectual contribution to the work and approved it for publication.

REFERENCES

Demirbas, A. (2004). Pyrolysis of municipal plastic wastes for recovery of gasoline-range hydrocarbons. *J. Anal. Appl. Pyrol.* 72 (1), 97–102. doi:10.1016/j.jaap.2004.03.001

Encinar, J. M., and González, J. F. (2008). Pyrolysis of synthetic polymers and plastic wastes. Kinetic study. *Fuel Process. Technol.* 89 (7), 678–686. doi:10.1016/j.fuproc.2007.12.011

Kumar, S., and Singh, R. K. (2013). Thermolysis of high-density polyethylene to petroleum products. *J. Pet. Eng.* 2013, 987568. doi:10.1155/2013/987568

Lee, K.-H., and Shin, D.-H. (2007). Characteristics of liquid product from the pyrolysis of waste plastic mixture at low and high temperatures: influence of lapse time of reaction. *Waste Manag.* 27 (2), 168–176. doi:10.1016/j.wasman.2005.12.017

More, B. P., Malve, M. K., Toche, R. B., and Shinde, D. B. (2012). Analysis of adulterant kerosene in diesel by kinematic viscosity measurement. *Int. J. Pharm. Biol. Sci.* 2 (4), 256–261.

Williams, P. T., and Slaney, E. (2007). Analysis of products from the pyrolysis and liquefaction of single plastics and waste plastic mixtures. *Resour. Conserv. Recycl.* 51 (4), 754–769. doi:10.1016/j.resconrec.2006.12.002

Conflict of Interest: The authors declare that the research was conducted in the absence of any commercial or financial relationships that could be construed as a potential conflict of interest.

Advantages of publishing in Frontiers

OPEN ACCESS
Articles are free to read for greatest visibility and readership

FAST PUBLICATION
Around 90 days from submission to decision

HIGH QUALITY PEER-REVIEW
Rigorous, collaborative, and constructive peer-review

TRANSPARENT PEER-REVIEW
Editors and reviewers acknowledged by name on published articles

Frontiers
Avenue du Tribunal-Fédéral 34
1005 Lausanne | Switzerland

Visit us: www.frontiersin.org
Contact us: frontiersin.org/about/contact

REPRODUCIBILITY OF RESEARCH
Support open data and methods to enhance research reproducibility

DIGITAL PUBLISHING
Articles designed for optimal readership across devices

FOLLOW US
@frontiersin

IMPACT METRICS
Advanced article metrics track visibility across digital media

EXTENSIVE PROMOTION
Marketing and promotion of impactful research

LOOP RESEARCH NETWORK
Our network increases your article's readership